Studies towards degradable polymers: new zinc(II) and palladium(II) complexes as catalysts for lactide polymerization and carbon monoxide/styrene copolymerization

A thesis presented in fulfilment of the requirements for the degree of

Doctor of Philosophy

In the Department of Chemistry

University of Cape Town

by

Peter Malatji

MSc (University of Cape Town)

BSc(Hons) (University of Limpopo)

August 2012

Plagiarism Declaration

I know the meaning of plagiarism and declare that all of the work in this thesis, save for that which is properly acknowledged, is my own

Name of candidate: Peter Malatji

Signature:…….....

Date:……..

Acknowledgements

I would like to thank the following for their contributions;

- Almighty God who makes everything possible.
- Associate Professor Alan T. Hutton and Professor Neil. J. Coville (University of Witwatersrand) for guidance, support, encouragement, and excellent supervision.
- Professor Selwyn Mapolie (University of Stellenbosch) and his research group members for allowing me to use their gel permeation chromatography instrument; thank you.
- Dr Sophie Rees-Jones for her support and assistance during the difficult time experienced after the fire accident in our laboratory.
- Mr P. Bennincassa for conducting microanalyses and EI mass spectral analysis; Mr Pete Roberts and Mr Noel Hendricks for measuring ^{1}H and ^{13}C NMR spectra; Dr Hong Su for the determination of X-ray single crystal structures; the University of Cape Town Proteomic Research Unit for MALDI TOF analysis and the University of Stellenbosch Mass Spectrometry Service for mass spectral analysis.
- Dr Maré Vlok for conducting MALDI-TOF analysis.
- My colleagues in the organometallic research group, particularly, Dr Feng Zheng, Dr Banothile C. E. Makhubela and Dr Emmah B. Hager for their valuable discussions.
- My wife Linah Shibambo for her moral support and understanding throughout; thank you.
- My family for all their support and encouragement.
- The National Research Foundation and the Equity Development Programme (UCT Chemistry Department) for funding.
- ***This thesis is dedicated to my first born son, Reatlegile Matthew Malatji!!!***

Abstract

In this study a range of new zinc and palladium complexes were synthesized, characterized and used in the production of degradable polymers. Zinc complexes were used for the production of polylactides (PLAs) functionalized with a drug candidate on a polymer tail. These functionalized polymers displayed slow drug release properties under physiological conditions. Palladium complexes were utilized for the production of a photodegradable CO/styrene copolymer (CP) which was subsequently reacted with lactide to form a new poly(lactide-*co*-CO/styrene) block copolymer. The following zinc complexes, of the type $Zn(N\text{^}O)_2$, (**39**) and (**40**), and of the type $Zn(N\text{^}S)_2$, (**45**), (**46**), (**47**) and (**48**) (see the table below) displayed different catalytic behaviour towards lactide polymerization when the reaction was conducted in toluene solvent at 70 ºC.

Complex $Zn(N\text{^}O)_2$	**Structure of drug candidate anion, $(N\text{^}O)^-$**	**Complex $Zn(N\text{^}S)_2$**	**Structure of drug candidate anion, $(N\text{^}S)^-$**
(**39**)	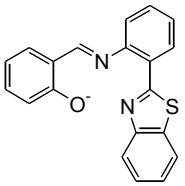 (**37**)$^-$	(**45**)	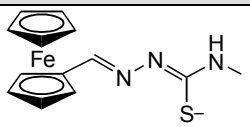 (**41**)$^-$
		(**46**)	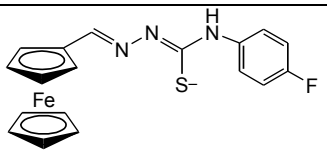 (**42**)$^-$
(**40**)	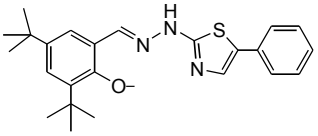 (**38**)$^-$	(**47**)	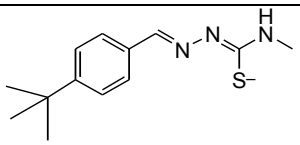 (**43**)$^-$
		(**48**)	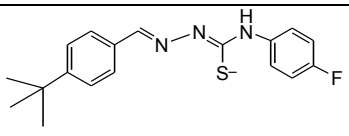 (**44**)$^-$

Complex (**39**) converted 95% of lactide monomer to form polylactide in 24 h while the same lactide conversion was achieved in 48 h when complexes (**45**) and (**46**) were utilized. Polymers having molecular weight of up to M_n = 4000 g/mol were isolated.

Abstract, continued

Polylactides functionalized with either (N^S) or (N^O) groups on the polymer backbone were successfully produced, thus presenting a new method for functionalization of polylactide. Complex $Zn(N^O)_2$ (**40**) did not convert lactide monomer to polylactide while complexes $Zn(N^S)_2$ (**47**) and (**48**) displayed the lowest activity. The following palladium complexes were investigated for CO/styrene copolymerization: [PdMe(MeCN)(N^N)]X, X = PF_6^- (**55**) or BF_4^- (**56**) and [PdMe(PPh_3)(N^N)]X, X = PF_6^- (**57**) or BF_4^- (**58**) [(N^N) = $CH_3(C_6H_4)C(O)N(C_5H_4N)_2$], as well as complexes [PdMe(MeCN)(N^N)]PF_6 (**59**) and [PdMe(PPh_3)(N^N)]PF_6 (**60**) stabilized with a (N^N) ligand containing a ferrocenyl group, [(N^N) = $FcC(O)N(C_5H_4N)_2$] (see the table below).

X^-, L	Compound	L'	Compound
PF_6, MeCN	(**55**)	MeCN	(**59**)
BF_4, MeCN	(**56**)		
PF_6, PPh_3	(**57**)	PPh_3	(**60**)
BF_4, PPh_3	(**58**)		

Catalyst behaviour in the CO/styrene copolymerization reaction was found to be influenced by several factors when the reaction was conducted in trifluoroethanol–dichloromethane mixture as the solvent medium and in the presence of benzoquinone as an oxidant at room temperature and carbon monoxide pressure of 1 bar. Higher catalyst activity of 203.60 g CP (g Pd)$^{-1}$ h^{-1} was observed when complex (**55**), containing the acetonitrile donor ligand and PF_6^- anion, was utilized for CO/styrene copolymerization as compared with compound (**56**) [2.60 mg CP (g Pd)$^{-1}$ h^{-1}], containing the same donor ligand but with the BF_4^- anion. Complex (**59**) with ferrocenyl group in its oxidized form, displayed improved activity of 143.60 mg CP (g Pd)$^{-1}$ h^{-1} when compared with the same complex (**59**) but with ferrocenyl group in neutral form [1.80 mg CP (g Pd)$^{-1}$ h^{-1}]. CO/Styrene copolymers having a molecular weight up to M_n = 3790 were isolated. Complexes (**57**), (**58**) and (**60**), containing the triphenylphosphine donor ligand, displayed lowest activity.

Contents

Contents, continued

Contents, continued

Contents, continued

Contents, continued

List of abbreviations

IR	Infrared
ν	Stretching frequency
TLC	Thin layer chromatography
NMR	Nuclear Magnetic Resonance (^{1}H or ^{13}C)
ppm	Parts per million
δ	Chemical shift
t	Triplet
s	Singlet
m	Multiplet
J	Coupling constant
CO	Carbon monoxide
PLA	Polylactide
ROP	Ring opening polymerization
CP	Copolymer
PDI	Polydispersity index
PPh_3	Triphenylphosphine
MeCN	Acetonitrile
M	Metal
Cp	Cyclopentadienyl
Fc	Ferrocenyl
BQ	Benzoquinone
Ph	Phenyl
L	Ligand
TFE	Trifluoroethanol
M_w	Molecular weight
M_n	Number average molecular weight
PGSE	Pulsed gradient spin-echo
DFT	Density functional theory
CV	Cyclic voltammetry
$E_{1/2}$	Half-wave potential
TBAP	Tetrabutylammonium perchlorate
ESI-MS	Electro-spray ionisation mass spectrometry

List of abbreviations, continued

FAB-MS	Fast-atom bombardment mass spectrometry
EI-MS	Electron impact mass spectrometry
MALDI TOF	Matrix assisted laser desorption ionization time of flight

CHAPTER 1: INTRODUCTION

1.1 Ring opening Polymerization of Lactide

Continuous gradual depletion of petrochemical feedstocks used to produce polymers, together with increasing environmental concerns, has led authorities to consider the use of cleaner plastics which are derived from natural resources. This has led to formulation of the Green Chemistry concept (see **Table 1.1.1**) in order to encourage good research practices which do not harm the environment.[1] The following principles are of particular interest considering the scope of the current study: Principle 1, on prevention; Principle 7, for use of renewable resources; Principle 9, for catalysis; and Principle 10, for promotion of production of degradable products.

TABLE 1.1.1: The twelve Principles of Green Chemistry[1]

1. Prevention It is better to prevent waste than treat or clean up waste after it has been created.
2. Atom Economy Synthetic methods should be designed to maximize the incorporation of all materials used in the process into the final product.
3. Less Hazardous Chemical Synthesis Wherever practicable, synthetic methods should be designed to use and generate substances that posses little or no toxicity to people or the environment.
4. Designing Safer Chemicals Chemical products should be designed to effect their desired function while minimizing their toxicity.
5. Safer Solvents and Auxiliaries The use of auxiliary substance (e.g., solvents or separation agents) should be made unnecessary whenever possible and innocuous when used.
6. Design for Energy Efficiency Energy requirements of chemical processes should be recognised for their environmental and economic impacts and should be minimized. If possible, synthetic methods should be conducted at ambient temperature and pressure.

TABLE 1.1.1: The twelve Principles of green chemistry[1], continued

7. Use of Renewable Feedstocks

A raw material or feedstock should be renewable rather than depleting, whenever technically and economically practicable.

8. Reduce Derivatives

Unnecessary derivatization (use of blocking groups, protection/de-protection, and temporary modification of physical/chemical processes) should be minimized or avoided if possible, because such steps require additional reagents and can generate waste.

9. Catalysis

Catalytic reagents (as selective as possible) are superior to stoichiometric reagents.

10. Design for Degradation

Chemical products should be designed so that at the end of their function they break down into innocuous degradation products and do not persist in the environment.

11. Real-time Analysis for Pollution Prevention

Analytical methodologies need further development to allow for real-time, in-process monitoring and control prior to the formation of hazardous substances.

12. Inherently Safer Chemistry for Accident Prevention

Substances and the form of substance used in chemical processes should be chosen to minimize the potential for chemical accidents, including releases, explosions and fires.

It has been reported that more than 150 million tonnes of petrochemical resources are consumed annually as raw material for plastic production.[2] It was for this reason that polylactide- or polylactic acid (PLA)-based plastics were considered as alternatives to petrochemical polymers. Polylactides maintain many of the desirable properties of traditional plastics. Lactide monomer is derived from agricultural renewable resources, such as beets and corn. The added bonus is that PLAs are also biocompatible, readily biodegradable and easily recycled.[3]

Existence of PLA dates from as far back as the sixteenth century, produced by the self-condensation of lactic acid to yield solid materials.[4] There are two methods that have been used for the preparation of polylactic acid: condensation of lactic acid and ring opening polymerisation (ROP) of lactide. The latter method was first reported by Carruthers *et al.* in 1932 and is commonly used for the commercial production of PLA.[5] Well-known medical applications of polylactide are its use for slow release drug delivery, tissue regeneration and biodegradable sutures.[6] However, its use as a commodity polymer has remained limited because of high production costs compared with conventional plastics, as well as poor activity and stereochemical control of available catalyst systems. Due to environmental legislations and also the increased demand for petrochemicals there have been concomitant increases in the prices of these resources. In 2002, Natureworks LLC, currently a joint venture between Cargill and Teijen Limited, opened a 300 million lb per year PLA production plant, making PLA the first commodity polymer to be derived from corn instead of fossil fuel.[7] Interestingly, this industrially produced PLA, fabricated in isotactic form, has physical properties similar to polyolefins and polystyrene. It also has found use in material applications such as bulk packaging and fibers (trade name Ingeo™).[7]

Production of PLA begins from a starch or sugar feedstock which is processed to yield D-glucose. As a result, optically pure L-lactic acid is generated by fermentation using bacteria of the genera *Lactobacillus*, *Streptococcus pediococcus*.[8] The low molecular weight pre-polymer (MW 1000 – 5000 g/mol) of poly(L-lactic acid) can be produced from lactic acid through condensation polymerization. The synthesis of lactide is then achieved by a depolymerization process to afford the lactide monomer (see **Scheme 1.1.1)**.

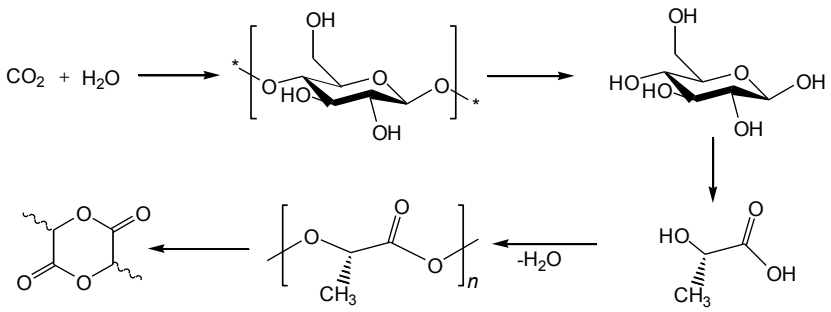

SCHEME 1.1.1: Synthesis of lactide monomer from natural resources.

The monomer is then used in the presence of a suitable catalyst to produce higher molecular weight polymers through a ring opening polymerization (ROP) mechanism. The resulting polymers are degraded by biological processes and the degradation products are carbon monoxide and water.

1.1.1 Ring opening polymerization mechanism

Lactide monomer possesses two stereocentres, and thus there exist three stereoisomers: L-lactide, its enantiomer D-lactide and the diastereomer *meso*-lactide.[9] As such, numerous types of ordered polymer microstructures are produced (see **Figure 1.1.1**). The resulting microstructures exhibit a crystallinity that depends on the stereochemistry of the monomer. Isotactic poly(L-Lactide) or PLLA, which is derived from pure L-Lactide monomer, is a crystalline thermoplastic with a glass transition (T_g) of approximately 60 °C and a melting temperature (T_m) of 170 – 180 ºC. In this case polymer preparation does not require any polymerization stereocontrol.

Syndiotactic PLA, however, can only be synthesized from *meso*-lactide and requires that the catalyst employed be selectively inserted at only one stereocentre (*R* or *S*) of the monomer. On the other hand, heterotactic PLA is an amorphous material produced from *rac*-lactide monomer by selective insertion of the D- or L-lactide isomer with opposite configuration to the previously inserted monomer. Catalysts which generate isotactic PLA from *rac*-lactide are also of importance since a mixture of isotactic PLLA and PDLA has been found to have bulk properties much different to that of pure PLLA (**Figure 1.1.1**).[10,11]

The ring opening polymerization of lactide to yield high molecular weight PLA is commonly initiated by a Lewis acid as a catalyst, e.g. metal complexes containing a metal-alkoxide bond. Organic compounds or enzymes in the presence or absence of alcohol as co-solvent have also been employed.[11] The mechanism of ring opening polymerization that has been proposed for lactide catalysed by a metal complex is represented in **Scheme 1.1.2**.[7,11,12]

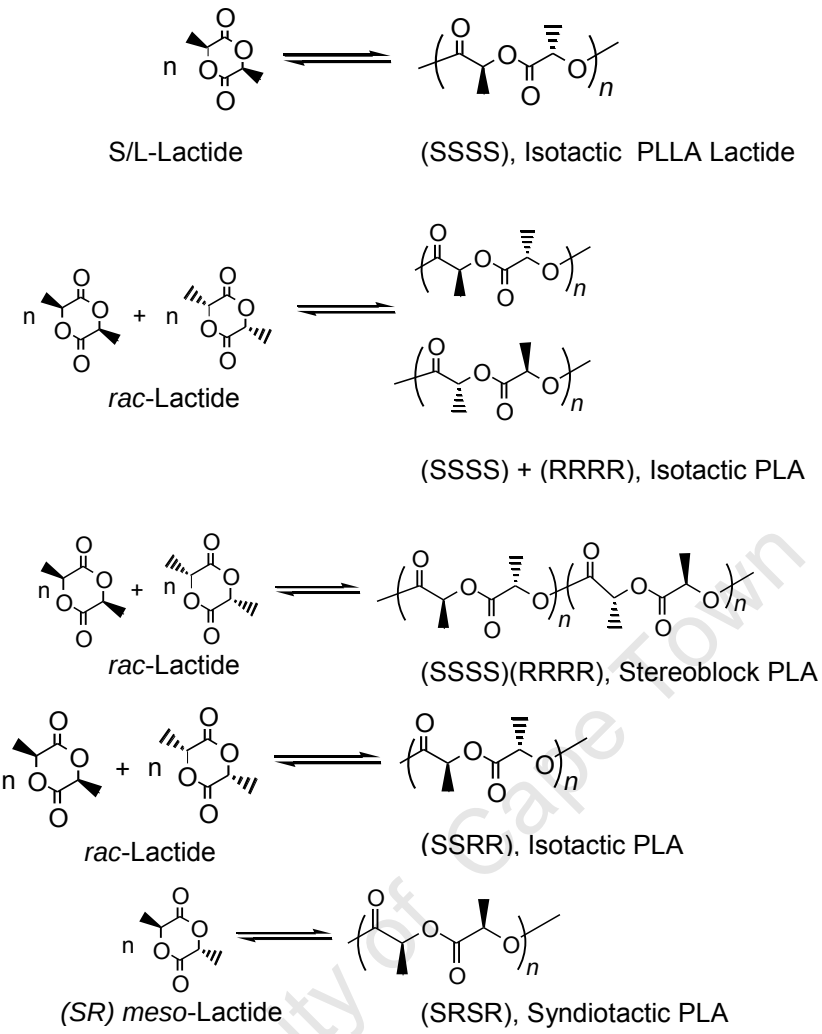

FIGURE 1.1.1: Isomers of lactide and possible polymers formed from a specific starting monomer.

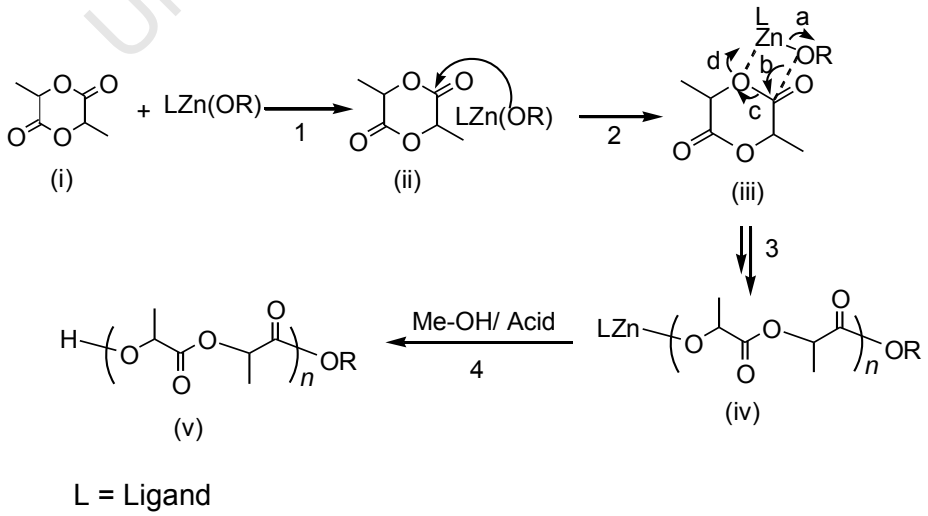

SCHEME 1.1.2: Proposed mechanism for the ring opening polymerization of lactide.[7,11,12,13]

The first step (1), of the polymerization process, as shown in **Scheme 1.1.2**, involves the attack on the acyl bond in the lactide monomer (i) by the nucleophilic alkoxide species which originally was bonded to a Lewis acidic metal centre. In step 2, the intermediate (ii) undergoes acyl-bond cleavage through four stages (a – d) shown in (iii). The generated intermediate, subsequently, forms a new metal alkoxide species which re-initiates the polymerization process in Step (3). The polymeric intermediate (iv) is finally quenched with acidified methanol in step (4) to form a polylactide (v) which is capped with an ester group on the initiating site and the hydroxyl group on the terminating site. Depending on the zinc initiator used, for example, when zinc amide (LZn-NR_2) or zinc acetate (LZnOAc) are used, the final polymer will be terminated with amide or acetate groups, respectively. The R group can be designed for desired applications e.g., it can be a drug molecule. Various methods which deal with functionalization of PLAs will be fully discussed later in **Section 1.1.4**. For the catalytic process to be successful, the conditions should satisfy certain minimum thermodynamic requirements.

The driving force of this catalytic process is the enthalpy of polymerization, more specifically the relief of ring strain, i.e. ΔH = 22.1 kJ mol^{-1} for 1 M solutions of lactide at room temperature. This energy enables the unfavourable entropy of polymerization to be overcome.[14] Whilst the polymerization equilibrium is determined thermodynamically, the polymerization control, stereoselectivity and the rate are governed by the choice of the initiator. Two types of possibly competing processes are believed to be involved during the polymerization process: the chain-end control and the enantiomorphic site-control.[15] The latter process occurs when the stereochemistry of the most recently inserted monomer influences the stereochemistry of the subsequent insertion. Such control is typically observed in catalytic systems which exploit bulky ligands to crowd the active-site. Alternatively, the enantiomorphic site control process relies on the chirality of the ancillary ligand, and hence, the catalyst itself is the source of the stereochemical selectivity due to steric interactions between the incoming monomer and the catalyst framework. In addition to thermodynamic properties, the choice of the initiator is also of importance.

1.1.2 Polymerization-initiator selection parameters

Early studies were focused on the utilization of homoleptic heterogeneous zinc oxides and some Group 2 metals ions, e.g. magnesium and calcium. The initiators such as carboxylates (e.g. stearate and acetate), halides (e.g. chloride and bromide), amino acid salts (e.g. glycinate) and alkoxides (e.g. lactate) have been employed.[11] However, since these complexes were insoluble in many organic solvents, polymerization reactions were performed under solvent free conditions or at high temperatures ranging from 110 – 200 °C. Whilst most of these salts were active to some extent, reactions were generally slow and epimerization side reactions occured.

The most desirable aspects of lactide polymerization catalysts are high activity, ability to controllably produce high molecular weight materials, production of monodispersed polymers and stereochemical control. In addition, the metal ion should be redox-inactive and inert to β-hydrogen atom abstraction from the growing alkoxide polymer chain, otherwise side reactions could lead to chain termination and loss of catalytic activity.[12] The inorganic template LM, on the other hand, should be inert with respect to ligand scrambling, otherwise oligomeric alkoxides could be formed through intermolecular exchange. The advantages of the single-site catalysis could then be lost and the process would be akin to catalysis by simple metal salts.[12]

The alkoxide initiator in the LMOR complex should be labile to alcohol exchange and be easily inserted into a C=O double bond. Chain transfer and functionalities could then be introduced into the polymer-backbone through such reactions. The key feature of the single site catalysts is the lability of the leaving group within the complex and various anionic leaving groups have been investigated for ROP of lactide. The rate of polymerisation, i.e. conversion of a given amount of a monomer in a given time, for anionic initiators has been observed to be as follows; RO^-> $(^iPr)_2N^-$> $(SiMe_3)_2N^-$> $(SiPh_3)O^-$> AcO^-.[7,11,12]

Homogeneous lactide polymerization processes which utilize heteroleptic-catalyst systems involving a single site alkoxide as initiator have been the most studied. On the other hand, heterogeneous polymerization processes involving suitable catalysts incorporating acetate ion (AcO^-) as a leaving group have been reported.[16] A wide

array of ligand frameworks has been employed generating a library of catalysts with substantial variation in both steric environment and Lewis acidity. The effect of the Lewis acidity of the metal on the activity, however, is still not well understood,[17] and is further complicated by the potentially chelating nature of the growing polymer chain that also affects the polymerization control.[18]

Other important initiator parameters are the polymerization control, rate of the polymerization reaction and stereo-control. Well-controlled polymerization processes are advantageous as they could enable tuning of the physical properties of the polymer. The degree of polymer control is judged by the fulfilment of the following: linear increase in M_n with respect to percent conversion, linear increase in M_n/[initiator]$_0$ ratio, polymers with narrow polydispersity index (PDI = 1), ability to undergo sequential monomer addition, high ratio of k_p/k_i (k_p = rate of propagation, k_i = rate of initiation) and finally, a high k_p/k_{tr} ratio (k_{tr} = rate of transesterification).

The ROP is rarely truly living due to side processes such as chain transfer by transesterification or hydrolysis reactions; however, these transfer reactions are often kinetically controlled. Two types of transesterification reaction exist and both result in polydisperse polymers (PDI > 1). The intramolecular side reaction leads to formation of cyclic oligomers or to the production of polymers with a range of chain lengths, (**Figure 1.1.2**).

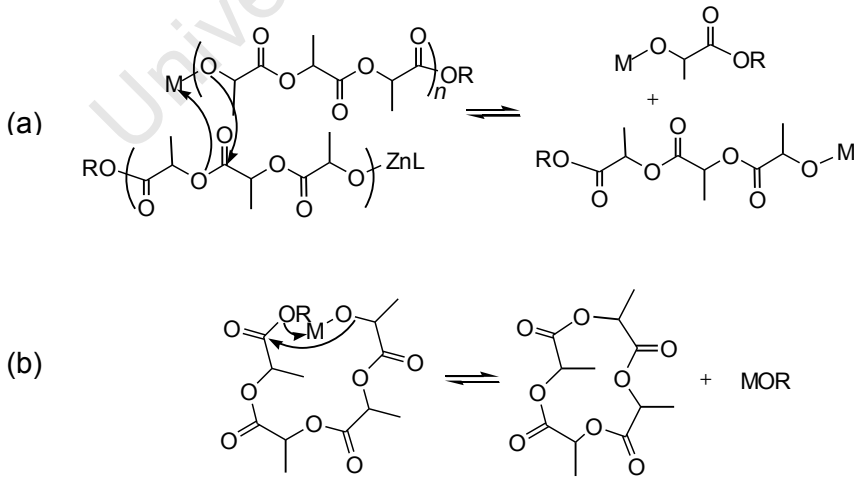

FIGURE 1.1.2: Transesterification reactions possibly taking place during polymerization: (a), intermolecular transestification, (b) intramolecular transestification (back-biting).[11]

The degree of esterification is usually determined with Gel Permeation Chromatography (GPC) through analysis of PDI. The greater the value of PDI (>1) the higher the degree of transestirification. In MALDI-TOF (matrix assisted laser desorption ionization time of flight) mass spectrometry molecular weights (M_w) occur which corresponds to cyclic structures or odd-numbered chains with lactic acid repeat units [i.e. $M_w = (72)n + 2$]. Homonuclear decoupled ^{1}H NMR spectroscopy is used to analyse polymers resulting from the *rac*-lactide monomer and to identify the tetrad level of the methine region at 5.20 ppm [according to Bernoulian statistics, there are five possible *tetrad* sequences, i.e. 3*iii*, 2*isi*, *sis*: *iis*, *sii*, which describe the ability of the catalyst to control racemic (*i*-dyad) and meso (*s*-dyad) connectivity of the monomer units].[19] The ^{1}H NMR spectra display main signals which have been denoted as *isi* or *iis* resonances.[19]

The extent of stereocontrol exerted by a particular initiator is also expressed in terms of the probability of certain stereosequences: the probability of isotactic enchainment (P_i), sometimes referred to as P_m, and the probability of syndio/heterotactic enchainment (P_s). These are determined from an analysis at the tetrad level of resonances observed in both the homonuclear-decoupled ^{1}H and ^{13}C NMR spectra. The calculation is performed by comparing the peak integrals with those predicted by Bernouillan statistics.[19]

While various catalysts containing transition metal ions, Zn^{2+}, Ti^{4+}, Zr^{4+}, Fe^{2+} and Fe^{3+},[11] main-group metal ions, Li^+, Mg^{2+}, Ca^{2+}, Al^{3+} and Sn^{2+},[12] and lanthanides, La^{3+}, Y^{3+} and Sc^{3+},[12] have been reported for lactide polymerization, in this review only catalysts containing Zn^{2+} will be discussed.

In cases where the polymer is to be used for medical purposes, the metal ion should be non-toxic, biocompatible and inexpensive. Traces of metal catalysts that remain in the final polymeric material can, under physiological conditions, be converted to harmful metal oxides or hydroxides.[11] Whilst metal-alkoxides of Groups 1 and 2, together with tin(II) are generally considered non-toxic, their hydroxides, which could form under physiological conditions, are strong bases, irritants and are harmful. The formation of these metal oxides or hydroxides in the human body is undesirable. Interestingly, zinc oxides have been reported to be less harmful, thus catalysts

utilizing this metal are mostly studied for the production of polymers for medical applications.[11,12]

1.1.3 Zinc(II) complexes for lactide polymerization

The first reported homoleptic complex used for ROP of lactide was bis(2-ethylhexanoate)tin(II) abbreviated as [$Sn(oct)_2$] [compound (i) shown in **Scheme 1.1.3**]. This commercially available complex, traditionally referred to as stannous octanoate, is easy to handle and is soluble in common organic solvents.[20] When this catalyst was utilized for ROP, surprisingly, no anhydride end-group was detected as expected in the polymer-backbone. Hydroxyl terminated polymers and macrocyclic molecules were detected. Various studies suggested that impurities such as water or alcohol, which are present in the polymerization solution, were the active ROP initiators.[21] It was only when benzyl-alcohol was added to the catalytic reaction solution that benzyl ester groups were detected on the polymer end, suggesting that the benzyloxy group was responsible for the polymerization initiation step. More specifically, the active catalyst was suggested to be a tin-benzyloxy species (ii), (see **Scheme 1.1.3**), which was generated *in situ.* These observations prompted researchers to investigate compounds containing various metal-alkoxy entities similar to single-site lactide ROP. To date, numerous reports exist on the polymerization of lactide utilizing various types of heteroleptic and homoleptic complexes.[7,11,12]

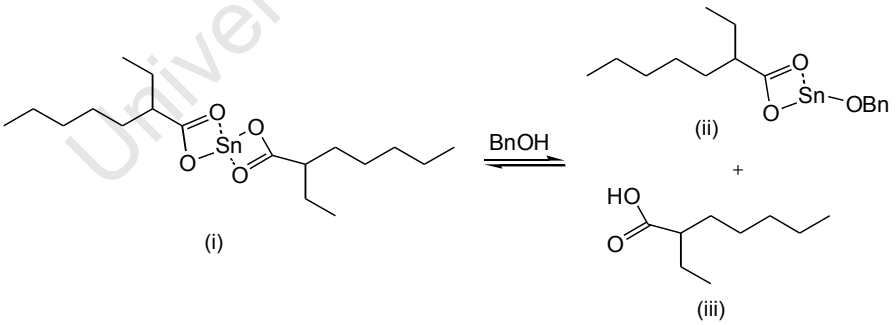

SCHEME 1.1.3: Ligand exchange of one octanoate group with benzyl alcohol in $Sn(octanoate)_2$ catalyst. [20]

It has been observed that heteroleptic complexes are the best alkoxide single-site initiators. A range of different ancillary ligands have been explored; however, excellent activities and remarkable selectivities were only observed when the following three types of ligand were utilized: β-diketiminates (BDI),[22] tris(pyrozolyl)hydroborates (Tp)[23] and bis(phenoxy diamine/diimine) ligands.[24-29]

The electron withdrawing feature of the ligands (*hard bases*) enable them to stabilize a range of metal-alkoxide complexes (*hard acids*) of the Main Group metals, as well as zinc. Zinc(II) and magnesium(II) have fully-filled outermost orbitals, which are $3d^{10}$ and $2s^2 2p^6$, respectively. The metal ions have similar ionic radii and share many similar properties; therefore, they are usually classified together.[30] The similarities of the metal ions make zinc(II) a pseudo-transition metal. The catalytic activity of zinc alkoxide complexes has been generally reported to be higher for complexes stabilized with phenoxy-amine ligands ($^{-}O\wedge NR_2$) than for BDI and Tp ligands. The higher activity has been postulated to be due to the greater Lewis acidity of the metal centre, thus making an alkoxy-group more nucleophilic.

A study by Chisholm[7] on pyrazole-donor-containing ligands has prompted a number of other researchers to investigate related tripodal frameworks bearing pyrazole donor groups. Carpentier *et al.*[7,28] isolated several zinc complexes stabilized with this ligand. Compound (**1**) as a catalyst displayed good activity and produced monodisperse polymers. In addition, 100% conversion of the monomer was achieved within 30 h at room temperature. The good activity was maintained even when a low catalyst loading of 0.25% was employed.

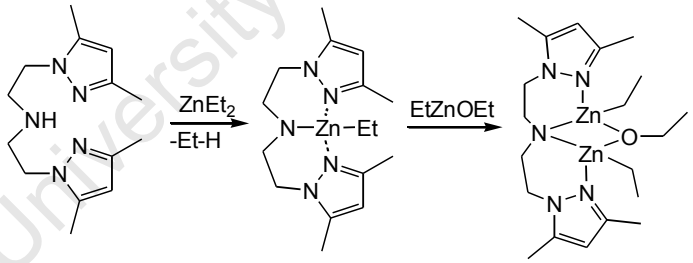

(**1**)

The investigation of the influence of the bulky groups on stereoselective lactide polymerization using a three-coordinate zinc-phenoxide complex (**2**) has been pursued by Chisholm *et al.*[31] The complex contains bulky *tert*-butyl and *iso*-propyl substituents on the ligand while the phenoxide-leaving group contained *ortho tert*-butyl substituents. It was observed that complex (**2**) catalysed ring-opening L-lactide polymerization to produce isotactic-PLA when the reaction was performed in benzene solvent at room temperature. Similarly, the complex catalysed *rac*-lactide to produce atactic poly(*rac*-lactide). The results confirmed that bulky groups on the ligands play

a role in the production of stereo-controlled polymers. When the ratio of $[LA]_0/ [Zn]_0$ ($[LA]_0$ and $[Zn]_0$ referes to initial molar concentration of lactide and zinc, respectively.) was 20:1, and with a catalyst loading of 5 mol%, polymerization occurred slowly at 25 ºC, proceeding to 90% conversion in 72 h. The low activity was attributed to the slow rate of initiation influenced by the bulky 2,6-*tert*-butylphenoxide leaving group.

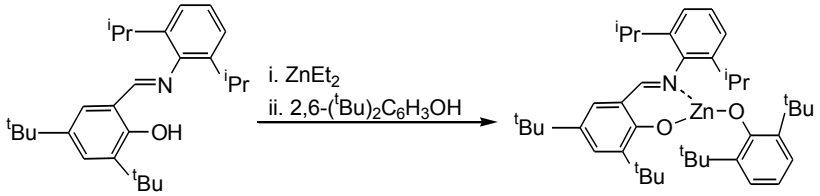

(**2**)

Research on a family of mononuclear phenoxy-supported zinc complexes bearing a single ethylenediamine tether at the *ortho* position have been carried out by Hillmyer, Tolman and co-workers.[32] Such complexes were produced by a reaction between salicylaldimine and diethyl zinc, followed by derivatization to the corresponding ethoxide after treatment with ethanol. Complex (**3**) has been established to exist as an alkoxy bridged dimer in the solid state. In addition, pulsed gradient spin-echo (PGSE) NMR measurements demonstrated that the complex dissociated in solution to be monomeric. The complex had an unusually high catalytic activity for the polymerization of lactide, even with a low catalyst loading of 0.15%; however, it has a drawback in that it produced polymers with slightly broad polydispersities (PDI = 1.34 – 1.42). At this catalyst loading, 96% of the original monomer was converted within 5 minutes of polymerization. On the other hand, 93% was converted within 18 minutes when the loading amount was decreased to 0.067%.

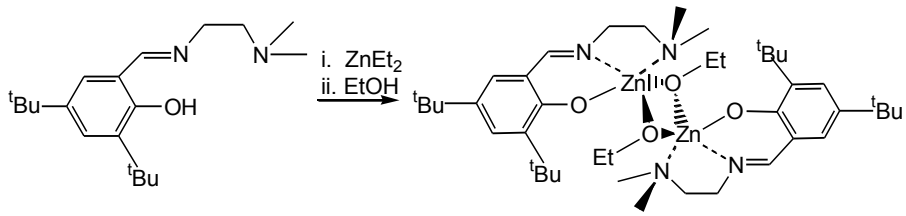

(**3**)

Various derivatives of complex (**3**) with a range of substituents on the benzene ring or with methyl or phenyl groups on the imine-carbon atom were explored by Lin and co-

workers [complexes (**4**) – (**14**)].[25] Although a range of ligand variants has been investigated, zinc alkoxide complex (**4**) has been the most thoroughly studied. Amongst all the complexes investigated for lactide polymerization, complex (**7**) was found to be inactive. The positive influence of the bulkier derivatives was observed when complex (**8**), bearing 4,6-*tert*-butyl substituents, was used. Molecular weight and stereochemical control (PDI = 1.13 and the degree of tacticity P_r = 0.74) was observed; however, the catalyst activity was reduced as 98% of the monomer was converted in 6 hours under similar conditions when compared to other derivatives.

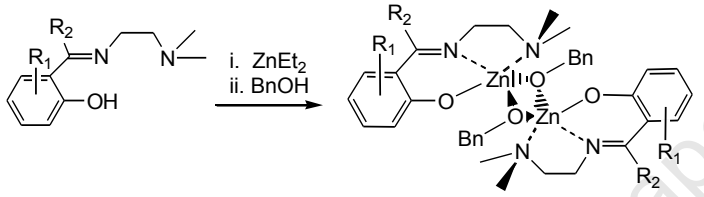

R_1	R_2	Complex
H	H	(**4**)
3,4-naphthyl	H	(**5**)
4-Cl	H	(**6**)
4-Br	H	(**7**)
4,6-di-^{t}Bu	H	(**8**)
H	Me	(**9**)
4-Cl	Me	(**10**)
4-Br	Me	(**11**)
4-OMe	Me	(**12**)
H	Ph	(**13**)
4-Cl	Ph	(**14**)

The bulkier monoether salicyldimene (Salen) Schiff base ligand and the corresponding zinc complex (**15**) has been synthesized by Wu *et al*.[33] In toluene solvent, complex (**15**) initiated polymerization of lactide at 60 °C and within 4 h, and lactide conversion of up to 96% was achieved when the ratio of $[LA]_0/[Zn]_0$ = 100 was employed. The experimental results showed all of the polymerization reactions were well-controlled, displaying sharp PDIs (1.03 – 1.10). The catalyst also showed good *rac*-Lactide selectivity and heterotactic polymers were produced in dichloromethane solvent.

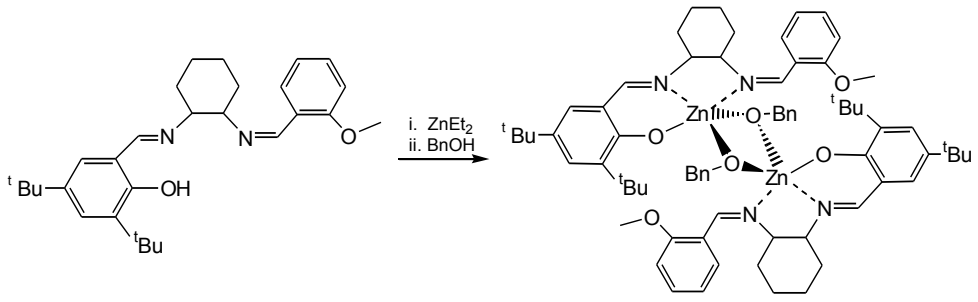

(**15**)

Phenoxy-based ancillary ligands possessing two ethylenediamine tethers installed at the *ortho* sites of the phenoxy ring were reported by Breyfogle *et al*.[26] Highly active

zinc alkoxide catalysts were prepared by reaction of the starting ligand with a mixture of EtZnCl and $ZnCl_2$, followed by treatment with ethanol. This afforded the binuclear monoalkoxide complex (**16**) in good yield. At a catalyst loading of 0.33%, complex (**16**) controllably polymerized *rac*-lactide, converting 90% of monomer within 30 minutes, producing almost monodisperse polymers (PDI = 1.19).

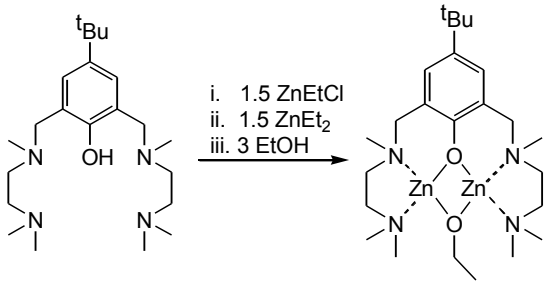

(**16**)

The same researchers reported the synthesis of complexes (**17**) and (**18**).[32] Complex (**17**) appeared to be dimeric with two five-coordinate Zn(II) centres, and this was confirmed by X-ray crystallography. Analysis of the complex mixture with PGSE NMR measurements and with laser desorption mass spectrometry (LDMS) showed that both complexes (**17**) and (**18**) cleaved into four-coordinate monomers in solution. A high activity for the polymerization of *rac*-LA in dichloromethane was displayed by complex (**17**) at ambient temperature, reaching 93% conversion after several minutes. The rate constant for ROP of lactide was, respectively, 5.1-, 8.2- and 1120-times higher than that of β-diketiminate,[19c,22a] dinuclear-(**3**)[24] and tris(pyrazolyl)-hydroborate-zinc ethoxy complexes.[23] Faster conversion reactions using a wide range of initial monomer to catalyst ratios were possible even up to $[LA]_0/[Zn]_0$ ratios of 1500. Polylactides with molecular weights as large as 130 kg mol^{-1} and with relatively narrow molecular weight distributions of PDI = 1.4 were observed.

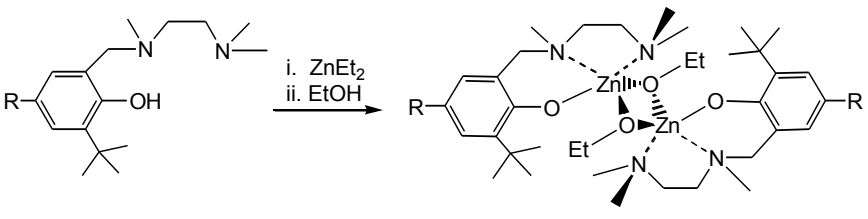

(**17**) R = ^{t}Bu, (**18**) R = Me

Sobota and co-workers have extensively studied both the hetero- and homo-leptic zinc complexes of a simple bidentate aminophenolate ligand incorporating 2,6-*tert*-butyl substituents.[34] Reaction of one or two equivalents of the ligand yielded complexes

(**19**) or (**20**), respectively. Both complexes were found to effectively initiate the polymerization of L-lactide at room temperature. Compound (**19**) achieved 98% conversion within two hours, while complex (**20**), upon addition of one equivalent of benzyl alcohol as a co-catalyst, required only one hour for near quantitative conversion. Molecular weight distributions of polymers produced with each catalyst were small (PDI = 1.09 and 1.16 respectively); however, neither catalyst was tested for stereoselective polymerization.

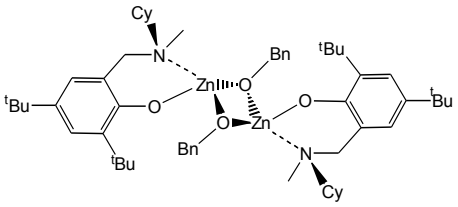

(**19**)

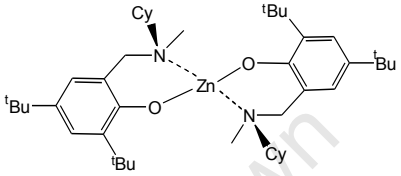

(**20**)

Wang and co-workers incorporated a pendant pyrazole ring into the salicylaldimine Schiff-base framework.[35] The authors managed to isolate the ethyl-zinc complex (**21**), although they were unable to isolate an alkoxide analogue. Nonetheless, complex (**21**) demonstrated catalytic competence for lactide polymerization at 80 ºC in toluene solvent. A relatively high catalyst loading (1.67 mol%) and six hours was required to achieve 92% *rac*-lactide conversion.

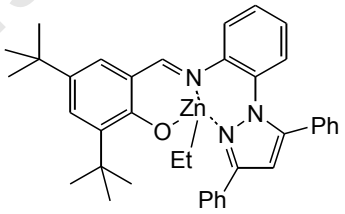

(**21**)

The resulting polymer had an extremely narrow molecular weight distribution (PDI = 1.03). The monodispersed polymers have been attributed to the influence of the bulky tertiary-butyl and phenyl substituents that are in close proximity to the ethyl-initiating group.

This section has highlighted characteristics which are required in a good catalyst. The next section goes on to discuss methods which have been investigated for functionalization of PLA in order to produce polymers with novel applications.

1.1.4 Developments of polylactide materials for delivery applications

Various species have been incorporated on the PLA-backbone and the materials have been used in the controlled release of drug molecules[36] or agrochemicals.[37] The most common method involves the use of a catalyst, commonly stannous octanoate or an aluminium complex, together with a substrate of choice as a polymerization initiator or terminator.[38] The chain-initiating substrates usually contain a hydroxyl group which is responsible for the process. On the other hand, the chain-terminating substrates usually contain an acid chloride group, which reacts with the metal-alkoxide at one end of the polymer, subsequently forming a polymer terminated with an ester-group.

Tong and Cheng reported the first PLA covalently bound with a drug molecule by incorporating a cancer drug, doxorubicin (Doxo), on a polymer backbone.[36] The conjugate material displayed well-controlled drug release without any noticeable burst release of the drug. The fluorophore, difluoroboron dibenzoylmethane, has also been incorporated on the PLA-backbone, using a similar method. The resulting functionalized polymer was employed for *in situ* live cell imaging. The authors demonstrated that the uptake of the polymeric material into the Hela cells was through endocytosis.[39]

The physical composite between PLA and another suitable substrate have been prepared by melt process. Polylactide and another componennt are mixed together and melted, the mixture is then allowed to solidify forming a polymeric matrix in the form of granules or films which are applied as drug delivery materials.[40] The third method, on the other hand, involves the use of modified lactide monomers which contain various functionalizable groups, such as an alkyne which is functionalized through a click chemistry method by a reaction with molecules containing an azide-group. Yang *et al*. prepared a series of hemilactide substrates containing functionalizable groups and tested them for ring opening polymerization with a catalyst (see **Figure 1.1.3**).[41]

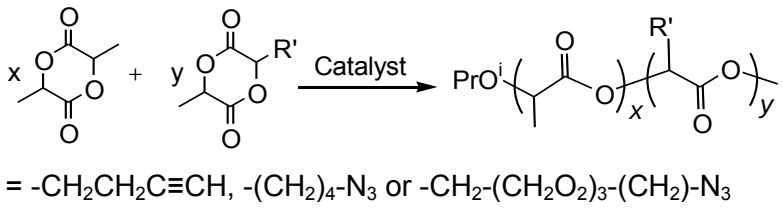

FIGURE 1.1.3: Polylactide co-polymer starting from lactide and lactide derivative monomer with R' -functionalizable group.[41]

PLA-block copolymers have also been reported as stable polymers for potential packaging applications.[42] These types of polymers were prepared by firstly producing PLA and instead of terminating the polymerization process with an alcohol, a second monomer was added to the polymer solution and the polymerization reaction was continued. Examples of such polymers are poly(lactic-*co*-glycolic)acid (PLA/PGA),[43] poly(lactide-*co*-ethylene oxide) (PLA/PEG) [44,45] and poly(styrene-*co*-lactide) copolymers (PS/PLA)[46] (**Figure 1.1.4**). All the copolymers displayed an increased stability compared to the pure polylactide. On the other hand, PLA/PGA and PLA/PEG displayed remarkable water solubility.

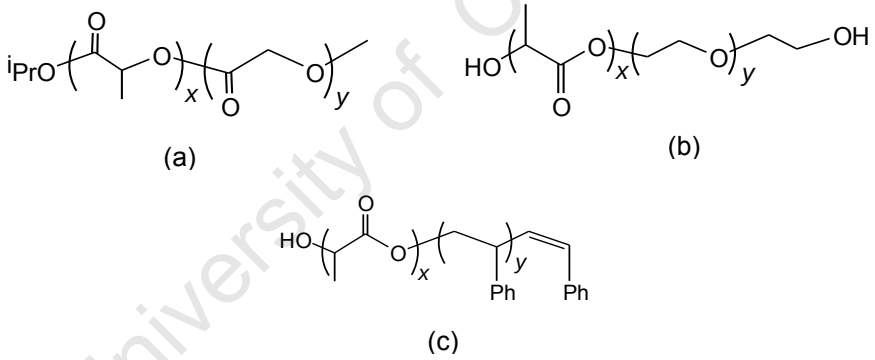

FIGURE 1.1.4: Polylactide block copolymers: (a) (PLA/PGA),[43] (b) (PLA/PEG)[45] and (c) (PLA/PS).[46]

Once functionalization of the polymers is completed, the process can then be followed by the design and production of advanced architectural structures. These include, stars, brushes, cyclics[47] microspheres,[47,48] hydrogels, microspheres, networks, nanoparticles[43] and cross-linked materials, which can then be used for various medical applications.[47] There is continuous research activity worldwide devoted to the production of new materials for drug delivery purposes.[47]

The use of erodible polymer vehicles for controlled drug delivery carriers dates back to the early 1970s.[49] Such carriers have been found to be advantageous in improving

the therapeutic effect, prolonging the biological activity, and controlling the drug release rate, thus decreasing the administration frequency. The advantage of controlled drug delivery vehicles is revealed in **Figure 1.1.5**.[43,50] There is a minimum amount of drug molecule which is required for treatment. When too much of a drug molecule is used an overdose can be reached which is a toxic level and can lead to side effects. An ideal administration of the drug requires that a drug be available in the system in acceptable levels and can only be excreted out of the body when the disease is cured. This phenomenon is regarded as controlled drug-release. When a drug is administered through an intravenous method, too much of a drug may be injected initially, reaching a toxic level, and it is also flushed out of the body with time before completely killing the disease cells. Administration of the drug in a tablet form also suffers from the drug availability problem. Drug molecules which are functionalized on various delivery vehicles have an added advantage since the size of drug molecules can be tuned to the nano-sized level, further improving the activity of the drug.

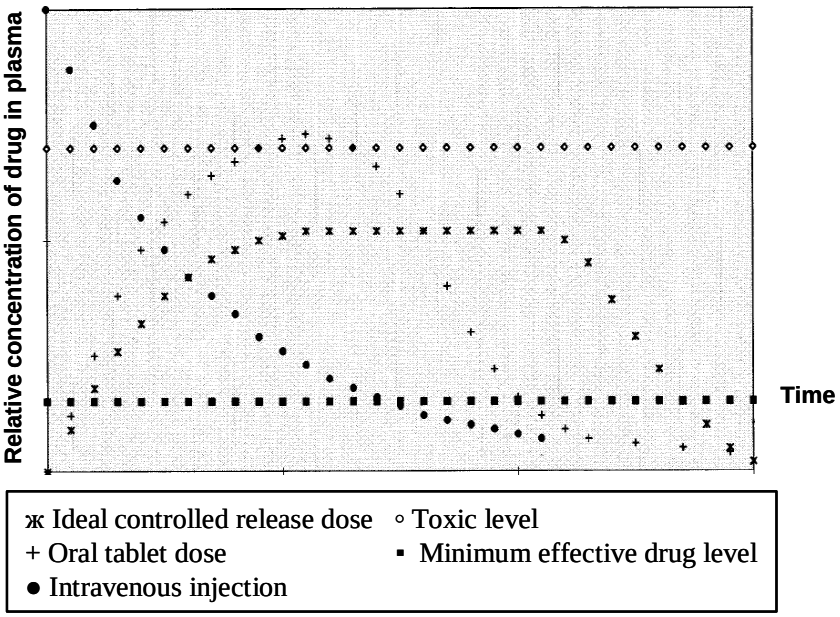

FIGURE 1.1.5: Illustration of plasma-drug concentration profiles for various methods of administration.[43,50]

Polyesters are the most studied polymers that have been used in various preclinical or clinical studies.[36] Several systems based on PLAs have been investigated for the long-term delivery of antimalarial drugs,[51] contraceptives[52] and eye healing drugs.[53] There has also been a consideration of intra-arterial embolization of unresectable primary

hepatocellular carcinoma and hepatic metastases with radioactive biodegradable microspheres for an effective treatment.[54] Holmium-labelled PLLA-microspheres have especially been developed for radioembolisation of liver malignancies.[55] In addition, microspheres have also been used for radioembolization of unresectable head and neck cancers.[56]

Noticeable successes exist for some materials which have been approved for clinical cancer therapy.[57] Lupron Depot is an example of a commercially successful injection-administered drug delivery system intended for endometriosis and prostate cancer therapy.[58,59] This system is composed of microspheres of PLGA copolymer containing leuprorelin acetate (LH-RH agonist and an anticancer drug).[58,59]

This part of the review has highlighted the intense research and development studies that have been undertaken with regards to the production of functionalized PLAs. Undoubtedly, polymers with unique properties are yet to be discovered. The research on the design and synthesis of zinc-containing catalysts for ring opening polymerization of lactide is of importance, especially in the production of polymers for medical and agricultural applications.

Factors such as the depletion of petrochemical feedstocks, environmental pollution caused by petrochemical polymers, and their production processes, are forcing authorities to consider the use of alternative products. Hence, the future of degradable PLA-copolymers is promising due to their less harmful nature to the environment and the fact that part of the resulting polymeric material is derived from renewable feedstocks.

As opposed to polystyrene, polyketones which are produced from copolymerization of styrene and carbon monoxide have been reported to be photodegradable. The second part of this review, **Section 1.2**, illustrates the progress made in the production of carbon monoxide/styrene copolymers. This section will provide the background to the production of PLA-*co*-CO/styrene copolymers. The ultimate goal of the research of this thesis is to make other types of degradable polymers.

1.2 Carbon Monoxide/Styrene Copolymerization

The alternating copolymerization reaction between carbon monoxide and olefins is metal-catalysed and usually performed in different phase systems. Catalysts containing palladium(II) metal ions are mostly employed for the process.[60] Polyketone products obtained through alternating copolymerization of carbon monoxide and one or more olefinic-unsaturated monomer represents a class of low-cost innovative thermoplastic. The properties and applications of these polymers is still the subject of intense fundamental research.[60] The properties of the resulting polymers can be finely tuned by an appropriate choice of a catalyst and an olefinic co-monomer. Cationic complexes of the type [PdMe(N^N')(L)]X, or dicationic complexes $[Pd(N^N')(L)_2]X_2$ (where N^N' = bidendate and L = monodentate donor ligand, and X is an anion with low coordination ability), are mostly utilized as the catalyst precursors. This review focuses on the monocationic Pd(II) complexes stabilized with N-N donor ligands. Dicationic Pd(II) complexes are not discussed here as they are outside the scope of the current study.

Various olefinic-unsaturated monomers such as ethene, propene, norbornene, styrene, methylacrylate have been successfully incorporated in the production of polyketones. In this thesis, however, only studies utilizing styrene and as co-monomer will be discussed. The first CO/olefin copolymerization reaction was reported in 1941 by Farbenfabriken Bayer,[61] where they produced a CO/ethylene copolymer. Since then, synthetic procedures for the production of polyketones have experienced constant improvement in terms of selectivity, productivity, environmental impact and economy.[62] The industrial production of CO/olefin copolymers is a reality and at least two products are already on the market, i.e. Carilon® from Shell[63] and Ketonex® from BP.[64] Companies such as BASF and EniChem have also filed an impressive number of patents covering different types of polyketones.[60c]

Applications of polyketones range from the production of objects to fibers, and include film coatings, adhesives, membranes, photoresists, and packaging materials. The continuous discovery of new structures forecasts a wealth of new applications though there are challenges in making these polymers in large scale. From the recyclability point of view, polyketones are photochemically degradable as they

contain a carbonyl group chromophore. Absorption of ultraviolet radiation leads to degradation by the Norrish Type I and II processes (**Scheme 1.2.1**),[65] all of which are typical photoreactions of the carbonyl chromophore. Once radicals are introduced into the system, chain degradation can occur by the auto oxidation mechanism (see **Scheme 1.2.2**).[65]

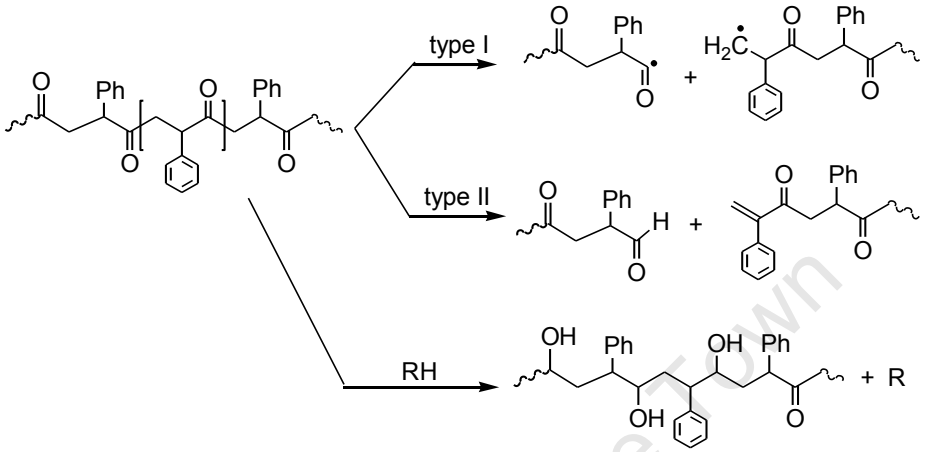

SCHEME 1.2.1: Photochemical degradation pathways for polymers containing carbonyl groups.[65]

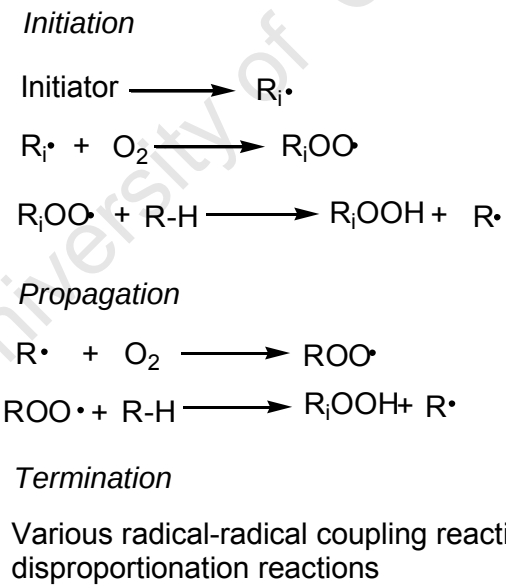

SCHEME 1.2.2: The auto oxidation mechanism for hydrocarbon materials.[65]

A particular hindrance to the ready commercialization of these thermoplastics, especially CO/styrene copolymers, results from their low stability. In particular, when exposed to high temperatures for extended periods or subjected to repeated cycles of melting and solidification they decompose. The propensity of metallic palladium to

plate out of the solution during both catalyst preparation and copolymer work-up is also a challenge. A wide range of improvements in both catalyst and material stability, as well as catalytic productivity, has been achieved; this is evidenced by continuous publications and patents dealing with olefins/CO copolymerization reactions over the last decade.[60]

1.2.1 CO/styrene copolymerization

Copolymerization of styrene or styrene-derivatives with CO requires the use of cationic palladium(II) catalysts containing N-N chelating ligands.[60] These catalyst systems containing nitrogen bidentate ligands generally produce CO/styrene copolymers with moderate to high molecular weight (4 - 10 x 10^3 g/mol). On the other hand, lower molecular weight oligomers are obtained when palladium catalysts stabilized with chelating phosphine ligands are utilized.[66] It is believed that the termination through β-H elimination prevails over polymer-propagation due to the higher electron density on the palladium centre in phosphine-modified catalysts when compared to nitrogen modified catalysts.[60d] It has also been suggested that the bis(diphenylphosphine)Pd-styryl intermediates formed during the initial steps in CO/styrene copolymerization are strongly stabilized by π-benzylic coordination inhibiting the CO insertion. The termination process then becomes favoured and subsequently oligoketones instead of polyketones are formed.[67] In addition, hydrogen gas has also been found to be a powerful polymerization inhibitor, leading to the formation of aldehydes and/or ketones, and the presence of H_2 has to be entirely eliminated.[68]

Copolymers of the general formula $[CH(Ar)CH_2CO]_n$ show regio- and stereoisomerism due to the presence of truly stereogenic centres in the polymer backbone.[69] Depending on the regioselectivity of the monomer insertion, primary (1,2-mode) or secondary (2,1-mode) arrangements, form three different polymer units: head-to-tail, head-to-head and tail-to-tail (see **Figure 1.2.1**). Styrene insertion into a Pd-acyl intermediate, however, has been found to occur exclusively in the 2,1-fashion. The occurrence of the same insertion mode during the chain growth leads only to head-to-tail units.

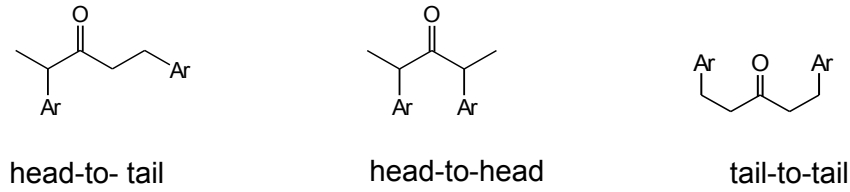

FIGURE 1.2.1: Regioselectivity of propagation during CO/styrene copolymerization.

Moreover, the sequence of the absolute configuration of the stereogenic centres in the backbone can control the formation of atactic, stereoregular, syndiotactic (SRSRSR-sequence) or isotactic (RRRRRR- or SSSSSS-sequence) copolymers (**Figure 1.2.2**).

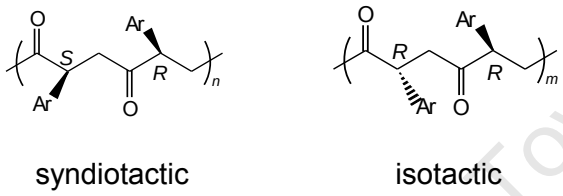

FIGURE 1.2.2: Syndiotactic and isotactic copolymers in CO/styrene copolymerization.

Syndiotactic and isotactic alternating copolymers are characterized by very small or high optical activities, respectively. The control of regio- and enantio-selectivities of styrene insertion, ultimately leading to stereoregular polyketones, can be achieved through a choice of a suitable bidentate chiral or achiral ligand. In general, copolymerization promoted by catalytic systems containing achiral ligands produces materials which show both head-to-tail regioselectivity and syndiotactic stereoselectivity.[60]

Techniques used to analyse polymers are ^{1}H- and ^{13}C-NMR spectroscopy and X-ray diffraction techniques. The head-to-tail selectivity (> 90%) is a consequence of the occurrence of consecutive secondary (2,1-mode) migratory insertions of styrene into a palladium-acyl intermediate during the chain growth,[60d] while the stereoselectivity is due to the chain end-controlled enantioface selection. The enatioface of the incoming styrene, which inserts almost exclusively in the 2,1-mode, is determined by the chirallity of the previously incorporated styrene.[60,62b] Extensive studies have been conducted on catalysts stabilized with various nitrogen donor ligands. Some of the ligands have shown improved productivity.[60]

1.2.2 Palladium catalysts stabilized by (N^N) ligands

The perfectly alternating copolymerization of CO with styrene or *p*-alkyl-styrene to give syndiotactic polyketones has been produced by the utilization of simple catalytic systems composed of chelating nitrogen bidentate ligands, i.e. bipyridine or phenanthroline, coordinated to palladium(II)acetate or trifluoroacetate. Initial reactions have been carried out in methanol as a solvent, a palladium catalyst, excess strong oxidants, such as 1,4-benzoquinone (BQ) and a suitable Brønsted acid e.g. triflic or tosyl acid, as cocatalyst. Using these conditions the active species Pd(N^N)triflate or tosylate are produced *in situ*. When the oxidant is omitted in the polymerization solution it has been found that polymer production is drastically reduced.[60,70]

Most catalysts suffered from decomposition when polymerization was performed in methanol as a solvent; however, it was later discovered when 2,2,2-trifluoroethanol (TFE) was used as a solvent or as a co-solvent the polymerization process improved and higher molecular weight copolymers were obtained. The polymer productivities were even higher than in the absence of the oxidant.[71] In particular, the softer oxygen-donor in TFE, which allowed for a *soft-acid-soft-base* match as compared to a harder oxygen-donor-stabilized Pd-alkoxy intermediate, avoided chain termination through alcoholysis. However, irrespective of the catalytic system, the catalytic activity of the catalysts has always been < 500 g (g Pd)$^{-1}$, while polymer molecular weights were not high enough to obtain materials with useful properties.[72]

The effect of various counter-anions on the performance of cationic catalysts with the general formula $[Pd(bipy)(\eta^1,\eta^2\text{-}C_8H_{12}OMe)]^+X^-$ (X^- = BPh_4, OTf, BF_4, PF_6, SbF_6, $B[3,5\text{-}(CF_3)_2C_6H_3]_4$ or BAr_4; ($C_8H_{12}OMe$ = methoxycyclooctenyl) for copolymerization has been studied in dichloromethane under mild conditions (at room temperature and 1 bar CO). The catalytic activity for the palladium compounds with the following anions have been observed: X^- = BPh_4 <<OTf <BF_4 <PF_6 < SbF_6< $B(3,5\text{-}(CF_3)_2C_6H_3)_4$. The influence of the anion has been related to the different strength of interionic interactions, i.e., an increase in the effectiveness of interionic interactions resulted in the decrease in productivity of polymers.[73] A similar order has been observed for most of the catalyst systems which are discussed below.

Syndiotactic copolymers have been obtained under mild conditions (25 ^{0}C, 1 bar CO) when using catalyst precursors (**22**), (**23**) and (**24**) containing unsymmetrical pyrazolyl chelating ligands. The variation in C_s-symmetry of the ligands did not affect the stereochemistry of the polymer, which was controlled by the main chain-end process. These catalyst systems produced polymers with a molecular weight of 20 – 70 kg mol^{-1} and with well-controlled polymerization (PDI = 1.1 – 1.3).[74]

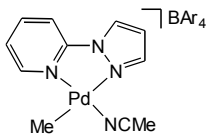

(**22**)

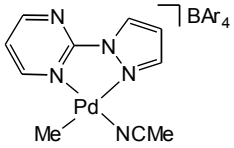

(**23**)

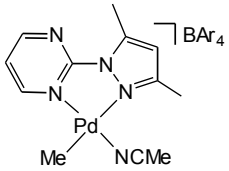

(**24**)

Various catalysts stabilized with chiral-ligands have been investigated for the production of stereo-controlled polyketones. These types of catalysts have been found to switch the chain-end control to enantiomorphic site control yielding regio-regular isotactic polyketones. The enantioface of the incoming styrene is controlled by the chiral ligand and not by the chain-end.

The first example of enantioselective copolymerization of styrene with CO was reported by Brookhart utilizing a cationic palladium catalyst (**25**) modified with an enantiomerically pure C_2-symmetric bisoxazoline ligand.[75] A reaction between *p-tert*-butylstyrene (TBS) with carbon monoxide (1 bar) under solvent free conditions at room temperature displayed a catalytic activity of 2.5 g (g Pd x h)$^{-1}$. The polymers produced had M_n = 26 kg mol^{-1} with PDI = 1.4 and were demonstrated by both isotactic microstructure and high optical activity. The presence of the methyl substituents in 3,5-positions of the oxazoline rings strongly controlled the orientation of the incoming styrene around the metal centre during the propagation process. On the other hand, the palladium catalyst (**26**) modified with pyridine-oxazoline ligands yielded polymers which were largely syndiotactic.[75] Therefore, the electronic properties of the ligands, together with chiral substituents, contributed to the tacticity of the resulting polymers.

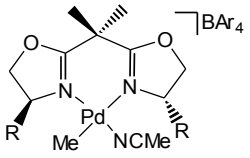

(**25**), R = $CHMe_2$ or Me

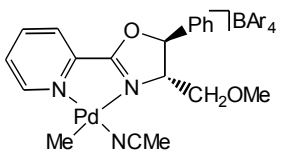

(**26**)

Reaction of another type of bisoxazoline complex (**27**) produced isotactic copolymers of CO/styrene or 4-methylstyrene.[76] The bisoxazoline ligand contained isopropyl groups at the 2,2'-positions that were closer to the catalytic site. The reactions were carried out employing a monomer itself as a solvent under 1 – 4 bar of CO pressure at room temperature. These reactions yielded the corresponding copolymers and a catalytic activity of 0.3 g CP (g Pd)$^{-1}$ h^{-1} has been observed. The lower activity has been attributed to the weak coordination ability of the bisoxazoline ligand which ultimately led to an unstable catalyst system under copolymerization conditions.

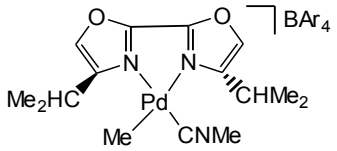

(**27**)

Complex (**28**) on the other hand, stabilized by an imine ligand containing bulky isopropyl substituents, produced syndiotactic copolymers of styrene or *p*-methylstyrene with CO under mild reaction conditions.[77] The difference in tacticity of polymers produced by compound (**28**) compared to those produced with compound (**27**) is presumably due to the electronic properties and geometry of the ligands.

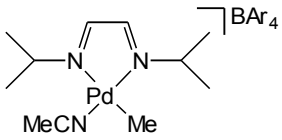

(**28**)

Palladium complexes (**29**) and (**30**), modified respectively with chiral diketimine or dialdimine with the formula [PdMe(N^N)(L)]$BAr_{4,}$ have been tested as catalyst precursors in the alternating copolymerization of tertiarybutylstyrene (TBS) and carbon monoxide in dichloromethane at ambient conditions.[78] The chirality of the complexes is based on the rotation of the dibenzyl rings due to the bulky substituents, which prefer to be as far from each other as possible.

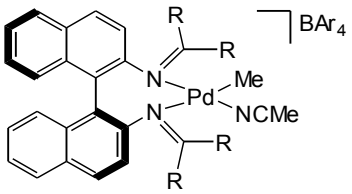

a, R = Ph

b, R + R = 2,2'-$(C_6H_4)_2$

c, R = *p*-$MeOC_6H_4$

d, R = *p*-ClC_6H_4

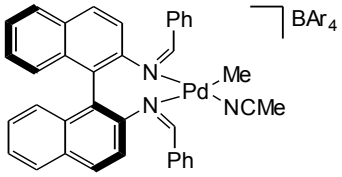

(**29**) (**30**)

The TBS/CO copolymers obtained with these catalysts under 1 bar CO pressure at room temperature, showed average molecular weights in the range from 40 to 50 kg mol^{-1} with a PDI = 1.2 and isotacticity > 97%. Interestingly, the diketimine complex (**29b**) and the dialdimine compound (**30**) were inactive. The inactivity of complex (**29b**) could be explained by the bulky fluorinyl groups, which hinder coordination of the monomers to the metal centre, while the electron deficient ligand in complex (**30**) stabilized the complex making it unreactive. Diketimine complexes (**29a**), (**30c**) and (**30d**), however, produced polyketones with activities of 4, 3 and 8 g CP (g Pd)$^{-1}$ h^{-1}, respectively. Optimised conditions improved the activity to 21 g CP (g Pd)$^{-1}$ h^{-1}.

D'Amora *et al.* investigated the influence of various substituents on the bipyridyl ligands attached to the palladium complexes on the formation of polyketones or oligoketones.[79] When the complexes were utilized as catalyst precursors, the authors found that at a CO pressure of 5 bar, the amount of polyketones produced was always more than that of oligoketones. The activity of the catalysts for the conversion of styrene decreased as follows (**31**)>(**32**)>(**33**)>(**34**). On the other hand, complex (**31**) only produced polyketones at CO pressures of 1 bar, and even at higher pressures up to 6 bar, the amount of polyketones dominated that of oligoketones. In addition, increasing the amount of BQ with respect to catalyst resulted in an increase in both the activity and polymer yields.

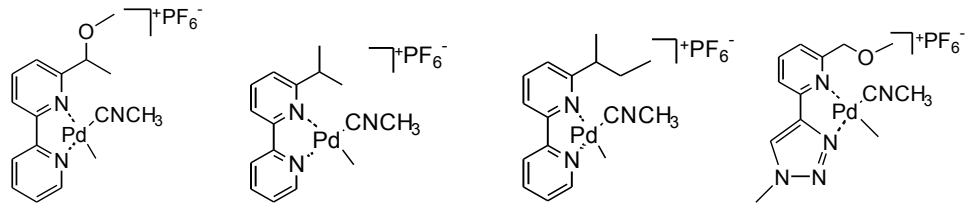

(**31**) (**32**) (**33**) (**34**)

Similar palladium catalysts (**35a, b and c**), stabilized with bipyridinyl derivatives, produced well-controlled CO/*p*-*tert*-butylstyrene copolymers (PDI = 1.6).[80] Catalyst

activities for compounds **35a, b** and **c** were 3.85, 1.85, and 1.68 x 10^4 gCP (g Pd)$^{-1}$ h^{-1}, when the polymerization reaction was performed in the range 0 – 25 ºC and 1 bar CO pressure for 24 h.

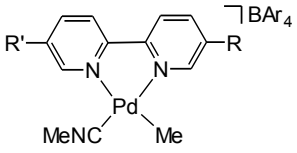

(**35**)

a, R = R' = H

b, R = H, R' = Me

c, R = R' = Me

1.2.3 Palladium catalysts stabilized by (P^N) ligands

The influence of the counterion on the cationic Pd(II) complexes can be realized in the complexes containing phosphorus donor atoms. It has been found that complexes stabilized by triflate (OTf^-) anions were more active than those containing the (BAr_4^-) anion. However, higher CO pressures were required for the production of polyketones as compared to when N^N stabilized complexes were employed. In addition, most complexes stabilized by P^N ligands are dicationic, so are not discussed here.

The palladium system (**36**), containing a phosphanyl-dihydrooxazole ligand, is so far the only reported catalyst stabilized with a P^N ligand to be active for CO/styrene copolymerization.[81] Polymer productivity of 975 g CP (g Pd)$^{-1}$ h^{-1} with molecular weight of 7.5 x 10^3 g/mol was obtained when a CO pressure of 320 bar was employed.

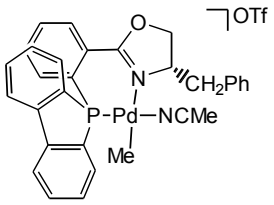

(**36**)

1.2.4 Mechanism of CO/styrene copolymerization

Simple cationic complexes with N^N chelating ligands [PdMe(NCMe)(N^N)]$^+$X$^-$ have been used to investigate the mechanism involved in the CO/styrene copolymerization process. The styrene derivatives, *p-tert*butylstyrene (TBS), or *p*-methylstyrene, were used as model reactants to study the reaction. Copolymerization

reactions using these monomers were found to be slow, making it possible to study the intermediates formed. NMR spectroscopy was used to analyze the intermediates and polymerization products *in situ*, while MALDI-TOF was used for end-group analysis of the polymeric materials.[60]

A possible mechanism that has been reported consists of two cycles, 1 and 2, each composed of three steps (A, B and C in cycle one and D, E and F in cycle two); see **Scheme 1.2.3**.[60,62a,81,82] Polymerization initiation takes place in steps A and D. Carbon monoxide firstly displaces a weakly coordinated solvent molecule, then it inserts between the Pd-methyl or Pd-alkoxide bond to form a Pd-acyl (i) or Pd-acetate (vi) intermediate, respectively. Propagation steps B and E involve coordination of the styrene followed by migratory insertion of styrene monomer (in this case a 1,2-mode of insertion takes place) followed by another CO insertion on the resulting η^3-π-benzyl intermediate (ii) or (iii). Subsequently, alternating CO/styrene insertion reactions take place repeatedly to form a growing polymer chain. Finally, termination steps C and F both consist of a fast β-hydride elimination of the last inserted styrene unit to form polymers (iv) and (viii), terminated by an inner alkenyl group. In the presence of an oxidant, such as benzoquione, any formed molecular Pd(0) due to reduction of unstable Pd(II)-H (v) is re-oxidized before it can form an inactive metallic Pd/Pd-black decomposition product.

Palladium catalysts are well known to be active in C-C bond formation.[83] The possible formation of a Pd-benzyl species during the copolymerization process was a motivating factor to investigate the possibility of coupling this alkenyl end of a CO/styrene copolymer with polylactide. The results for this investigation will be further discussed in Chapter 5.

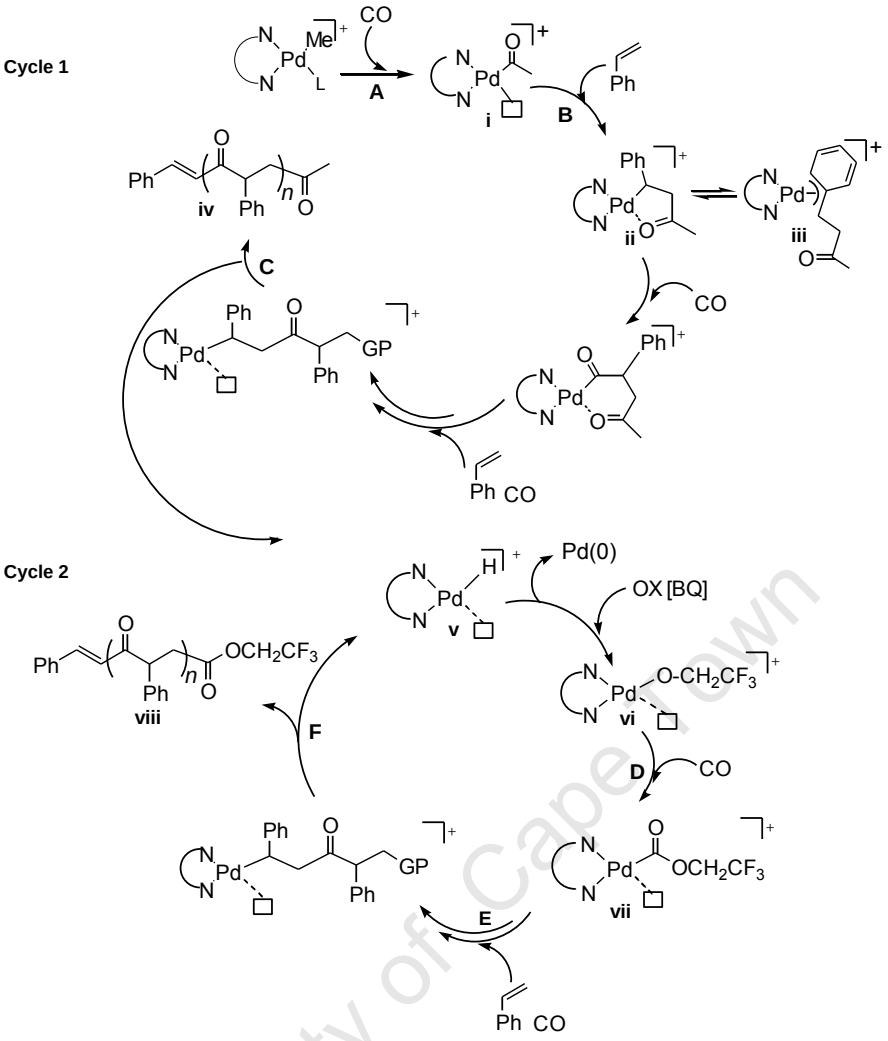

SCHEME 1.2.3: Proposed mechanism of CO/olefin copolymerization catalysed by N^N palladium(II) precursors in trifluoroethanol as a solvent (GP = Growing Polymer).[60,62a,81,82]

1.3 Aims and objectives

Catalyst systems that are active for polylactide production and the different methods that have been used for polylactide functionalization, as well as the applications of the resulting polymers, especially in drug delivery systems, have been described in **Section 1.1.** The survey suggested the starting point for the research for this thesis. This project, consisting of two different parts, aimed at producing different forms of functionalized PLAs using new catalytic methods. The aim of the first part of this research was as follows:

- To synthesize and characterize new homoleptic zinc catalysts of the type $Zn(N\text{^}O)_2$ [(**39**) and (**40**)], and of the type $Zn(N\text{^}S)_2$ [(**45**) – (**48**)], where $(N\text{^}O^-)$ and $(N\text{^}S^-)$ are drug candidate ligands (see **Table 1.3.1**).
- To investigate these complexes for lactide polymerization. The main goal was to investigate if drug candidates which were initially bonded to the zinc ion could act as chain initiators for lactide polymerization, thereby ultimately producing polylactides functionalized with the drug candidates. The polymers produced could be expected to be biodegradable and might be suitable for use in drug delivery.

TABLE 1.3.1: Zinc complexes synthesized

$Zn(N\text{^}O)_2$	$Zn(N\text{^}S)_2$
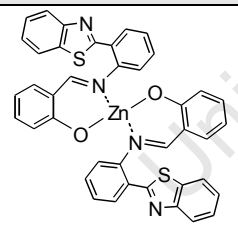 (**39**)	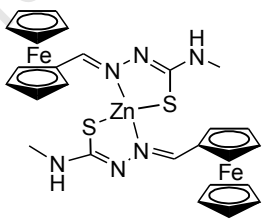 (**45**) 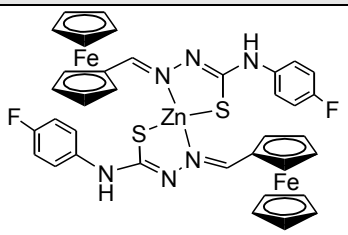 (**46**)
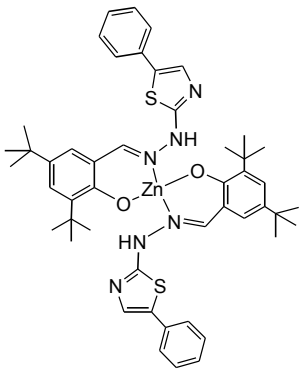 (**40**)	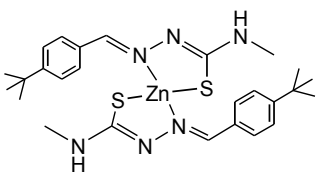 (**47**) 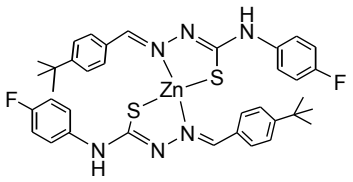 (**48**)

It was described in **Section 1.1.4** that polystyrene is a non-degradable polymer that has been successfully incorporated on a polylactide tail to form block-copolymers with improved glass transition (T_g) and thermal stability. Moreover, the resulting polymers were partially degradable. Various catalyst systems and reaction conditions utilized for CO/styrene polymerization were also discussed in **Section 1.2,** providing motivation from the progress made in the production of stable polymers for the second part of this thesis. The objectives in this part of the research, therefore, were as follows:

- To synthesize and characterize new palladium complexes of the type [PdMe(N^N)(L)]X, L = MeCN or PPh_3, X = BF_4^- or PF_6^-(**55**) – (**58**), (see **Table 1.3.2**).

TABLE 1.3.2: Palladium complexes synthesized

Pd(N^N) complexes

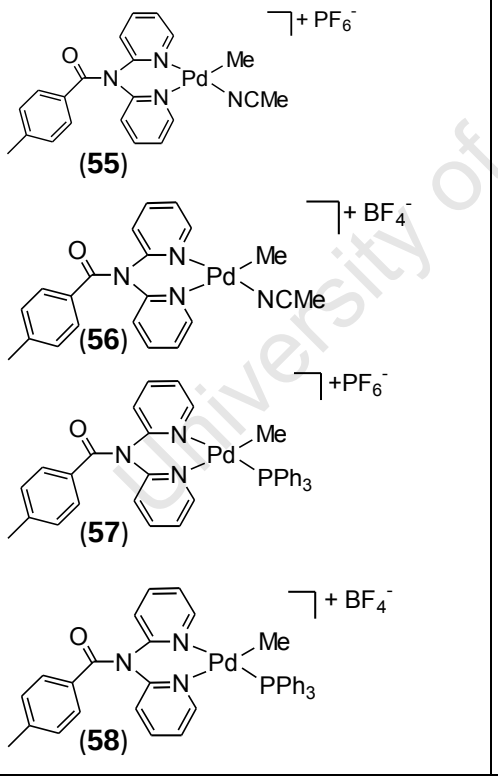

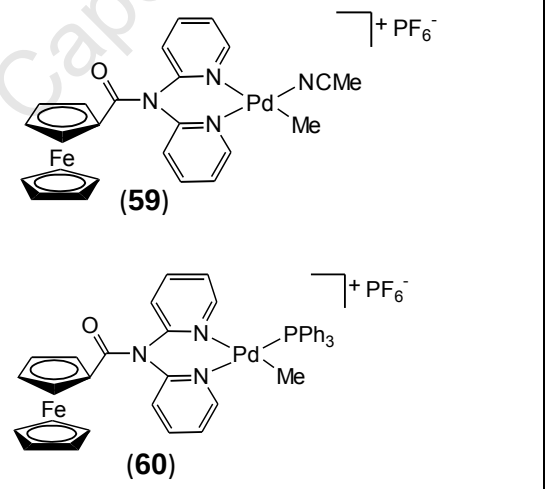

- To investigate these complexes as catalysts for CO/styrene copolymerization.
- To synthesize and characterize the new palladium complexes [PdMe{Fc(N^N)}(L)]PF_6, L = MeCN (**59**) and L = PPh_3 (**60**) (see **Table 1.3.2**), which contain the ferrocenyl group in the ligand scaffold.

- Complexes (**59**) and (**60**) would be prepared in order to investigate the influence of changing the oxidation state of the ferrocenyl group and changing the donor ligands, i.e. MeCN and PPh_3, on the activity of the resulting complexes towards the CO/styrene copolymerization reaction.
- To investigate a new method to synthesize poly(LA-*co*-CO/styrene) block copolymer. In view of Green Chemistry principles, it is believed that the resulting block copolymer will be environmentally friendly since the CO/styrene copolymer is photodegradable in contrast to the more stable polystyrene.

1.4 References

1. (a) M. Lancaster, *Green Chemistry: An Introductory Text*, Royal Society of Chemistry, Great Britain, 2002, p 5. (b) J. Clark and D. Macquarrie, *Handbook of Green Chemistry and Technology*, Blackwell Science Ltd, Great Britain, 2002, pp 3 – 9.
2. M. Biron, in *Thermosets and Composites: Technical Information for Plastic User*s, Elsevier Ltd., 1st ed., 2003, Chapter 2, p. 32.
3. R. E. Drumright, P. R. Gruber and D. E. Henton, *Adv. Mater*., 2000, **12**, 1841.
4. A. Södergård and M. Stolt, *Prog. Polym. Sci*., 2002, **27**, 1123.
5. W. H. Carruthers, G. L. Dorough and F. J. van Natta, *J. Am. Chem. Soc.*, 1932, 761.
6. Y. Ikada and H. Tsuji, *Macromol. Rapid Commun*., 2000, **21**, 117.
7. C. A. Wheaton, P. G. Hayes and B. J. Ireland, *Dalton Trans*., 2009, 4832.
8. A. N. Vaidya, R. A. Pandey, S. Mudliar, M. S. Kumar, T. Chakrabarti and S. Devotta, *Crit. Rev. Environ. Sci. Technol*., 2005, **35**, 429.
9. P. R. Gruber, E. S. Hall, J. J. Kolstad, M. L. Iwen, R. D. Benson and R. L. Borchardt, *US Pat*., 5484 881, 1996.
10. D. Brizzolara, H. J. Cantow, K. Diederichs, E. Keller and A. J. Domb, *Macromolecules*, 1996, **29**, 191.
11. R. H. Platel, L. M. Hodgson and C. K. Williams, *Polym. Rev.*, 2008, **48**, 11.
12. J. Wu, T-L. Yu, C-T. Chen, C-C. Lin, *Coord. Chem. Rev.*, 2006, **250**, 602.

13. (a) P. Dubois, C. Jacobs, R. Jérôme and P. Teyssié, *Macromolecules*, 1991, **24**, 2266; (b) H. R. Kricheldorf, M. Berl and N. Scharnagl, *Macromolecules*, 1988, **21**, 286 ; (c) J. L. Eguiburu, M. J. Fernandez-Berridi, F. P. Cossío and J. San Román, *Macromolecules*, 1999, **32**, 8252 ; (d) A. Kowalski, A. Duda and S. Penczek, *Macromolecules*, 2000, **33**, 7359 ; (e) E. L. Marshall, V. C. Gibson and H. S. Rzepa, *J. Am. Chem. Soc*., 2005, **127**, 6048; (f) M. Ryner, K. Stridsberg, A. C. Albertson, H. von Schenck and M. Svensson, *Macromolecules*, 2001, **34**, 3877.
14. A. Duda, S. Penczek, *Polymers from Renewable Resources; Biopolymers and Biocatalysis*; C. Scholz, R. A. Gross, Eds, ACS Symposium Series, Oxford University Press USA, Washington DC, 2000, Vol. 764, pp. 160-199.
15. M. H. Chisholm, N. J. Patmore and Z. Zhou, *Chem. Commun*., 2005, 127.
16. M. D. Jones, M. G. Davidson, C. G. Keir, L. M. Hughes, M. F. Mahom and D. C. Apperley, *Eur. J. Inorg. Chem*., 2009, 635.
17. (a) L. M. Alcazar-Roman, B. J. O'Keefe, M. A. Hillmyer and W. B. Tolman, *Dalton Trans*., 2003, 3082; (b) J. Lewinski, P. Horeglad, E. Tratkiewicz, W. Grzenda, J. Lipkpwski and E. Kolodziejczyk, *Macromol. Rapid Commun*., 2004, **25**, 1939.
18. J. Lewinski, P. Horeglad, K. Wojcik and Justyniak, *Organometallics*, 2005, **24**, 4588.
19. (a) J. Coundane, C. Usttariz-Peyret, G. Schwach and M. Vert, *J. Polym. Sci. Polym. Chem*., 1997, **35**, 1651; (b) H. R. Kricheldorf, C. Boetttcher and K. U. Tonnes, *Polymer*, 1992, **33**, 2817; (c) B. M. Chamberlain, M. Cheng, D. R. Moore, T. M. Ovitt, E. B. Lobkovsky and G. W. Coates, *J. Am. Chem. Soc*., 2001, **123**, 3229.
20. (a) H. R. Kricheldorf, J. M. Jonté and M. Berl, *Macromol. Chem. Phys. Suppl*., 1985, 25; (b) O. Dechy-Cabaret, B. Martin-Vaca and D. Bourissou, *Chem. Rev*., 2004, **104**, 6147.
21. P. Dubois, N. Ropson and R. Jerome, P. Teyessie, *Macromolecules*, 1996. **29**, 1965; (b) J. Libszowski, A. Kowalski, A. Duda and S. Penczek, Macromol. *Chem. Phys*., 2002, **203**, 1694; (c) H. R. Kricheldorf, I. Kreiser-Saunders and A. Stricker, *Macromolecules*, 2000, **33**, 702.

22. (a) M. Cheng, A. B. Attygalle, E.B. Lobkovsky, E. B. Coates, *J. Am. Chem. Soc. 1999,* **121**, 11583; (b) A. P. Dove, V. C. Gibson, E. L. White, A. J. P. White and D. J. Williams, *Dalton Trans*., 2004, 570.
23. M. H. Chisholm, N. W. Eilerts, J. C. Huffman, S. S. Iyer, M. Pacold and K. Phomphrai, *J. Am. Chem. Soc*., 2000, **122**, 11845.
24. C. K. Williams, N. R. Brooks, M. A. Hillmeyer and W. B. Tolman, *Chem. Commun*., 2002, 2132.
25. H. Y. Chen, H. Y. Tang and C. C. Lin, *Macromolecules*, 2006, **39**, 3745.
26. L. E. Breyfogle, C. K. Williams, V. G. Young, M. A. Hillmyer and W. B. Tolman, *Dalton Trans*., 2006, 928.
27. J. Ejfler, M. Kobylka, L. B. Jerzykiewicz and P. Sobota, *Dalton Trans*., 2005, 2047.
28. B. Lian, C. M. Thomas, O. L. Casagrande Jr., C. W. Lehmann, T. Roisnel and J. F. Carpentier, *Inorg. Chem.*, 2007, **46**, 328.
29. C. K. Williams, L. E. Breyfogle, S. K. Choi, W. W. Nam, V. G. Young, Jr., M. A. Hillmyer and W. B. Tolman, *J. Am. Chem. Soc*., 2003, **123**, 3229.
30. F. A. Cotton, E. Wilkinson, C. A. Murrillo, M. Bochmann, *Advanced Inorganic Chemistry*, 6th ed., John Wiley and Sons, New York, 1999, p. 1302.
31. M. H. Chisholm, J. C. Gallucci, H. S. Zhen, *Inorg. Chem*., 2001, **40**, 5051.
32. C. K. Williams, L. E. Breyfogle, S. K. Choi, W. Nam, V. G. Young Jr., M. A. Hillmyer and W. B. Tolman, *J. Am. Chem. Soc*., 2003, **125**, 11350.
33. J. Wu, B. H. Huang, M. L. Hsueh, S. L. Lai, C.-C. Lin, *Polymer*, 2005, **46**, 9784.
34. J. Ejfler, S. Szafert, K. Mierzwicki, L. B. Jerzykiewicz and P. Sobota, *Dalton Trans*., 2008, 6556.
35. C. Zhang and Z. -X. Wang, *J. Organomet. Chem*., 2008, **693**, 3151.
36. R. Tong and J. Cheng, *J. Am. Chem. Soc*., 2009, **131**, 4744.
37. P. A. Holmes, *Phys. Technol*., 1985, **16**, 32.
38. (a) M. J. Stanford and A. P. Dove, *Macromolecules*, 2009, **42**, 141; (b) F. K. Wolf, A. M. Hofman and H. Frey, *Macromolecules*, 2010, **43**, 3314; (c) M. B. Runge, S. Dutta and N. B. Bowden, *Macromolecules*, 2006, **39**, 498; (d) M. Pitet and M. A. Hillmyer, *Macromolecules*, 2009, **42**, 3674; (e) W. Zhao, Dongmei, X. Liu and X. Chen, *Macromolecules*, 2010, **43**, 6678; (f) R. O. MacRae, C. M. Pask, L. K. Burdsall, R. S. Blackburn, C. M. Rayner and C. McGowan, *Angew. Chem. Int. Ed*., 2011, **50**, 291.

39. J. Contreras, J. Xie, Y. J. Chen, H. Pei, G. Zhang, C. L. Fraser and S. F. Hamm-Alvarez, *ACS Nano.*, 2010, **4**, 2735.
40. (a) J. Zhao and R. M. Wilkins, *J. Agric. Food Chem*., 2005, **53**, 4076; (b) S. Bocchini, K. Fukushima, A. Di Blasio, A. Fina, A. Frache and F. Geobaldo, *Biomacromolecules*, 2010, **11**, 2919.
41. M. Rubinstein, C. R. James, J. L. Young, Y. J. Ma, Y. Kobayashi, N. C. Gianneschi and J. Yang, *Org. Lett*., 2010, **12**, 3560.
42. (a) A. L. Brody, *Packaging Materials, Encyclopaedia of Polymer Science and Engineering*, 1987, **10**, 684; (b) D. M. Bigg, *Advances in Polymer Technology*, 2005, **24**, 69; (c) E. S. Stevens, *Green Plastics; An Introduction to the New Science of Biodegradable Plastics*, Princeton University Press, United States of America, 2002, pp 128 – 130.
43. W. Amass, A. Amass and B. Tighe, *Polym. Int.*, 1998, **47**, 89.
44. M. A. Kandadai, P. Praveena, G. Lin, A. Butterfield, M. Skliar and J. J. Magda, *Langmuir*, 2010, **26**, 4655.
45. Y. Nagasaki, T. Okada, C. Scholz, M. Iijima, M. Kato and K. Kataoka, *Macromolecules*, 1998, **31**, 1473.
46. A. S. Zalusky, R. Olayo-Valles, J. H. Wolf and M. A. Hillmyer, *J. Am. Chem, Soc*., 2002, **124**, 12761.
47. (a) A-C. Albertsson and I. K. Varma, *Biomacromolecules*, 2003, **4**, 1466; (b) H. J. Sanders, *Chem. Eng. News*, 1985, **63**, 30.
48. L. Zhang, J. M. Chan, F. X. Gu, J-W. Rhee, A. Z. Wang, A. F. Radovic-Moreno, F. Alexis, R. Langer and O. C. Farokhzad, *ACS Nano.*, 2008, **2**, 1696.
49. (a) S. Yolles, *Polym. Sci. Technol*., 1975, **8**, 245; (b) S. Yolles, J. E. Eldridge and J. H. R. Woodland, *Polym. News*, 1971, **1**, 9.
50. K. S. Soppimath, T. M. Aminabhavi, A. R. Kulkarni and W. E. Rudzinski, *J. Contr. Rel.*., 2001, **70**, 1.
51. D. L. Wise, G. J. McCormick, G. P. Wilet, *Life Sciences*, 1976, **19**, 1867.
52. (a) A. Schindler, R. Jeffcoat, G. L. Kimmel, C. G. Pitt, M. E. Wall and R. Zweidinger *Cont. Topics Polym. Sci.*, 1977, **2**, 251; (b) L. R. Beck, D. R. Coswar, D. H. Lewis, J. W. Gibson and C. E. Flowers, *Am. J. Obstet. Gynecol*., 1979, **135**, 419.
53. A. S. Michaels, U. S. Patent, 3, 962,414, 1976.
54. Y. X. Li, J. Northnagel and T. Kissel, *Polymer*, 1997, **38**, 6197.

55. R. R. Nijsen, B. A. Zonnerberg, J. R. W. Woittiez, D. W. Rook, I. A. Sweldens-Van Woundenberg, P. P. Van Rijk and A. D. Van Het Schip, *J. Nucl. Med*., 1999, **26**, 699.
56. R. J. J. Van Es, J. F. W. Nijsen, A. D. Van Het Schi, H. F. J. Dullens, P. J. Slootweg and R. Koole, *J. Oral Maxillofac. Surg*., 2001, **30**, 407.
57. V. Wagner, A. Dullaart, A. K. Bock, A. Zweck, *Nat. Biotechnol*., 2006, **24**, 1211.
58. H. Okada, Y. Ogawa, T. Yashiki, U.S. Patent, 4,652,441, 1987.
59. H. Okada, M. Yamamoto, T. Heya, Y. Inoue, S. Kamei, Y. Ogawa and S. Toguchi, *J. Contr. Rel.*, 1994, **28**, 121.
60. (a) A. Nakamura, S. Ito and K. Nozaki, *Chem. Rev.*, 2009, **109**, 5234; (b) J. Durand, B. Milani, *Coord. Chem. Rev*., 2006, **250**, 542; (c) C. Bianchini and A. Meli, *Coord. Chem. Rev*., 2002, 35; (d) G. W. Coates, *Chem. Rev*., 2000, **100**, 1242; (d) E. Drent and P. H. M. Budzelaar, *Chem. Rev*., 1996, **96**, 663; (e) A. Nakamura, K. Munakata, T. Kochi and K. Nozaki, *J. Am. Chem. Soc.*, 2008, **130**, 8128; (f) A. Sen and Z. Jiang, *Macromolecules*, 1993, **26**, 911.
61. F. Ballauf, O. Bayer and L. Leichmann, G. Pat., 863711, 1941.
62. (a) A. Sen, *Acc. Chem. Res*., 1993, **26**, 303; (b) K. Nozaki and T. Hijima, *J. Organomet. Chem*., 1999, **576**, 248.
63. Shell Carilon® Thermoplastic Polyketone, Information Sheet, 1994, www.shell.com, production discontinued in year 2000, Shell Carilon® DP R1000 www.matweb.com.
64. European Plastics News, October, 1995, p. 57.
65. D. R. Tyler, *Coord. Chem. Rev*., 2003, **246**, 291.
66. (a) M. Barsacchi, G. Consiglio, L. Medici, G. Petrucci and U. W. Suter, *Angew. Chem. Int. Ed. Engl*. 1991, **30**, 989; (b) M. Barsacchi, A. Batistini, G. Consiglio and U. W. Suter, *Macromolecules*, 1992, **25**, 3604; (c) K. Nozaki, N. Sato and H. Takaya, *J. Am. Chem. Soc*., 1995, **117**, 9911; (d) K. Nozaki, N. Sato, Y. Tonomura, M. Yasutomi, H. Takaya, T. Hiyama, T. Matsubara and N. Koga, *J Am. Chem. Soc*., 1997, **119**, 12779.
67. B. Milani, F. Baronetto and E. Zangrando, *J. Chem. Soc, Dalton, Trans*., 2000, 3055.
68. C. Pisano, G. Consiglio, A. Sironi and M. Moret, *J. Chem. Soc. Chem. Commun*., 1991, 421.

69. S. Bruckner, C. De Rosa, P. Corradini, W. Porzio and A. Musco, *Macromolecules*, 1996, **29**, 1535.
70. A. Sommazzi and F. Garbassi, *Prog. Polym. Sci*., 1997, **22**, 1547.
71. B. Milani, A. Anzilutti, L. Vicentini, A. S. o Santi, E. Zangrado, S. Geremia and G. Mestroni, *Organometallics*, 1997, **16**, 5064.
72. R. A. Koster, R. H. Birk, *Polym. Prepr. (Am. Chem. Soc. Div. Polym. Chem.)*, 1996, **37**, 525.
73. A. Macchioni, G. Bellachioma, G. Cardaci, M. Travaglia, C. Caragna, M. Formica, *Organometallics*, 1999, **18**, 3061.
74. A. Bastero, C. Claver, A. Ruiz, A. M. Guerriero, F. Jalon and B. R. Manzano, *J. Organomet. Chem.*, 2001, **619**, 287.
75. M. Brookhart, M. I. Wagner, G. G. A. Balavoine and H. A. Haddou, *J. Am. Chem. Soc*., 1994, **116**, 3641.
76. S. Bartolini, C. Carfanga and A. Musco, *Macromol. Rapid Commun*., 1995, **16**, 9.
77. C. Carfagna, M. Formica, G. Gatti, A. Musco, A. Pierleoni, *Chem. Commun*., 1998, 1113.
78. M. T. Reetz, G. Haderlein and K. Angermund, *J. Am. Chem. Soc*., 2000, **122**, 996.
79. A. D'Amora, L. Fanfoni, D. Cozzula, N. Guidolin, E. Zangrando, F. Felluga, S. Gladiali, F. Benedetti and B. Milani, *Organometallics*, 2010, **29**, 4472.
80. B. Soro, S. Stoccoro, M. A. Gimellu, G. Minghetti, A. Zucca, A. Bastero and C. Claver, *J. Organomet. Chem*., 2004, **689**, 1521.
81. A. Aeby and G. Consiglio, *Dalton Trans*., 1999, 655.
82. (a) G. P. C. M. Dekker, C. J. Elsevier, K. Vrieze, P. W. N. M. Van Leeuwen and C. F. Roobeek, *J. Organomet. Chem*., 1992, **430**, 357; (b) A. Batistini and G. Consiglio, *Organometallics*, 1992, **11**, 1766.
83. (a) J. Dupont, C. S. Consorti and J. Spencer, *Chem. Rev*., 2005, **105**, 2527; (b) V. Polshettiwar, C. Len and A. Fihri, *Coord. Chem. Rev*., 2009, **253**, 2599; (c) J. G. de Vries, *Dalton Trans.*, 2006, 421.

CHAPTER 2: SYNTHESIS AND CHARACTERIZATION OF LIGANDS AND COMPLEXES

2.1 General

Methods for the preparation of zinc and palladium complexes together with the corresponding ligands that were attached to these metals are discussed in this Chapter. The ligands and complexes were characterized using various analytical techniques, such as ^{1}H and ^{13}C NMR, mass spectrometry (MS), infrared (IR) spectroscopy, melting points and elemental analysis. The single crystal X-ray diffraction technique was used to study compounds which yielded suitable crystals. Phosphorus-containing compounds were analysed with ^{31}P NMR spectroscopy while cyclic voltammetry (CV) was used for ferrocenyl-containing compounds. Important aspects of the characterization data are discussed in each section (i.e. for zinc complexes in Section 2.2 and for palladium complexes in Section 2.3). Full characterization data and preparative procedures are listed in the experimental section (Chapter 7).

2.2 Zinc complexes and corresponding ligands

2.2.1 Introduction

There are numerous reports in which thiazole-containing compounds have been investigated as potential drug candidates.[1] The compounds have displayed biological properties including anticancer, antimalaria and antiamoebic activity.[1] In addition, compounds which displayed activity as agrochemicals have also been reported. Riluzole [IUPAC name = 6-(trifluoromethoxy)benzothiazol-2-amine] is an example of a commercially available drug. The molecule is marketed by Sanofi-Aventis with the brand name Rilutek® and is used to treat amyotrophic lateral sclerosis. There is no doubt that the thiazole group (see below) has unique biological properties.

Thiosemicabazone-containing compounds have also been found to display biological activities as drug candidates.[2] The activities generally are similar to those observed for their thiazole-containing counterparts. The thiosemicarbazone group can be considered as an acyclic analogue of the cyclic-thiazole molecules. Indeed, in some

cases thiosemicarbazone compounds are used as precursors for the preparation of thiazole derivatives (see below).[3]

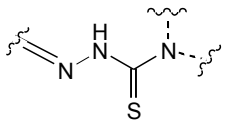

thiosemicarbazone group

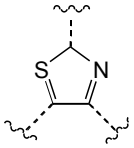

thiazole group

Despite the fact that many compounds have been reported as lead molecules, most of the compounds do not reach laboratory investigations for *in vivo* animal testing trials. The issues of insolubility and lack of selectivity shown by some of these compounds have been found to contribute to their failure to reach the application stages. Fortunately, a method of drug delivery has been proposed as a possible solution to these problems and some compounds have been able to reach development or even commercialization stages.[4] These various methods of drug delivery have been described in some detail in the literature review, presented in Chapter 1.

The current study, therefore, aimed to develop an alternative method of incorporating a drug on a polylactide backbone. This section deals with synthetic methods and a discussion of the characterization of the ligands and corresponding homoleptic zinc complexes. Two types of ligands, both containing a drug moiety and their corresponding zinc complexes, were prepared. The first ligand type contained a thiazole group, when the resulting complexes were of the type $Zn(N\hat{}O)_2$. The second ligand type contained a thiosemicarbazone moiety and yielded the corresponding $Zn(N\hat{}S)_2$ complexes. The data obtained when utilizing the ligands and complexes for lactide polymerization will be discussed in Chapter 3.

The thiazole derivatives were prepared following the Schiff-base method employing the reaction between a suitable primary amine and salicylaldehyde or a salicylaldehyde-derivative. Ligand (**37**) was prepared by the reaction between 2-Amino-benzothiazole with 2-hydroxybenzaldehyde in ethanol as a solvent. Ligand (**38**), on the other hand, was prepared from a reaction between 3,5-di-*tert*-butyl-2-hydroxythiosemicarbazone (which was prepared following a literature procedure)[3] and α-bromoacetophenone in ethanol as a solvent. The zinc complexes were then prepared by reacting two equivalents of the ligand with one equivalent of diethylzinc

or zinc acetate. The reaction route illustrating the synthesis of the ligands and their zinc complexes is shown in **Figure 2.2.1**.

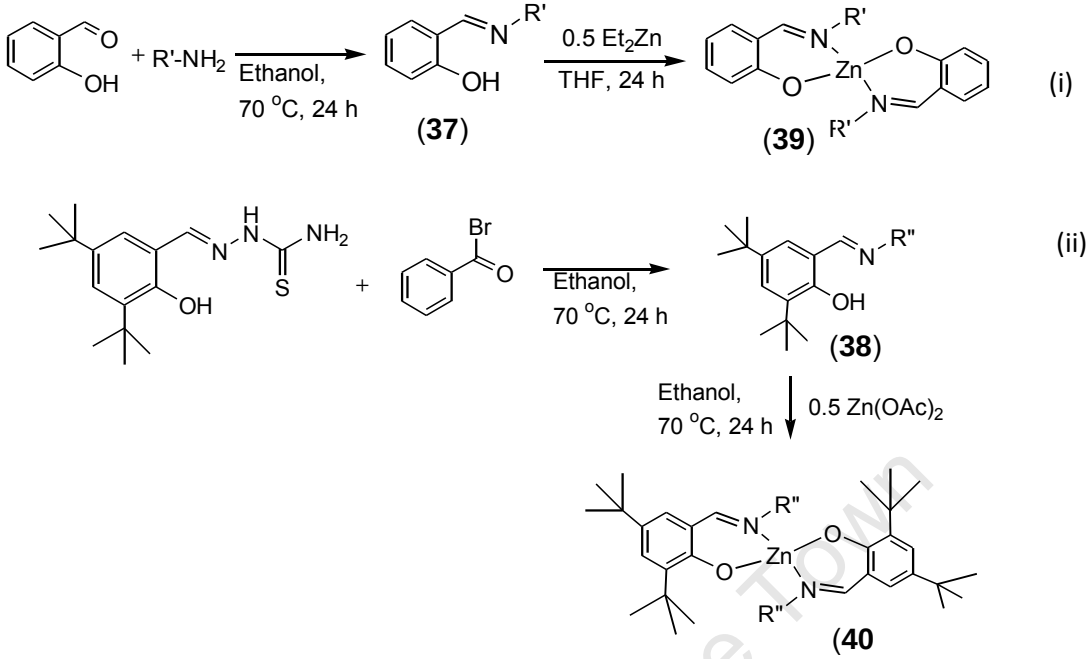

Reaction scheme	Substituent	Ligand	Complex
(i)	R' = 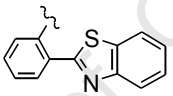	(**37**)	(**39**)
(ii)	R'' = 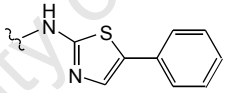	(**38**)	(**40**)

FIGURE 2.2.1: The reaction route for the preparation of thiazole-ligands and their corresponding $Zn(N\hat{}O)_2$ complexes.

The thiosemicarbazone ligands were also prepared following a conventional Schiff-base reaction. In this case, the thiosemicarbazide derivative was reacted with either 4-*tert*-butyl-benzaldehyde or ferrocenecarboxyaldehyde. As an example, ferrocenecarboxyaldehyde and 4-methylthiosemicarbazide were reacted in methanol as a solvent under reflux to form ligand (**41**). The reactions for the production of aromatic compounds (**43**) and (**44**) took longer than those for the production of (**41**) and (**42**) the ferrocenyl analogues. This was because the ferrocenyl group is a good donor compared to aromatic groups, and therefore faster reaction times were observed.[5] Thiosemicarbazone compounds interconvert between the thione- and thiol-forms and this occurs faster when the solutions are heated; see **Figure 2.2.2**.[6,7]

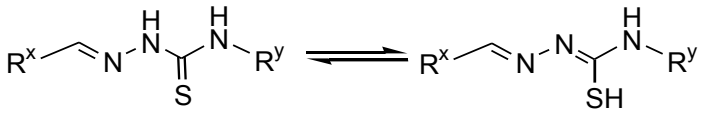

thione form thiol form

FIGURE 2.2.2: The two forms of thiosemicarbazone compounds.[6,7]

When reacted with metal salts the complexes have mostly been found to adopt an (N^S) coordination mode in which the imine-nitrogen is involved in the metal-coordination sphere.[7] In this study, the zinc complexes $Zn(N^S)_2$ were prepared from a reaction between two equivalents of the ligand (**41**), (**42**), (**43**) or (**44**) and one equivalent of zinc acetate in methanol as a solvent at 70 ºC. The reaction route for the preparation of the ligands and complexes is shown in **Figure 2.2.3**.

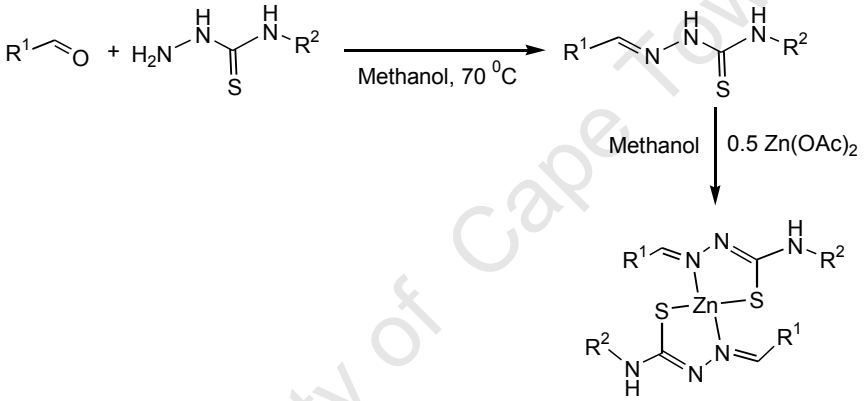

R^1	R^2	Ligand	Complex
Fc	Methyl	(**41**)	(**45**)
Fc	4-Fluorophenyl	(**42**)	(**46**)
4-^{t}Bu-C_6H_4	Methyl	(**43**)	(**47**)
4-^{t}Bu-C_6H_4	4-Fluorophenyl	(**44**)	(**48**)

FIGURE 2.2.3: General reaction scheme for the preparation of thiosemicabazone ligands and corresponding $Zn(N^S)_2$ complexes.

2.2.2 Characterization of thiazole-containing (N^O) ligands (**37**) *and* (**38**)

The ligand (**37**) was isolated as a grey microcrystalline solid which melted in the range 130 – 131 ºC. All the expected peaks for compound (**37**) appeared in the ^1H and ^{13}C NMR spectra. The numbering system followed for the assignment of proton and carbon atoms in the NMR spectra is shown in **Figure 2.2.4**.

The azomethine hydrogen (*H*^{7}C=N) appeared at 8.61 ppm, while the hydroxyl proton (O*H*) resonated at 12.49 ppm.

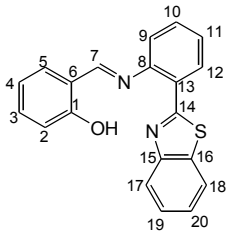

FIGURE 2.2.4: The numbering system followed for assignment of proton and carbon atoms in the ^{1}H and ^{13}C NMR spectra of ligand (**37**).

In the ^{1}H NMR spectrum proton signals were observed in the range 6.98 – 8.40 ppm. An HMQC NMR spectral analysis was also conducted in order to further confirm the atom assignments. The ^{1}H and ^{13}C NMR spectra of ligand (**37**) are shown in **Figure 2.2.5**.

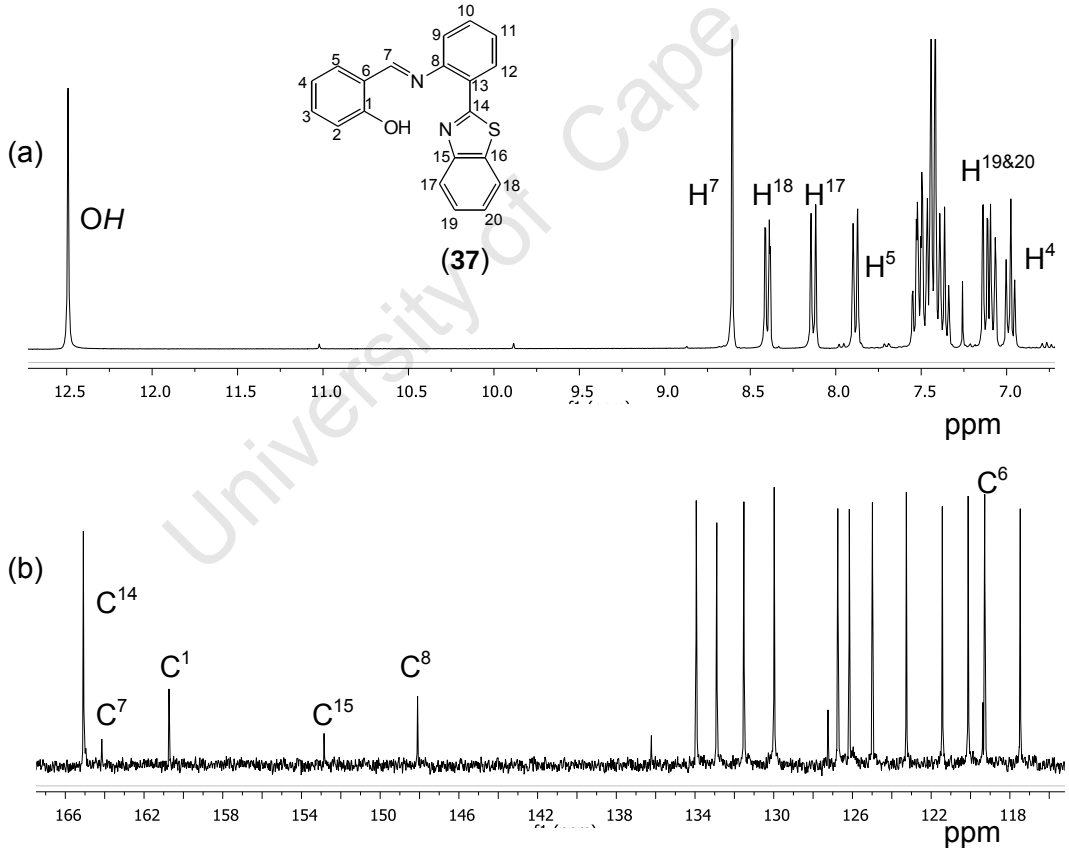

FIGURE 2.2.5: NMR spectra of compound (**37**) in C_6D_6 at ambient temperature: (a) ^{1}H NMR spectrum and (b) ^{13}C NMR spectrum, (selected atoms are assigned).

In the ^{13}C NMR spectrum, carbon signals appeared in the range 117.5 – 165.1 ppm. Attention was focused on the chemical shifts of C^{1}, C^{6}, C^{7} C^{8}, C^{9} and C^{13} as they are

closer to the oxygen- and azomethine nitrogen-coordinating groups and would be most affected when the ligand is coordinated to zinc in the complex. Chemical shifts for the selected carbon atoms were observed as follows: 160.7 (C^1), 117.5 (C^2), 119.3 (C^6), 164.1 (C^7), 148.1 (C^8), 120.1 (C^9) and 131.5 ppm (C^{13}). Although ligands prepared from salicylaldehyde derivatives with substituent 3-^{t}Bu (**49**) or 3,5-^{t}Bu (**50**) groups were isolated (see full characterization data in experimental section), their zinc complexes could not be isolated. It was concluded that this type of complex was not tolerant to the bulkier substituents since, for example, the starting ligands were obtained unchanged after attempts to react the ligand with diethylzinc or zinc acetate using various reaction conditions. The infrared spectrum displayed the imine bond ν(C=N) vibration at 1611 cm^{-1}, while the ν(OH) band appeared at 3200 cm^{-1}. Electron impact mass spectra displayed the molecular ion peak, $[M]^+$ = 330.40 (100%) which matched with the proposed molecular formula $C_{20}H_{14}N_2OS$ of compound (**37**). The elemental analysis was in agreement with the proposed compound (see Experimental Chapter).

In the preparation of compound (**38**), the thiosemicarbazide precursor was prepared from a reaction between hydrazine and 3,5-di-*tert*-butyl-2-hydroxybenzaldehyde.[3] The product which was formed, 3,5-di-*tert*-butyl-2-hydroxythiosemicarbazone was further reacted with α-bromoacetophenone in ethanol by heating the reaction mixture under reflux overnight. Ligand (**38**) was isolated as a brown microcrystalline solid. The ^{1}H NMR spectrum of the compound recorded in DMSO-d^6 displayed aromatic peaks ($7H^{5,9,16-18}$) in the range 7.25 – 7.83 ppm, an alkenyl proton (H^{13}) at 7.83 ppm and the aliphatic proton signals H^4 and H^8 appeared at 1.24 and 1.38 ppm, respectively. The numbering system which was followed in assignment of atoms in the ^{1}H and ^{13}C NMR spectrum is illustrated in **Figure 2.2.6.**

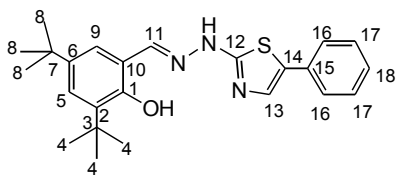

FIGURE 2.2.6: Numbering of atoms for ligand (**38**) followed for assignment of chemical shifts in the ^{1}H and ^{13}C NMR spectra.

The azomethine hydrogen (H^{11}) resonated at 8.26 ppm and the hydrazide proton (N*H*) appeared at 7.81 ppm; the hydroxyl proton resonated at 10.80 ppm. Moreover, the ^{13}C

NMR spectrum displayed eighteen expected signals. In particular the signals which were assigned as follows were observed: 147.6 (C^1), 118.1 (C^9), 154.2 (azomethine carbon, C^{11}), 167.6 (C^{12}), 128.3 (C^2) and 125.4 (C^5). The ^1H and ^{13}C NMR spectra of compound (**38**) are shown in **Figure 2.2.7**.

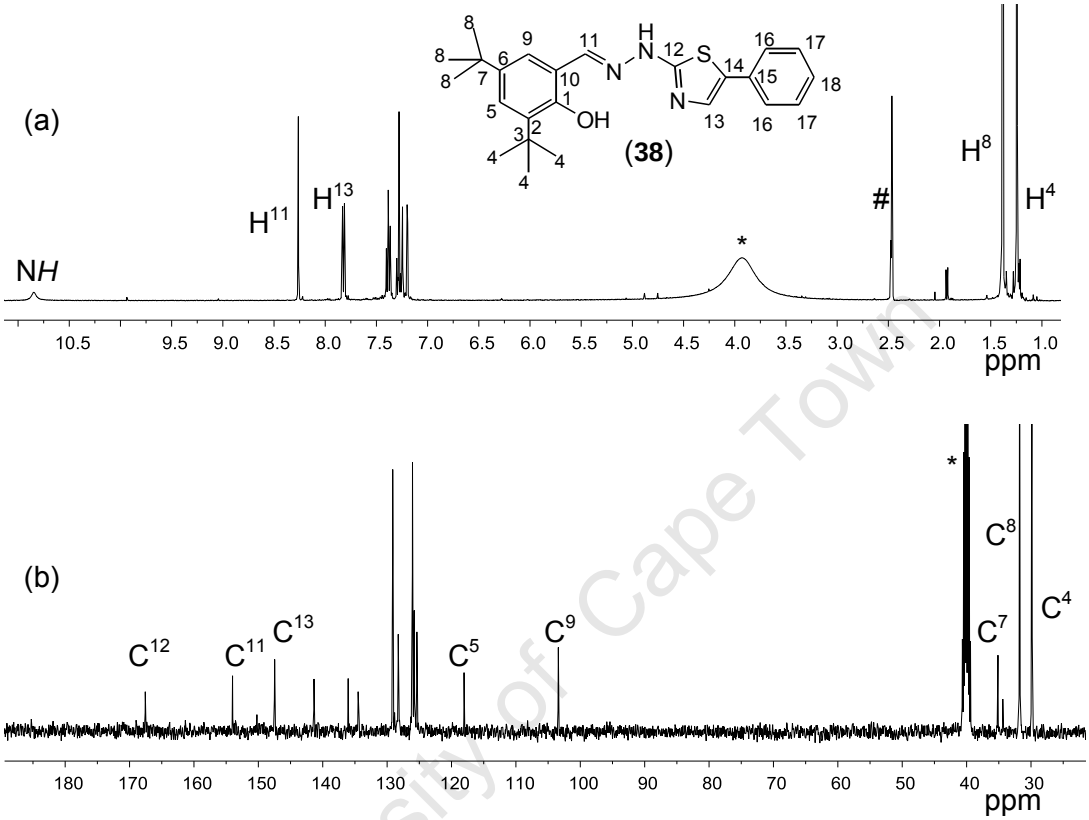

FIGURE 2.2.7: NMR spectra of compound (**38**) in DMSO-d^6 at ambient temperature, selected atoms are assigned: (a) ^1H NMR spectrum and (b) ^{13}C NMR spectrum. #Residual water in deuterated solvent; *solvent residual peak, broadening explained as hydrogen bonding interaction with the sample.

The infrared spectrum displayed signals for ν(C=N) at 1622 and 1587 cm^{-1}, which were attributed to the stretching vibration associated with the aliphatic and aromatic (in the thiazole ring) azomethine bonds, respectively.[3] The ν(O-H) band appeared at 3134 cm^{-1}, while the ν(N-H) band was observed at 3052 cm^{-1}. The mass spectrum displayed the molecular ion peak, $[M]^+$ = 406.80 (100%), which matched the proposed molecular formula of $C_{24}H_{29}N_3OS$ for compound (**38**). The purity of the ligand was confirmed by elemental analyses (see Experimental, Chapter 7).

2.2.3 Homoleptic Zn(N^O)$_2$ complexes (**39**) and (**40**)

Complex (**39**) was isolated as a yellow powder, melting by decomposition at 220 ºC for the compound was obtained. The downfield shift of the azomethine proton (H^7) to 8.87 ppm and the disappearance of the hydroxyl proton in the ^{1}H NMR spectrum confirmed the formation of the complex. Moreover, the chemical shifts for carbon atoms in the ^{13}C NMR spectra appeared between 119.0 – 174.5 ppm. Signals due to the following carbon atoms were observed: 164.0 (C^1), 119.0 (C^2), 120.8 (C^6), 170.0 (C^7), 153.9 (C^8), 125.1 (C^9) and 136.7 ppm (C^{13}). The downfield shift of the carbon signals, in particular of C^1, C^7 and C^8, further confirmed the coordination of azomethine-nitrogen and phenolate oxygen of the ligand to zinc.

A probably insignificant IR frequency shift was observed for the imine bond at 1609 cm^{-1} compared to the ligand. Similar behaviour has been observed for various other related zinc complexes.[8] As expected, the band due to ν(O-H) stretching disappeared in the IR spectra, confirming the complex formation. The percentage composition of the atoms as determined by elemental analysis corresponded to the proposed chemical formula. The complex, however, required numerous recrystallization from a mixture of tetrahydrofuran and hexane to achieve acceptable elemental analysis which was in good agreement with the calculated values. Electron spray ionization mass spectrometry displayed a molecular ion peak (M^+) at *m/z* 722.08 (2%). Some fragments which were observed at *m/z* 650.02, 616.11, 486.32 and 381.20 corresponded to a stepwise fragmentation of the samples starting from the thiazole group. The proposed fragmentation ions are shown in **Figure 2.2.8.**

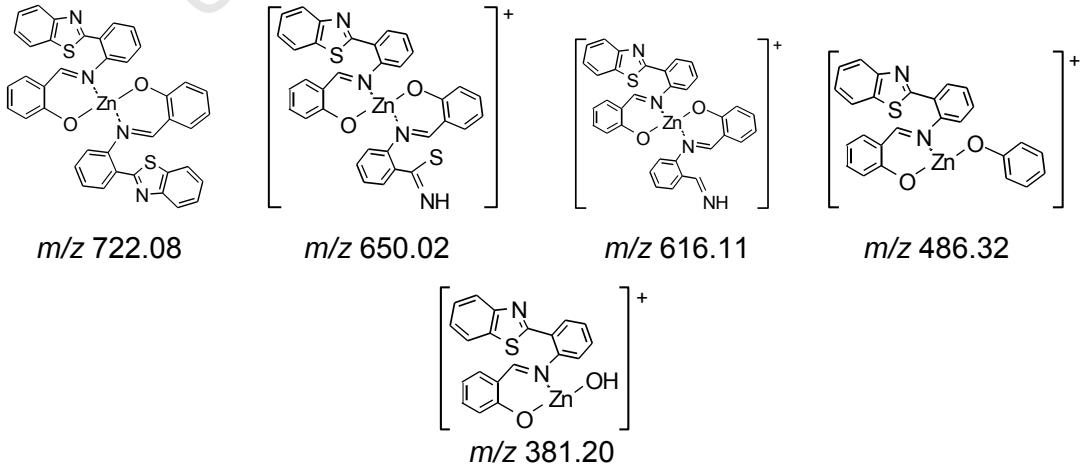

FIGURE 2.2.8: Proposed assignments of fragments which appeared in the mass spectrum (ESI) of zinc complex (**39**).

Similar observations were made for complex (**40**), isolated as a brown microcrystalline solid melting in the range 228 – 233 °C. The disappearance of the hydroxyl proton in the ^{1}H NMR spectrum of this compound (**40**) suggested the formation of the complex. The signal for azomethine (H^{11}C=N) proton shifted downfield from 8.26 for the ligand (**38**) to 8.38 ppm for complex (**40**). The signals for other protons, however, did not show any shifts compared to the signals observed in the spectrum of the ligand (**38**).

The carbon-signals in the ^{13}C NMR spectra also did not show any shifts in the complex compared to that of the ligand. The infrared spectrum, however, displayed a lower frequency for ν(C=N) band of the azomethine linkage at 1607 cm^{-1} while ν(C=N) band for the thiazole showed a probably insignificant increase of 2 cm^{-1}. Similar observations have been made for related compounds containing both the aliphatic azomethine bond and thiazole goups[3,8]. On the other hand, the ν(O-H) band did not appear in the spectrum of the complex. The ν(N-H) vibration appeared at 3168 cm^{-1}.

The mass spectrum (FAB MS) confirmed the formation of the compound by the appearance of a peak at *m/z* 877.02, which corresponded with the proposed molecular formula of $C_{48}H_{56}N_6O_2S_2Zn$ for compound (**40**). A similar fragmentation pattern to that of the ligand was observed. The elemental analysis corresponded with the calculated values for the complex. Full characterization data for these ligands and complexes are listed in the experimental section, Chapter 7.

2.2.4 Characterization of thiosemicarbazone (N^S) ligands (**41**) – (**44**)

The ^{1}H NMR spectra of ligands (**41**) and (**42**) dissolved in DMSO-d^{6} displayed signals attributed to the ferrocenyl protons in the range 4.21−4.74 ppm. The aromatic protons in ligand (**42**) appeared as doublets at 7.52 and 7.14 ppm for H^{8} and H^{9}, respectively. The numbering system for the protons of these ligands is illustrated in **Figure 2.2.9**. The methyl protons (3H^{7}) for ligand (**41**) appeared as a doublet at 2.94 ppm. Two signals for the azomethine protons, N-N*H*-(CS)^{2} and (CS)-N*H*R^{2}, appeared at 11.51 and 9.71 ppm, and at 11.10 and 8.07 ppm, in compounds (**42**) and (**41**), respectively. The azomethine proton (H^{5}) was observed at 7.97 and 7.84 ppm in compounds (**42**) and (**41**), respectively. The ^{1}H NMR shifts

were comparable to those of similar compounds reported in literature.[8,9] The ^{1}H and ^{13}C NMR spectra of compound (**41**) are shown in **Figure 2.2.10**.

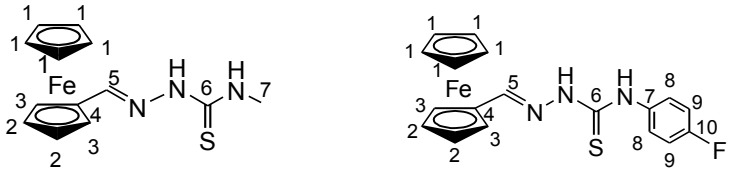

(**41**) (**42**)

FIGURE 2.2.9: The numbering system followed for assignment of proton and carbon atoms in the ^{1}H and ^{13}C NMR spectra.

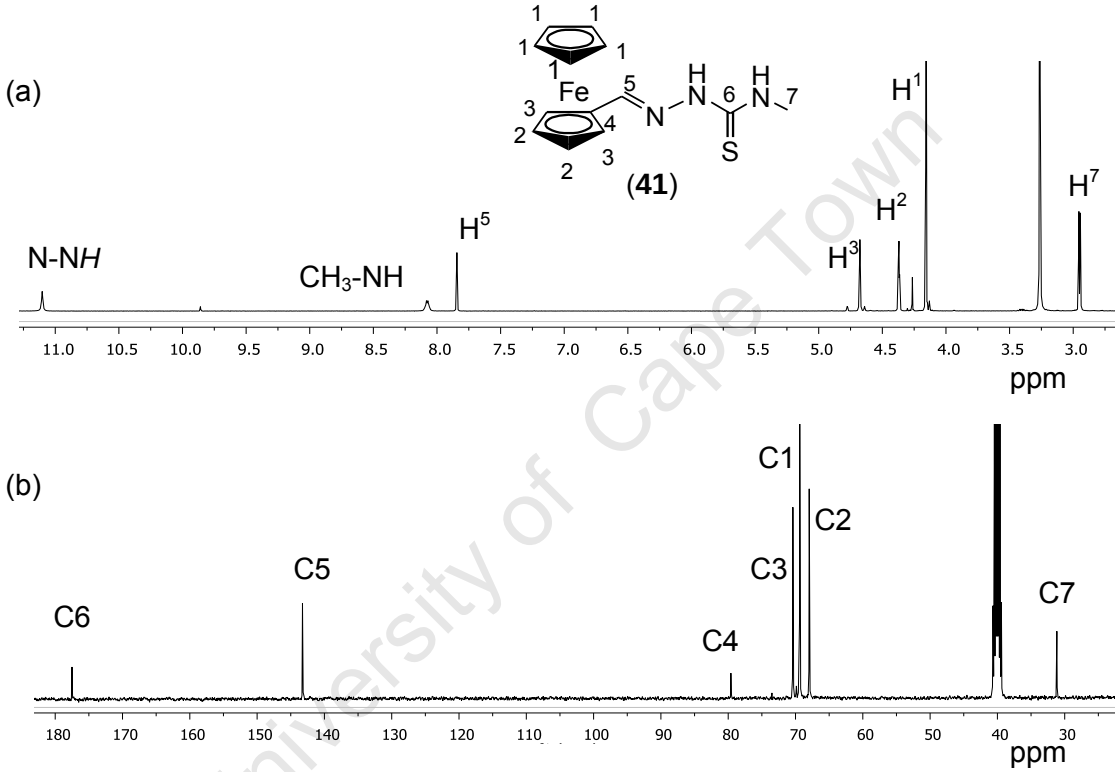

FIGURE 2.2.10: The spectra of compound (**41**) in DMSO-d^{6}: (a) ^{1}H NMR spectrum and (b) ^{13}C NMR spectrum.

The effect of the R^{2} (ie. methyl or 4-flurophenyl) group on the chemical environment of azomethine-protons was observed by the behaviour of the chemical shifts of the protons. The fluorophenyl substituent in compound (**42**) had a deshielding effect on the adjacent azomethine proton, while the methyl substituent in compound (**41**) displayed the opposite effect. The difference in the electronic properties of the compounds influenced their catalytic activity for lactide polymerization. Surprisingly, ligand (**42**) was found to be more active for lactide polymerization while ligand (**41**) was not active. The results of these studies will be discussed in the next chapter.

Determination of the electron density using molecular modelling calculations further supported the electrophilic character of the N-NH imino group in compound (**42**), while the same group displayed nucleophilic character in compound (**41**). Simulated molecular structures and electronic properties are shown in **Figure 2.2.11**.

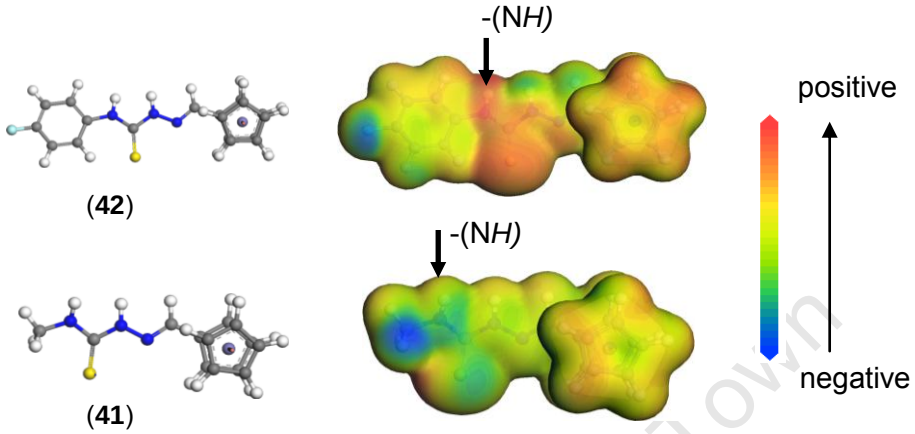

FIGURE 2.2.11: DFT-estimated nucleophilic site for compounds (a); (**42**) and (b); (**41**) deduced from the total electron density of the molecule. Red-yellow indicates the electrophilic regions and green-blue the nucleophilic regions.

The *tert*-butyl-substituted compounds displayed similar spectral data when compared to the ferrocenyl analogues. The numbering system of atoms used in the NMR spectra of compounds (**43**) and (**44**) is shown in **Figure 2.2.12**.

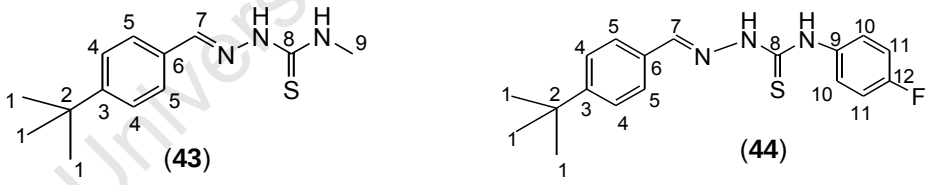

FIGURE 2.2.12: The numbering system followed for assignment of proton and carbon resonances in the ^{1}H and ^{13}C NMR spectra for compounds (**43**) and (**44**).

The protons of the *tert*-butyl substituent on the aromatic ring appeared at 3.02 ppm. The aromatic protons (H^4, H^5, H^{10} and H^{11}) in compound (**44**) appeared as four sets of doublets, each integrating for two protons in the range 7.17–7.81 ppm. The azomethine proton appeared at 8.14 (H^7) while the two amino protons resonated at 11.76 and 10.11 ppm for (-N-N*H*-C) and (-CN*H*-R^2), respectively. Similar resonances appeared at 8.04 (H^7), 11.32 (-N-N*H*-) and 8.34 ppm (C-N*H*-R^2) in the ^{1}H NMR spectrum of compound (**43**).

Similar deshielding of the secondary amine proton (N-N*H*) by the 4-fluorophenyl substituent in compound (**44**) was observed as found in the ferrocenyl analogue (**42**), when compared to their methyl-substituted counterparts. The azomethine protons (H^7) in aromatic analogues (**43**) and (**44**), notably, resonated downfield at 8.04 and 8.14 ppm when compared to the proton (H^5) in ferrocenyl analogues (**41**) and (**42**), which resonated at 7.84 and 7.97 ppm, respectively. As already mentioned, the difference in electronic properties of the compounds had an effect on the polymerization activity of the compounds, the results of which will be discussed in Chapter 3.

The ^{13}C NMR spectra for these *tert*-butyl-substituted aromatic compounds displayed the aromatic carbon atoms in the range 125.7 – 142.2 ppm; the imino carbon (C^7=N) appeared at 152.7 ppm, while the thione carbon (C^8=S) resonated at 177.1 ppm. The ^{1}H and ^{13}C NMR spectra for compound (**44**) are shown in **Figure 2.2.13**.

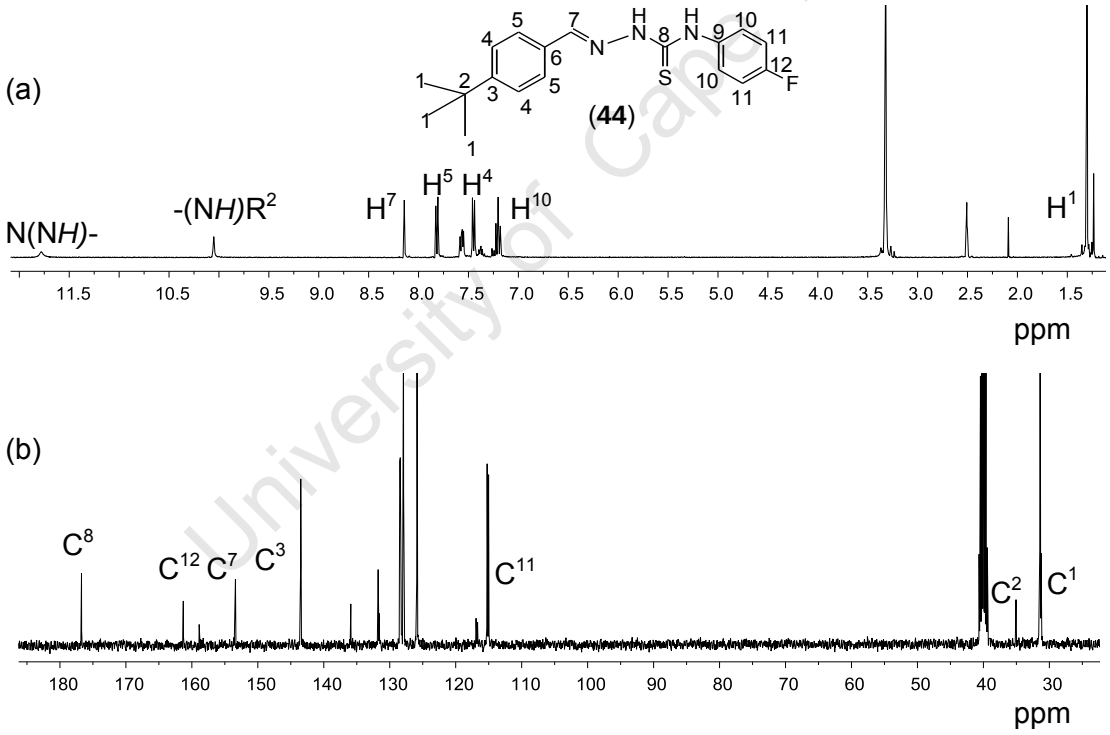

FIGURE 2.2.13: The spectra of compound (**44**) in DMSO-d^6 at ambient temperature: (a) ^{1}H NMR spectrum and (b) ^{13}C NMR spectrum.

Mass spectra displayed molecular ion peaks for each of the thiosemicarbazone ligands (**41**), (**42**), (**43**) and (**44**). A similar fragmentation trend was observed for all the ligands. The most intense signals corresponded to sequential fragmentation starting with loss of the C(S)-NH- substituent, *viz.* a 4-fluorophenyl or a methyl group (see **Figure 2.2.14** for the proposed ionization fragments). In addition, peaks

corresponding to either 4-*tert*-butyl-fluorophenyl derivative or the ferrocenyl substituent were observed for each type of compound. As an example, the following *m/z* values were measured for the 5-methylferrocenylthiosemicarbazone (**41**): 301.05 $[M]^+$, 284.71 (73%), 271.00, 238.59, 226.68 and 212.02, see **Figure 2.2.14.**

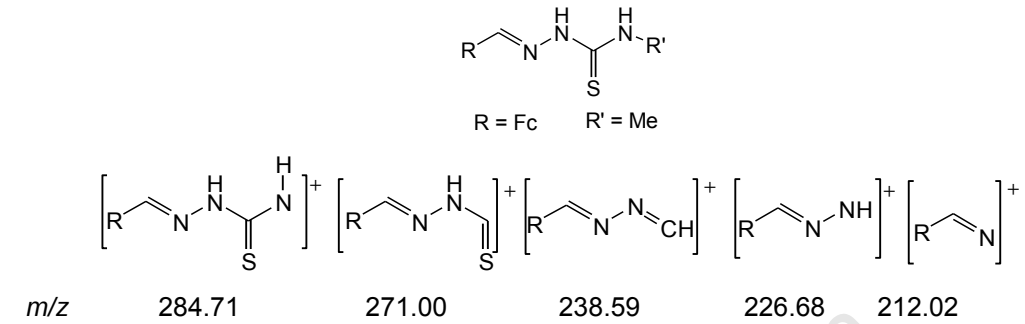

FIGURE 2.2.14: Proposed ionization fragments observed in an electron impact mass spectrum for thiosemicarbazone ligands (**41**).

2.2.5 Homoleptic Zn(N^S)$_2$ complexes (**45**) - (**48**)

The reaction of zinc acetate with two equivalents of the corresponding ligand (**41**) (in methanol) or (**42**) (in methanol) yielded the complexes (**45**) and (**46**), respectively, as red powders. When the reaction mixture was heated under reflux at 60 ºC, the ligand, which was converted to thiol-form,[6,7] reacted with zinc acetate. There was a disappearance of the imino proton [N(N*H*)C] in the ^{1}H NMR spectra of the complexes compared to that of the respective ligands. There was also broadening of the proton signals. In addition, the signals assigned to the C*H*^{5}=N and the imino proton [C(N*H*)R^2] shifted upfield upon complexation. The azomethine proton (H^7) in the aromatic analogues (**47**) and (**48**), however, did not show a significant shift. The azomethine proton resonated at 7.84 ppm while the imino protons were observed at 11.10 (-NN*H*-C) and 8.07 ppm (CN*H*R^2), for the ligand (**41**). The spectrum of complex (**45**) displayed a broad signal integrating for two protons per ligand (*H*^{5}C=N and CN*H*R^2) at 7.30 ppm and the peak which was assigned to NN*H*C for the free ligand disappeared. The imino protons (C-N*H*R^2) resonated at 8.33 and 9.48 ppm in the spectra of the aromatic analogues (**47**) and (**48**), respectively.

The ^{13}C NMR spectra of the complexes further confirmed complex formation. The upfield shift of the C^8 atom in the aromatic complexes (**47**) and (**48**) and C^6 atom in the ferrocenyl complexes (**45**) and (**46**) was due to the formation of a new C=N

double bond (azomethine) [-N=*C*-S$^-$)] in the complexes after conversion of the thione bond [–(NH)-*C*=S] which existed in the ligands to the thiolate form.[6,7] The azomethine carbon atom resonated in the region 151.2 – 177.6 ppm in the spectra of these complexes. The chemical shifts of atoms in the ^{13}C and ^{1}H NMR spectra are illustrated in **Table 2.2.1.**

TABLE 2.2.1: Comparison of chemical shifts for selected hydrogen and carbon atoms of compounds (**41**) – (**48**) in ^{1}H and ^{13}C NMR spectra conducted in DMSO-d^6

Compound	^{1}H NMR			^{13}C NMR	
	(HC=N)	-C(N*H)*R^2	-N(N*H)*-	*C*=S	*C-S*
(**41**)[a]	7.84	8.07	11.10	177.6	-
(**45**)[b]	7.30	7.30	-	-	151.2
(**42**)[a]	7.97	9.71	11.51	175.6	-
(**46**)[b]	7.48	9.41	-	-	170.1
(**43**)[a]	8.04	8.34	11.32	177.1	-
(**47**)[b]	8.04	8.33	-	-	173.1
(**44**)[a]	8.14	10.11	11.76	176.9	-
(**48**)[b]	8.19	9.50	-	-	172.0

[a]ligand, [b]complex

The IR spectra of the ferrocenyl analogues (**45**) and (**46**) displayed bands due to the ν(C=N) stretching frequency, which shifted to slightly lower frequencies as compared to the corresponding uncoordinated ligands. The ν(C=N) bands for aromatic analogues (**47**) and (**48**), however, appeared at slightly higher frequencies. It was noted that for ligand (**44**), two bands were observed in which one band appeared as a shoulder. The bands could possibly be due to the presence of isomers (thione and thiol form) thus giving rise to two C=N bands. A new ν(C=N) band was observed due to the formation of another type of a azomethine bond [-C=N-C(S$^-$)-] during complex formation.[6,7] On the other hand, the band originally observed in the region 835 – 854 cm^{-1} which was postulated to ν(C=S) in the ligands disappeared and was replaced by a new band in the region 815 – 839 cm^{-1} due to ν(C-S) in the complexes.[9] An insignificant shift of 1 cm^{-1} in the stretching frequency of the C-S bond was observed for complex (**48**) when compared to be ν(C=S) for corresponding ligand, (**44**). The

band due to ν[N(N-H)C] did not appear in the spectra as was expected, while ν[C(N-H)R^2] stretch shifted to lower frequency when compared with that of the ligand, for example, for the ferrocenyl analogue (**42**) a shift from 3129 to 3306 cm^{-1} was observed, while for aromatic complex (**48**) a shift from 3065 to 3069 cm^{-1} was observed. Surprisingly, there was no shift in the stretching frequency of the imino bond for complex (**47**) when compared to that of the corresponding ligand (**43**). The ν[C(N-H)R^2] and ν[N(N-H)C] assignments were based on literature reports for similar thiosemicarbazone compounds.[6,7,9] Comparison of the stretching frequencies for selected bonds in complexes and ligands is given in **Table 2.2.2**. The infrared spectra obtained for complex (**46**) and ligand (**42**) are shown in **Figure 2.2.15**.

TABLE 2.2.2: Stretching frequencies of selected functional groups observed in the infrared spectra (KBr) of ligands (**41**) – (**44**) and corresponding complexes (**45**) – (**48**)

(Ligand) (Complex)	Stretching frequency, (cm^{-1})					
	C(*C=N*)N	S(*C=N*)N	N(*N-H*)C	C(*N-H*)R^2	C=S	C-S
(**41**)	1609	-	3297	3336	854	-
(**45**)	1598	1495	-	3349	-	815
(**42**)	1604	-	3323	3129	850	-
(**46**)	1600	1527	-	3306	-	839
(**43**)	1609	-	3319	3177	835	-
(**47**)	1613	1579	-	3177	-	831
(**44**)	1607	-	3198	3065	836	-
(**48**)	1609	1592	-	3069	-	835

Molecular ion peaks of the ferrocenyl complexes were observed in their respective mass spectra (ESI). For aromatic compounds (**40**), (**47**) and (**48**) FAB MS was utilized. A molecular ion signal for complex (**46**) appeared at *m/z* = 824.00 and the peak corresponded with the proposed molecular formula of $C_{36}H_{32}N_6F_2S_2Fe_2Zn$. Intense signals were observed which were attributed to stepwise fragmentation [usually by the initial loss of the R^2 substituent (-CH_3 or 4-F-C_6H_4)] as was observed in the mass spectra of the complexes (*cf.* fragmentation ions in **Figure 2.2.14**). Full characterization data for these compounds, including melting points and elemental analyses, are listed in the Experimental Section (Chapter 7).

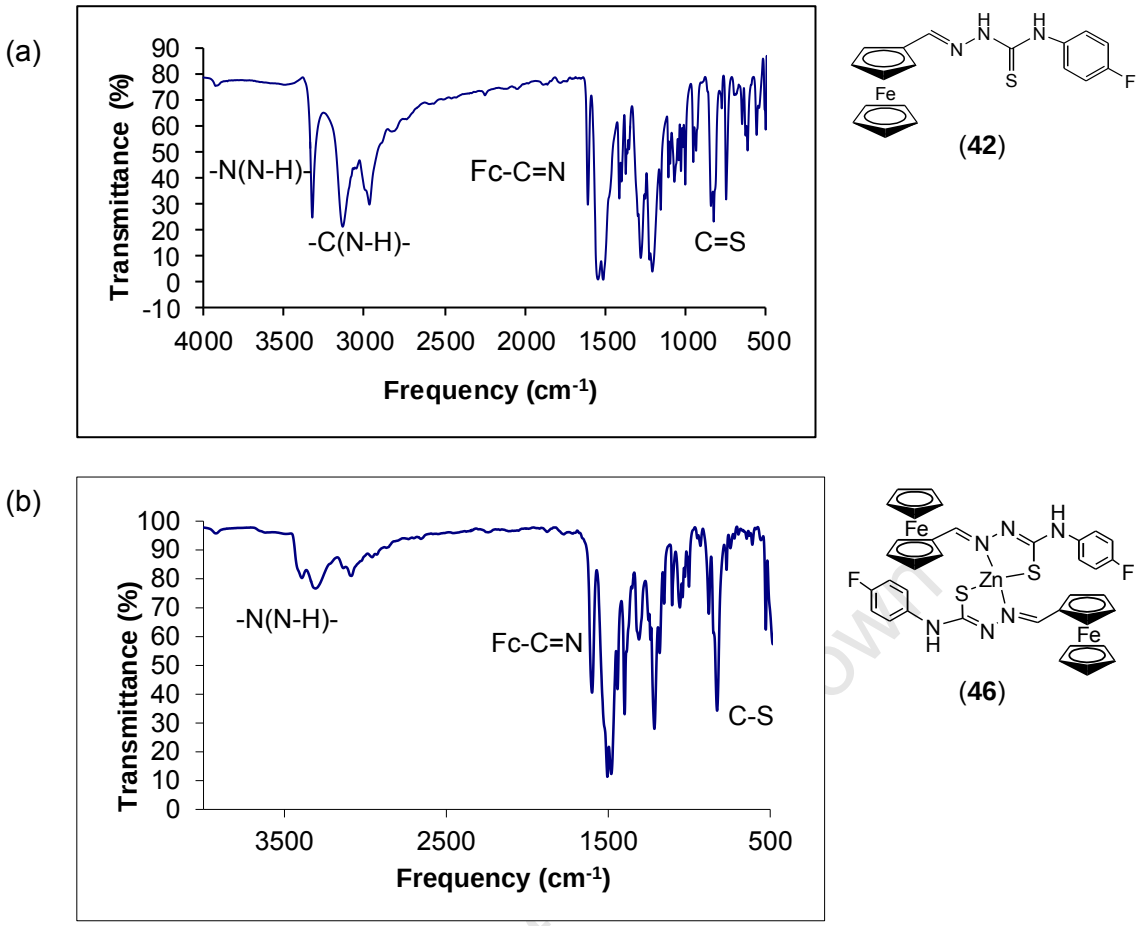

FIGURE 2.2.15: The solid state infrared spectra (KBr) of compounds: (a) (**42**) and (b) (**46**). Assignment of stretching frequencies for selected bonds is shown.

In a series of cyclic voltammetry experiments it was found that the half-wave potential ($E_{1/2}$) of the ferrocene/ferrocenium couple of the ferrocenyl group in the ligands and complexes was higher than that of the couple in ferrocene itself. The ferrocenyl group in complex (**42**) was more difficult to oxidize compared to the same group in ligand (**41**), the $E_{1/2}$ values of the compounds being 372 and 352 mV, respectively. The potential difference compared to the Fc/Fc^{+} couple in ferrocene itself was $\Delta E_{1/2}$ = +105 and +125 mV for compounds (**41**) and (**42**), respectively. The observed half-wave potentials were consistent with the ^{1}H NMR results and computational calculations on the electron withdrawing nature of the 4-fluorophenyl substituent in compound (**42**) (see Section 2.2.4).

The ferrocenyl group in the complexes (**45**) and (**46**) was found to be even more difficult to oxidize than in the respective ligands and ferrocene itself. A comparison of the potentials observed for the ligands and their respective complexes is illustrated in

Table 2.2.3, while representative cyclic voltammograms which were obtained are illustrated in **Figure 2.2.16.**

TABLE 2.2.3: Electrochemical potentials (mV, vs. Ag/Ag^{+}) of the ferrocenyl redox couple in ferrocenyl compounds in dichloromethane solution (1.5 mM, scan rate 100 mVs^{-1})

Compound	E_{pa} (mV)	E_{pc} (mV)	ΔE_p(mV) [a]	$E_{1/2}$(mV)[b]	$\Delta E_{1/2}$(mV)[c]
(**Fc**)	281	212	69	247	0
(**41**)	383	321	62	352	+105
(**45**)	412	347	65	380	+133
(**42**)	401	342	59	372	+125
(**46**)	442	382	60	412	+165

[a]$\Delta E_p = E_{pa} - E_{pc}$, [b]$E_{1/2} = (E_{pa} + E_{pc})/2$, precision of data is ±5 mV. [c]$\Delta E_{1/2} = E_{1/2}$compound $- E_{1/2}$Fc

In all voltammograms obtained for the complexes, only one redox couple was observed, suggesting that there was no communication between the two ferrocenyl groups. The peak currents (i_p mA) were slightly higher in the voltammograms of the complexes than in those of the ligands, with similar sample concentrations. This suggested that there were more ferrocenyl groups in the complexes than in the ligands, further confirming complex formation.

The half-wave potential of the ferrocenyl moieties in complex (**45**) was $E_{1/2}$ = 380 mV, while that of compound (**46**) was found to be $E_{1/2}$ = 412 mV, consistent with the electron withdrawing nature of the 4-fluoro-phenyl substituent in complex (**46**). In all cases the difference in anodic (E_{pa}) and cathodic (E_{pc}) peak potentials was in the range ΔE_p = 59 - 69 mV, confirming that a one electron transfer in the redox-cycle was taking place. Apart from the ferrocenyl wave, no other redox activity was observed for these ligands and complexes in the solvent/electrolyte window.

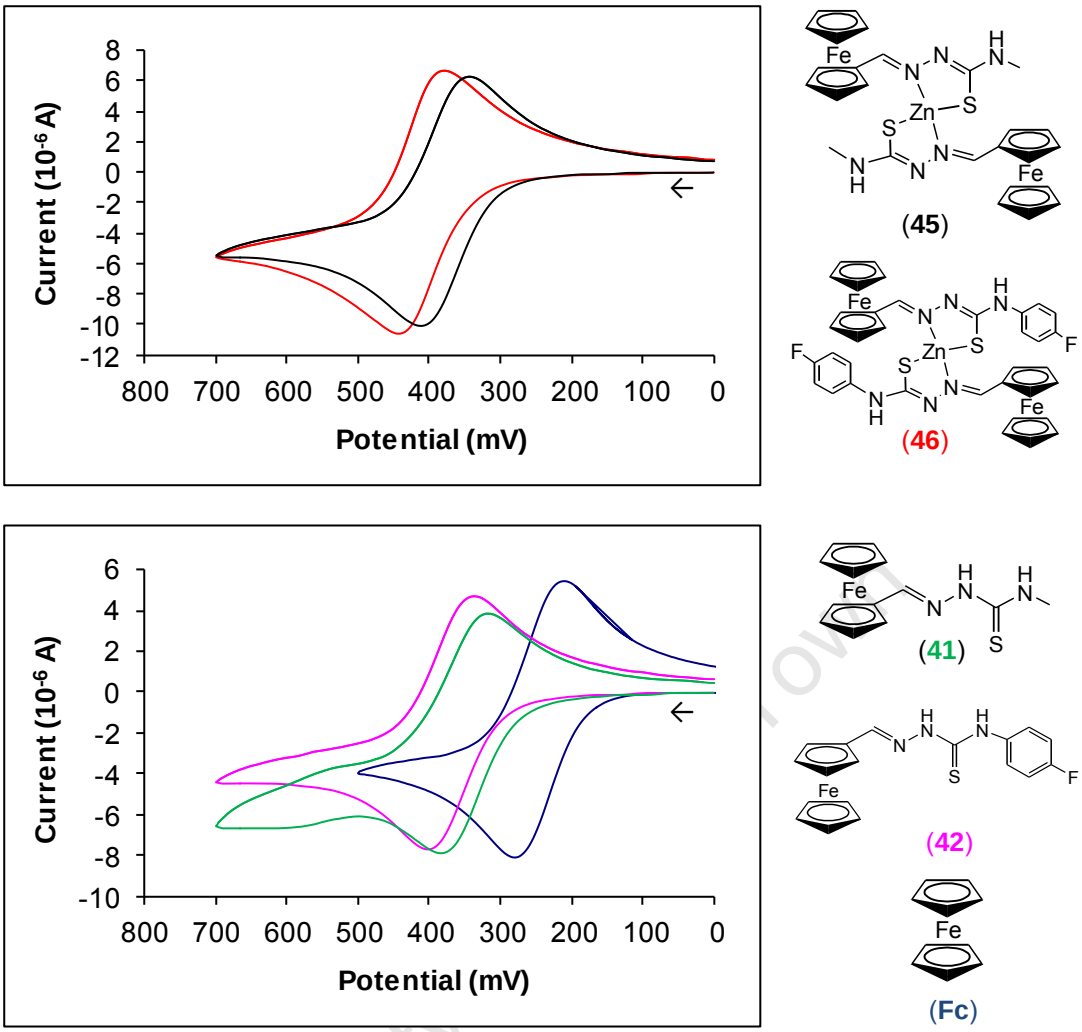

FIGURE 2.2.16: Comparison of cyclic voltammograms of ferrocenyl compounds (1.5 mM in dichloromethane). The potential is referenced to Ag/Ag^{+} (see Experimental).

2.3 Palladium complexes and corresponding ligands

2.3.1 Introduction

As already mentioned in Chapter 1, the choice of the ligand containing an amide-group was inspired by the fact that a carbon nanotube surface can be oxidized to introduce a layer of carboxylic acid groups by treatment with nitric acid.[10] Reaction of the acid groups with thionyl- or oxalyl chloride produces acid chloride groups which can be reacted with a suitable amine. Therefore, the mononuclear palladium complexes (**55**) – (**58**) prepared in this study serve as model compounds for future heterogeneous-type catalysts. Various examples of heterogeneous catalysts have been reported where the *N*,*N*-di(2-pyridyl)amine has been functionalized on the carbonaceous-supports.[11]

Most of the systems which have been reported displayed catalyst recyclability of up to four cycles without loss of catalyst activity for Heck reactions.[11b] Ferrocenyl analogues (**59**) and (**60**), on the other hand, were prepared to investigate the redox properties of the complexes and, subsequently, the effect of electronic properties on the CO/styrene copolymerization reaction. When oxidized by chemical or electrochemical processes, ferrocenyl-containing complexes might display improved activity for CO/styrene copolymerization. The synthetic route for the ligands and complexes prepared in this study are illustrated in **Figure 2.3.1.**

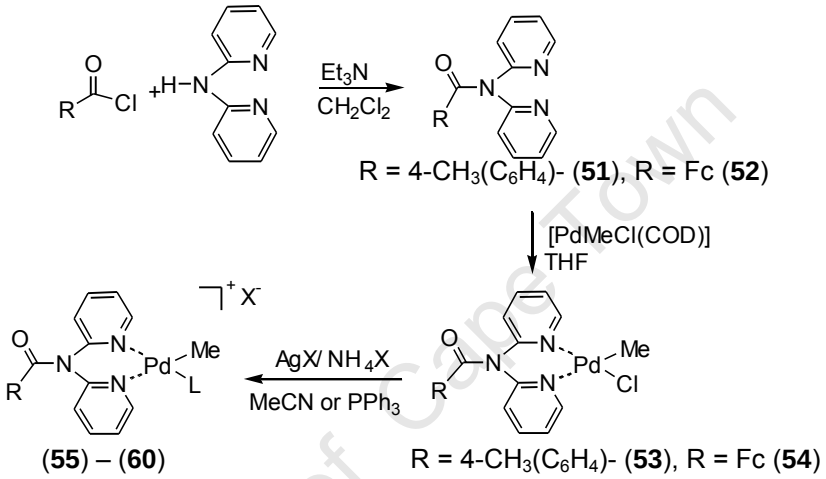

R = 4-$CH_3(C_6H_4)$-		R = $(C_5H_5)Fe(C_5H_4)$-	
X^-, L	Compound	X^-, L	Compound
PF_6, MeCN	(**55**)	PF_6, MeCN	(**59**)
BF_4, MeCN	(**56**)		
PF_6, PPh_3	(**57**)	PF_6, PPh_3	(**60**)
BF_4, PPh_3	(**58**)		

FIGURE 2.3.1: General reaction scheme for the preparation of ligands and cationic palladium complexes: amide ligands (**51**) and (**52**); neutral palladium complexes (**53**) and (**54**), cationic palladium complexes (**55**) – (**60**).

The reaction between *N*,*N*-di(2-pyridyl)amine and toluoyl chloride or chlorocarbonylferrocene produced the desired amide ligands (**51**) and (**52**), respectively, in high amounts; usually a minimum of 60% yield of ligands was obtained. This was followed by the preparation of neutral palladium complexes from a reaction of the ligand with [PdMeCl(COD)].[12] Subsequently, the neutral complexes were further reacted with a silver or ammonium salt (i.e. AgX or NH_4X, X = BF_4^- or PF_6^-) in the presence of a donor ligand (i.e. CH_3CN or PPh_3) to form the cationic complexes (**55**)-(**60**).

2.3.2 Characterization of ligands (**51**) *and* (**52**)

The amide ligand 4-methyl-*N*,*N*-di(2-pyridyl)benzamide (**51**), was isolated as a white microcrystalline solid. It was prepared from a reaction between *N*,*N*-di(2-pyridyl)amine and toluoyl chloride in the presence of triethylamine in dicloromethane (or tetrahydrofuran used) as solvent at room temperature for 24 h. The characterization data for this new ligand (**51**) were similar to related compounds in the literature.[13] The numbering system used for the assignment of proton and carbon chemical shifts for ligand and complexes is represented in **Figure 2.3.2.**

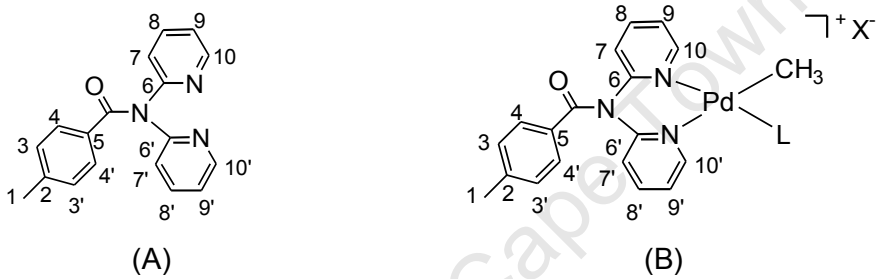

FIGURE 2.3.2: Atom numbering used in the assignments of the ^{1}H and ^{13}C NMR spectra. of (A) ligand (**51**) and (B) complexes (**55**) – (**58**).

The ^{1}H NMR spectra showed four doublet signals for the pyridinyl substituents and two sets of doublets for the aromatic protons. The assignments were further confirmed by (2D) COSY, HSQC and HMBC NMR spectroscopy. The protons from each pyridinyl group resonated at the same chemical shifts since the molecule is symmetric about the amide nitrogen. Thus the ^{1}H NMR spectrum of the ligand (**51**) in $CDCl_3$ displayed seven signals. Six of these signals appeared in the range δ 7.02 – 8.40 ppm and each signal integrated for two protons, while the remaining signal integrated for the three protons of the methyl substituent, which resonated at δ 2.29 ppm. The most deshielded hydrogen atoms H^{10} and $H^{10'}$ resonated downfield at δ 8.40 ppm, splitting to generate a doublet with coupling constants $J_{10\text{-}9,8,7}$ or $J_{10'\text{-}9',8',7'}$ = 3 Hz. The coupling behaviour was typical of multiple bond coupling of proton H^{10} or $H^{10'}$ and with the neighbouring protons $H^{9,8,7}$ or $H^{9',8',7'}$, respectively.

It is common behaviour for the protons in the substituted pyridine ring to display long range coupling.[14] As a result, the signals appeared as doublets in the ^{1}H NMR spectrum. The coupling behaviour was confirmed using (2D) HSQC NMR analysis. The most shielded protons numbered H^{9} and $H^{9'}$ resonated upfield as a doublet at δ 7.02 ppm integrating for two protons. Protons H^{7} and $H^{7'}$ resonated at δ 7.12 ppm as a doublet with a coupling constant of 3 Hz. Another doublet was observed at δ 7.40 ppm which was assigned to protons numbered H^{8} and $H^{8'}$, and displayed a coupling constant of J = 9 Hz and was attributed to be due to $J_{9\text{-}10,8,7}$ or $J_{9'\text{-}10',8',7'}$.

A multiplet was observed at δ 7.66 ppm for the tolyl protons H^{4} and $H^{4'}$, which are *ortho* to an electron-withdrawing amide substituent. On the other hand, the protons H^{3} and $H^{3'}$ resonated upfield at δ 7.25 ppm, due to the shielding effect of the electron-donating methyl group. The ^{13}C NMR spectrum of ligand (**51**) displayed a total of eleven signals, which resonated in the range δ 121.4 – 172.0 ppm for the aromatic carbon atoms (C^{2} – C^{10}), while the carbons of the methyl substituent and the carbonyl group resonated at 21.4 (C^{1}) and 156.2 ppm (C=O).

The electron impact ionisation mass spectrum (EI MS) displayed a molecular ion peak for ligand (**51**) at $[M]^{+}$ = 289.33 as a base peak (100% intensity). The infrared spectrum showed a carbonyl stretching frequency at 1656 cm^{-1} while the imino-pyridyl ν(C=N) stretching frequency was observed at 1609 cm^{-1}. CHN analysis agreed with the calculated values for $C_{18}H_{15}N_{3}O$. The melting point in the range of 125 -130 ºC for the ligand was obtained.

A ferrocenyl ligand (**52**) was isolated as a yellow microcrystalline solid from a reaction between chlorocarbonylferrocene and *N*,*N*-di(2-pyridyl)amine in dichloromethane as a solvent. Chlorocarbonylferrocene was firstly prepared following a literature procedure from a reaction between ferrocenecarboxylic acid and oxalyl chloride.[15] The compound was immediately used in the subsequent steps without further purification. The numbering system used to label protons and carbon atoms is shown in **Figure 2.3.3**.

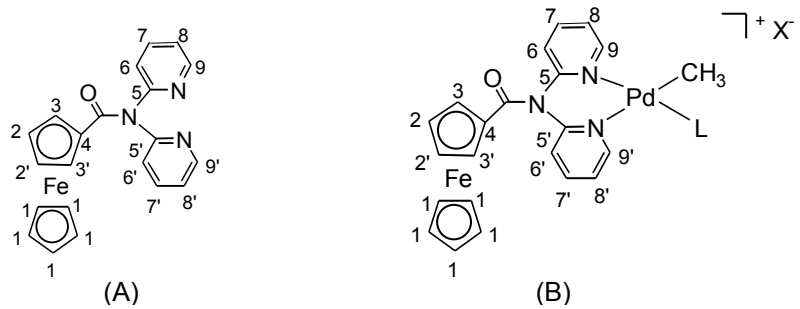

FIGURE 2.3.3: Atom numbering used in the assignments of the ^{1}H and ^{13}C NMR spectra of (A) ligand (**52**) and (B) complexes (**59**) and (**60**).

The ^{1}H NMR spectrum of *N*,*N*-di(2-pyridyl)ferrocenylamide (**52**) in $CDCl_3$ displayed peaks which were attributed to ferrocenyl protons: a multiplet at δ 4.21 ppm for the substituted cyclopentadienyl (Cp) ring (H^3 , $H^{3'}$, H^2 and $H^{2'}$), and a singlet at δ 4.28 ppm due to protons ($5H^1$, C_5H_5) in the unsubstituted Cp ring. The pyridinyl protons (H^9 and $H^{9'}$), on the other hand, resonated at 8.44 ppm as a doublet (J = 9 Hz). The peaks for the other pyridinyl protons, H^6 – H^8, resonated between 7.10 – 7.72 ppm.[16]

The ^{13}C NMR spectrum displayed peaks for all expected carbon atoms in the range 121.3 - 155.6 ppm for the carbon atoms in the pyridinyl rings, while the carbon atoms C^2 and C^3 in the substituted Cp ring resonated at 70.4 and 71.1 ppm, respectively. Finally, the carbon atoms ($5C^1$) in the unsubstituted Cp ring resonated at 70.2 ppm. The *ipso* carbon (C^4), however, did not appear in the spectrum. The lack of detection of this carbon is common in many substituted ferrocenyl compounds.[16b,c]

The electron impact ionisation mass spectrum (EI MS) displayed a molecular ion peak for ligand (**52**) at $[M]^+$ = 383.20 as a base peak (100% intensity). The infrared spectrum displayed the carbonyl stretching frequency at 1674 cm^{-1}, while the azomethine ν(C=N) stretching frequency was observed at 1567 cm^{-1}. Furthermore, the ν(C-C) and ν(C-H) stretching frequencies appeared, respectively, at 1435 and 3058 cm^{-1}. CHN analysis agreed with the calculated values for $C_{21}H_{17}N_3OFe$. The purity of the ligand was further confirmed by a relatively sharp melting point of 150 − 153 ºC. Full characterization data are listed in the experimental section, Chapter 7.

2.3.3 Characterization of cationic palladium complexes (**55**) – (**60**)

The cationic complexes were found to be stable and melting points by decomposition of 190 °C or above were obtained. Their colours changed from yellow or orange to black as they decomposed during heating for melting point determination. CHN elemental analysis confirmed the purity of the complexes. Full characterization data are shown in the experimental section, Chapter 7.

The neutral [PdMeCl(N^N)] precursors (**53**) and (**54**) were characterized by NMR, infrared spectroscopy, mass spectrometry and elemental analysis. Only ^{1}H NMR spectral analysis was performed on compound (**53**) as it displayed poor solubility in deuterated organic solvents, such as $CDCl_3$, C_6D_6 and D_6-DMSO. Confirmation of the formation of the complexes was observed from a shift of the imino-pyridinyl stretch and the carbonyl stretching frequencies. The ν(C=N) stretching frequencies were observed at 1600 cm^{-1} for compound (**53**) while two stretching frequencies, at 1632 and 1594 cm^{-1}, for compound (**54**) were observed. The carbonyl stretching frequencies ν(C=O) appeared at 1690 or 1656 cm^{-1} for compounds (**53**) or (**54**), respectively. The difference in ν(C=O) stretch when compared to ligand (**51**) is due to the difference in the ring size of the substituents, i.e. to the five- and six-membered rings in (**52**) and (**51**), respectively.[17] Smaller ring sizes cause a decrease in the angles of sp^2-hybridized atoms resulting in an increased stretching frequency.

^{1}H NMR spectra were measured and the influence of anions (BF_4^- or PF_6^-) and donor ligands (PPh_3 or MeCN) on the Pd-C*H*$_3$ protons was investigated. The presence of the acetonitrile group in complex (**56**) was confirmed by methyl protons resonating at δ 1.93 ppm while in complex (**55**) these methyl protons resonated at δ 2.05 ppm in deuterated acetone (these protons resonated at the same position as residual deuterated acetone). The same protons resonated at δ 2.53 for complex (**56**) in $CDCl_3$; compound (**55**), however, was not completely soluble in $CDCl_3$. ^{31}P NMR spectra for complexes (**57**) and (**58**) displayed phosphorus signals at δ 39.94 and a septet signal at -144.34 ppm which were assigned to the phosphorus atoms in triphenylphosphine and the hexafluorophosphate anion, respectively. In tolyl cationic complexes, the pyridinyl protons generally appeared in the range 6.80 – 8.78 ppm. A comparison of selected proton chemical shifts for the compounds prepared here is given in **Table 2.3.1.**

TABLE 2.3.1: Summary of chemical shifts for selected protons in ligands and palladium complexes. Unless otherwise indicated, the solvent was $CDCl_3$.

Compound	Chemical shift (ppm)			
	-(*H*)C=N-, H^{9}, $H^{9'}$ or H^{10}, $H^{10'}$	Pd-CH_3	^{31}P	N≡CCH_3
R = Tolyl				
(**51**), ligand	8.40[a], 8.16[b]			
(**53**)	9.02, 8.63	1.11		
(**55**)	8.76, 8.75[b]	1.05	-[c]	2.05
(**56**)	8.78, 8.40	1.01	-	2.53
(**56**)	8.72, 8.57[b]	0.96	-	1.93
(**57**)	8.78, 8.60	0.78	39.94	-[d]
(**58**)	8.60, 7.91	0.82	39.94	-
R = Fc				
(**52**), ligand	8.44[a]			
(**54**)	9.03, 8.67	1.13		
(**59**)	8.84, 8.50	1.12	-	2.52
(**60**)	8.60, 7.90	0.72	39.54	-

[a]Ligand only displayed one proton signal for this group in $CDCl_3$ also in acetone. [b]Sample analysed in acetone-d^6. [c]Compound does not contain triphenylphosphine group. [d]Compound does not contain acetonitrile group.

Upon complexation of ligand (**51**) when the cationic complexes were formed, loss of symmetry, which originally existed for the ligand, was noticed. The loss of symmetry resulted from the difference in electronic properties of the methyl- and donor-ligand-groups bonded to palladium. The pyridinyl protons appeared as two signals, each integrating for one hydrogen atom. The chemical shifts for H^9 and $H^{9'}$ shifted downfield in the cationic complexes when compared to protons in the ligand. The counter-ions did not display any effect on the resonance of methyl protons (Pd-CH_3) in the palladium complexes. The chemical shifts of the donor ligands and the Pd-CH_3 resonance protons were similar in all complexes. On the other hand, an effect on the Pd-CH_3 was found to be due to the donor ligands. The triphenylphosphine donor group showed a shielding effect, causing the methyl protons to resonate upfield around δ 0.80 ppm compared to a downfield shift at δ 1.05 ppm due to the acetonitrile ligand. The methyl protons in complex (**57**) and (**58**) both appeared as doublets with a coupling constant of J_{PH} = 3 Hz due to coupling of the methyl protons with the phosphorus atom in PPh_3.[18] The pyridinyl protons in ferrocenyl complexes (**59**) and (**60**) split into two signals compared to the original

ligand. The signals appeared in the range δ 7.00 – 8.84 ppm. The protons numbered $H^{9/9'}$ appeared as distinct signals at 8.84 and 8.50 ppm for compound (**59**) while for compound (**60**) the protons resonated at 8.60 and 7.90 ppm. The $H^{9/9'}$ protons for the ligand (**52**) resonated at δ 8.44 ppm. Methyl protons for Pd-CH_3 appeared at 1.12 ppm for compound (**59**) and at δ 0.72 ppm for compound (**60**). Again, the protons in Pd-CH_3 appeared as a doublet (J_{PH} = 3 Hz) for compound (**60**) due to coupling of these protons with the phosphorus atom in PPh_3. Broad signals were observed in the ferrocenyl region between 3.99 and 4.43 ppm for the complexes (**59**) and (**60**). The broadening of these peaks has been attributed to the fluxional behaviour of the ferrocenyl group which has been observed in many substituted ferrocenyl compounds.[19]

Density Functional Theory calculations allowed for the determination of electron density in complexes (**55**) and (**57**) and confirmed the behaviour of the observed chemical shifts in the ^{1}H NMR spectra (see **Figure 2.3.4**).

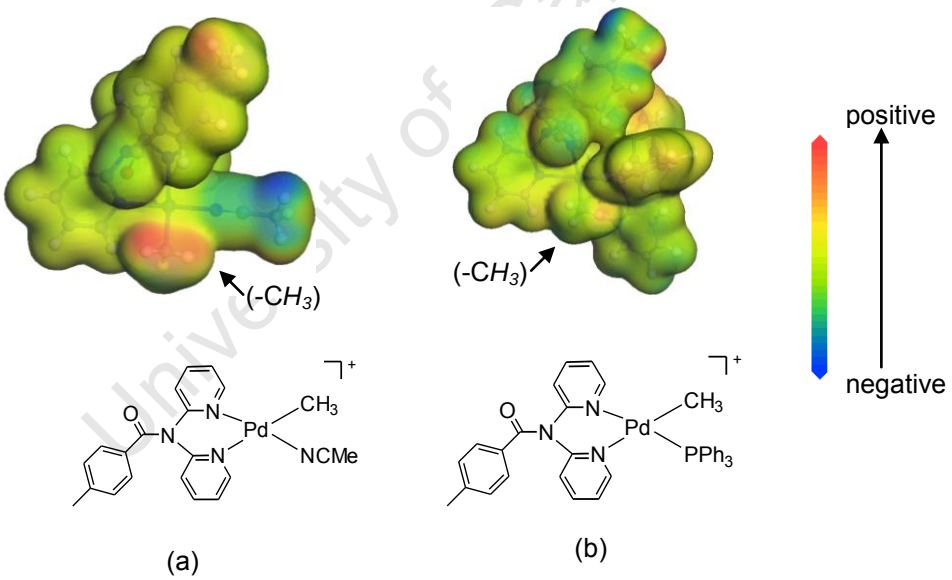

FIGURE 2.3.4: DFT calculations for determination of the electron density for simulated palladium complexes: (a) $[PdMe(N\text{^}N)(MeCN)]^+$ (**55**), (b) $[PdMe(N\text{^}N)(PPh_3)]^+$ (**57**). Red-yellow indicates the electrophilic regions and green-blue the nucleophilic regions.

The Pd-CH_3 protons of compound (**55**) displayed an electrophilic environment, explaining the downfield shift in the ^{1}H NMR spectrum of compound (**55**). On the other hand, methyl protons in complex (**57**), which are nucleophilic, appeared upfield in the ^{1}H NMR spectrum. In addition, the resonances of PdCH_3 shifts for complexes (**55**) and (**57**) could also have been as a result of the shielding effect of bulky PPh_3

when compared to acetonitrile. Typical ^{1}H, ^{13}C and ^{31}P NMR spectra obtained for complex (**57**) are shown in **Figure 2.3.5,** and the ^{1}H and ^{13}C NMR spectra for complex (**56**) are shown in **Figure 2.3.6.**

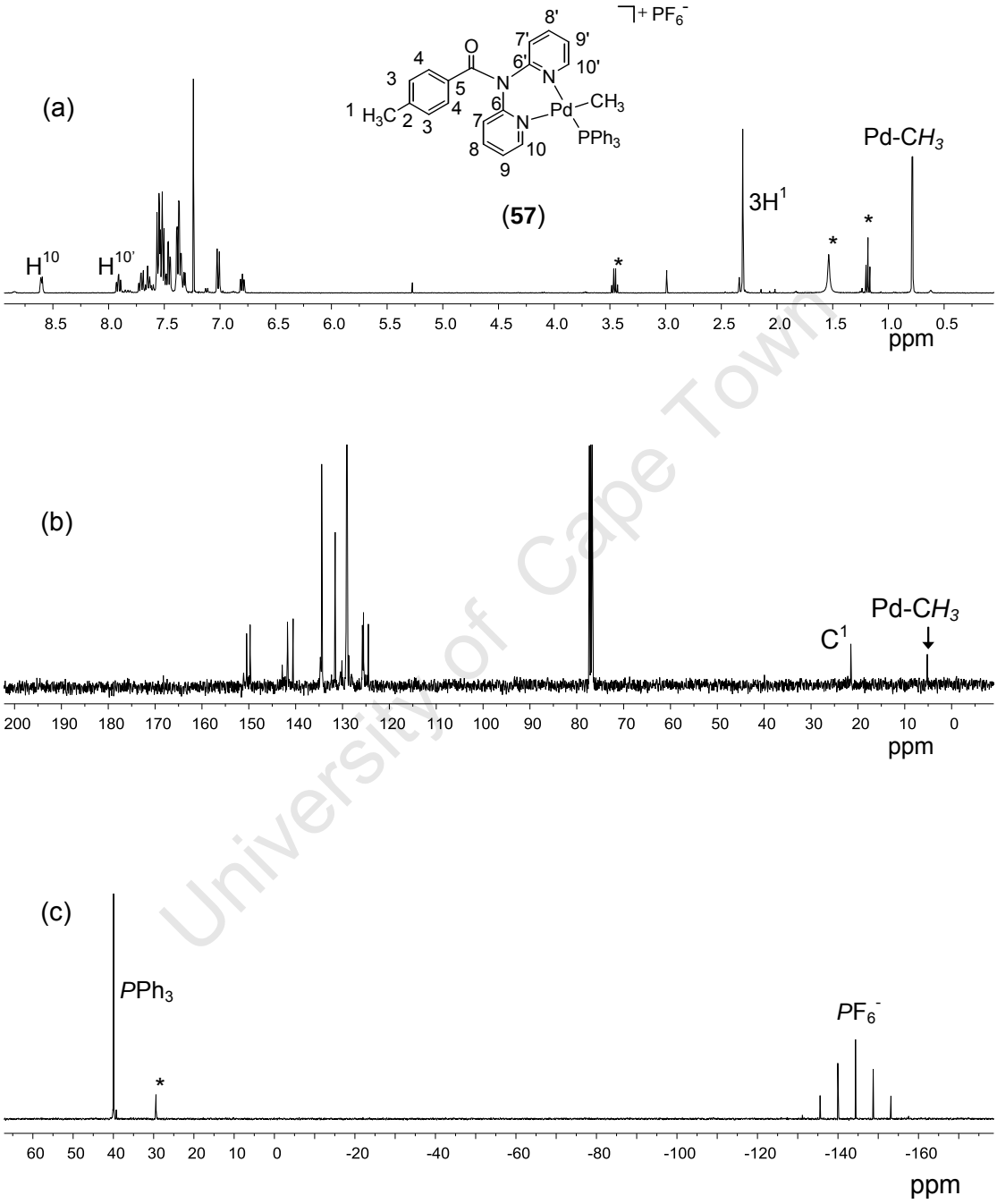

FIGURE 2.3.5: The NMR spectra of compound (**57**) in $CDCl_3$: (a) ^{1}H spectrum, (b) ^{13}C spectrum and (c) ^{31}P spectrum. Assignment of selected resonances is illustrated. *Impurities: residual solvent (H_2O) and Et_2O in (a), triphenylphosphine oxide in (c).

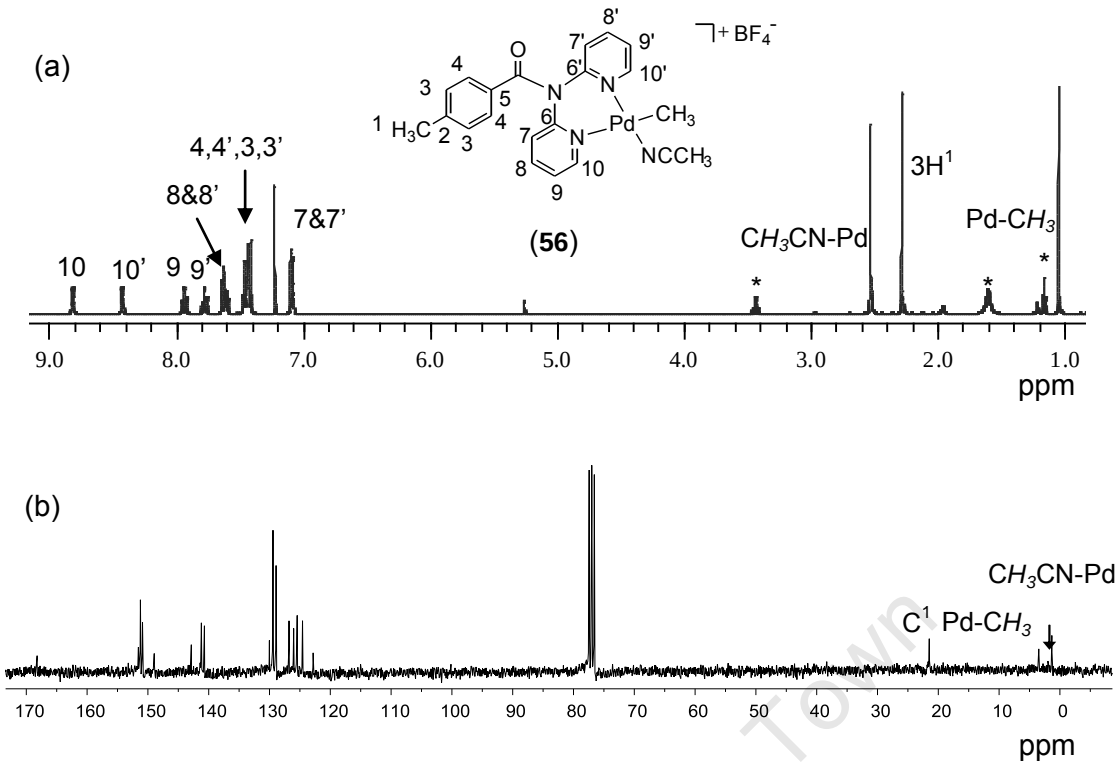

FIGURE 2.3.6: The NMR spectra of compound (**56**) in $CDCl_3$: (a) ^{1}H spectrum and (b) ^{13}C spectrum. Assignment for selected resonances is illustrated. * Solvent impurity.

The molecular weights of compounds were determined by Electron Spray Ionization Mass Spectrometry (ESI MS). All cationic complexes displayed [M - counter anion]$^{+}$ as the major peak (with 100 % intensity) when the spectra were recorded in a positive ion mode. For example, complexes (**55**) and (**56**), with the neutral acetonitrile ligand, showed fragmentation ions at *m/z* 451.00 [PdMe(N^N)(MeCN)]$^{+}$ for the fragment after the BF_4^- or PF_6^- counter ions were lost. The chemical structure of the fragment is illustrated in **Figure 2.3.7**. The decomposition behaviour was not unexpected since there is only a weak intermolecular interaction between the counter ion and palladium complex.[20]

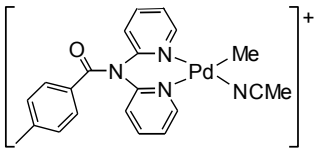

m/z 451.00

FIGURE 2.3.7: Main fragment-ion observed in mass spectra of complexes (**55**) and (**56**).

The mass spectral analysis of complexes (**57**) and (**58**) stabilized with neutral triphenyphosphine showed similar fragmentation when compared to compounds (**55**)

and (**56**). However, in addition to the main fragment-ion, a peak at *m/z* 672.06 (80%) in complexes (**57**) and (**58**) was observed. The signal was assigned to $[PdMe(N\text{^}N)(PPh_3)]^+$. The fragment-ions at *m/z* 528.03 (8%) and 470.02 (2%) and were also observed for complexes (**57**) and (**58**). The signals corresponded, respectively, to $[PdMe(PPh_3)(BF_4)]^+$ and $[PdMe(PPh_3)(PF_6)]^+$.Furthermore, both compounds showed a fragment-ion at *m/z* 383.12 (100%) which was attributed to $[PdMe(PPh_3)]^+$. Chemical structures representing the *m/z* values observed in the mass spectra of complexes (**57**) and (**58**) are shown in **Figure 2.3.8**.

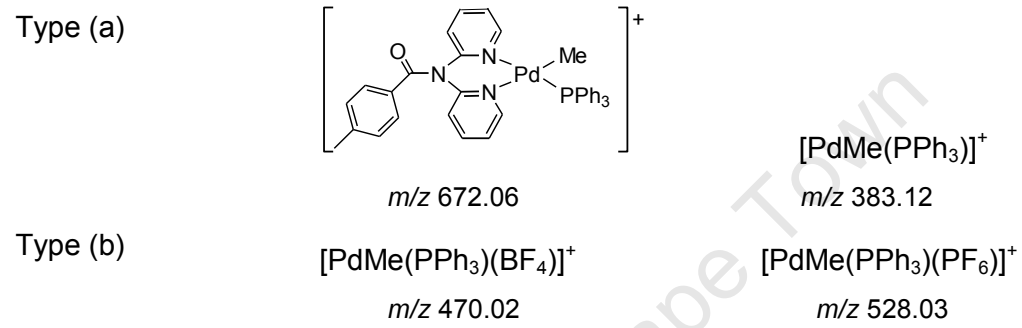

FIGURE 2.3.8: Proposed main fragmentation ions observed in mass spectral analysis: Type (a) appear in spectra of both complexes (**57**) and (**58**); Type (b) appear in spectra of complex (**58**) and (**57**), respectively.

The fragmentation behaviour confirmed the stability of these complexes that were stabilized by the strong π-acceptor (triphenylphosphine) compared to those stabilized by the weak π-acceptor (acetonitrile) ligands. The negative mode analysis, on the other hand, confirmed the presence of the BF_4^- counter ion at *m/z* 87.00 (100% intensity) for complexes (**56**) and (**58**), while the PF_6^- counter ion at *m/z* 145.00 (100% intensity) was observed for complexes (**55**) and (**57**). The positive and negative mode analysis confirmed the formation of the respective cationic palladium complexes.

A similar fragmentation pattern was observed in the mass spectra of the ferrocenyl analogues (**59**) and (**60**) when compared to the tolyl analogues (**55**) – (**58**). In this case, the main peaks were those of $[PdMe\{(C_5H_5)Fe(C_5H_4)C(O)N(C_5H_4N)_2(L)]^+$, which appeared at *m/z* 545.00 and 767.00 for compounds (**59**) and (**60**), respectively. In addition, a peak at *m/z* 185.00 was attributed to the ferrocenyl fragment.

The infrared spectra of the complexes of the tolyl analogues (**55**) – (**58**) displayed a shift to lower wavenumbers of the ν(C=N) stretching frequency compared to the free ligand (**51**). The peaks appeared as broad signals, suggesting that there might have been two bands which were not clearly resolved. Ideally, two bands appearing at different stretching frequencies would be expected due to the difference in the electronic properties of the *trans* atoms.

The pyridinyl-azomethine (C=N) vibration, however, did not differ significantly in all the tolyl complexes. On the other hand, the ν(C=O) stretching frequency shifted to higher wavenumbers in complexes compared to the free ligand. The IR spectra of complexes displayed a ν(C=N) stretch in the range 1598 – 1609 cm^{-1}, while the ν(C=O) stretching frequency was observed in the range 1669 – 1690 cm^{-1}.

The similarity in ν(C=N) stretching frequencies for the complexes suggested that there was no major influence of anions or donor ligands on the imine bond in the complexes. The carbonyl stretching frequency of the complexes containing the PF_6^- anion appeared at 1690 and 1675 cm^{-1} for compounds (**55**) and (**57**), respectively. Compounds (**56**) and (**58**), containing the BF_4^- anion, showed the ν(C=O) stretching frequency at 1686 and 1669 cm^{-1}, respectively.

Interestingly, the carbonyl vibration frequency shifted to much higher values for complexes (**55**) and (**56**) (containing the MeCN ligand) than for complexes (**57**) and (**58**) (containing the PPh_3 ligand). The behaviour confirms that variation in the ligand properties did affect the carbonyl group, thus suggesting an electronic interaction and ultimately a communication between these groups. The data displaying comparisons of IR stretching frequencies of various groups for the complexes prepared here are summarized in **Table 2.3.2**.

The IR spectra of complexes (**55**) and (**56**), which contain a neutral acetonitrile donor ligand, each exhibited two bands: at 2232 and 2306 cm^{-1} in complex (**55**) and at 2297 and 2328 cm^{-1} in complex (**56**). The bands correspond to the asymmetric and symmetric ν(C≡N) stretching frequencies. Similar stretching frequencies have been observed in related complexes containing the acetonitrile donor ligand.[21]

TABLE 2.3.2: Summary of IR stretching frequencies for selected functional groups in palladium complexes

Compound, anion	Stretching frequency ν (cm^{-1}) of the functional group		
	C=N	C=O	C≡N
R = Tolyl			
(**51**)[a]	1609	1656	
(**53**), neutral[b]	1600	1690	
(**55**), PF_6^-	1602	1690	2232, 2306
(**56**), BF_4^-	1598	1686	2328, 2297
(**57**), PF_6^-	1604	1675	-[c]
(**58**), BF_4^-	1602	1669	-
R = Fc			
(**52**)[a]	1567	1674	
(**54**), neutral[b]	1632	1656	
(**59**), PF_6^-	1632	1667	2331, 2302
(**60**), PF_6^-	1658	1710	-

[a]Ligand. [b]PdMeCl(N^N). [c]Compounds do not contain acetonitrile group but triphenylphosphine as a donor ligand.

The IR spectra of the ferrocenyl analogues displayed broad peaks attributed to the stretch of azomethine bond at 1632 and 1658 cm^{-1} for compounds (**59**) and (**60**), respectively. The azomethine stretch of ligand (**52**) appeared at 1567 cm^{1}. The stretching frequency of the carbonyl group shifted to lower wavenumber (1667 cm^{-1}) for compound (**59**) and a shift to higher wavenumber (1710 cm^{-1}) was observed for compound (**60**), compared to the ν(C=O) of the ligand at 1674 cm^{-1}. The observed shifts were attributed to the effect of electronic properties of the donor ligands. The IR spectra of complexes (**55**), (**57**) and (**60**) are shown in **Figure 2.3.9.**

The complexes were further characterized using cyclic voltammetry to investigate the effect of the donor ligands on the ferrocenyl moiety. The ferrocenyl group in complex (**60**) (with PPh_3 donor ligand) ($E_{1/2}$ = 546 mV) was more difficult to oxidise when compared to the ferrocenyl group in compound (**59**) (with acetonitrile donor ligand) ($E_{1/2}$ = 528 mV). Cyclic voltammograms of ferrocenyl compounds are shown in **Figure 2.3.10** while the electrochemical data are summarized in **Table 2.3.3**.

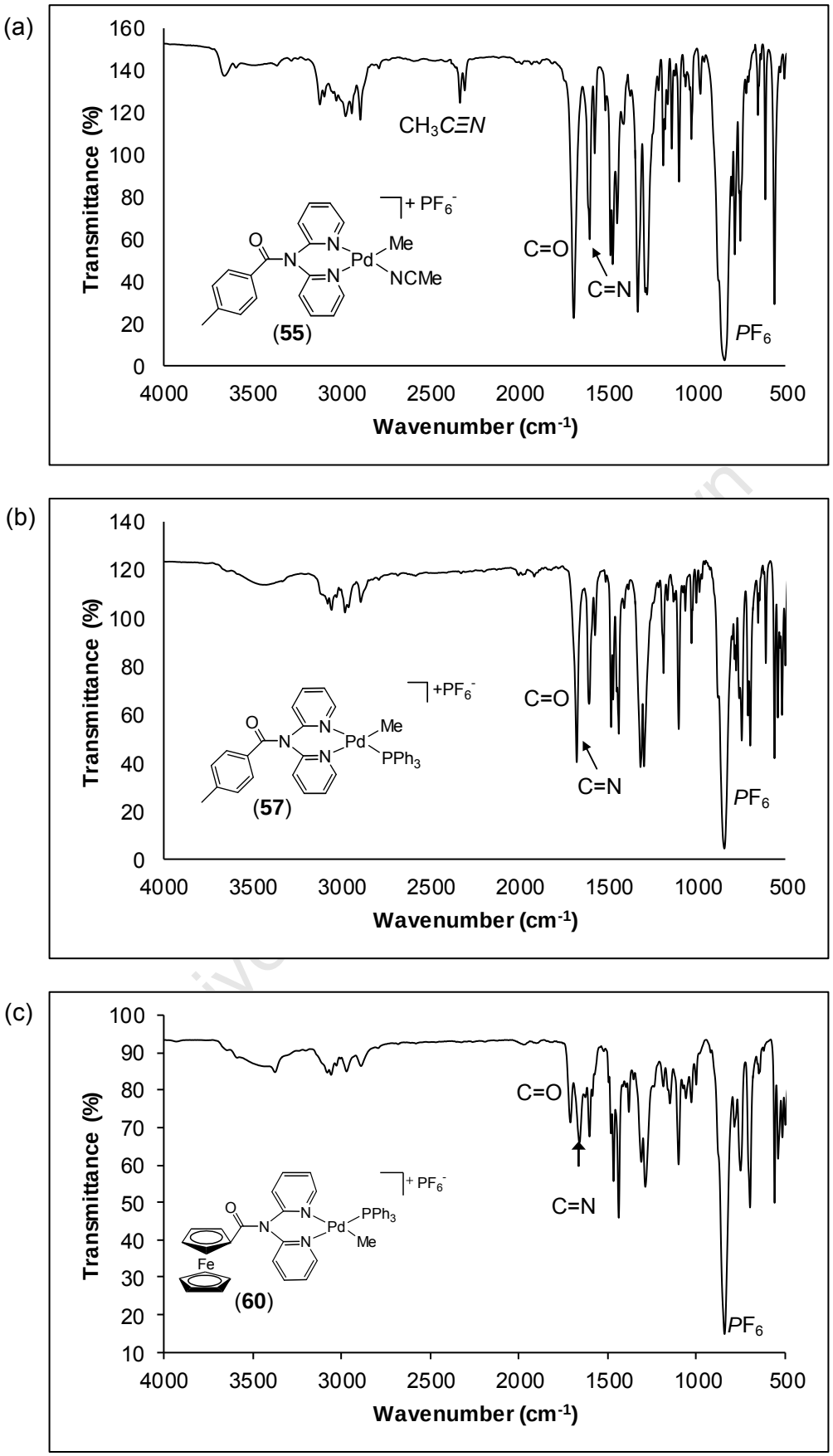

FIGURE 2.3.9: The solid state Infrared spectra (KBr discs) of compounds; (a) (**55**), (b) (**57**) and (c) (**60**). The assignment for vibration frequencies of selected functional groups is shown.

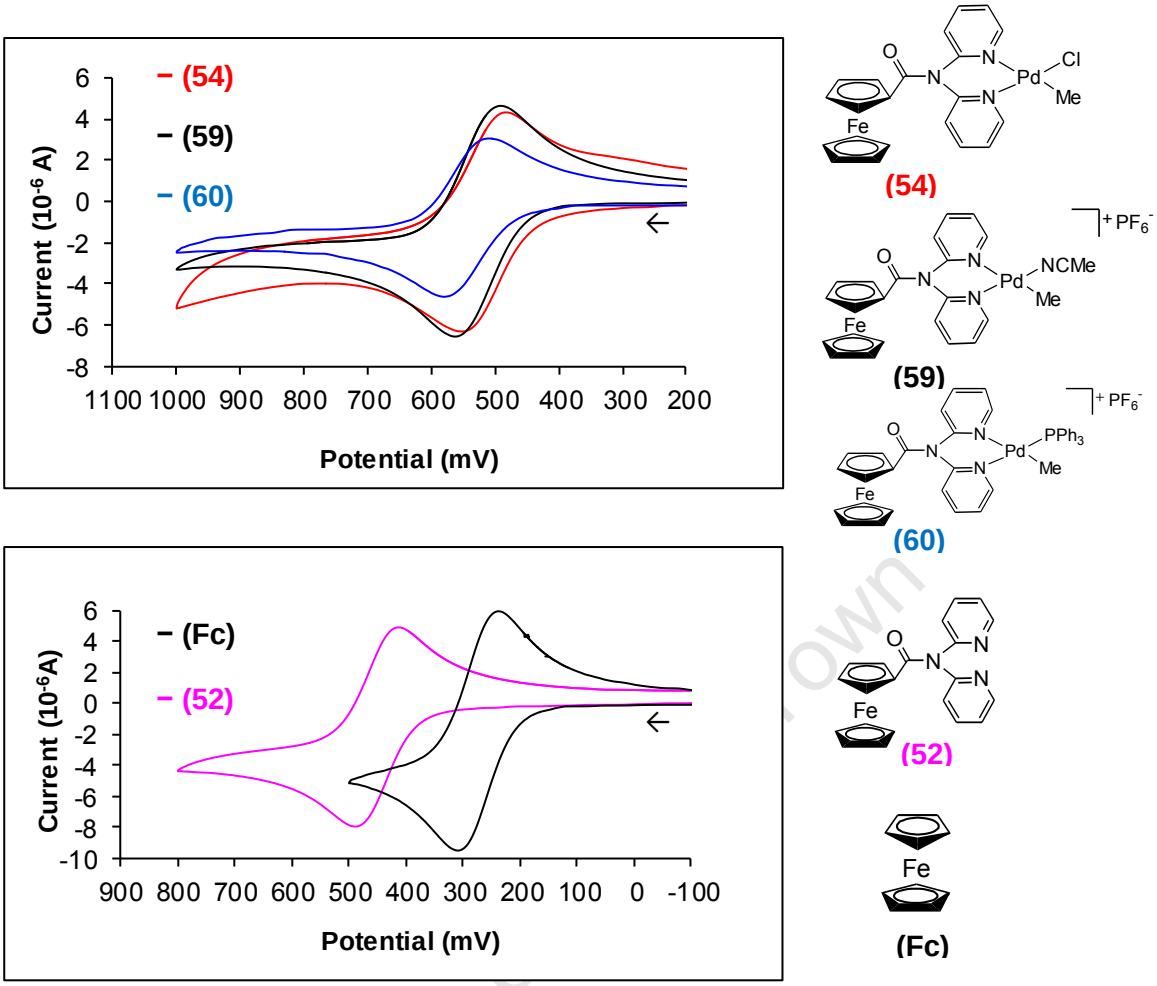

FIGURE 2.3.10: Comparison of cyclic voltammograms of ferrocenyl compounds (1.5 mM) in dichloromethane. The potential is referenced to Ag/Ag^+ (see Experimental).

TABLE 2.3.3: Electrochemical data (mV vs. Ag/Ag^+) for the ferrocenyl redox couple in ferrocenyl compounds in dichloromethane solution (1.5 mM); scan rate 100 mV/s

Compound	E_{pa} (mV)	E_{pc} (mV)	ΔE_p(mV)[a]	$E_{1/2}$(mV)[b]	[c]$\Delta E_{1/2}$(mV)
(**Fc**)	308	241	67	274	0
(**52**)	482	414	68	448	+173
(**54**)	548	485	63	517	+242
(**59**)	564	492	62	528	+254
(**60**)	581	510	71	546	+272

[a]$\Delta E_p = E_{pa} - E_{pc}$, [b]$E_{1/2} = (E_{pa} + E_{pc})/2$, precision of data is ±5 mV. [c]$\Delta E_{1/2} = E_{1/2}$compound $- E_{1/2}$Fc

The redox behaviour of the ferrocenyl group in the complexes was attributed to be due to the influence of the difference in electronic properties of donor atoms (Phosphorus in triphenylphosphine or Nitrogen in acetonitrile) on the palladium

centre. The strong electronic interaction between Pd(II) centre which is a *soft-acid* and phosphorus atom which is a *soft-base* resulted in the electron-withdrawing effect. On the other hand, the nitrogen atom (which is a *hard-base*), displayed an electron-donating effect. Both cationic complexes were found to be difficult to oxidize when compared to oxidation potential of ferrocene ($E_{1/2}$ = 274 mV) or the ligand (**52**) ($E_{1/2}$ = 448 mV). The difference in $E_{1/2}$ values of the (Fc/Fc^{+}) redox couple in the complexes confirmed the communication of the ligand groups (PPh_3 or MeCN) through the Pd centre with ferrocenyl moiety. The redox effect on ferrocenyl group was also noted on neutral palladium complex (**54**) (containing chlorine ion) in which $E_{1/2}$ of (Fc/Fc^{+}) was 517 mV. Chloride ion, same as nitrogen is a *hard-base* thus will be expected to display electron donating behaviour, however, since complex (**59**) is cationic, the observed redox behaviour of ferrocenyl group on the complexes is expected, as it would be difficult to withdraw an electron from electron-deficient a cationic species.

2.3.4. Crystallographic characterization of compounds (**57**) and (**60**)

Crystals suitable for X-ray diffraction analysis were obtained for cationic complexes (**57**) and (**60**). The full crystal refinement data including the cif files are presented on the CD-Rom in the Appendix section. Crystals suitable for X-ray analysis were obtained through recrystallization from a mixture of dichloromethane and hexane for complex (**57**). The molecular structure of compound (**57**) is shown in **Figure 2.3.11**.

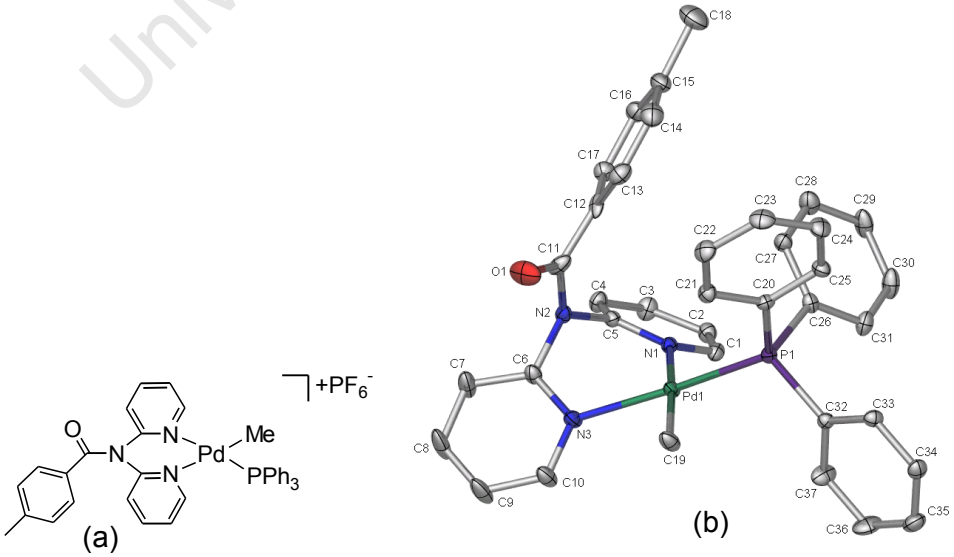

FIGURE 2.3.11: The structures of compound (**57**): (a) chemical structure, and (b) molecular structure of the complex. Hydrogen atoms and PF_6^- counter-ion are omitted for clarity.

As in the case of many palladium complexes containing a similar *N*,*N*-bipyridinyl ligand, a six-membered ring involving the palladium ion formed a distorted chair-like structure (*cf*. geometric conformations of cyclohexane).[17] The two pyridinyl rings appeared tilted in opposite directions. Details of the crystal and structure refinement data are summarised in **Table 2.3.4,** while selected bond lengths and bond angles are shown in **Table 2.3.5.** The compound crystallized in the monoclinic, $P2_1/c$ space group and the following bond angles around the metal centre were in the range 85 - 100º: N(1)-Pd(1)-N(3), C(19)-Pd(1)-P(1), P(1)-Pd(1)-N(1) and C(19)-Pd(1)-N(3), while those of C(19)-Pd(1)-N(1) and P(1)-Pd(1)-N(3) were 173 and 172º, respectively. These bond angles confirmed a distorted square-planar geometry around the palladium centre similar to other Pd(II) complexes reported in the literature.[16a] The Pd(1)-P(1) bond length found of 2.2235(14) Å was comparable to similar complexes reported in the literature.[22] The palladium-nitrogen bond lengths did not differ significantly. However, the Pd-N(3) bond length for the nitrogen atom *trans* to the phosphorus atom was slightly shorter than the Pd-N(1) bond length for the nitrogen atom *trans* to the methyl group.

TABLE 2.3.4: Crystal and structure refinement data for compound (**57**)

Empirical formula	$C_{37}H_{33}F_6N_3OP_2Pd$	
Formula weight	818.04	
Temperature	173(2) K	
Crystal system	Monoclinic,	
Space group	$P2_1/c$	
Unit cell dimensions	a = 10.6052(12) Å	α = 90º
	b = 23.346(3) Å	β = 109.080(3)º
	c = 15.341(2) Å	γ = 90º
Volume	3589.6(8) Å^3	
Z	4	
Crystal size	0.18 x 0.16 x 0.14 mm	
Reflections collected / unique	43920 / 8917 [R(int) = 0.0772]	
Absorption coefficient	0.672 mm^{-1}	
Goodness-of-fit on F^2	1.035	
Final R indices [I>2sigma(I)]	R_1 = 0.0652, wR_2 = 0.1454	
R indices (all data)	R_1 = 0.1011, wR_2 = 0.1624	

TABLE 2.3.5: Selected bond lengths (Å) and angles (º) for the cationic palladium complex (**57**)

Bond angles		**Bond lengths**	
Atoms	Angle (º)	Atoms	Length (Å)
C(19)-Pd(1)-N(3)	89.8(2)	Pd(1)-C(19)	2.047(6)
C(19)-Pd(1)-P(1)	84.78(16)	Pd(1)-P(1)	2.2235(14)
C(19)-Pd(1)-N(1)	173.2(2)	Pd(1)-N(3)	2.141(4)
P(1)-Pd(1)-N(1)	100.27(12)	Pd(1)-N(1)	2.158(4)
P(1)-Pd(1)-N(3)	171.78(13)	N(1)-C(1)	1.346(7)
N(1)-Pd(1)-N(3)	85.67(16)	N(1)-C(5)	1.336(6)
C(6)-N(2)-C(5)	114.7(4)	N(3)-C(10)	1.336(7)
N(2)-C(11)-C(12)	120.6(5)	N(3)-C(6)	1.344(7)
N(2)-C(11)-O(1)	118.3(6)	C(11)-C(12)	1.435(9)
C(12)-C(11)-O(1)	121.0(6)	C(11)-O(1)	1.218(7)
		C(11)-N(2)	1.391(7)

This small difference in the Pd-N(3) and Pd-N(1) bond lengths was not surprising since the *trans* Pd-P(1) bond is a coordination type which is weaker than the sigma Pd-C(19) bond. As expected, the carbonyl oxygen atom did not coordinate to the metal centre. Most palladium complexes with nitrogen donor atoms have been found to display bond lengths ranging from 2.10 – 2.20 Å for the Pd-N bond with nitrogen atom *trans* to a methyl group.[18c, 20a,b] Generally Pd-C bond lengths in the range 2.02 – 2.09 Å have been observed and the Pd-C(19) distance found here falls in the middle of this range.[23]

Single crystals of the ferrocenyl compound (**60**) suitable for X-ray crystallography were also obtained from slow diffusion of hexane into a dichloromethane solution. The compound crystallized in a monoclinic system in the $P2_1/n$ space group was observed. The molecular structure of complex (**60**) is shown in **Figure 2.3.12**. The crystal refinement data are illustrated in **Table 2.3.6** while the selected bond angles and bond lengths are shown in **Table 2.3.7**. The structure of compound (**60**) for the N^N donor site was similar to that of compound (**57**) and the bond lengths around C(11) were also similar to those observed in complex (**57**).

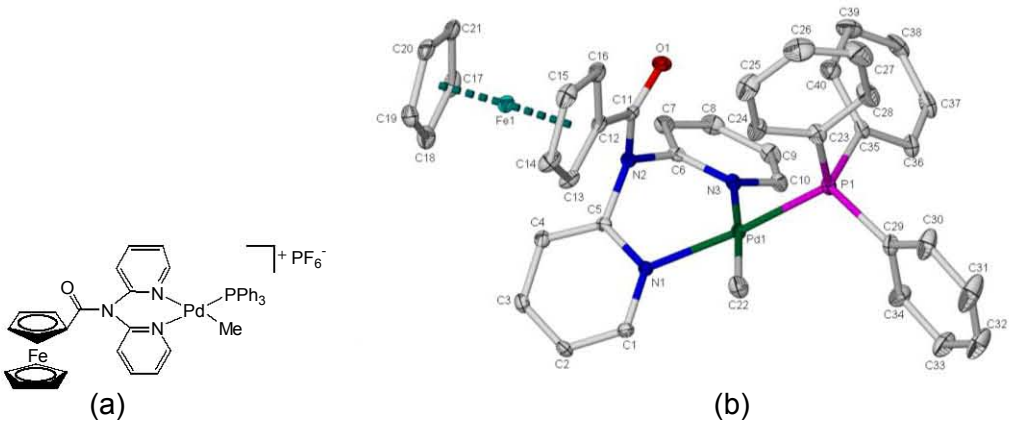

(a) (b)

FIGURE 2.3.12: The structures of compound (**60**): (a) chemical structure, and (b) molecular structure of the complex. Hydrogen atoms and PF_6^- counter-ion are omitted for clarity.

TABLE 2.3.6: Crystal and structure refinement data for compound (**60**)

Empirical formula	$C_{40}H_{35}F_6N_3OP_2FePd$	
Formula weight	911.90	
Temperature	173(2) K	
Crystal system	Monoclinic	
Space group	$P2_1/n$	
Unit cell dimensions	a = 15.8450(13) Å	α = 90º
	b = 8.5116(6) Å	β = 96.807(2)º
	c = 27.783(2) Å	γ = 90º
Volume	3720.5(5) $Å^3$	
Z	4	
Crystal size	0.22 x 0.14 x 0.02 mm	
Reflections collected / unique	9282 / 6818 [R(int) = 0.0772]	
Absorption coefficient	1.027 mm^{-1}	
Goodness-of-fit on F^2	0.999	
Final R indices [I>2sigma(I)]	R_1 = 0.0323, wR_2 = 0.0612	
R indices (all data)	R_1 = 0.0584, wR_2 = 0.0691	

TABLE 2.3.7: Selected bond lengths (Å) and angles (º) for cationic palladium complex (**60**)

Bond angles		**Bond lengths**	
Atoms	Angle (º)	Atoms	Length (Å)
C(22)-Pd(1)-P(1)	86.87(8)	Pd(1)-C(22)	2.024(3)
C(22)-Pd(1)-N(1)	90.48(10)	Pd(1)-P(1)	2.2342(7)
C(22)-Pd(1)-N(3)	173.26(10)	Pd(1)-N(1)	2.1365(3)
P(1)-Pd(1)-N(1)	172.21(5)	Pd(1)-N(3)	2.160(2)
P(1)-Pd(1)-N(3)	98.88(5)	N(1)-C(1)	1.3342(3)
N(1)-Pd(1)-N(3)	85.67(16)	N(1)-C(5)	1.346(3)
C(6)-N(2)-C(5)	115.39(19)	N(3)-C(10)	1.345(7)
C(12)-C(11)-O(1)	121.4(2)	N(3)-C(6)	1.335(7)
N(2)-C(11)- O(1)	117.9(2)	C(11)-C(12)	1.478(4)
N(2)-C(11)- C(12)	120.6(2)	C(11)-O(1)	1.214(3)
		C(11)-N(2)	1.402(3)

The bond lengths between Pd(1) and the following atoms: N(1), N(3), P(1) and C(22), were similar to those observed in the molecular structure of complex (**57**). The Pd(1)-C(22) bond length in complex (**60**) was slightly smaller when compared to the corresponding bond length observed in complex (**57**); these bond lengths were 2.047(6) and 2.024(3) Å for complexes **(57**) and (**60**), respectively. The bond angles around the palladium centre displayed distorted square-planar geometry. The two cyclopentadienyl rings of the ferrocenyl group displayed an eclipsed form and were approximately parallel to each other. The bond distances between the Fe(1) and the cyclopentadienyl carbon atoms were found to be in a range 2.053(3) – 2.046(3) Å. The bond length of 2.053(3) Å for Fe(1)-C(21) was found to be the longest of all Fe-C distances.

2.4 Catalyst precursors utilized for functionalization of the lactide

2.4.1 Palladacycle complex (**63**) *for C-C coupling reaction*

Palladacycles prepared by aromatic C-H bond activation have been reported to be active catalyst precursors for C-C coupling reactions, particularly of the Heck- and

Suzuki-type reactions.[24] In the vast majority of these cases the palladacycles serve as a reservoir of catalytically active Pd(0) species. For this reason, the cationic palladacycle (**63**) was prepared and used for the coupling reaction of 4-bromobenzyl alcohol with an alkenyl group [(COP)-CH=CH-Ph] (COP = copolymer), in the CO/styrene copolymer tail. It was anticipated that the cationic complex would enable coordination of the alkenyl group to the metal centre.

The Schiff base ligand (**61**) was firstly prepared by acid-catalysed reaction (of benzophenone and *N*,*N*-dimethyl-ethane-1,2-diamine).[25] Palladacycle (**62**) was then prepared by treatment of the ligand with Na_2PdCl_4 (or Li_2PdCl_4 was also used) in the presence of sodium acetate in dry methanol as a solvent under nitrogen atmosphere. Finally, the neutral palladium chloride complex (**62**) was reacted with silver tetrafluoroborate to form the desired cationic palladacycle catalyst precursor (**63**). The procedure is outlined in **Figure 2.4.1.**

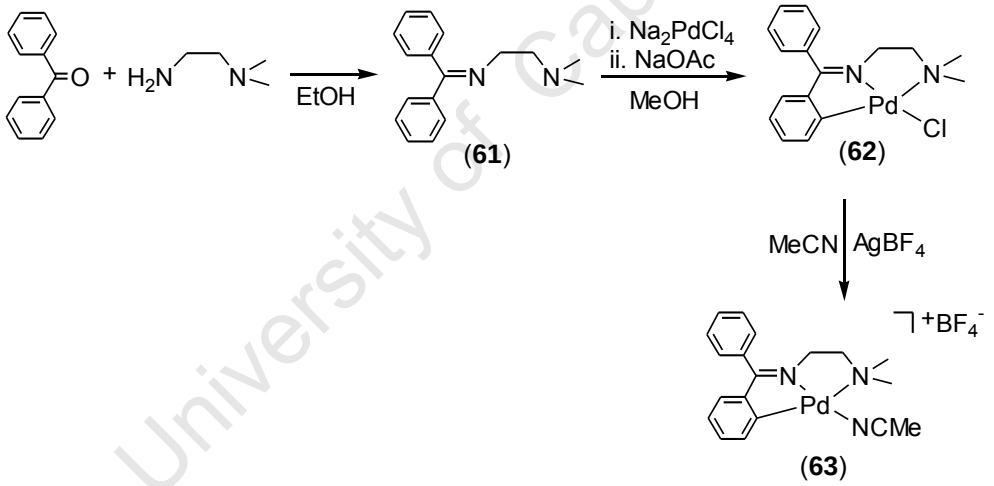

FIGURE 2.4.1: The reaction route for the preparation of cationic palladacycle (**63**).

The ^{1}H NMR spectrum of (**61**) displayed the expected peaks: aromatic protons resonated between δ 7.12 – 7.76 ppm, the amino methyl protons [$N(CH_3)_2$] appeared at 2.19 ppm, while the methylene protons resonated at 3.49 ppm (=N-CH_2-CH_2NMe_2) and 2.60 ppm (=NCH_2-CH_2-NMe_2). After C-H bond activation was complete, a downfield shift of aliphatic protons was observed. In the cationic palladacycle compound (**63**) the methylene signals resonated at δ 3.70 and 2.85 ppm, while the amino methyl protons appeared at 2.78 ppm. In addition, the signal attributed to the coordinated acetonitrile resonated at 2.62 ppm. Splitting of the aromatic protons was

also observed. Furthermore, the total number of protons in the aromatic region integrated for nine protons, confirming that C-H bond activation was successful.

The shift of the imine bond stretch ν(C=N) to lower frequency at 1604 cm^{-1} for complex (**63**) when compared to that of the ligand (**61**) at 1658 cm^{-1} also confirmed coordination of the imine-nitrogen to the palladium ion. Of particular interest, the ^{13}C NMR spectrum showed that the aromatic carbon was bonded to palladium, as the atom resonated at δ 157.1 ppm, similar to other cyclopalladated complexes.[26] Further characterization using elemental analysis confirmed the formation of palladacyle (**63**). Full details are shown in the experimental section in Chapter 7.

Single crystals suitable for X-ray crystallography were obtained from slow diffusion of hexane into a dichloromethane solution. The molecular structure of palladium complex (**63**) is shown in **Figure 2.4.2.** The compound crystallized in the triclinic system with a *P*-1 space group. Crystal structure refinement data are represented in **Table 2.4.1** while selected bond lengths and bond angles are shown in **Table 2.4.2**.

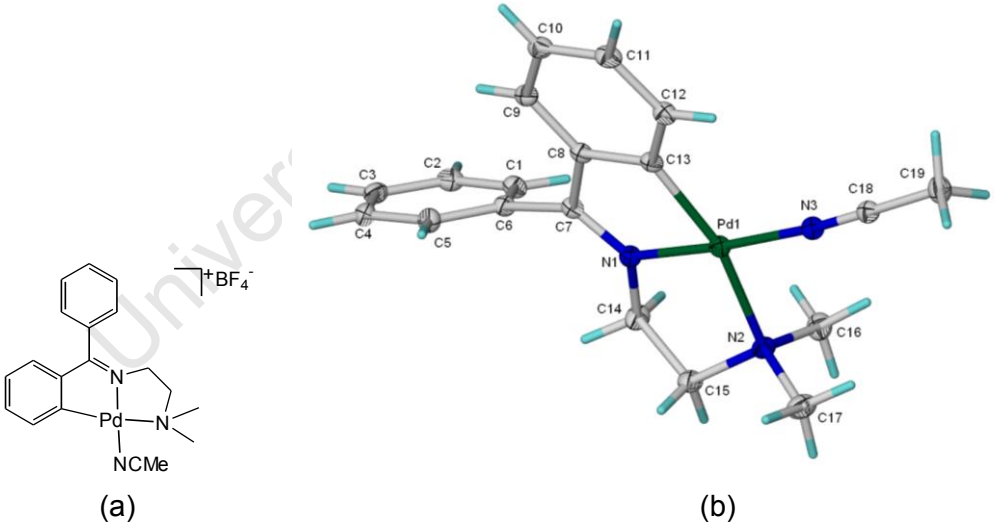

(a) (b)

FIGURE 2.4.2: The structures of compound (**63**): (a) chemical structure, and (b) molecular structure of the complex. The BF_4^- counter-ion is omitted for clarity.

The following *cis* bond angles around the palladium centre were observed: 81.16(10)º for C(13)-Pd(1)-N(1), 83.20(9)º for N(1)-Pd(1)-N(2), 99.24(9)º for N(2)-Pd(1)-N(3) and 96.61(10)º for N(3)-Pd(1)-C(13). In addition, the following *trans* bond angles were observed: 163.87(10)º for N(2)-Pd(1)-C(13) and 175.84(9)º for N(1)-Pd(1)-N(3).

TABLE 2.4.1: Crystal and structure refinement data for compound (**63**)

Empirical formula	$C_{19}H_{22}BF_4N_3Pd$	
Formula weight	485.61	
Temperature	173(2) K	
Crystal system	Triclinic	
Space group	*P*-1	
Unit cell dimensions	*a* = 9.2266(3) Å	α = 110.936(2)º
	b = 10.5143(4) Å	β = 99.171(2)º
	c = 11.2312(4) Å	γ = 92.067(2)º
Volume	999.46(6) $Å^3$	
Z	2	
Crystal size	0.16 x 0.15 x 0.13 mm	
Reflections collected / unique	4942 / 3994 [*R*(int) = 0.0367]	
Absorption coefficient	0.973 mm^{-1}	
Goodness-of-fit on F^2	1.049	
Final *R* indices [*I*>2sigma(*I*)]	R_1 = 0.0359, wR_2 = 0.0845	
R indices (all data)	*R*1 = 0.0520, wR_2 = 0.0915	

TABLE 2.4.2: Selected bond lengths (Å) and angles (º) for the cationic palladium complex (**63**)

Bond angles		**Bond lengths**	
Atoms	Angle (º)	Atoms	Length (Å)
N(1)-Pd(1)-C(13)	81.16(10)	Pd(1)-C(13)	1.989(3)
N(1)-Pd(1)-N(3)	175.84(9)	Pd(1)-N(1)	1.966(2)
C(13)-Pd(1)-N(3)	96.61(10)	Pd(1)-N(3)	2.015(2)
N(1)-Pd(1)-N(2)	83.20(9)	Pd(1)-N(2)	2.177(2)
C(13)-Pd(1)-N(2)	163.87(10)	N(2)-C(16)	1.484(4)
N(3)-Pd(1)-N(2)	99.24(9)	N(2)-C(15)	1.491(4)
C(7)-N(1)-C(14)	125.8(2)	N(3)-C(18)	1.132(4)
C(14)-N(1)-Pd(1)	115.65(18)	C(6)-C(7)	1.481(4)
C(17)-N(2)-C(16)	108.36(3)	C(7)-C(8)	1.476(4)
C(15)-N(2)-Pd(1)	102.29(17)	C(8)-C(13)	1.410(4)
C(18)-N(3)-Pd(1)	171.7(2)	C(18)-C(19)	1.457(4)
N(3)-C(18)-C(19)	178.9(3)		

These bond angles suggested a distorted square-planar geometry for the palladium complex. A bond length of 1.989(3) Å was observed for Pd(1)-C(13), while a bond length of 2.015 Å for Pd(1)-N(3) for the coordinated acetonitrile was observed. The bond lengths were comparable to those observed in similar complexes.[27,28]

2.4.2 Ligand (**65**) *for stabilization of a zinc complex utilized in ring-opening polymerization of lactide in a functionalization reaction*

The use of ferrocenyl hydroxyl derivatives for *in situ* stabilization of diethylzinc has been employed in asymmetric catalysis for the reduction of aldehydes.[29] The authors suggested the formation of a seven-membered ring for the ethylzinc complex [Zn(CH_2CH_3)(N^O)] (see **Figure 2.4.3** for typical N^O ligand) in which a zinc atom is bonded to amine and oxygen atoms and the cyclopentadienyl ring.[29a] With this idea in mind the ferrocenyl derivative (**65**) was prepared with the aim of utilizing it for an *in situ* preparation of an ethylzinc complex. A literature procedure was followed for the preparation of methiodide (**64**) in which lithiated *N,N*-dimethylaminomethylferrocene was reacted with benzophenone.[30] Subsequent treatment of a tertiary amine intermediate with methyl iodide yielded the methiodide salt (**64**) as a yellow solid. The salt was then treated with picolyl amine in the presence of potassium carbonate in acetonitrile as solvent to afford the desired product (**65**); see the reaction scheme in **Figure 2.4.2.**

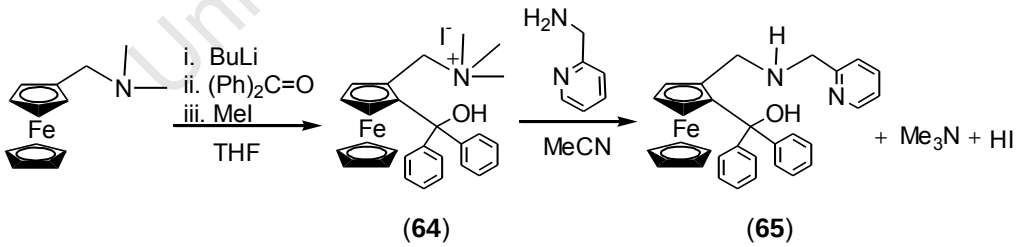

(**64**) (**65**)

FIGURE 2.4.3: Reaction scheme for the preparation of ligand (**65**).

The ^{1}H NMR spectrum of compound (**65**) displayed peaks in the aromatic region as a broad signal in the range δ 7.20 – 7.40 ppm [$10H^{1-3}$, 2x(C_6H_5)]. The numbering system used for assignment of the atoms is shown in **Figure 2.4.4**. The pyridinyl protons appeared as doublets at δ 8.58 ppm (H^{18}), 7.63 ppm (H^{17}) and two overlapping peaks at 7.49 ppm ($2H^{15,16}$).

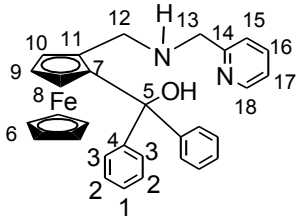

FIGURE 2.4.4: Numbering of atoms of ligand (**65**) used for assignment of the ^{1}H and ^{13}C NMR spectra.

A peak attributed to the unsubstituted Cp ring was found δ at 4.33 ppm ($5H^{6}$), while three broad signals for the protons in the substituted Cp ring resonated at 4.13 (H^{9}), 4.02 (H^{8}), and 3.48 (H^{10}) ppm. Finally, four peaks for the aliphatic protons appeared as doublets and each integrated for one proton at 3.80 ($H^{13'}$), 3.67 (H^{13}), 3.20 ($H^{12'}$) and 2.64 ppm (H^{12}). The protons of the N*H* and O*H* groups did not appear in the ^{1}H NMR spectrum and this is most likely the result of exchange with H_2O. The infrared spectrum, however, displayed stretching frequencies for ν(O-H) at 3297 cm^{-1} and ν(N-H) at 3060 cm^{-1}. Further characterization using ^{13}C NMR spectroscopy, melting point and elemental analysis was conducted; see full details in the experimental section in Chapter 7.

X-ray quality crystals were obtained from a mixture of dichloromethane and hexane, and the molecular structure was determined (see **Figure 2.4.5**). The molecule crystallized in an orthorhombic crystal system and a *Pbca* space group was observed. The crystal and structure refinement data are summarized in **Table 2.4.3** while the selected bond lengths and angles are shown in **Table 2.4.4**. Intramolecular hydrogen bonding interactions were observed in the unit cell. The hydrogen bonding interaction between the hydroxyl proton and the amino nitrogen (−HN···HO−) with a bond distance of 1.772(7) Å (N(1)···H(1)) was observed in the molecular structure determined using X-ray analysis. The cyclopentadienyl rings in the ferrocenyl group appeared in a staggered orientation.

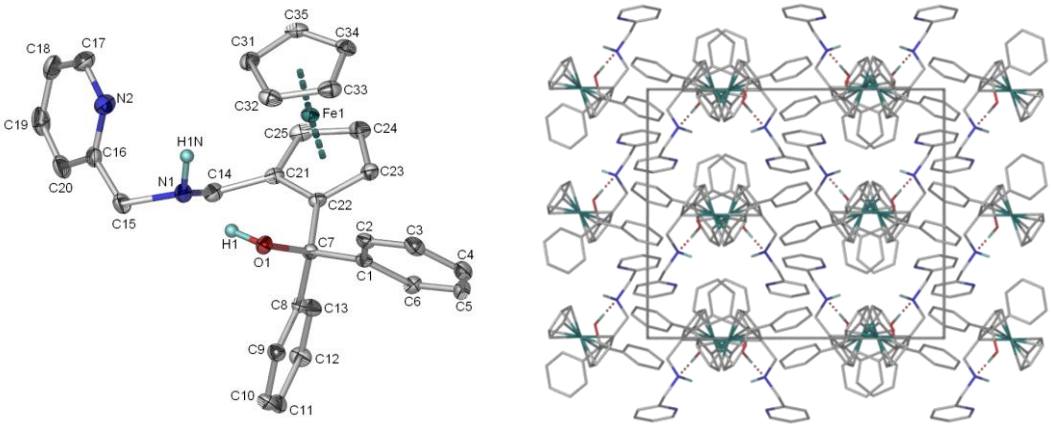

(a) (b)

FIGURE 2.4.5: The structures of compound (**65**): (a) molecular structure, (b) projection view of themolecular packing diagram down [z axis] displaying hydrogen bonding interactions between N(1) and H(1). Hydrogen atoms were omitted for clarity.

TABLE 2.4.3: Crystal and structure refinement data for compound (**65**)

Empirical formula	$C_{30}H_{28}N_2OFe$
Formula weight	488.39
Temperature	173(2) K
Crystal system, space group	Orthorhombic, *Pbca*
Unit cell dimensions	*a* = 17.3492(10) Å α = 90º *b* = 15.2030(10) Å β = 90º *c* = 18.1362(11) Å γ = 90º
Z	8
Volume	4783.6(5) $Å^3$
Absorption coefficient	0.656 mm^{-1}
Crystal size	0.15 x 0.12 x 0.10 mm^3
Reflections collected / unique	21831 / 5960 [*R*(int) = 0.0435]
Goodness-of-fit on F^2	1.004
Final *R* indices [*I*>2sigma(*I*)]	R_1 = 0.0367, wR_2 = 0.0816
R indices (all data)	R_1 = 0.0641, wR_2 = 0.0929

TABLE 2.4.4: Selected bond lengths (Å) and angles (º) for compound (**65**)

Bond angles		**Bond lengths**	
Atoms	Angle (º)	Atoms	Length (Å)
C(34)-Fe(1)-C(24)	106.32(8)	Fe(1)-C(24)	2.0378(19)
C(32)-Fe(1)-C(21)	117.28(8)	Fe(1)-C(35)	2.0384(18)
C(32)-Fe(1)-C(22)	112.36(7)	Fe(1)-C(33)	2.0391(18)
C(7)-O(1)-H(1)	107.9(14)	Fe(1)-C(32)	2.0443(19)
C(14)-N(1)-C(15)	112.19(15)	Fe(1)-C(21)	2.0507(17)
C(14)-N(1)-H(1N)	109.1(13)	O(1)-C(7)	1.426(2)
C(15)-N(1)-H(1N)	106.5(13)	O(1)-H(1)	0.965(5)
C(17)-N(2)-C(16)	117.33(18)	N(1)-C(14)	1.467(2)
O(1)-C(7)-C(1)	106.33(13)	N(1)-C(15)	1.471(2)
C(22)-C(7)-C(1)	109.74(14)	N(1)-H(1N)	0.966(5)
O(1)-C(7)-C(8)	108.80(14)	N(2)-C(17)	1.332(3)
C(22)-C(7)-C(8)	109.65(14)	N(2)-C(16)	1.340(3)
C(1)-C(7)-C(8)	110.10(14)	C(7)-C(22)	1.528(2)
N(1)-C(15)-C(16)	111.34(16)	C(14)-C(21)	1.495(3)
N(2)-C(16)-C(20)	122.5(2)		
C(25)-C(21)-C(22)	107.23(16)		
C(23)-C(22)-C(21)	107.37(15)		

2.5 Concluding remarks

Benzothiazole ligands (N^O), (**37**) and (**38**) and thiosemicarbazone (N^S) ligands, (**41**) – (**44**) together with the corresponding homoleptic Zn(II) complexes (**39**), (**40**) and (**45**) – (**48**) were successfully prepared using the synthetic routes described above. The complexes and ligands were tested for ring-opening polymerization of lactide, the results of which are described in Chapter 3.

The (N^N) donor ligands and corresponding cationic palladium complexes (**55**) – (**60**) were successfully prepared. All the complexes were tested for CO/styrene copolymerization, and the results are described in Chapter 4.

The palladacycle complex (**63**) was prepared and utilized in a C-C coupling reaction, while the ferrocenyl hydroxyl ligand (**65**) was prepared for *in situ* stabilization of a Zn(II) complex in preliminary reactions for functionalization of lactide. The results of these experiments are also described in Chapter 5. All compounds were characterized using spectroscopic and analytical techniques, while several new complexes were structurally characterized by X-ray diffraction.

2.6 References

1. (a) D. X. West, H. Beraldo, A. Nassar, F. A. Ei-Saied and M. I. Ayad, *Trans. Met. Chem*., 1999, **24**, 421; (b) I. Dilović, M. Rubćić, V. Vrdoljak, S. Pavelić, M. Kralj, I. Piantanida and M. Cindrić, *Bioinorg. Med. Chem.*, 2008, **16**, 5189; (c) I. Hutchinson, S. A. Jennings, B. R. Vishnuvajala, A. D. Westwell and M. F. G. Stevens, *J. Med. Chem.*, 2002, **45**, 744; (d) A. Dömling, *Chem. Rev*., 2006, **106**, 17.
2. (a) S. Signh, N. Bharti and P. P. Mohapatra, *Chem. Rev*., 2009, **109**, 1900; (b) A. Y. Louie and T. J. Meade, *Chem. Rev*., 1999, **99**, 2711.
3. (a) S. K. Bharti, G. Nath, R. Tilak and S. K. Singh, *Eur. J. Med. Chem.*, 2010, **45**, 651; (b) V. Vrdoljak, I. Đilovic, M. Rubčić, S. Pavelić, M. Kralj, D. Matković-Calogović, P. Novak, A. Rožman, I. Piantanida and M. Cindrić, *Eur. J. Med. Chem.*, 2010, **45**, 38; (c) T. D. Thangadurai and S.-K. Ihm, *Trans. Met. Chem*., 2004, **29**, 189; (d) I. Yilmaz and A. Çukurovali, *Synth. React. Inorg. Met.-Org. Chem.*, 2003, **33**, 657.
4. (a) H. Okada, Y. Ogawa, T. Yashiki, U.S. Patent 4,652,441, 1987; (b) V. Wagner, A. Dullaart, A. K. Bock and A. Zweck, *Nat. Biotechnol*., 2006, **24**, 1211; (c) A.-C. Albertsson and I. K. Varma, *Biomacromolecules*, 2003, **4**, 1466; (d) H. Okada, M. Yamamoto, T. Heya, Y. Inoue, S. Kamei, Y. Ogawa and S. Toguchi, *J. Controlled Release*, 1994, **28**, 121.
5. N. J. Long, *Metallocenes, Introduction to Sandwich Complexes*, Blackwell Science Ltd., United Kingdom, 1998, pp. 123 – 137.
6. (a) K. N. Zelenin, O. B. Kuznestsova, V. V. Alekseyev, P. B. Terentyev, V. N. Torocheshnikov and V. V. Ovcharenko, *Tetrahedron*, 1993 **49**, 1257; (b) R. Prabhakaran, R. Huang, S. V. Renukadevi, R. Karvembu, M. Zeller and K. Natarajan, *Inorg. Chim. Acta*, 2008, **361**, 2547.

7. (a) S. Halder, R. J. Butcher and S. Bhattacharya, *Polyhedron*, 2007, **26**, 2741; (b) S. Halder, S.-M. Peng, G-H. Lee, T. Chatterjee, A. Mukherjee, S. Dutta, U. Sanyal and S. Bhattacharya, *New J. Chem*., 2008, **32**, 105.
8. (a) C. Zhang and Z.-X. Wang, *J. Organomet. Chem*., 2008, **693**, 3151; (b) J.-C. Wu, B.-H. Huang, M.-L. Hsueh, S.-L. Lai and C.-C. Lin, *Polymer*, 2005, **46**, 9784.
9. R. Mukhopadhayay, S. Bhattacharjee and R. Bhattacharya, *J. Chem. Soc., Dalton. Trans.*, 1994, 2799.
10. (a) D. J. Guo and H. L. Li, *Electrochem. Commun.*, 2004, **6**, 999; (b) D. J. Guo and H. L. Li, *J. Colloid Interface Sci*., 2005, **286**, 274, (b) K. Flavin, H. Kopf, E. L. Canta, C. Navio, C. Butencourt and S. Giodarni, *J. Mater. Chem*., 2011, **21**, 17881; (c) R. Czerw, Z. Guo, P. M. Ajayan, Y.-P. Sun and D. L. Carroll, *Nano Letters*, 2001, **1**, 423; (d) A. Contescu, C. Contescu, K. Putyera and J. A. Schwartz, *Carbon*, 1997, **35**, 83.
11. (a) D. Hu, W. Huang, S. Gou, S. Chantrapromma, H.-K. Fun and Y. Xu, *Synth. React. Inorg. Met.-Org. Chem*., 2002, **32**, 127; (b) H. Azoui, K. Baczko, S. Cassel and C. Larpent, *Green Chem*., 2008, **10**, 1197; (c) B. Karimi, A. Zamani, S. Abedi and J. H. Clark, *Green Chem*., 2009, **11**, 109; (d) C. Tu, J. Lin, Y. Shao and Z. Guo, *Inorg. Chem*., 2003, **42**, 5795; (e) B. Feng, L. Hua, Z. Hou, H. Yang, Y. Hu, H. Li and X. Zhao, *Catal. Commun*., 2009, **10**, 1542.
12. (a) D. Drew, J. R. Doyle, *Inorg. Synth.*, 1972, **13**, 52; (b) B. Milani, A. Marson, E. Zangrando, G. Mestroni, J. M. Ernsting, C. J. Elsevier, *Inorg. Chim. Acta*, 2002, **327**, 188.
13. (a) T. J. Mooibroek, G. Aeomi, M. Quesada, O. Roubeau, P. Gamez, S. D. George, J. Van Slageren, S. Yasin, E. Ruiz and J. Reedijk, *Inorg. Chem*., 2009, **48**, 10643; (b) M. D. Živković, S. Rajković, U. Rychewska, B. Warżajtis, M. I. Djuran, *Polyhedron*, 2007, **26**, 1541; (c) M. Burgos, O. Crespo, M. C. Gimeno, P. G. Jones and A. Laguna, *Eur. J. Inorg. Chem.*, 2003, 2170; (d) B. Antonioli, J. Bray, J. K. Clegg, K. Gloe, A. Jäger, K. A. Jolliffe, O. Kataeva, L. F. Lindoy, P. J. Steel, C. J. Sumby and M. Wenzel, *Polyhedron*, 2008, **27**, 2889.
14. B. S. Furniss, A. J. Hannaford, P. W. G. Smith, A. R. Tatchell, *Vogel's, Textbook of Practical Organic Chemistry*, 5th Edn., Longman Scientific and Technical, United Kingdom, 1989, p. 1429.

15. (a) C. T. Cioffi, A. Palkar, F. Melin, A. Kumbhar, L. Echeqoyen, M. Melle-Framco, F. Zerbertto, G. M. Aminu-Rahman, C. Ehli, V. Sgobba, D. M. Guldi and M. Prato, *Chem. Eur. J.*, 2009, **15**, 4419; (b) A. S. Batsanov, D. Herault, J. A. K. Howard, L. G. F. Patrick, M. R. Probert and A. Whiting, *Organometallics*, 2007, **26**, 2414.
16. (a) J. E. Aguado, O. Crespo, M. C. Gimeno, P. G. Jones, A. L. Laguma and Y. Nieto, *Eur. J. Inorg. Chem.*, 2008, 3031; (b) S. Quintal, M. Gimeno, A. Laguma, M. J. Calhorda, *J. Organomet. Chem*., 2010, **695**, 558, (c) S. Quintal, S. Fedi, J. Barbetti, P. Pinto, V. Félix, M. G. B. Drew, P. Zanello, M. J. Calhorda, *J. Organomet. Chem*., 2011, **696**, 2142.
17. Ref. 14, pp. 296 – 309.
18. (a) G. Muller, M. Klinga, P. Osswald and M. Leskela and B. Rieger, *Z. Naturforsch,* 2002, **57b**, 803; (b) A. R. Shaffer and J. A. R. Schmidt, *Organometallics*, 2009, **28**, 2494; (c) C. M. Kapteijn, M. P. R. Spee, D. M. Grove, H. Kooijman, A. L. Spek and G. Van Koten, *Organometallics,* 1996, **15**, 1405.
19. Ref. 5, p. 165.
20. (a) M. C. Done, T. Ruther, K. J. Cavell, M. Kilner, E. J. Peacock, N. Braussaud, B. W. Skelton and A. White, *J. Organomet. Chem*., 2000, **607**, 78; (b) A. Bastero, A. Ruiz and C. Claver, *Organometallics*, 2002, **21**, 5820.
21. (a) R. A. Walton, *Can. J. Chem.*, 1966, **44**, 1480; (b) R. A. Adrian, G. A. Broker, E. R. T. Tiekink, J. A. Walmsley, *Inorg. Chim. Acta*, 2008, **361**, 1261.
22. (a) J. S. Brumbaugh, R. R. Whittle, M. Parvez and A. Sen, *Organometallics*, 1990, **9**, 1735; (b) R. McCrindle, G. Ferguson, A. J. McAlees, G. J. Arsenault, A. Gupta and M. C. Jennings, *Organometallics,* 1995, **14**, 2741.
23. (a) A. Scarel, J. Durand, D. Franchi, E. Zangrado, G. Mestroni, C. Carfagna, L. Mosca, R. Seraglia, G. Consiglio and B. Milani, *Chem. Eur. J*., 2005, **11**, 6014. (b) C. Carfagna, G. Gatti, D Martini and Claudio Pettinari, *Organometallics*, 2001, **20**, 2175.
24. (a) J. Dupont, C. S. Consorti and J. Spencer, *Chem. Rev*., 2005, **105**, 2527; (b) V. Polshettiwar, C. Len and A. Fihri, *Coord. Chem. Rev*., 2009, **253**, 2599; (c) J. G. de Vries, *Dalton Trans.*, 2006, 421.
25. M. Cohen and D. H. Smith, *J. Med. Chem*., 1981, **24**, 336.

26. P. L. Alters, J. Boersma, W. J. J. Smeets, A. L. Spek and G. van Koten, *Organometallics*, 1993, **12**, 1639.
27. (a) Y. Motoyama, H. Kawakami, K. Shimozono, K. Aoki and H. Nishiyama, *Organometallics*, 2002, **21**, 3408; (b) S. Lentijo, J. A. Miguel and P. Espinet, *Dalton Trans*., 2011, **40**, 7602; (c) J. M. Chitanda, S.-C. Wua, J. W. Quail and S. R. Foley, *Inorg. Chim. Acta*, 2011, **379**, 122; (d) H. R. Thomas, R. J. Deeth, G. J. Clarkson and J. P. Rourke, *Organometallics*, 2011, **30**, 5641; (e) K. Gopi, N. Thirupathi and M. Nethaji, *Organometallics*, 2011, **30**, 572; (f) J. L. Serrano, L. García, J. Perez, E. Perez, J. García, G. S. P. Sehnal, S. De Ornellas, T. J. Williams and I. J. S. Fairlamb, *Organometallics*, 2011, **30**, 5095.
28. (a) A. D'Amora, L. Fanfoni, D. Cozzula, N. Guidolin, E. Zangrado, F. Felluga, S. Gladiali, F. Benedetti and B. Milani, *Organometallics*, 2010, **29**, 4472; (b) R. A. Adrian, G. A. Broker, E. R. T. Tiekink and J. A. Walmsley, *Inorg. Chim. Acta*, 2008, **361**, 1261.
29. (a) M. Watanabe, S. Araki and Y. Butsugan, *J. Org. Chem*., 1991, **56**, 2218; (b) C. Bolm, K. Muńiz-Fernández, A. Seger, G. Raabe and K. Günther, *J. Org. Chem*., 1998, **63**, 7860; (c) O. Riant, O. Samuel, T. Flessner, S. Taudien and H. B. Kagan, *J. Org. Chem*., 1997, **62**, 6733.
30. D. W. Slocum, B. W. Rocket and C. R. Hauser, *J. Am. Chem. Soc*., 1965, **87**, 1241.

CHAPTER 3: LACTIDE POLYMERIZATION

3.1 Introduction

Very few reports exist on the utilization of zinc(II) complexes for functionalization of polylactide. Some of these studies have already been discussed in Chapter 1.[1] In these studies, it was indicated that research had been devoted to complexes that had been used as initiators for the production of high molecular weight polymers, with $M_n > 10^4$ g/mol.[2] The aim of most studies has been to produce biodegradable polymers with properties suitable for packaging applications, which potentially can be used to replace petrochemically derived plastics. On the other hand, for biological applications, functionalized-PLA has been reported to display biocompatibility under physiological conditions (pH 7.4 at 37 ºC).[3] PLA based delivery materials for agrochemicals have also been reported.[4]

The primary goal at the outset of this study, was to prepare homoleptic zinc complexes (**39**) and (**40**) that were conjugated with a potential drug and/or pesticide moiety. The synthetic procedures and characterization of ligands and corresponding complexes were discussed in Chapter 2. The catalysts were tested for ring-opening polymerization of lactide at 50 or 70 °C in toluene, tetrahydofuran or dichloromethane as solvent medium. Full experimental conditions for the polymerization reactions are shown in experimental section in Chapter 7. It was hypothesized that by utilizing the homoleptic type complexes one might successfully prepare functionalized PLA. Moreover, the resulting material could act as a drug or pesticide delivery system. This proposal was based on the ROP mechanism.[2]

A range of variables were studied to investigate their effect on the polymerization reaction: use of different solvents, conducting polymerization at different temperature and modifying the duration of the reaction. The conditions which would produce polymers in a controlled manner were of interest, e.g. when the lactide concentration is increased in different independent experiments there should be a proportional increase in polylactide molecular weight. In addition, ideally polymers with narrow molecular weight distributions (PDI = 1) should be produced. Furthermore, the polymer molecular weights determined with gel permeation chromatography (GPC)

[M_n(GPC), the experimental value] should be comparable to those calculated [M_n(calc), the theoretical value]. Polymer formation was confirmed using ^{1}H and ^{13}C NMR spectral analysis. The colours of the isolated polymers were light yellow, light red or light orange, with the colour dependent on the catalyst used, thus further confirming drug functionalization on a polymer backbone. Coloured polymers were also observed by other researchers.[5]

The molecular weights of the polymers together with the polymer molecular weight distributions were analysed using gel permeation chromatography (GPC). Qualitative analysis of drug incorporation on the polymer back-bone was performed using matrix-assisted laser desorption ionization time of flight (MALDI-TOF) and electron spray ionization (ESI) mass spectral analysis. Experiments on the drug-releasing ability of the polymers were conducted and studied by ^{1}H NMR spectroscopy. The results of these catalytic investigations and the data obtained on the polymer characterization, together with the drug delivery studies, are discussed in this Chapter.

3.2 Results and Discussion on Lactide Polymerization

3.2.1 Lactide polymerization using Zn(N^O)$_2$ **(39)**

The zinc catalyst **(39),** stabilized with a benzothiazole ligand, produced polymers with narrow molecular weight distributions and medium size molecular weights (M_n = 1.28 – 5.05 x 10^3). Independent reactions were conducted employing an increasing concentration of lactide while keeping the catalyst concentration constant in toluene as a solvent (70 ºC for 24 h). There was no systematic increase in polymer molecular weight for independent experiments conducted employing different lactide concentrations (see **Table 3.2.1).** The polymerization experiments were not in general duplicated, as four repetitions of the reaction for entries 1 and 4 gave M_n(corr) values that differed by not more than 10 g/mol.

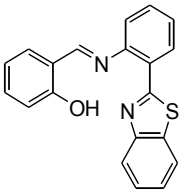

(**37**)

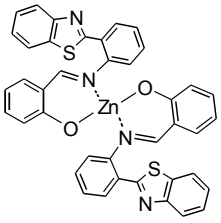

(**39**)

The absence of a linearity increase suggested a lack of polymerization control for this catalyst. Molecular weights determined by GPC were corrected using the accepted formula as employed in the literature,[6] namely, molecular weight determined by GPC times the correction factor 0.58. On the other hand, the theoretical molecular weights were calculated using the formula: M_n = [M_w(benzothiazolimine) + M_w(Lactide) x (Lac/Cat)] x (% conversion).[7] The percentage conversion was determined using ^{1}H NMR spectroscopy and found to be 95%. This was achieved by using the methine proton peak intensity (resonating at 5.05 ppm, further discussed in the next section) in all experiments performed here, however, there was a difference in time for various catalysts to achieve 95% conversion. The proposed structure of the polymer used in the calculation is shown in **Figure 3.2.1.**

TABLE 3.2.1: Polymerization of of *rac*-lactide by catalyst (**39**) at 70 ºC in toluene[a]

Entry	[Lactide] mol l^{-1}, Cat:Lac	M_n x10^3, GPC[b] [M_n(corr)][d]	M_n x10^3,calc[c]	PDI[b]
1	[0.11], 1:20	2.21 [1.28]	2.91	1.46
2	[0.42], 1:30	8.71 [5.05]	4.19	1.08
3	[0.55], 1:40	8.02 [4.65]	5.48	1.15
4	[0.69], 1:50	5.68 [3.29]	6.78	1.10
5	[1.10], 1:80	7.83 [4.54]	10.67	1.09
6[e]	[0.55], 1:20	1.93 [0.75]	2.91	2.16

[a]Conditions: 10 ml of toluene, 70 ºC for 24 h, Cat. (0.01 mmol). [b]Determined by GPC analysis and calibrated using polystyrene standards. [c]Calculated using the formula M_n = [330 + 144 x (lac/Cat)] x (% conversion). [d]Corrected by using formula M_n(corr) = M_n(GPC) x 0.58.[6] [e]Moles of Lac = 0.01 mol, Cat = 0.21 mmol, 20 ml toluene.

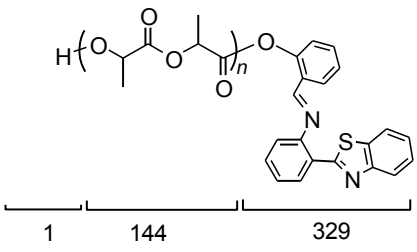

FIGURE 3.2.1: Proposed structure of the polymer produced assuming a well-controlled polymerization process.

Lower values of corrected molecular weights [M_n(corr)], when compared to the calculated molecular weights M_n(calc) were observed (see **Table 3.2.1**, entries 1, 3, 4, 5 and 6), i.e. M_n(corr) < M_n(calc). However, for entry 2 it was noted that M_n(corr) > M_n(calc). The difference in molecular weights determined using GPC, relative to the calculated molecular weights, could be due to side reactions taking place during the polymerization reaction. It is also the case that transestirification reactions, slow or incomplete initiation relative to the propagation step, could result in the formation of macrocycles and oligomers with a range of molecular weights. The data obtained in this study to confirm formation of side reactions is discussed in Section 3.3.2. Side reactions have been observed to be prevalent at higher polymerization temperatures, at high concentrations of lactide, and at longer reaction times.[8] The formation of polymers with a range of molecular weights accounts for the lower M_n(corr) compared to M_n(calc) as the latter assumes perfect polymerization control. M_n(corr) < M_n(calc) has generally been observed for other catalysts.[7]

Polymers with quite narrow molecular weight distributions were produced (PDI = 1.08 – 1.15). The only exception was in entry 1, where a polymer with PDI = 1.46 was obtained. The lactide concentration employed in this particular experiment was the lowest (0.11 M); for experiment in which a lactide : catalyst of ratio of 20 : 1 was employed. On the other hand, when a ratio of lactide : catalyst of 20 : 1 was employed but with an increased amount of monomer and catalyst (entry 6) a polymer with a larger molecular weight distribution was produced (PDI = 2.16). This suggested that the concentration of the reagents (more than just their amounts) was important for the production of narrow molecular weight distribution polymers.

Employing a lower lactide concentration (0.11 M, entry 1), resulted in polymers with a broader molecular weight distributions compared to when higher lactide concentrations were used (entries 2 - 4). The broad molecular weight distribution observed here could possibly be due to transesterification side reactions which are favoured at lower concentration of lactide. This is also seen when larger amounts of low lactide concentrations were employed at a reaction temperature of 70 ºC.[9] The peaks which were attributed to formation of oligomers and macrocycles were obsereved in the MALDI-TOF mass spectrum of polymers obtained in this study (this is Further discussed in Section 3.3.2).

3.2.1.1 Effect of varying the polymerization temperature

When the polymerization temperature was reduced from 70 ºC to 50 ºC (toluene as the solvent, while lactide: catalyst (**39**) ratio of 20 : 1 was employed), polymers with an improved molecular weight distribution were produced, see **Table 3.2.2** (entry 1). This observation suggests that at the lower temperature, transestification side reactions were less favoured.

TABLE 3.2.2: Polymerization of *rac*-lactide by catalyst (**39**) at 50 ºC in toluene[a]

Entry	[Lactide] M, Lac/ Cat	M_n x10^3, GPC[b] [M_n(corr)[d]	M_n x10^3, calc[c]	PDI[b]
1	[0.11], 20	5.62 (3.25)	2.91	1.11
2	[0.42], 30	18.21 (10.56)	4.19	1.22
3	[0.69], 50	6.97 (4.04)	6.78	1.09

[a]Conditions: Catalyst (0.01 mmol) in 10 ml of toluene at 50 ºC for 3 days. [b]Determined by GPC analysis and calibrated by polystyrene standard. [c]Calculated using the formula M_n = [330 + 144 x (Lac/Cat)] x (% conversion). [d]Corrected by using formula M_n(corr) = M_n(GPC) x 0.58.[6]

There were no major differences in the polydispersity indices of the polymers produced when lactide concentrations of 0.42 and 0.69 M were employed at this temperature (50 °C) compared to experiments conducted at 70 ºC. Even though the polymerization was better controlled at this temperature, the rate of polymerization was very slow (three days of reaction were required for 95% of lactide monomer to be converted to a polymer). A similar observation was made by other reserachers.[10] Interestingly, polymers with increased molecular weights were obtained at 50 ºC as compared to 70 ºC.

3.2.1.2 Effect of changing the polymerization solvent

Solvents which are commonly employed for lactide polymerization are non-polar and aprotic organic solvents, such as toluene, tetrahydrofuran and dichloromethane. Polymerization reactions have also been conducted in supercritical carbon dioxide.[7e] In this study, the effect of changing the solvent from toluene to dichloromethane at 50 ºC was investigated. The polymerization reactions were conducted for three days

as was done for the reactions in toluene at 50 ºC. Experiments were conducted employing lactide concentrations of 0.11 and 0.42 M and Cat:Lac ratio of 1:20 and 1:30, respectively was used. The data obtained for duplicate experiments are summarized in **Table 3.2.3**. A better controlled polymerization was observed as the PDI values were close to one. However, M_n(corr) was higher than M_n(calc) for polymers obtained when employing a lactide concentration of 0.11 M (entry 1) (same as for toluene. When increasing the lactide concentration to 0.42 M, it gave a M_n(corr) that was much smaller than M_n(calc) (entry 2). This suggested that at higher concentrations there was poor polymerization control.

Interestingly, in dichloromethane higher molecular weight polymers were obtained when a lactide concentration of 0.11 M was employed when compared to polymers obtained at 50 ºC in toluene (when the same lactide concentration was employed). On the other hand, an increase in lactide concentration to 0.42 M resulted in the production of lower molecular weight polymers compared to those obtained using toluene as a solvent and at 50 °C. The data suggest that the change of polymerization solvent did indeed affect the polymerization process, as found by other researchers. This is possibly because of high solubility of lactide in dichloromethane when compared to toluene at 50 °C. Higher concentration of lactide, restrict chain growth, favouring faster chain termination step, resulting in polymers with shorter chains.

TABLE 3.2.3: Polymerization of *rac*-lactide by catalyst (**39**) at 50 ºC in dichloromethane[a]

Entry	[Lactide] mol l^{-1}, Cat:Lac	M_n x10^3, GPC[b] [M_n(corr)][d]	M_n x10^3,calc[c]	PDI[b]
1	[0.11], 1:20	11.19 [6.49]	2.91	1.11
2	[0.42], 1:30	1.21 [0.70]	4.19	1.28

[a]Conditions: Catalyst (0.01 mmol) in 10 ml of dichloromethane at 50 ºC for 3 days. [b]Determined using GPC analysis and calibrated using polystyrene standard. [c]Calculated using the formula M_n = [330 + 144 x(Lac/Cat)] x (% conversion). [d]Corrected by using formula M_n(corr) = M_n(GPC) x 0.58.[6]

*3.2.2 Attempted lactide polymerization using Z*n(N^O)$_2$ (**40**)

As discussed in the previous chapter, difficulty was experienced in isolating zinc complexes of benzothiazolyl-imine derivatives bearing substituents on the aromatic

ring. Other similar complexes were thus investigated. Complex (**40**), with bulky *tert*-butyl substituents on the phenolate ring was isolated from a reaction between ligand (**38**) and zinc salt, as discussed in Chapter 2.

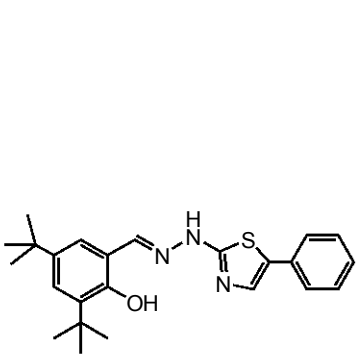

(**38**)

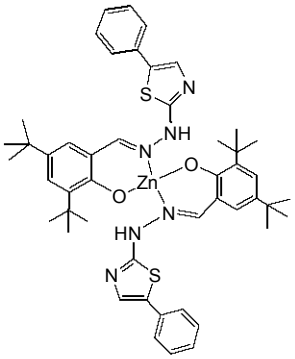

(**40**)

A bulky substituent which is close to the initiating group has been found to promote polymerization control;[11] For this reason, complexes containing *tert*-butyl groups were of interest. Both the ligand (**38**) and complex (**40**) were tested for lactide polymerization and, as expected, no polymer formation was observed when ligand (**38**) was utilized (in toluene as a solvent at 70 °C for a minimum of 24 h, The full experimental details are shown in Chapter 7). The complex also was not active even when using a range of reaction conditions. It was concluded that the bulky groups hindered the interaction of the incoming monomer to the phenolate initiating group.

3.2.3 Ring opening polymerization of lactide using Zn(N^S)$_2$, (**45**) and (**46**)

The study was further extended to incorporate thiosemicabazone derivatives (S^N) on the PLA-backbone. Unlike the homoleptic complexes (**39**) and (**40**), which were stabilized with the *hard* phenolate anion [Zn(O^N)$_2$], complexes (**45**) and (**46**) were stabilized with the *soft* thiolate anion [Zn(S^N)$_2$]. Ligands (**41**) and (**42**) were initially tested for lactide polymerization in toluene as a solvent at 70 ºC for 24 h. The ^{1}H NMR spectra of the product from the polymer reaction displayed contrasting behaviour: there was no sign of polymer formation for a sample isolated when ligand (**41**) was utilized. Surprisingly, the sample isolated from a polymerization reaction utilizing (**42**), displayed peaks corresponding to polylactide. Polymerization of lactide was not expected when using the ligands in control experiments.

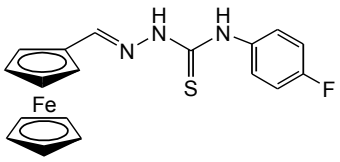

(**42**)

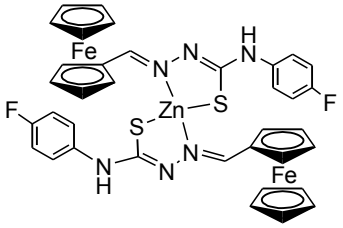

(**46**)

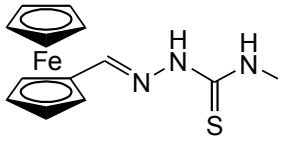

(**41**)

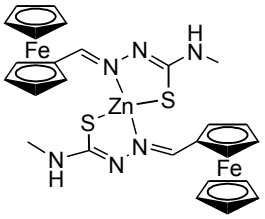

(**45**)

Various organocatalysts have been utilized for lactide polymerization, such as thiourea-amines,[12] carbenes,[13] and tertiary amines.[7e, 14] In addition, ring-opening polymerization of lactide monomer utilizing triflate ion ($CF_3SO_3^-$) from triflic acid or as a counter ion in organometallic complexes has also been reported.[15,16] The mechanism of action proposed for lactide ROP by organocatalysts has been referred to as cationic polymerization. Polymerization is believed to be initiated by an activated monomer due to highly electrophilic protons on the catalyst. Some of the organocatalysts previously employed are shown in **Figure 3.2.2**: those containing a tertiary amine without an amino proton are shown in A (i- iv), and others with both tertiary amine and an amino proton, in B (i- iii).

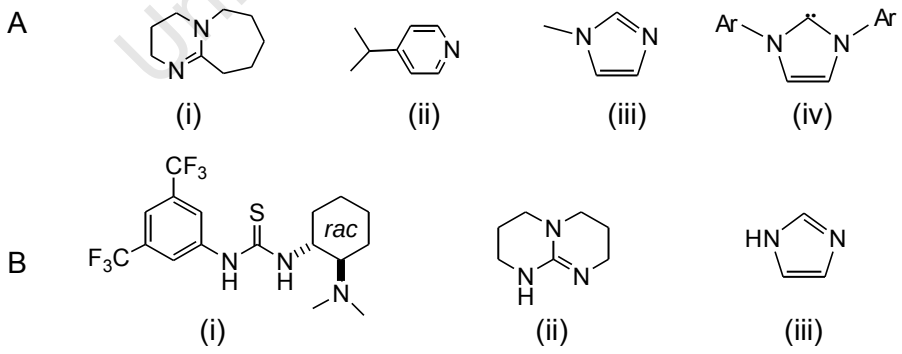

FIGURE 3.2.2: Organocatalysts which have been found to be active for ring-opening polymerization of lactide through the activated monomer mechanism: (A) compounds containing amine group but without amino proton; (B) compounds containing both amine group and amino proton.

Of particular interest is the thiourea derivative **Figure 3.2.2** [B(i)], because the thiourea group is similar to that found in ligand (**42**). The thiourea compound has been found to be active for ROP of lactide only in the presence of an alcohol.[12] The authors attributed the activity of the compound to the synergistic effect of the electrophilic protons (-N*H*-(CS)-N*H*-), which are believed to interact with the carbonyl oxygen on the lactide monomer, thereby activating it. The amine group, on the other hand, assists in deprotonation of the alcohol in order to initiate polymerization. ^{1}H NMR scale experiments were conducted utilizing a thoroughly dried sample of ligand (**42**). No polymer formation was observed in the spectrum after 48 h of heating a mixture of compound (**42**) and lactide, and also when heating a mixture of lactide and methanol. Upon addition of ten equivalents of methanol to the lactide and ligand (**42**) reaction mixture and heating for 24 h, new peaks attributed to polylactide were observed (see **Figures 3.2.3** and **3.2.4).** In addition, the material which was isolated from the reaction mixture and analysed by mass spectrometry further suggested polymer formation.

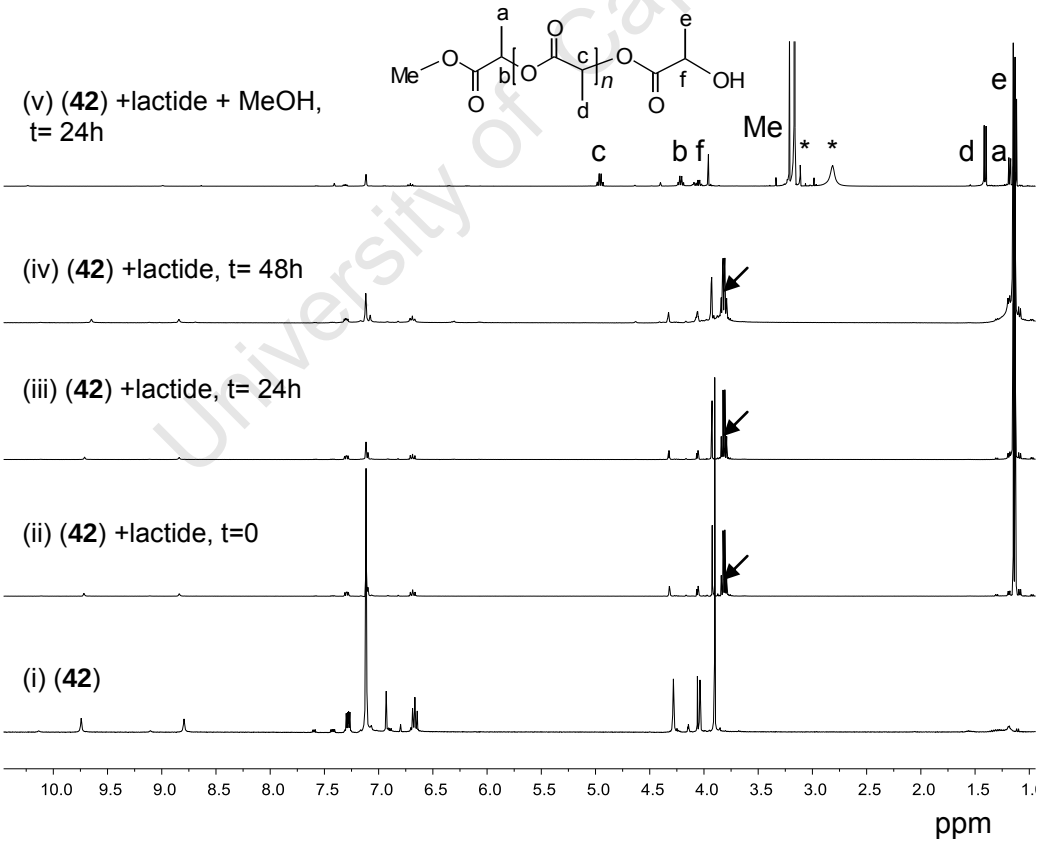

FIGURE 3.2.3: ^{1}H NMR spectra showing the reaction monitoring of compound (**42**) to investigate the influence of methanol in the solution of lactide and the ligand. *Methanol. ↙ = Methine peaks of lactide monomer.

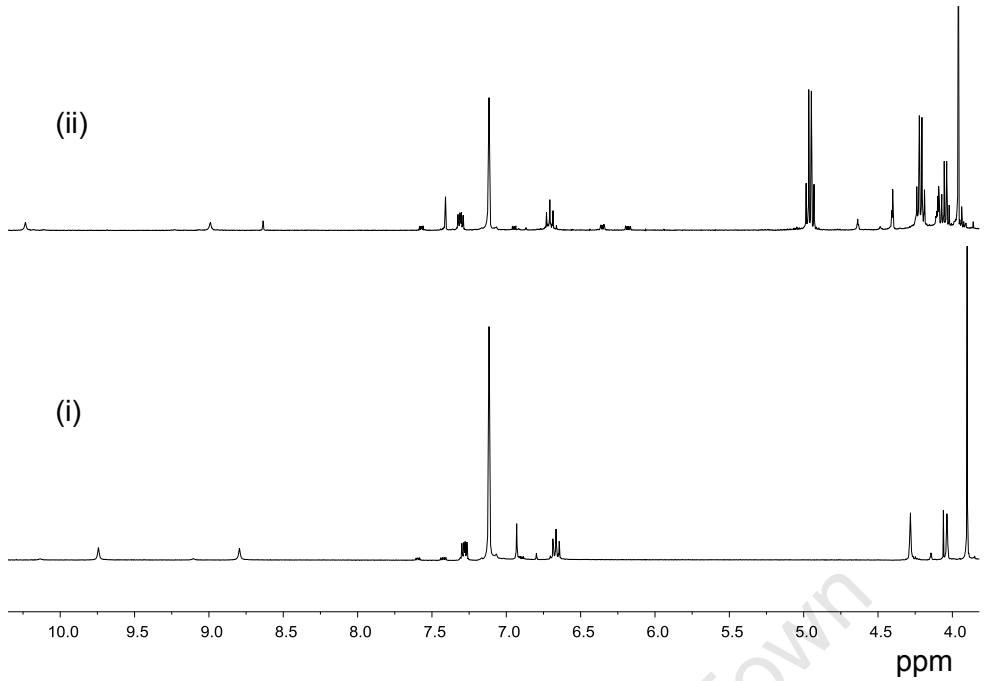

FIGURE 3.2.4: ^{1}H NMR spectra in region (δ 4.00 – 10.5 ppm): (i) of compound (**42**) and (ii) of compound (**42**) in the presence of polylactide.

Interestingly, an intermolecular interaction between polylactide and compound (**42**) in the solution was observed. There was a downfield shift of the following proton signals: –C*H*=N-, NN*H*C(S) and C(S)N*H*(C_6H_4F) which resonated at δ 7.41, 9.00 and 10.25 ppm, respectively. A fresh solution of compound (**42**) gave peaks that resonated at 6.81, 8.30 and 9.75 ppm, respectively (see **Figure 3.2.4)**. Further investigations on the polymeric system shown were not conducted. However, it is believed that further studies could lead to the development of thiosemicarbazone-polylactide materials which could serve as controlled drug delivery vehicles.

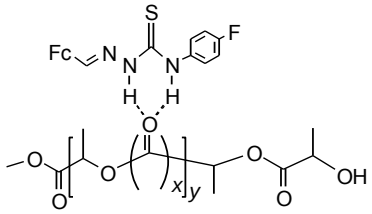

With reference to the NMR scale experiments already discussed, it can be concluded that the polymerization reaction when compound (**42**) was first utilized was activated by the trace amount of methanol which remained from the reaction workup. The possible mechanism shown in **Figure 3.2.5**, which is similar to the one reported for the thiourea derivative on lactide polymerization, is consequently proposed here.[7e,14]

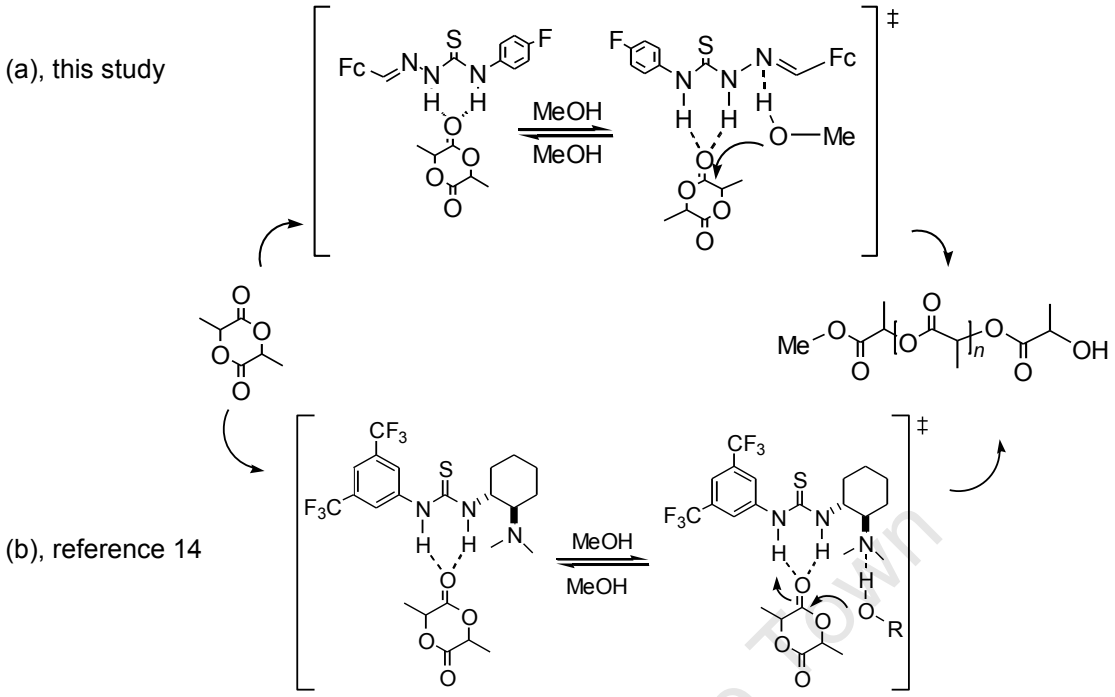

FIGURE 3.2.5: Proposed monomer-activated mechanism taking place during lactide polymerization with thiourea derivative.[7e,14]

In Chapter 2 the highly electrophilic nature of the following protons: NN*H*C(S) and C(S)N*H*R in compound (**42**) compared to (**41**) was discussed. The difference in the electronic properties of the compounds was suggested to play a role in the observed activity. The ring-opening polymerization of lactide by compound (**42**) as observed here will undoubtedly open up a new area of research in which various thiosemicabazones could be investigated for lactide polymerization.

The corresponding complexes (**45**) and (**46**), likewise, displayed activity towards lactide polymerization, while compound (**46**) was the most active of the two. The activity observed for both complexes [Zn(S^N)$_2$] were, however, low when compared to the activity of the phenolate analogue (**39**), [Zn(O^N)$_2$]. This could be due to the basicity of the *hard* oxygen anion as a polymerization initiator which is more basic than the *soft* thiolate ion, thus compound (**39**) was more active for lactide polymerization. The lactide conversion of 60% of the monomer was achieved after three days of reaction when compounds (**45**) and (**46**) were utilized as catalysts. Molecular weights of polymers obtained when compounds (**45**) and (**46**) were used as catalysts for lactide polymerization were determined using ESI mass spectrometry.

Polymers with M_w = 741 and 1231 were observed when compounds (**45**) and (**46**) were utilized for polymerization, respectively. The ESI mass spectrum of the sample obtained from catalytic reaction of lactide and compound (**46**) displayed peaks at *m/z* 548, 620 and 764 corresponding to thiosemicarbazone group incorporation onto one, two and three repeating lactide units of the polymer (see **Figure 3.2.6**).

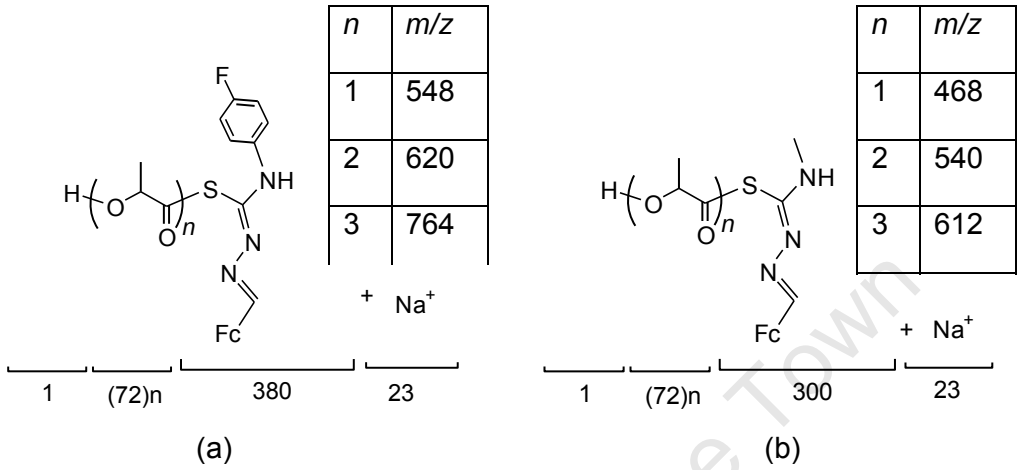

FIGURE 3.2.6: Proposed structures of the polymers produced for the lactide polymerization process utilizing zinc catalysts: (a) using compound (**46**), *m/z* = 404 + (72)*n*; (b) using compound (**45**), *m/z* = 324 + (72)*n*.

The spectrum also displayed peaks which corresponded to various polylactide chains, up to ten lactide repeating units, i.e. *m/z* = 764 was observed [*m/z* = (72)n + 26], which were not functionalized with a drug-like molecule. Similar mass spectral behaviour was observed for the sample obtained on polymerization using compound (**45**). A typical mass spectrum for the polymers obtained when using compound (**45**) is shown in **Figures 3.2.7** and **3.2.8** (page 100 and 101).

The substituted phenyl analogues, ligands (**43**) and (**44**), were inactive towards polymerization of lactide.

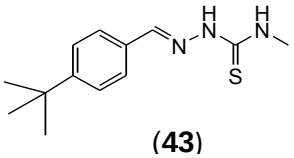

(**43**)

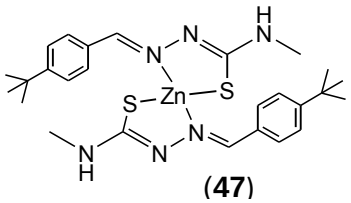

(**47**)

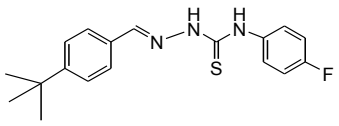

(**44**)

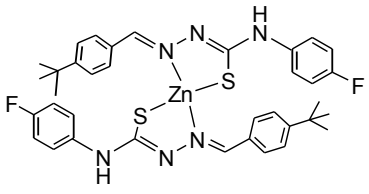

(**48**)

This behaviour was attributed to the donor ability of the ferrocenyl group compared to the 4-*tert*-butylphenyl group. On the other hand, the corresponding complexes (**47**) and (**48**) displayed lower activity towards lactide polymerization. Polymers with a molecular weight of M_n = 800 g/mol were obtained when utilizing these complexes, and also, at least three days were required to convert 50% of lactide monomer to polylactide. The polymers displayed a broad molecular weight distribution behaviour, with the PDI = 1.92.

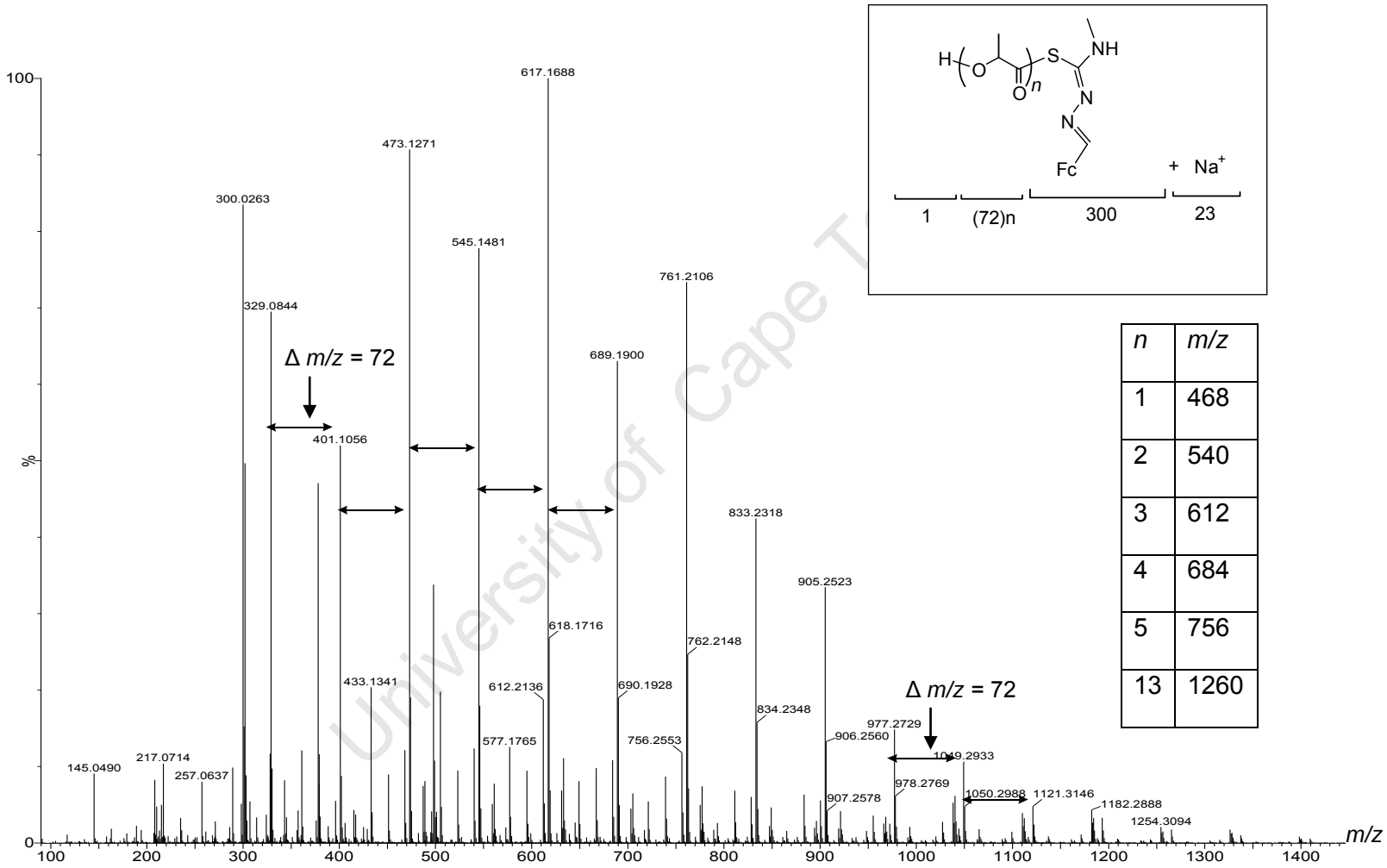

n	*m/z*
1	468
2	540
3	612
4	684
5	756
13	1260

FIGURE 3.2.7: The mass spectrum (ESI) of functionalized polylactide obtained when using catalyst (**45**).

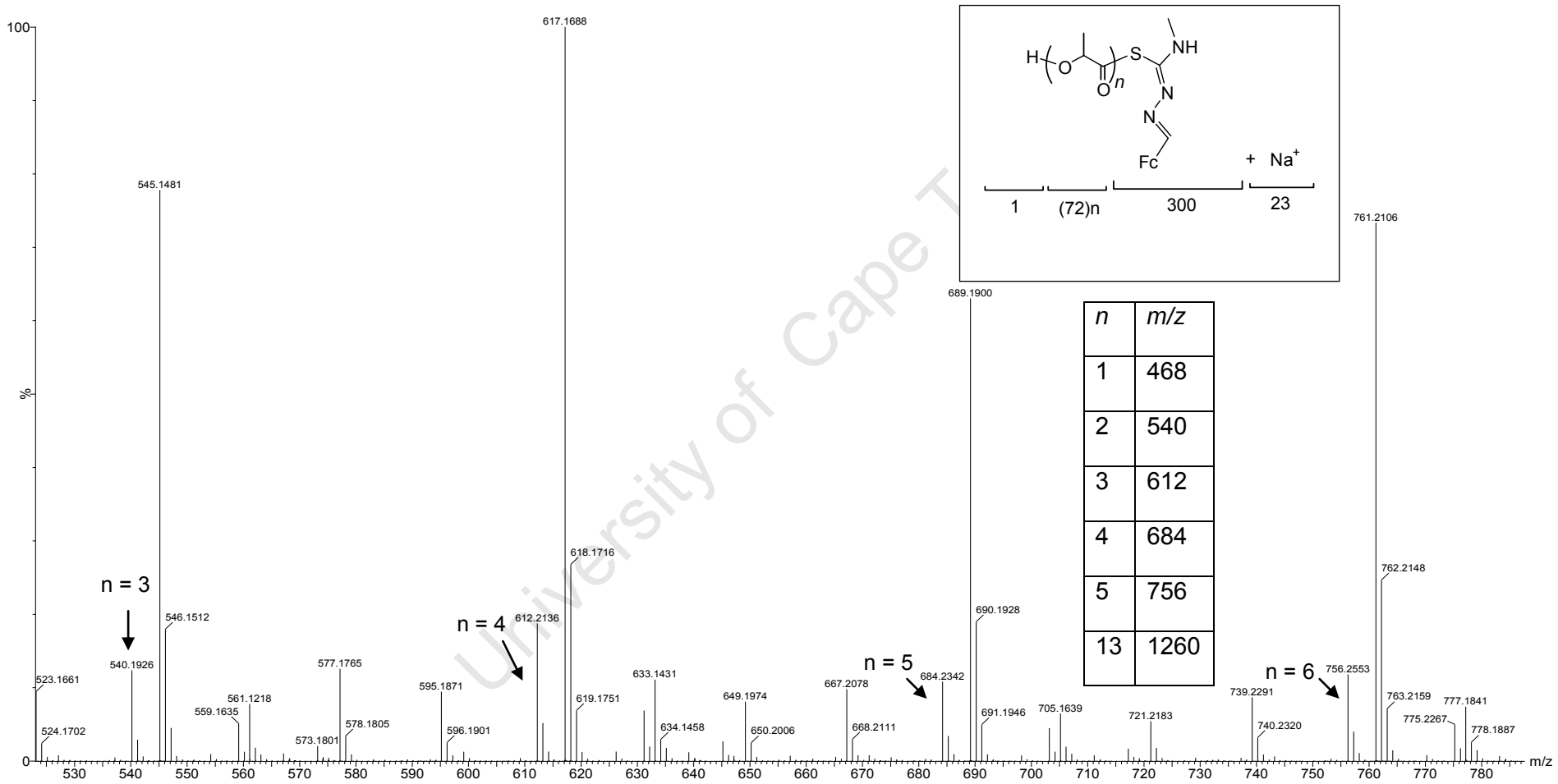

n	*m/z*
1	468
2	540
3	612
4	684
5	756
13	1260

FIGURE 3.2.8: The mass spectrum (ESI), in the range *m/z* = 500 – 800 of functionalized polylactide obtained when using catalyst (**45**).

3.3 Characterization of functionalized polylactide

3.3.1 Characterization using ^{1}H and ^{13}C NMR Spectroscopy

The polymers produced here were studied by ^{1}H and ^{13}C NMR spectroscopy, with the samples dissolved in C_6D_6. The formation of a polymer was confirmed by the appearance of polymer methine protons as a broad signal which resonated at δ 5.05 ppm ($H^{f\&i}$) compared to the methine signal of the starting *rac*-lactide monomer resonating at 3.85 ppm (H^{2}) (see **Figure 3.3.1)**. The appearance of the methine peak as a broad signal was attributed to the formation of various polymer stereoisomers; the stereochemical analysis required the use of homonuclear-decoupled ^{1}H NMR and was not conducted here.[1,7] The broadening of the signals for the polymer were also due to the protons of polymers with various molecular weights. In addition, macrocyclic side-products have also been found to resonate at a similar chemical shift. A doublet signal which was assigned to methyl protons was observed at 1.18 ppm for *rac*-lactide and at 1.25 ppm for polylactide.[1,7]

It is interesting to note that the methine protons in the polymer resonated at similar chemical shifts whether measured in C_6D_6 or $CDCl_3$. The exception was observed with the methine group in the lactide monomer, which resonated at δ 3.85 and 5.00 ppm in C_6D_6 and $CDCl_3$, respectively. Polymerization reactions were also conducted in a Young's NMR tube in order to monitor the reaction progress. No polymer formation was observed when the reaction was conducted with the ligand alone and lactide at 70 ºC in deuterated benzene (C_6D_6). The same spectrum shown in **Figure 3.3.1** (i), was obtained at the start and after 24 h of the reaction. This confirmed that the ligand alone was not responsible for lactide polymerization. When the catalyst was introduced in the reaction, the new peaks due to polymer formation appeared at 5.05 ppm ($H^{f\&i}$) and 1.02 ppm ($H^{e\&h}$ and $H^{c\&l}$) after 5 h of reaction. At the same time, the methine peak (H^{2}) of the lactide monomer decreased in intensity. The lactide conversion to the polymer was almost complete after 24 h [see **Figure 3.3.1** (ii) and (iii)]. In addition, the peaks attributed to the benzothiazole moiety were observed in the aromatic region. Thus, the sample analysed after quenching the polymerization reaction with acidified methanol displayed the

formation of the polymer functionalized with a benzothiazole group (see **Figure 3.3.2** (insert)].

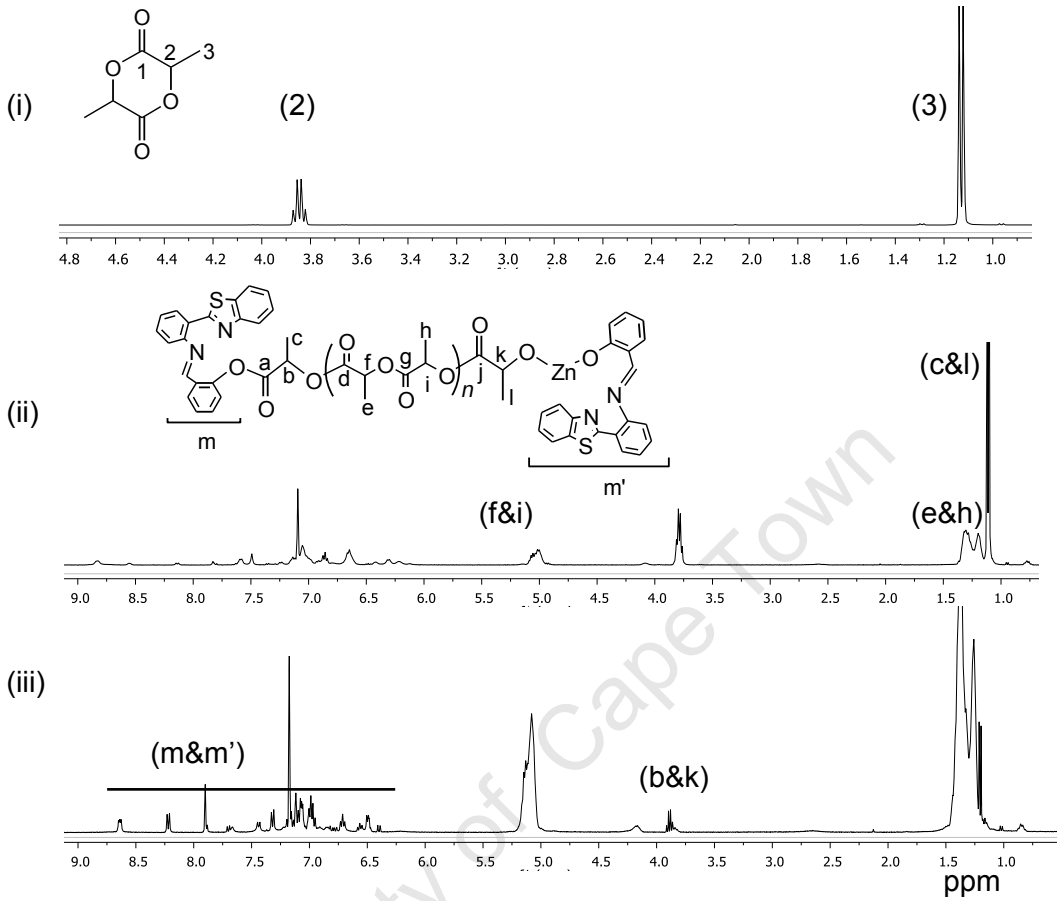

FIGURE 3.3.1: ^{1}H NMR spectra (C_6D_6) showing chemical shifts of protons in lactide monomer and in polylactide: (i) heated solution of lactide without catalyst; (ii) polymerization with zinc catalyst (**39**) after 5 h of reaction; and (iii) polymerization with zinc catalyst (**39**) after 24 h of reaction.

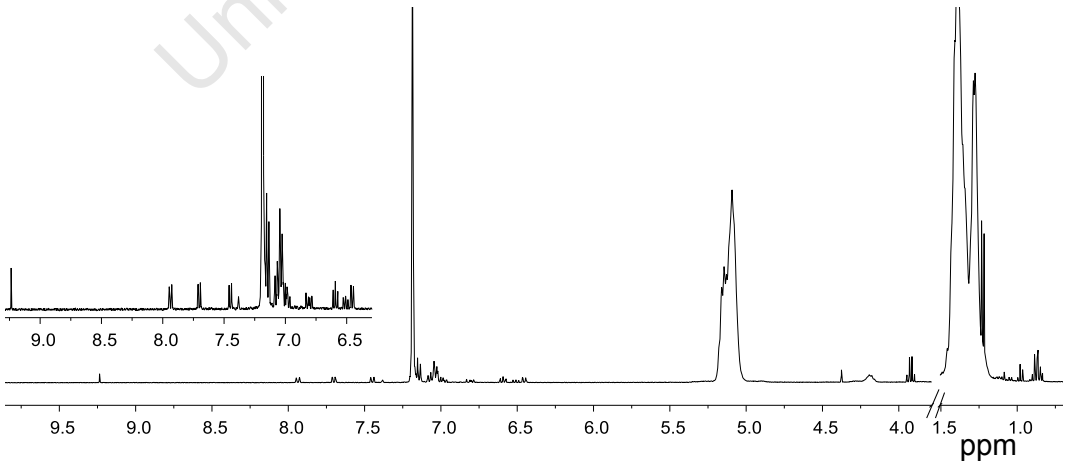

FIGURE 3.3.2: ^{1}H NMR spectrum (in C_6D_6) of the sample analysed after quenching the polymerization reaction with acidified methanol. The insert displays the peaks due to the benzothiozole-imine moiety.

The polymerization quenching process did not hydrolyse the ester bond connecting the polymer and the benzothiazole moiety; instead, the Zn(II)-PLA bond was hydrolysed as expected. The ^{13}C NMR spectra obtained for *rac*-lactide monomer conducted in C_6D_6 displayed peaks resonating at the following chemical shifts: δ 15.0 (C^3), 71.5 (C^2) and 166.2 ppm (C^1). Upon polymerization, new peaks were observed: a downfield shift for the methyl carbon atoms at 16.5 and 16.6 ppm (C^e and $C^{c\&l}$), an upfield shift for methine-carbons at 69.3 and 69.5 ppm ($C^{f\&i}$ and $C^{b\&k}$) and multiple peaks for carbonyl-carbon atoms appeared downfield in the range δ 169.2 – 170.0 ppm (C^a, $C^{d\&g}$ and C^j) (see **Figure 3.3.3**). Peaks due to macrocyclic side-products were not observed in the spectrum. The formation of macrocyclic side-products, however, was not ruled out, as their presence was observed in the MALDI-TOF spectrum, which will be discussed in the next section. It is possible that their concentrations were too small to be detected by ^{13}C NMR analysis. The spectra further supported the formation of the polymers in this study and the spectral data were comparable to the literature reports.[10]

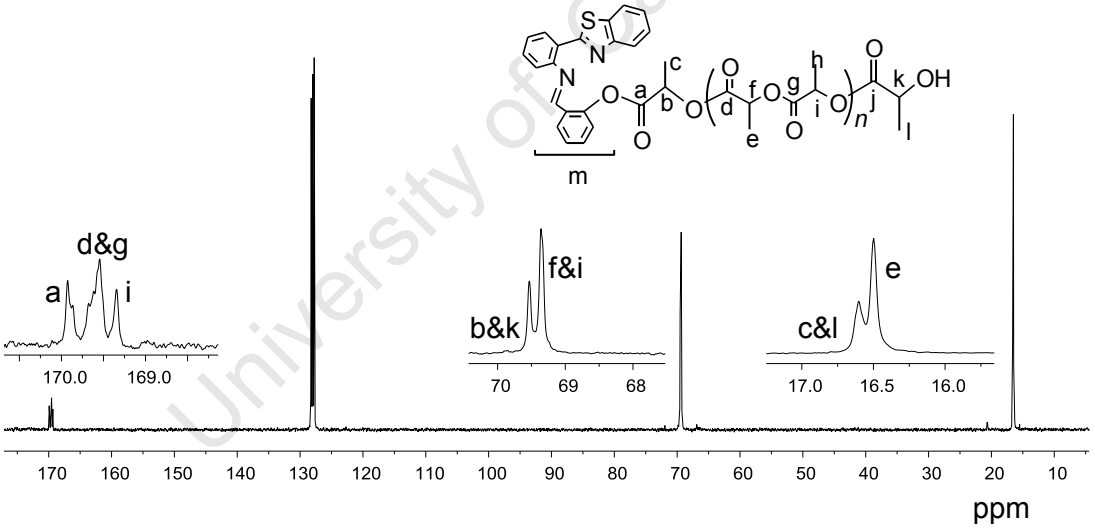

FIGURE 3.3.3: ^{13}C NMR spectrum (in C_6D_6) showing chemical shifts of functionalized polylactide prepared by zinc catalyst (**39**) at 70 °C for 24 h in toluene.

3.3.2 Characterization using MALDI-TOF mass spectrometry

Polymeric samples were analysed using MALDI-TOF mass spectrometry to confirm the benzotiazole group incorporation on the polymer. The following formula: M_w = 330 + 144(n), n = number of inserted lactide monomers, was used for the calculation of the molecular weight of the functionalized polymers. The MALDI-TOF spectra

displayed peaks with *m/z* values attributable to drug incorporation on the polymer backbone. The peaks with 20% intensity and above corresponded to polymers in which n = 4, 5, 6 and 7, and the corresponding molecular weights were; 905.1, 1049.2, 1193.3 and 1337.4, respectively (see **Figure 3.3.4**).

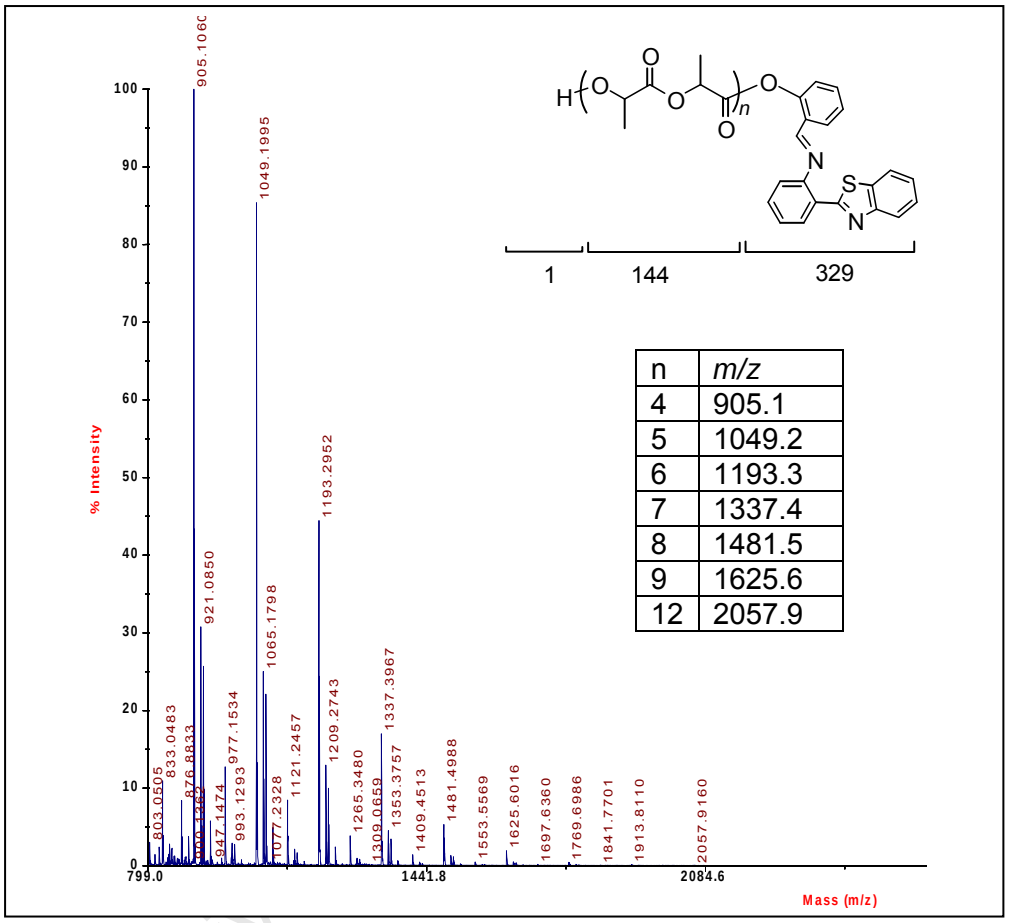

FIGURE 3.3.4: MALDI-TOF mass spectrum of benzothiazolimine-PLA_n obtained when polymerization was conducted employing (**39**): [(Lac/(**39**) = 20], Lac = 0.20 mmol, Cat = 0.01 mmol, in toluene for 24 h at 70 ºC. Observed *m/z* were identical to the calculated M_w of benzothiazolimine-PLA_n, M_w = 330 + (144 x n); matrix used was 2,5-dihydroxybenzoic acid.

Additional peaks which appeared in the spectra did not correspond to values for the substitution of n with a whole number and were attributed to the presence of various polymeric side-products, see **Figure 3.3.5**. Similar observations have been reported by other researchers reporting on the MALDI-TOF mass spectra obtained for their polymers.[7a,e,14c] The peaks at *m/z* = 1008, 1152, 1296 and 1140, for example, were believed to be due to macrocyclic polymers formed through a back-biting process. This behaviour was discussed in Chapter 1. Other smaller peaks could be due to intermolecular transestification side products.[7a,e,14c,17]

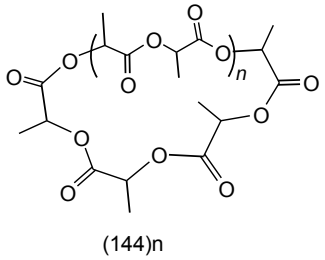

n	*m/z*
6	864
7	1008
8	1152
9	1296
10	1440

FIGURE 3.3.5: Possible cyclic oligomer side-products formed during the polymerization reaction.

Similar spectra were observed for samples obtained when catalysis was conducted employing catalyst: lactide molar ratios of 1:30, 1:40, 1:50 and 1:80 in toluene at 70 °C, 1:20 in toluene at 50 ºC and 1:20 dichloromethane at 50 ºC. This suggests that under the conditions investigated here, the longest possible polymer chain is the one containing twelve inserted lactide monomers (n = 12, M_n = 2057.9). On the other hand, the concentration of the polymer was just above detection limit. Furthermore, there was a mixture of polymers with various lengths: some were functionalized, while others were unfunctionalized side-products. When the amounts of lactide and catalyst were increased while keeping the catalyst : lactide ratio constant at 1 : 20, functionalized polymers with increased chain length were observed (see **Figure 3.3.6)**. In this case, the longest functionalized polymer had a molecular weight of M_w = 3499, corresponding to n = 22. The data suggest that the increased amounts of reactive species promote the number of inserted monomers, thus producing longer functionalized polymers. The large number of polymers with different molecular weights observed in the mass spectra also explains the high PDI value of 2.16 under these conditions (see entry 6 in **Table 3.2.1**, in **Section 3.2.1**).

The production of material which contains functionalized polymers with various molecular weights is an added advantage for drug delivery applications. This is so because the rate of polymer degradation, together with the water-solubility, has been found to be inversely proportional to the polymer molecular weight.[1d] Higher molecular weight polymers are generally less soluble in most solvents and they degrade slowly as compared to smaller molecular weight polymers. However, the properties and characteristics of drug delivery agents are usually optimized during the development stage of a drug delivery system.

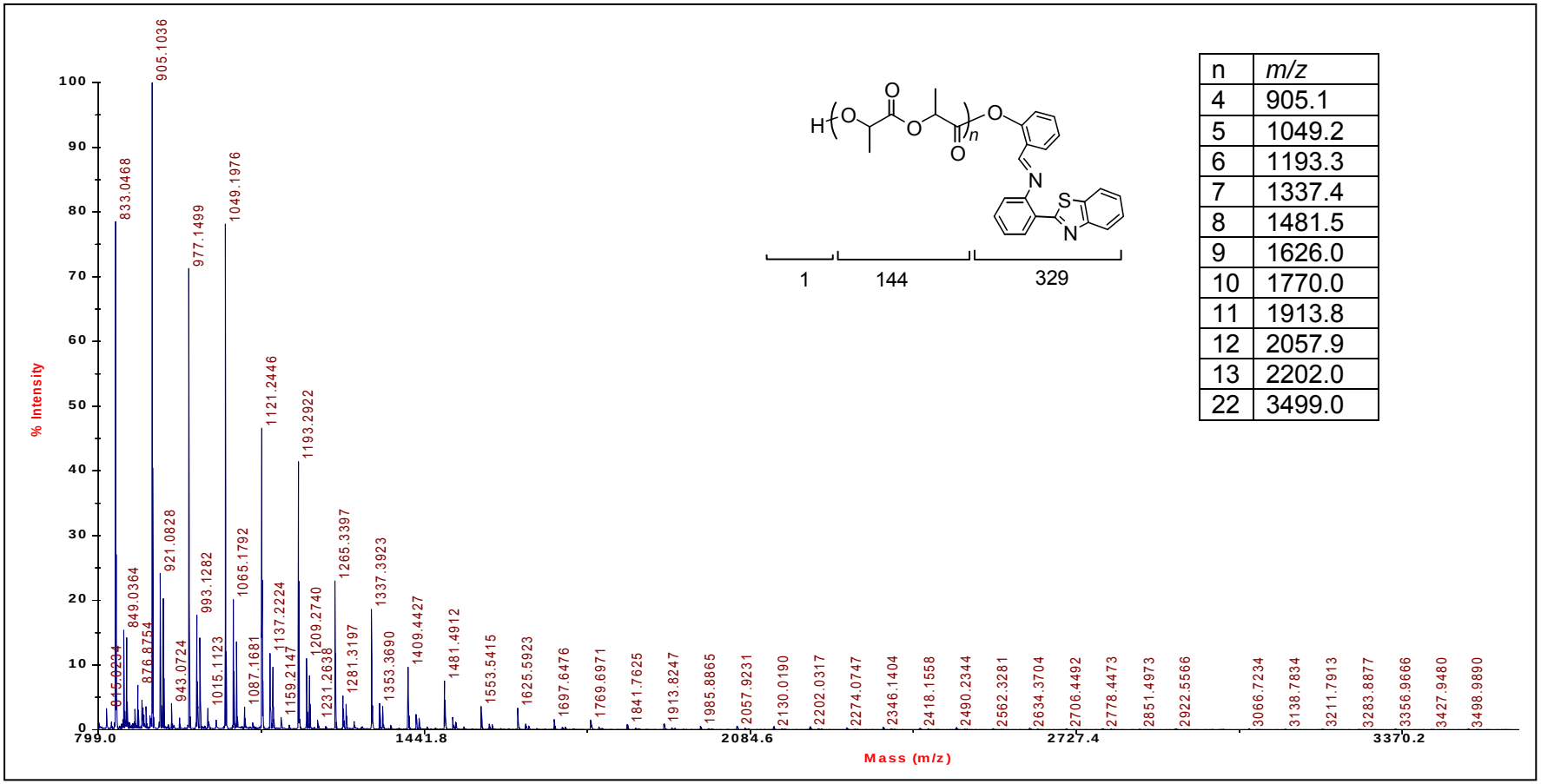

n	*m/z*
4	905.1
5	1049.2
6	1193.3
7	1337.4
8	1481.5
9	1626.0
10	1770.0
11	1913.8
12	2057.9
13	2202.0
22	3499.0

FIGURE 3.3.6: MALDI-TOF mass spectrum of benzothiazolimine-PLA$_n$ obtained when polymerization was conducted employing (**39**); [(Lac/(**39**) = 20], Lac = 0.42 mmol, Cat = 0.21 mmol, in toluene for 24 h at 70 ºC. Observed *m/z* are identical to the calculated M_w of benzothiazolimine-PLA$_n$, M_w = 330 + (144 x n); matrix used was 2,5-dihydroxybenzoic acid.

3.4 Polymer degradation studies

Preliminary studies were then conducted to investigate possible drug delivery applications. It has been reported that degradation takes place through a hydrolytic reaction which involves cleavage of the ester linkages; as a result, PLA oligomers are formed.[18a] The degradation process has been found to be accelerated by the ability of the polymer to absorb water. The lower molecular weight PLA oligomers then continue to break down to form lactic acid molecules, which ultimately are metabolized by the lactate dehydrogenase enzyme which is present in the metabolic system or in the environment. The process known as the pyruvate cycle then takes place to break down lactic acid and finally CO_2 and H_2O are formed as degradation products.

Folkman was the first researcher to demonstrate the controlled release of biological molecules using polymers.[18b] These studies have enabled the development of antiangiogenic drug delivery systems for cancer therapy and have also opened up new areas for the delivery of macromolecules.[18] In addition, the uptake of functionalized PLAs by cells has been investigated.[19] The slow release of pesticides by polylactide has also been observed.[4]

In this study the same amounts of polymer (50 mg) were added into six different sample vials containing phosphate buffer solution (PBS, 30 ml, 0.50 M) at blood pH = 7.4.[3] The ligand was treated in the same way as functionalized polymer samples. The mixture was then stirred at 37 ºC and at regular intervals the flask would be removed from the oil bath and the contents transferred to a separating funnel. The mixture was extracted with chloroform and the organic layer was collected, dried with anhydrous magnesium sulfate and filtered. The filtrate was concentrated to dryness and then analysed by ^{1}H NMR spectroscopy.

The ^{1}H NMR spectrum was initially recorded for one of the samples immediately after the polymer had been added to the PBS solution and shaken vigorously for 10 min (see **Figure 3.4.1)**. The spectra were then recorded after 2, 4, 14, 21 and 45 days. The spectra obtained for samples analysed after two and four days were similar to the spectrum obtained at t = 0.

Interestingly, new peaks were observed in the aromatic region of the ^{1}H NMR spectrum for a sample analysed after 14 days [see **Figure 3.4.1** (iii)]. The signals, surprisingly, did not correspond to those of benzothiazole molecule; instead, they corresponded to those of salicylaldehyde: δ 10.23 ppm (-CO*H*), 7.72 (H^2), 7.61 (H^4), 7.42 (H^3) and 6.92 (H^5) (see inset in **Figure 3.4.1**). On the other hand, the ^{1}H NMR spectra obtained for samples analysed after 21 and 45 days displayed a dramatic decrease in intensity of the polymer peaks.

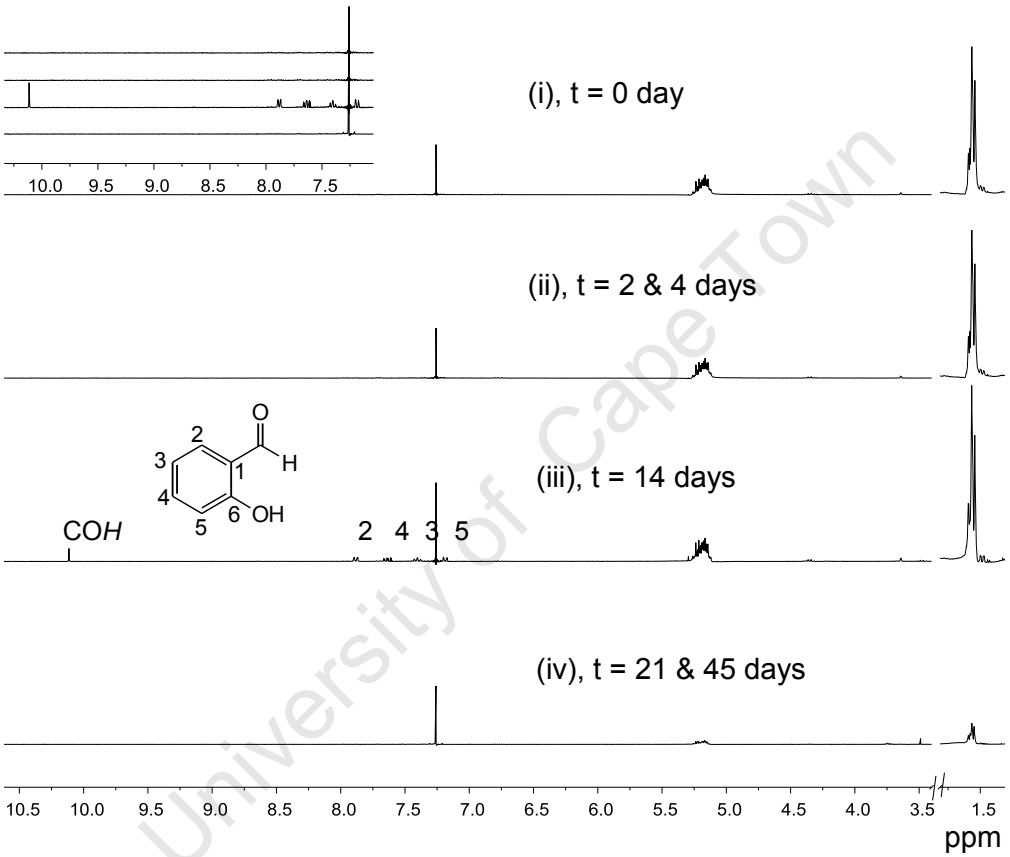

FIGURE 3.4.1: ^{1}H NMR spectra (C_6D_6) for samples analysed during functionalized-polylactide degradation studies in PBS, at pH 7.4 and 37 ºC: (i) sample analysed immediately at t = 0 day; (ii) sample analysed after 2 and 4 days; (iii) sample analysed after 14 days and (iv) sample analysed after 21 and 45 days. Inset: zoom in the aromatic region δ 7 – 10.5 ppm.

On the basis of the appearance of the ^{1}H NMR spectrum obtained for the sample analysed after 14 days, it is proposed that the imine bond connecting the benzothiazole and salicylaldehyde moieties was hydrolysed by the acid in the buffer solution. Ultimately, the aminobenzothiazole group was retained in the acidic aqueous phase during extraction with chloroform. The proposed degradation process taking place is shown in **Figure 3.4.2**. It is not clear why the

salicylaldehyde signals were not visible in the spectra analysed after 21 and 45 days, as would be expected. Ideally, when the polymer is further hydrolysed the peak intensities of the salicylaldehyde signals should increase; however, that was not the case here. It is possible that prolonged exposure of salicylaldehyde to the buffer solution which contained conjugate base could have deprotonated the hydroxyl protons, making the deprotonated molecule less likely to be found in the organic phase.

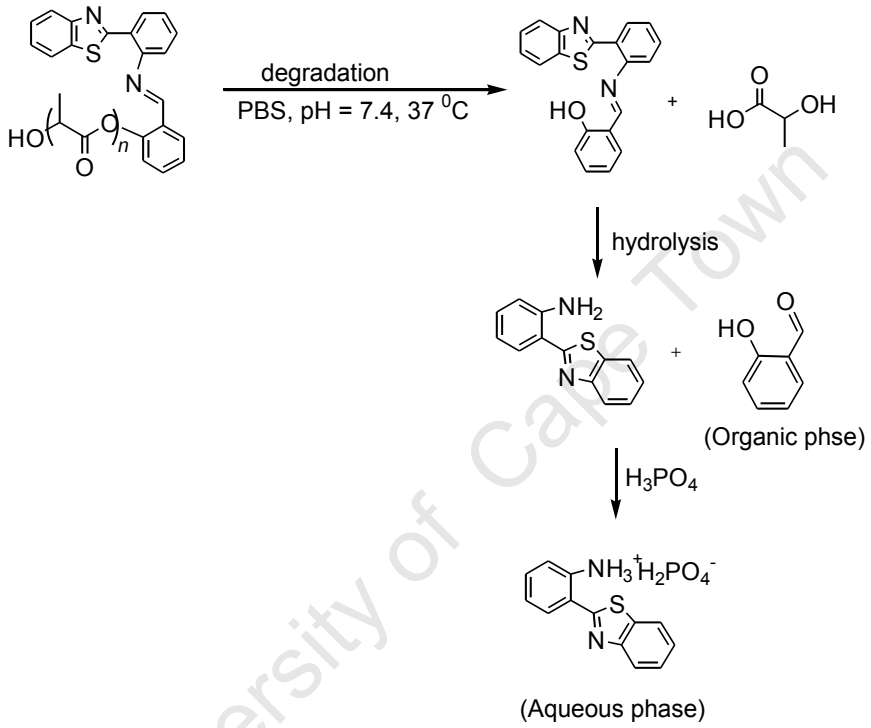

FIGURE 3.4.2: Proposed degradation process of functionalized polylactide (benzothiazole-PLA) taking place in PBS at pH 7.4 and 37 ºC.

The infrared spectrum obtained from the analysis of the dried material remaining from the aqueous phase was difficult to interpret. The stretching vibrations of phosphate salts absorb in a similar range to the carbonyl group (in the salicylaldehyde) and the amino and imine groups (in the benzothiazole).[20] However, analyses of the degradation mixture using other techniques, such as high performance liquid chromatography (HPLC) and differential scanning calorimetry (DSC) and thermo gravimetric analysis (TGA), might provide further insight on the degradation process.

The fact that salicylaldehyde signals appeared in the ^{1}H NMR spectrum after 14 days of exposure in PBS solution indicates that the benzothiazole molecule was detached from the polymer in a controlled manner. Notably, samples analysed for the benzothiazole ligand suspended in the PBS solution displayed the same ^{1}H NMR spectra even after 45 days of exposure. This suggested that the imine bond was not hydrolysed as the ligand was not soluble in the PBS solution. This observation confirms that the polymer also improved the solubility of the benzothiazolimine molecule. This study demonstrated that ^{1}H NMR spectroscopy is a useful technique to study polymer degradation and drug release.

3.5 Concluding remarks

The homoleptic zinc catalyst (**39**), [Zn(N^O)$_2$], stabilized with the benzothiazole group, was found to be active towards lactide polymerization. It has been shown for the first time here that the zinc(II) homoleptic complex (**39**) produces functionalized polymers which were terminated with the drug-like benzothiazole group. It was observed that by changing the solvent polymers could be prepared with different chain lengths and PDI values. Incorporation of the drug-like moiety on the polymer back-bone was observed. The functionalized polymer displayed potential drug delivery properties

The phenylbenzothiazolyl complex (**40**), with bulky *tert*-butyl groups was inactive for lactide polymerization. The ferrocenyl thiosemicarbazone ligand (**42**) containing the electron-withdrawing 4-fluorophenyl substituent was unexpectedly found to be active for lactide polymerization in the presence of methanol. On the other hand, the zinc complexes stabilized with the ferrocenyl thiosemicarbazone group (**42**) and (**45**), [Zn(N^S)$_2$] displayed poor activity towards lactide polymerization. The 4-*tert*-butylphenyl analogues (**47**) and (**48**) of the thiosemicarbazone complexes displayed the lowest activity towards lactide polymerization. A summary of the lactide polymerization studies reported in this Chapter is given in **Table 3.5.1**)

Table 3.5.1: Summary of lactide polymerization studies with compounds prepared in this study

Compounds	Ref.	Comments
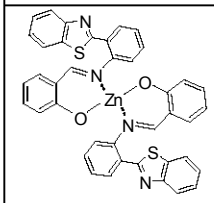	(**39**)	The catalyst produced polymers terminated with benzothiazolimine group.
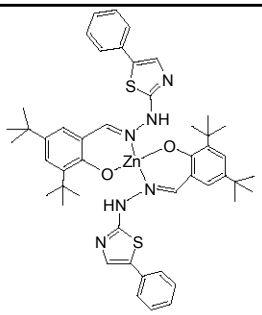	(**40**)	The catalyst was inactive for lactide polymerization due to bulky *tert*-butyl groups which presumably hindered access to the metal centre by lactide monomer.
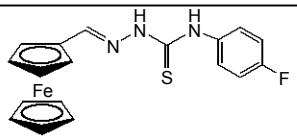	(**42**)	The ligand has unexpectedly displayed activity towards lactide polymerization; the activity was attributed to activation of lactide monomer by electrophilic amino protons. Similar observation has been made for thiourea compounds.
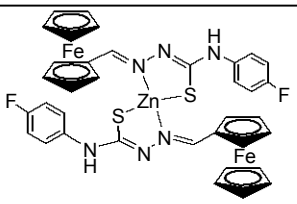	(**46**)	The catalyst displayed activity towards lactide polymerization; however, conversion of lactide monomer to form polylactide took longer, due to *soft* thiolate-anion which is a weak polymerization initiator.
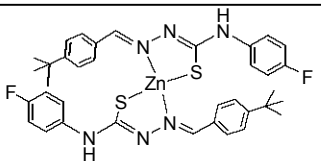	(**47**)	The catalyst displayed low activity towards lactide polymerization, possibly, due to the combination of a weak donor group; *tert*-butylphenyl (when compared to Fc) and also to the *soft* thiolate-anion which is a weak polymerization initiator.
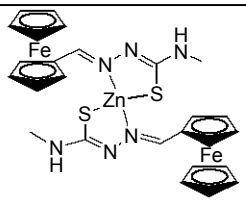	(**45**)	The catalyst displayed activity towards lactide polymerization; however, conversion of lactide to form PLA took longer, possibly, due to the combination of nucleophilic effects of methyl group and also to the *soft* thiolate-anion which is a weak polymerization initiator.
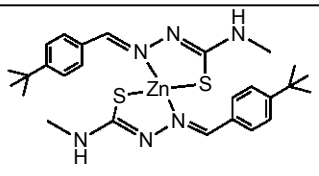	(**43**)	The catalyst displayed very low activity towards lactide polymerization, possibly, due to the combination of weak donor *tert*-butylphenyl group and nucleophilic methyl group, and also to the *soft* thiolate-anion, which is a weak polymerization initiator.

3.6 References

1. (a) R. O. MacRae, C. M. Pask, L. K. Burdsall, R. S. Blackburn, C. M. Rayner and C. McGowan, *Angew. Chem. Int. Ed*., 2011, **50**, 291; (b) W. Zhao, Dongmei, X. Liu and X. Chen, *Macromolecules*, 2010, **43**, 6678; (c) F. K. Wolf, A. M. Hofman and H. Frey, *Macromolecules*, 2010, **43**, 3314; (d) R. Tong and J. Cheng, *J. Am. Chem. Soc*., 2009, **131**, 4744; (e) M. J. Stanford and A. P. Dove, *Macromolecules*, 2009, **42**, 141; (f) M. Pitet and M. A. Hillmyer, *Macromolecules*, 2009, **42**, 3674; (g) M. B. Runge, S. Dutta and N. B. Bowden, *Macromolecules*, 2006, **39**, 498.
2. (a) R. H. Platel, L. M. Hodgson and C. K. Williams, *Polym. Rev.*, 2008, **48**, 11; (b) J. Wu, T-L. Yu, C-T. Chen, C-C. Lin, *Coord. Chem. Rev*., 2006, **250**, 602.
3. (a) E. Luiz de Paula, V. Mano, F. V. Pereira, *Polym. Degrad and Stabil*., 2011, **96**, 1631; (b) M.-R. Jung, I.-K. Shim, E-S. Kim, Y.-J. Park, Y.-L. Yang, S.-K. Lee, S.-J. Lee, *J. Contr. Rel*., 2011, **152**, 294.
4. (a) J. Zhao and R. M. Wilkins, *J. Agric. Food Chem*., 2005, **53**, 4076; (b) P. A. Holmes, *Phys. Technol*., 1985, **16**, 32.
5. R. O. MacRae, C. M. Pask, L. K. Burdsall, R. S. Blackburn, C. M. Rayner and P. C. McGowan, *Angew. Chem. Int. Ed., 2011*, **50**, 291.
6. (a) M. Save, M. Schappacher and A. Soum, *Macromol. Chem. Phys*., 2002, **203**, 889; (b) J. Baran, A. Duda, A. Kowalski, R. Szymanski and S. Penczek, *Macromol. Rapid Commun*., 1997, **18**, 325.
7. (a) L. Wang, J. Zhang, L. Yao, N. Tang and J. Wu, *Inorg. Chem. Commun*., 2011, **14**, 859; (b) W. Zhao, D. Cui, X. Liu and X. Chen, *Macromolecules*, 2010, **43**, 6678; (c) M. J. Stanford and A. P. Dove, *Macromolecules*, 2009, **42**, 141; (d) D. J. Darensbourg, W. Choi, O. Karroonnirum and N. Bhuvanesh, *Macromolecules*, 2008, **41**, 3493; (e) I. Blakey, A. Yu, S. M. Howdle, A. K. Whittaker and K. J. Thurecht, *Green Chem*., 2011, **13**, 2032.
8. (a) P. L. Arnold, I. J. Casely, Z. R. Turner, R. BellaBarba and R. B. Tooze, *Dalton Trans*., 2009, 7263; (b) H. Du, A. H. Velders, P. J. Dijkstra, Z. Zhong, X. Chen and J. Feijen, *Macromolecules*, 2009, **42**, 1058; (c) W.-C. Hung and C.-C. Lin, *Inorg. Chem*., 2009, **48**, 728; (d) H.-Y. Chen, M.-Y. Liu, A. K. Sutar and C.-C. Lin, *Inorg. Chem*., 2010, **49**, 665; (e) W.-C. Hung, Y. Huang, C.-C. Lin, *J. Polym. Sci.: Part A: Polym. Chem.*, 2008, **46**, 6466.

9. H.-Y. Chen, H.-Y. Tang and C.-C. Lin, *Macromolecules*, 2006, **39**, 3745.
10. (a) J. Eijfler, S. Szafert, K. Mierzwicki, L. B. Jerzykiewicz and P. Sobota, *Dalton Trans*., 2008, 6556; (b) H. R. Kricheldorf, M. Berl and N. Scharnagl, *Macromolecules*, 1988, **21**, 286.
11. (a) C.-Y. Li, C.-Y. Tsai, C.-H. Lin, B.-T. Ko, *Dalton Trans.*, 2011, **40**, 1880; (b) C. Zhang, Z-X. Wang, *J. Organomet. Chem*., 2008, **693**, 3151.
12. (a) A. P. Dove, R. C. Pratt, B. G .G. Lohmeijer, R. M. Waymouth and J. L. Hendrick, *J. Am. Chem. Soc*., 2005, **127**, 13798; (b) B. G. G. Lohmeijer, R C. Pratt, F. Leibfarth, J. W. Logan, D. A. Long, A. O. Dove, F. Nederberg, J. Choi, C. Wade, R. M. Waymouth and J. L. Hedrick, *Macromolecules*, 2006, **39**, 8574.
13. (a) O. Coulembier, B. G. G. Lohmeijer, A. P. Dove, R. C. Pratt, L. Mespoulie, D. A. Culkin, S. J. Benight, P. Dubois, R. M. Waymouth and J. L. Hedrick, *Macromolecules*, 2006, **39**, 5617; (b) A. P. Dove, R. C. Pratt, B. G. G. Lohmeijer, D. A. Culkin, E. C. Hagberg, G. W. Nyce, R. M. Waymouth and J. L. Hedrick, *Polymer*, 2006, **47**, 4018; (c) E. F. Connor, G. W. Nyce, M. Myers, A. Möck and J. L. Hedrick, *J. Am. Chem. Soc*., 2002, **124**, 914.
14. (a) R. C. Pratt, B. G. G. Lohmeijer, D. A. Long, R. M. Waymouth and J. L. Hedrick, *J. Am. Chem. Soc*., 2006, **128**, 4556; (b) G. Theryo, F. Jing, L. M. Pitet and M. A. Hillmyer, *Macromolecules*, 2010, **43**, 7394; (c) H. R. Kricheldorf, N. Lomadze and G. Schwarz, *Macromolecules*, 2008, **41**, 7812.
15. (a) M. Basko and P. Kubisa, *J. Polym Sci.: Part A: Polym. Chem*., 2010, **48**, 2650; (b) D. Bourissou, B. Martin-Vaca, A. Dumitrescu, M. Graullier and F. Lacombe, *Macromolecules*, 2005, **38**, 9993.
16. N. K. Lim, K. J. Yaccato, R. D. Dghaym and B. A. Arndtsen, *Organometallics*, 1999, **18**, 3953.
17. (a) T. Liu, T. L. Simmons, D. A. Nohnsack, M. E. Mackay, M. R. Smith, III and G. L. Baker, *Macromolecules*, 2007, **40**, 6040; (b) G. Montaudo, M. S. Montaudo, C. Puglisi, F. Samperi, N. Spassky, A. LeBorgne and M. Wisniewski, *Macromolecules*, 1996, **29**, 6461.
18. (a) F. Alexis, *Polym. Int.*, 2005, **54**, 36; (2005); (b) L. R. Folkman, *Nature*, 1976, **263**, 5580; (b) R. Dinarvand, N. Sepehri, S. Manoochehri, H. Rouhani, and F. Atyabi, *Int. J. Nanomed.*, 2011, **6**, 877.

19. J. Contreras, J. Xie, Y. J. Chen, H. Pei, G. Zhang, C. L. Fraser and S. F. Hamm-Alvarez, *ACS Nano*, 2010, **4**, 2735.
20. A. D. Cross and R. A. Jones, *An Introduction to Practical Infra-red Spectroscopy*, 3rd Edn., Butterworth, Ltd., London, 1969, p. 97.

CHAPTER 4: CARBON MONOXIDE/STYRENE COPOLYMERIZATION

4.1 Introduction

Cationic palladium catalysts which have been found to be active towards CO/styrene copolymerization were highlighted in Chapter 1. Thus far, catalysts which have shown activity are those bearing N^N ligands.[1] It has been generally found that the catalysts which are stabilized with P^N ligands are inactive for CO/styrene copolymerization. A few of these catalysts have been found to display low activity when conducting polymerization using higher CO pressures and temperatures. The π-acceptor ability of the phosphorus atom has been proposed to be stabilizing the styryl-allyl intermediate, thus hindering polymerization.[1] In this case, mostly oligoketones have been observed as products. The N^N catalyst systems, however, have been found to be the best candidates for CO/olefin copolymerization.[2] In order to promote catalyst recyclability, which is a principle (Principle 4) of Green Chemistry (see Chapter 1). Various conditions have been proposed to be play a role in the copolymerization reaction, such as the amount of the benzoquinone oxidant, the amount of catalyst, the amount of trifluoroethanol as a solvent or co-solvent, and the pressure of the reaction.[2] On the other hand, the electronic properties of the stabilizing N^N ligand have been shown to influence the performance of resulting catalysts as well as stereochemistry of copolymers.[1,2]

In this study, several new compounds bearing the pyridyl nitrogen donor group (i.e. *N,N*-di(2-pyridyl) were investigated. These were the type one compounds, [tol-(CO)N(N^N) Pd(MeCN)Me]X, X = PF_6^- and BF_4^-, (**55**) and (**56**), the type two compounds, [tol-(CO)N(N^N)(PPh_3)PdMe]X, X = PF_6^- and BF_4^-, (**57**) and (**58**), and the last type of compounds were the ferrocenyl analogues, [Fc-(CO)N(N^N)Pd(L)Me]PF_6, L = MeCN and PPh_3, (**59**) and (**60**) (see **Figure 4.1.1**). The tolyl analogues served as model compounds for a future heterogeneous catalyst system. Once the compounds were fully characterized and their catalytic activity investigated, then the ligand might be functionalized on carbon nanotubes (CNTs), followed by complexation to prepare supported catalysts.

The supported catalysts could improve catalyst activity since the carbon nanotubes would electronically stabilize palladium(II) species thus the copolymerization reaction will continue for longer times. However, the main aim would be catalyst recyclability. The reaction route which illustrates the preparation of supported catalyst systems on CNTs is shown in **Figure 4.1.2**.

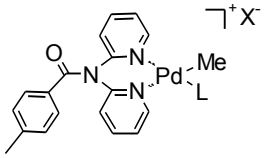

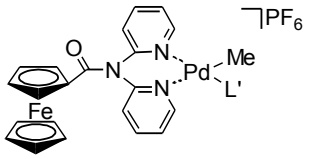

Tolyl analogues		Ferrocenyl analogues	
X^-, L	Compound	L'	Compound
PF_6, MeCN	(**55**)	MeCN	(**59**)
BF_4, MeCN	(**56**)		
PF_6, PPh_3	(**57**)	PPh_3	(**60**)
BF_4, PPh_3	(**58**)		

FIGURE 4.1.1: New compounds prepared and investigated for CO/styrene copolymerization.

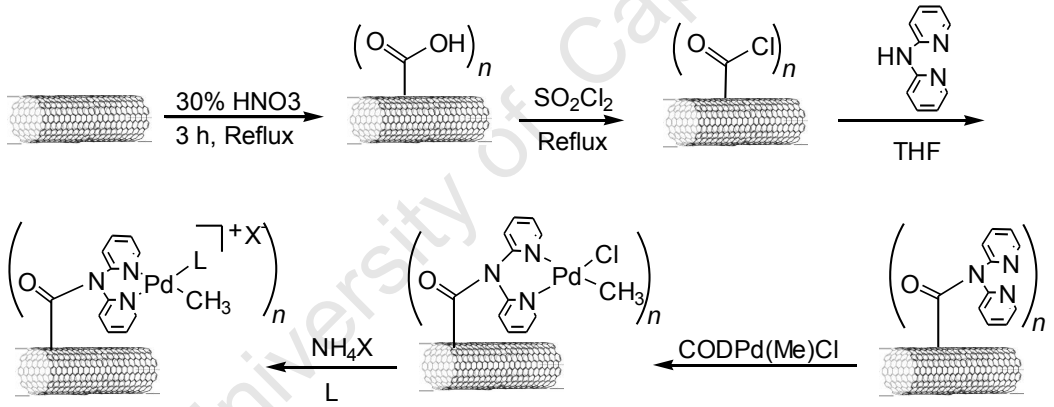

FIGURE 4.1.2: Reaction scheme illustrating the preparation of palladium catalysts supported on carbon nanotubes.

The ferrocenyl analogues were prepared in order to investigate the effect of changing the oxidation state of the ferrocenyl group in the complexes on the catalytic process. Compounds containing the triphenylphosphine donor ligand were prepared to investigate their activity, since most catalysts in the literature are those stabilized with a P^N bidentate ligand. To the best of our knowledge, the new type of complexes with phosphine as a monodentate ligand prepared in this study has never been explored for CO/styrene copolymerization. In addition, the phosphorus-

containing catalysts prepared here, will be of interest when expanding the study for CO/olefin copolymerization in the future.

Experiments were conducted in order to investigate the effects of reaction conditions on the production of CO/styrene copolymers. The optimum system would be the one producing a narrow distribution of polymers (with PDI ≈ 1), in high yield and with large molecular weight. In particular, the effects of varying the amount of catalyst, benzoquinone, trifluoroethanol, carbon monoxide pressure and temperature on the copolymerization reaction were investigated. The polymers prepared here were then utilized for functionalization with lactide, the results of which will be discussed in the next chapter.

4.2 Results and Discussion on CO/styrene polymerization

The complexes containing triphenylphosphine as a donor ligand displayed poor activity or no activity compared to compounds containing acetonitrile donor ligands under the catalytic conditions employed in this study. All compounds prepared here were inactive at elevated CO pressures of above 1 atm. Compound (**55**) containing the PF_6^- anion displayed better activity than compound (**56**) stabilized with the BF_4^- anion. For the ferrocene-containing complexes, compound (**59**) displayed activity while complex (**60**) was inactive. The results on polymer yields and catalytic activity were obtained from three repeat experiments and the data were reproducible. The results obtained from the catalyst testing studies and the characterization of the isolated polymers are discussed in this chapter.

4.2.1 Catalytic activity of palladium complexes at ambient conditions

The catalysts were employed for styrene/carbon monoxide copolymerization at room temperature under 1 atm, in the presence of benzoquinone as the oxidant in dichloromethane as solvent and trifluoroethanol as a stabilizing co-solvent, full experimental details are described in the experimental section (Chapter 7). When the polymerization was conducted in dichloromethane or methanol as solvents, catalysts (**55**), (**56**) and (**59**) decomposed to form palladium black upon introduction of carbon monoxide. Similar behaviour has been observed for other related catalysts

stabilized with N^N ligands.[1] This decomposition has been postulated to be due to the unstable palladium-acyl intermediate in these solvents which leads to the cleavage of the (N^N)-Pd bonds, resulting in aggregation of palladium atoms to produce metallic palladium black.[1] This behaviour, however, was not observed when compounds (**57**), (**58**) and (**60**) were utilized under the same conditions. The donor ability of phosphorus group which is better than acetonitrile, stabilized palladium complexes (**57**), (**58**) and (**60**) in dichloromenthane or methanol in the presence of CO.

Production of copolymers (CP), however, was successful when trifluoroethanol was introduced to the reaction. Trifluoroethanol is believed to stabilize the palladium species which is forming after the first catalytic cycle; and also to initiate the polymerization step in the subsequent cycles thus forming polymers terminated with trifluoromethoxy (CF_3CH_2O-) group.[2] Palladium complexes (**55**), (**56**), (**57**) and (**59**) displayed activity at ambient conditions while compound (**44**), displayed the highest activity. On the other hand, catalyst (**59**) with ferrocenyl group in its oxidised form, obtained by adding $AgBF_4$ to the reaction mixture, displayed best copolymer yield (**Table 4.2.1)**. The results represent an average of three repeat experiments and the data were reproducible (M_n values did not differ by more than M_n = 10 g/mol).

TABLE 4.2.1: Results for Carbon monoxide/styrene copolymerization when utilizing palladium complexes prepared in this study[a]

Catalyst	CP yield (mg)[b] [Activity, g CP (g Pd)$^{-1}$ h^{-1}]	Mn[c] x10^3	PDI[c]
(**55**)	390, [203.60]	2.51	2.34
(**56**)	5, [2.60]	0.91	2.22
(**57**)	2.3, [1.20]	0.24	1.16
(**58**)	-[d]	-	-
(**59**)[e]	7, [1.80]	1.25	2.34
(**59**)[f]	550, [143.60]	1.47	2.24
(**60**)	-	-	-

[a]Reaction conditions: dichloromethane (4 ml), trifluoroethanol (1 ml), styrene (5 ml), benzoquinone 20 x 10^{-6} mol, room temperature, 1 atm carbon monoxide, Pd contend in catalyst (1 x 10^{-6} mol), time = 18 h. [b]Mass of isolated polymer. [c]Determined by GPC analysis. [d]No polymer was isolated. [e]Pd contend in catalyst (2 x 10^{-6} mol) and BQ (40 x 10^{-6} mol). [f]Oxidized ferrocenyl group.

Polymers obtained when using catalyst (**55**) had a medium molecular weight (M_n = 2.51 x 10^3) with PDI = 2.34. On the other hand, catalyst precursor (**59**) in its oxidized form displayed highest copolymer yield of 550 mg. Generally, catalysts which displayed better activity were those stabilized with the acetonitrile ligand and the PF_6^- anion when compared to those bearing the BF_4^- anion. The produced polymers had medium size molecular weights and broad polymer distribution coefficients PDI = 2.22 – 2.34. The catalysts stabilized with the triphenylphosphine ligand displayed low activity; for example, catalyst (**57**) produced 5 mg of low molecular weight polymer (M_n = 0.91 x 10^3) with slightly improved polymer distribution (PDI = 1.16). Catalysts (**58**) and (**60**) were inactive.

A discussion of the results shown in **Table 4.2.1** now follows: it was observed in Chapter 1 that the increase in catalyst performance for cationic complexes is related to low interionic interaction between the metal centre and the anion, i.e. BF_4^- interacts strongly with Pd(II) when compared to the PF_6^- anion, leading to lower activity.[2] Complex (**48**), on the other hand, displayed low activity while compound (**58**) was inactive. The low activity of complexes (**57**) and (**58**) was postulated to be due to the hindrance of styrene insertion by either the strong donor triphenylphosphine ligand or stabilization of the Pd-(η^3)-styryl intermediate by triphenylphosphine through π-back donation.[3]

The effect of phosphorus donors on the CO/styrene copolymeriztion reaction has been studied in great detail.[2] These researchers have observed that the back-donation process favours the β-hydride elimination reaction, resulting in the formation of lower molecular weight oligoketones. This behaviour was confirmed in the present study since a low molecular weight oligo-ketone with $M_n \approx 240$ was obtained when catalyst (**57**) was utilized. Further experiments utilizing compound (**57**) were therefore conducted in a different solvent and varying temperature conditions. The results obtained will be discussed in **Section 4.2.7**.

The ferrocene-containing catalysts displayed low activity when compared to the tolyl analogues. As was discussed in Chapter 2, the ferrocenyl group is a better electron donor than the tolyl group, so the poor activity of compound (**59**) compared to that of complex (**55**) is attributed to the higher electron density in the

palladium centre in this compound. Palladium complexes with electron donating ligands have been found to be less active towards CO/styrene copolymerization.[4] Interestingly, an *in situ* oxidation of the ferrocenyl group with $AgBF_4$ in a solution of catalyst (**59**) resulted in a remarkable increase in productivity of polyketones. The increase in productivity corresponded to 80-fold improvement in the catalyst activity compared to the un-oxidized ferrocenyl moiety. No polymers were isolated from the control experiments conducted using $AgBF_4$, ferrocenyl ligand (**52**) or with both $AgBF_4$ and ligand (**52**) in the reaction mixture. This proved that the observed improved catalytic activity of catalyst (**59**) with ferrocenyl group in its oxidized form was not due to $AgBF_4$, ligand (**52**) or combination of these two. The ferrocenium moiety had an overall electron withdrawing property that reduced electron density at the palladium centre, generating an improved catalyst (see **Table 4.2.1**).

Electronic properties of the ligands play an important role in CO/styrene copolymerization reactions. The N^N(CO)Pd-acyl species (iii) shown in **Figure 4.2.1** has been found to be stabilized by the presence of electron-rich ligands.[4]

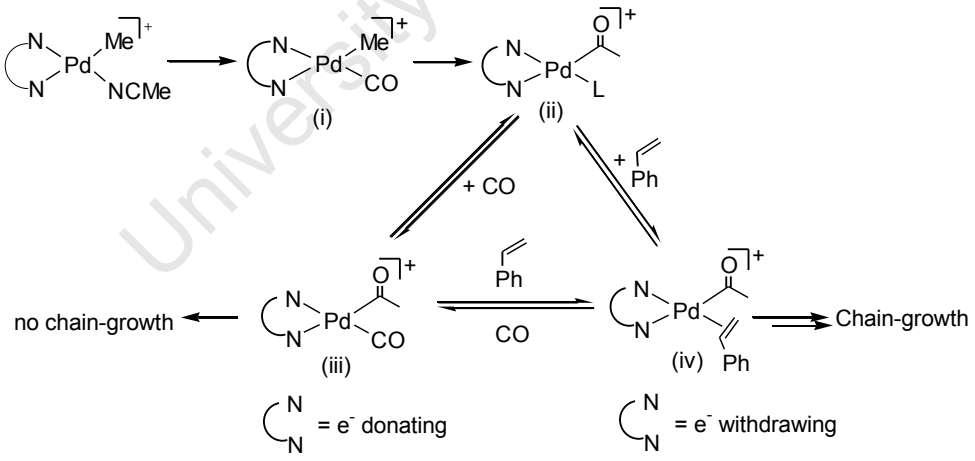

FIGURE 4.2.1: Observed catalytic behaviour for catalysts stabilized with ligands bearing different electronic propeties.[4]

The formation of the Pd-acyl-alkene intermediate (iv), on the other hand, is favoured with ligands bearing electron-withdrawing substituents.[4] The triphenylphosphine complex (**60**) was inactive. These results confirm the influence that electronic properties of the ligands have on the catalytic behaviour. Since

catalyst (**55**) displayed better activity than the other catalysts it was further investigated.

4.2.2 Effect of varying the temperature and pressure when using catalyst [tol-(CO)N(N^N)Pd(MeCN)Me]PF_6 (**55**)

It was observed that no solid material was obtained when experiments were conducted at room temperature employing CO pressures of 5, 10, 20 and 30 bar. Even when the temperature was increased from 30 to 50 ºC at 5 bar CO pressure no polymer was isolated. Surprisingly, using all the conditions described no palladium black was detected. This suggests that the lack of activity was not due to catalyst decomposition. The catalyst behaviour is in contrast to other N^N stabilized catalysts which required high CO pressures to produce polyketones.[5] Conversely, Reiser and co-workers observed a decrease in catalytic activity when the CO pressure was increased from 1 to 40 bar for their oxazoline-palladium complexes.[4] In their work, an increase in temperature from 30 ºC to 50 ºC resulted in a decrease in catalytic activity.

D'Amora *et al.*, investigated the formation of oligoketones using substituted bipyridyl-palladium complexes.[5] In contrast to what was observed in the present study, their catalysts were stabilized with electron-withdrawing N^N ligands and yielded only oligoketones at low CO pressure of less than 2 bar, but with an increase in CO pressure from 1 – 6 bar there was an increase in the amount of polyketones, while the oligoketone yield decreased.[5] The electron-withdrawing ligands resulted in a decrease in electron density on the metal centre which favoured the β-hydride elimination reaction and, subsequently, oligoketones were produced at ambient conditions. Increasing the pressure promoted the CO insertion reaction resulting in lower yields of polyketones. Catalyst (**55**) yielded polymers with medium molecular weight at 1 atm CO pressure, but at high CO pressures, no polymer was isolated. From this obrsevations it can be concluded that the complexes stabilized by N^N ligand investigated in this study are not suitable for high pressure or high concentrations of CO. It is possible that the electronic properties of the ligands promotes oligoketone formation at this conditions, however, formation of the oligoketones was not confirmed.

*4.2.3 Effect of varying the amount of benzoquinone at ambient conditions when using catalyst (**55**)*

The effect of the amount of oxidant, 1,4-benzoquinone (BQ), in relation to the palladium complex on the catalytic behaviour was investigated. In Chapter 1 the oxidation of molecular palladium(0) by BQ was discussed. It was observed that when BQ was not employed no polyketones were isolated and palladium black was formed. Interestingly, when ten equivalents of BQ were employed for 18 h reaction, a small amount (25 mg) of polyketone was isolated (see **Figure 4.2.2)**, similar observations were made by Scarel and D'Amora research groups[4,5] A further increase in BQ to 20 equivalents resulted in a further increase in the yield of polyketones to 39 mg, while higher molecular weight polymers were also obtained. In all cases when BQ was varied the reaction time was 18 h.

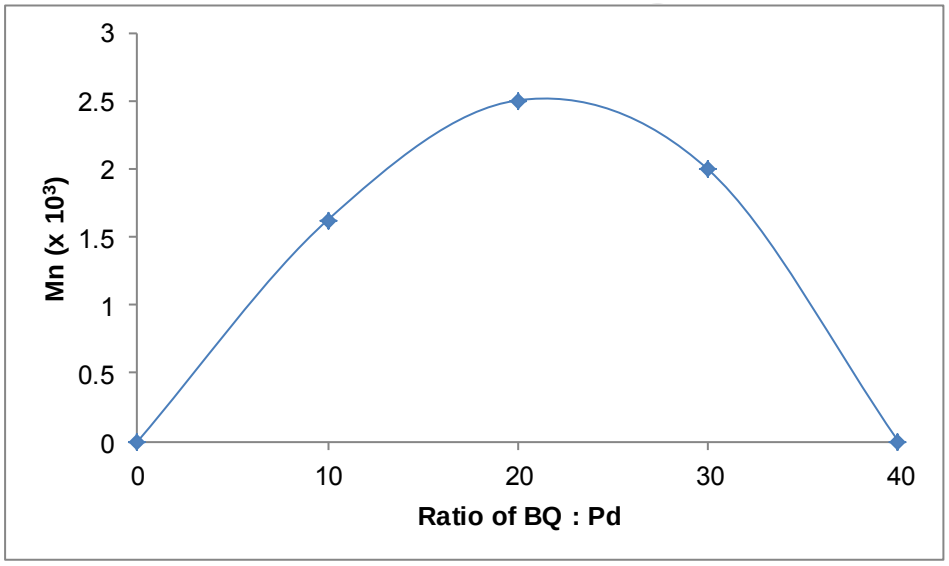

FIGURE 4.2.2: Styrene/Carbon monoxide copolymerization utilizing compound (**55**) to investigate the effect of varying the amount of the oxidant benzoquinone. Reaction conditions: see Table 4.2.1, except for increasing amount of BQ.

A further increase in the amount of BQ to 40 equivalents impacted negatively on the production of polyketones as no solid material was isolated. The large amount of BQ beyond 20 equivalents could have hindered the access of the monomer to the catalytic centre, thus affecting the catalyst performance. Similar observations were made by Guo *et al*. on their catalyst which was supported on a resin.[6] This observation suggested use of a Pd : BQ ratio of 1 : 20, and this ratio was employed in all further catalytic investigations. It is worth noting that studies which have been

conducted on various N^N-stabilized catalyst systems revealed an opposite behaviour to what was observed to in this current study. For example, increasing BQ from 5 to 40 equivalents has been observed result in a concomitant increase in polyketone formation.[4,5,7] However, they did not report the molecular weight of the polymers they isolated. On the other hand, Reiser and co-workers observed a decrease in catalyst activity when the BQ : Pd ratio was increased from 30 to 40.[4] A decrease in molecular weight for the isolated copolymers was also observed. It can be concluded that the best BQ to Pd(II) ratio depends on the type of the catalyst investigated. In the subsequent experiments, when the effect of catalyst loading was investigated, a Pd : BQ ratio of 1 : 20 was always employed and reaction time was 18 h.

4.2.4 Effect of catalyst (**55**) *loading at ambient conditions*

Catalyst (**55**) displayed activity when using catalyst amount as low as 0.005 g (0.01 mmol) which corresponded to 1.06 mg of Pd. The following activities g CP (g Pd)$^{-1}$ h^{-1} were observed when different amounts of catalyst was used: 203.60 (0.005 g), 33.8 (0.01 g) and 78.6 (0.015 g). The activity is defined as the amount of polymer produced per amount of palladium content per hour, i.e. g CP (g Pd)$^{-1}$ h^{-1}. However, polymers with similar molecular weights were isolated when different catalyst loading was used. Polymer yields were 390, 129 and 450 mg, when catalyst amounts of 0.005, 0.01, and 0.015 g were used, respectively (see **Figure 4.2.3)**. The results represent an average of three repeat experiments and the data were reproducible.

A marginal improvement in the dispersity of the polymers was noticed when the catalyst loading was increased. The molecular weight of the polymers was not affected when the catalyst loading was varied. Utilization of a large amount of catalyst in the reaction is not generally a disadvantage, particularly if the catalyst can be recycled. Rcyclability of the catalyst can be challenging in this case, since palladium species can be enrapped within the polymer sample and finaly be leached out. From an economic point of view it is necessary to keep the palladium content as low as possible.

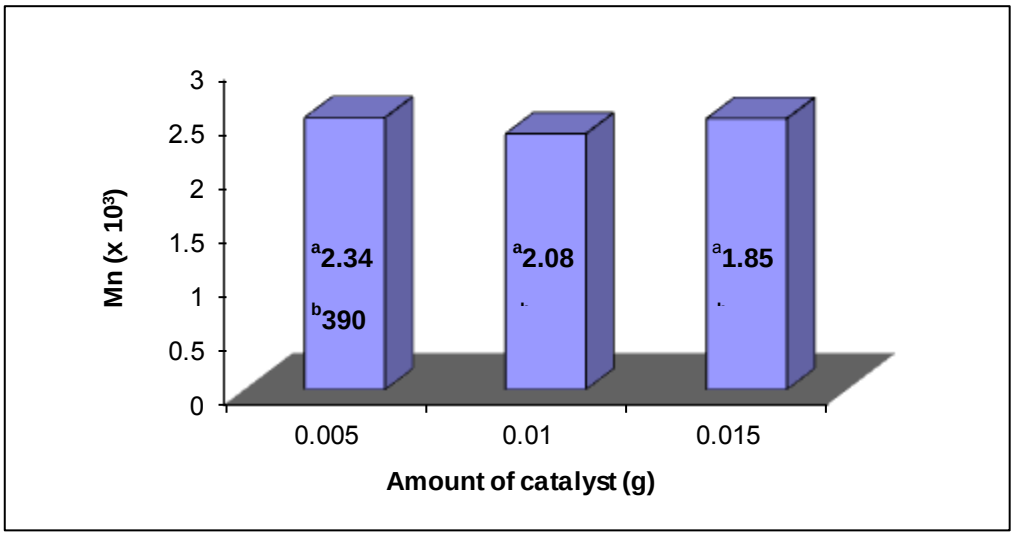

FIGURE 4.2.3: Carbon monoxide/Styrene copolymerization: effect on Mn, PDI and polymer yield when using different amounts of catalyst (**55**). For reaction conditions see Table 4.2.1, except for increasing amount of catalyst precursor. [a] PDI of isolated polymer analysed by GPC. [b]Mass of isolated Polymer (mg).

The catalyst loadings employed in this study are comparable to those utilized by other researchers. The advantage of the ligands employed here is that they can be functionalized and attached to various supports such as carbon nanotubes, which could enable catalyst recycling since CNTs interact strongly with palladium species.

4.2.5 Effect of varying the concentration of styrene monomer on copolymerization when using catalyst (**55**)

The variation of styrene concentration in relation to palladium content was investigated. As expected, when employing styrene concentration of of 175 , 400 and 1050 M, an increase in polymer molecular weight, M_n = 1690, 2510 and 3790, respectively, was observed. However, a further increase in styrene concentration (1400 M) resulted in loss of catalyst performance and polymers with M_n = 810 were obtained (see **Table 4.2.2**).

The volume of styrene used corresponded to styrene : Pd molar ratios of 2000:1, 4000:1, 10000:1 and 14000:1, respectively. The results suggest that when concentrations of styrene are increased, the rate of monomer insertion is favoured over β-hydride elimination, thus delaying the termination process. This leads to an increase in polymer molecular weight. However, the polymers produced in these experiments had a broad PDI; better polymer dispersity was observed when 1050 M

of styrene was used (see Table 4.2.2, entry 3). A drop in catalyst activity when concentration of styrene was further increased (Entry 4, corresponding to styrene/Pd ratio of 14 000), the termination is faster under this conditions resulting in polymers with smaller M_n value.

TABLE 4.2.2: Carbon monoxide/Styrene copolymerization: effect of varying the concentration of styrene using catalyst (**55**)[a]

Entry	Styrene/ Pd[b]	CP Yield (mg),[c] [Activity g CP (g Pd)$^{-1}$ h^{-1}]	M_n[d] (x10^3)	PDI[d]
1	1750	150, [78.10]	1.69	2.13
2	4000	390, [203.10]	2.51	2.34
3	10500	150, [78.10]	3.79	1.48
4	14000	53, [27.90]	0.81	2.64

[a]Reaction conditions: see Table 4.2.1, except for varying volume of styrene. [b]Molar ratio of styrene/ Pd. [c]Mass of isolated polymer. [d]Determined by GPC analysis using polystyrene standards.

4.2.6 Effect of varying the concentration of trifluoroethanol for catalyst (**55**) *at ambient conditions*

As already mentioned in Chapter 1, Section 1.2.3, researchers have discovered that trifluoroethanol (TFE) plays a major role in stabilizing palladium(II) ions in the solution after the first cycle of polymerization reaction. The use of TFE is employed mostly when the catalysts stabilized by N^N bidentate ligands are used in the CO/styrene copolymerization reaction.[4,7a,8,9] It is believed that this is due to its low nucleophilicity compared to methanol. Trifluoroethanol can also stabilize the active species, thus improving the catalyst lifetime. The effect of varying the concentration of TFE was investigated using catalyst (**55**). As expected, no polymer was produced when the experiment was conducted in the absence of TFE. When catalysis was conducted in dichloromethane or methanol solvents without TFE, palladium black was observed. Polymers were successfully isolated when TFE was introduced into the reaction mixture (see **Table 4.2.3**).

TABLE 4.2.3: Carbon monoxide/styrene copolymerization: effect of varying concentration of trifluoroethanol using catalyst (**55**)[a]

Entry	TFE (ml)	DCM (ml)	CP Yield (mg),[b] [Activity, g CP (g Pd)$^{-1}$ h^{-1}]	Mn[c] x10^3	PDI[c]
1	0	5	–[d]	–[e]	–
2	1	4	390, [207.41]	2.51	2.34
3	1.5	3.5	300, [157.89]	2.35	1.41
4	2.5	2.5	400, [210.53]	2.15	1.48
5	5.0	0	600, [315.79]	2.93	1.68

[a]Reaction conditions: see Table 4.2.1, except for varying amount of TFE. [b]Mass of isolated polymer. [c]Determined by GPC analysis using polystyrene standards. [d] No polymer was isolated. [e]Not determined.

An increase in volume of TFE while keeping the total volume of the catalytic system constant resulted in a concomitant increase in polymer yield, the catalyst activity and the molecular weight of the polymer. Moreover, the catalyst showed the best activity when only TFE was utilized as a solvent (**Table 4.2.3,** entry 5). Better polymerization control was achieved when the TFE volume was 1.5 and 2.5 ml, where PDI values of 1.41 and 1.48, were obtained. These results confirmed the important role played by TFE. In summary, an increase in the concentration of TFE results in an increased yield of polymers.

4.2.7 Effect of catalytic reaction time on CO/styrene copolymerization using catalyst (**55**)

Experiments were conducted at a constant catalyst : styrene molar ratio of 1 : 4000. In some experiments, 5 mg of catalyst and 400 M of styrene was employed, while in other experiments 10 mg of catalyst and 1050 M of styrene was used. It was observed that when reactions were conducted for 36 h each experiment yielded polymers with molecular weight of M_n = 1170. The molecular weights of isolated polymers were smaller than those obtained when reactions were run for 18 h under the same conditions.

Since M_n is a number average molecular weight of various polymers formed during catalysis, it is possible that when the reaction time is prolonged a number of active sites are hindered, which leads to the formation of large amounts of small-chain

polymers. The overall molecular weight of the polymeric material will then be smaller. On the other hand, a decreased yield of polymers produced was observed when reaction was conducted for 36 h. Polymer yields of 300 mg (PDI = 1.44) and 120 mg (PDI = 1.54), respectively, were observed when 5 and 10 mg of catalysts were employed for reaction times of 36 h. From these studies, it can be concluded that longer reaction times affects the polymer yields for reactions when same amount of catalyst is used. This could mean that the steady state was reached during 18 h of reaction.

4.2.8 Catalytic behaviour of complexes (**57**) *and* (**58**) *stabilized with a triphenylphosphine donor ligand*

As has already been mentioned in Chapter 1, stabilized with triphenylphosphine catalysts are generally known to require high CO pressures (320 bar) in order to produce CO/styrene copolymers. In this study, using the new catalysts a CO pressure of 50 bar was employed for investigations on the catalytic activity of complexes with triphenylphosphine, *viz.* [tol-(CO)N(N^N)PdMe(PPh_3)]X, X = PF_6 (**57**) and X = BF_4 (**58**) and [Fc-(CO)N(N^N)PdMe(PPh_3)]PF_6 (**60**). Catalysts (**57**), (**58**) and (**60**) were inactive for CO/styrene copolymerization at ambient conditions when compared to catalysts (**55**) and (**56**) investigated in this study.

To study this inactivity problem, NMR studies were conducted. The ^{13}C, ^{1}H and ^{31}P NMR spectra were recorded for compound (**57**) in $CDCl_3$ at room temperature. The NMR tube containing catalyst (**57**) was left standing under atmosphere of carbon monoxide (using a balloon) while shaking occasionally for ten minutes and the spectra were recorded again. Full details of experimental protocols employed are described in the experimental section in Chapter 7.

There was no difference between the original spectra and those obtained after reaction mixture was exposed to CO atmosphere for ten minutes. The reaction mixture was then further exposed to CO atmosphere for 18 h, and the insertion of carbon monoxide in the catalyst was observed (see **Figure 4.2.4)**.

A doublet signal due to the Pd-CH_3 resonance at δ 0.79 ppm disappeared and was replaced by a doublet at 2.12 ppm, which was attributed to the formation of the Pd acyl group (Pd-(C=O)-CH_3). A doublet due to the 6-pyridyl proton slightly shifted from 8.52 ppm as a broad signal to 8.48 ppm. The signal did not correspond to the 6-pyridyl proton of an uncoordinated ligand which resonated at 8.40 ppm. However, these chemical shifts are within the NMR accuracy, therefore, one could not rule out the dissociation of one nitrogen atom of the ligand from the metal centre to form (iii) (see **Figure 4.2.5**).

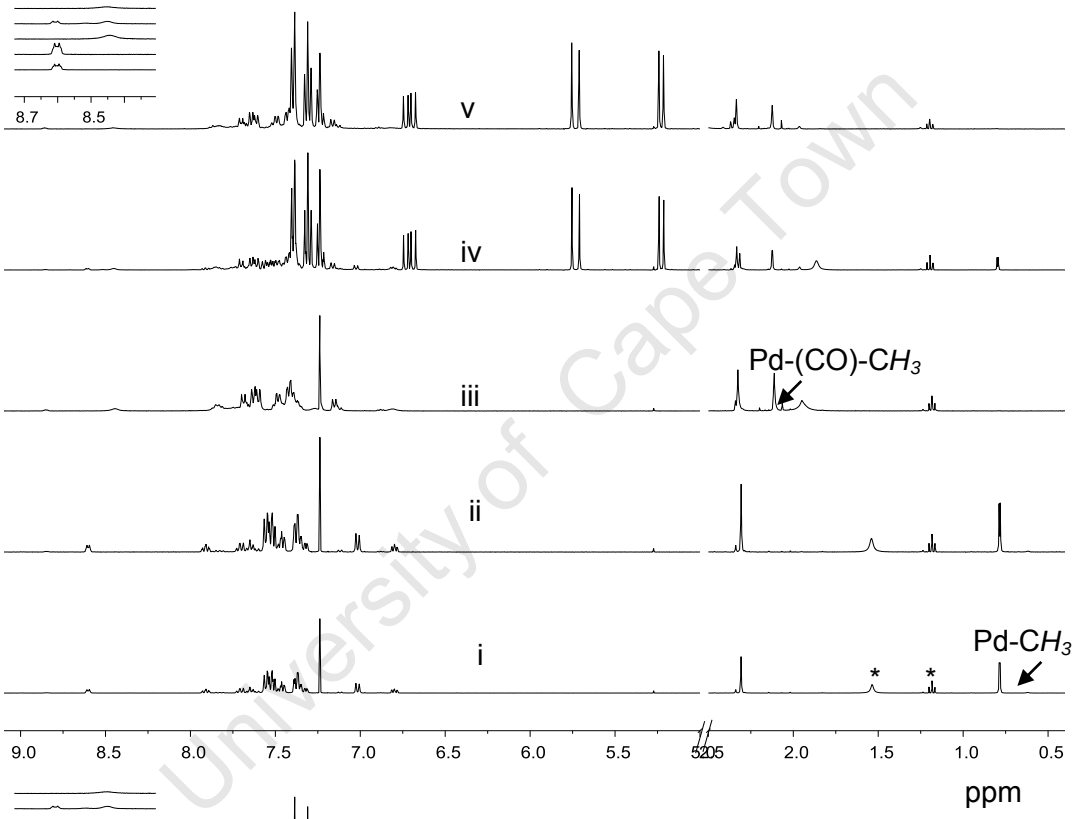

FIGURE 4.2.4: The ^{1}H NMR spectra in $CDCl_3$ of (**57**) during the investigation of carbon monoxide interaction with the catalyst precursor; (i) fresh solution of (**57**); (ii) compound (**57**) exposed to carbon monoxide atmosphere for ten minutes; (iii) solution exposed to CO atmosphere for 18 h; (iv) (**57**) and 3 equivalents of styrene under atmosphere of CO for 18 h; (v) the solution under the atmosphere of CO for 36 h. * Solvent impurity.

When three mole equivalents of styrene were introduced to the NMR solution, the rate of CO coordination in the catalyst slowed, since the signals due to the original catalyst were still visible even after 18 h of bubbling CO through the mixture. However, the signals disappeared after 36 h. There could have been a competition between styrene and CO for coordination to palladium, thus slowing the rate of CO coordination. The diffusion of carbon monoxide in the solvent mixture, especially

in the narrow NMR tube, could have also slowed the coordination process.[10,11] The studies confirmed that a methyl migration reaction took place in the presence of CO, while the dissociation of the pyridyl-amine ligand could not be ruled out (**Figure 4.2.5**, path B).

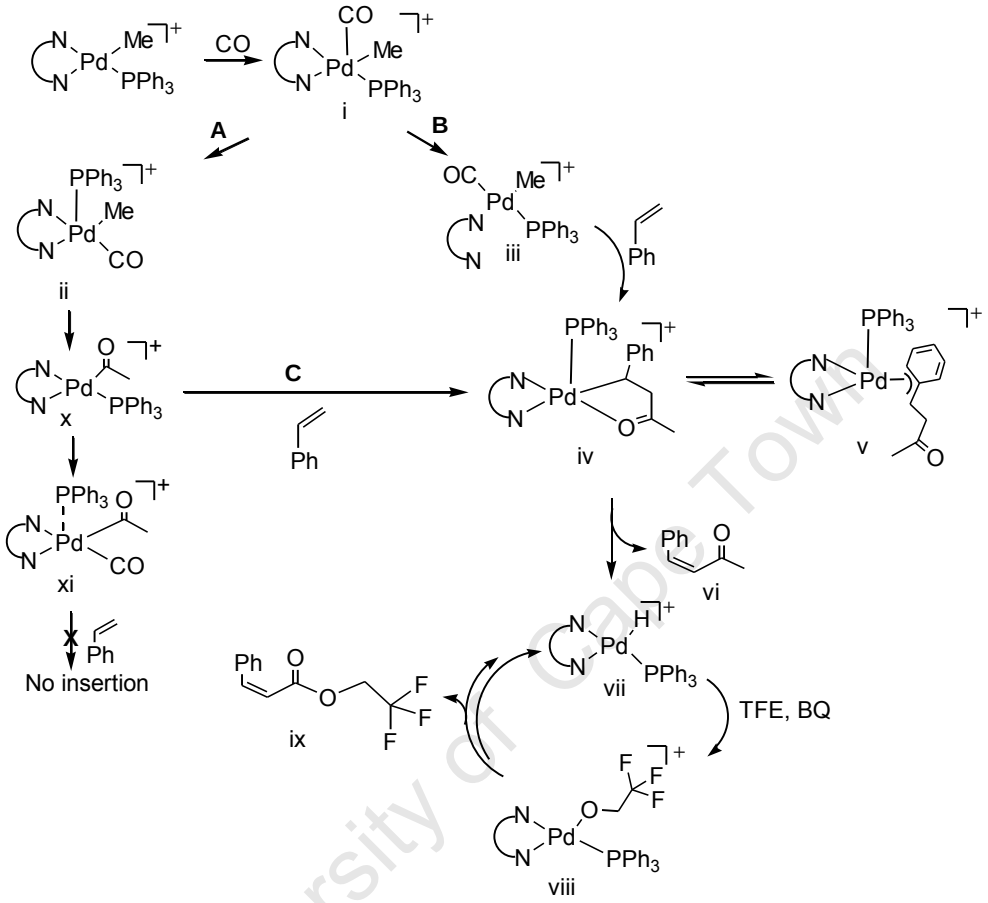

FIGURE 4.2.5: Proposed steps taking place during styrene/CO copolymerization to explain the catalytic behaviour of complexes $[PdMe(PPh_3)(N\hat{}N)]PF_6$ (**57**) and $[PdMe(PPh_3)(N\hat{}N)]BF_4$ (**58**).

The similarity of the spectra run immediately after sample preparation and after 18 and 36 h of bubbling with CO suggested the styrene monomer did not insert in the Pd-acyl bond. The 1H NMR signals for the styrene protons resonate at δ 5.25, 5.60 and 6.60 ppm and were visible even after 36 h [**Figure 4.2.5** (iv) and (v)]. It was thus concluded that under these conditions, styrene insertion did not take place.

The ^{13}C NMR spectrum in the aliphatic region for complex (**57**) displayed a signal due to Pd-CH_3 at 5.2 ppm; the signal disappeared after bubbling with CO for 18 h. Two new peaks were observed at 36.6 and 36.4 ppm. The new signals were attributed to the carbon atoms of the methyl group of a four coordinate species (x)

[(N^N)Pd(CO)(CO)-CH_3]$^+$ or a five coordinate species (xi) [(N^N)Pd(PPh_3)(CO)(CO)-CH_3]$^+$ (**Figure 4.2.5**). In the aromatic region, two signals were observed at δ 207.0 and 203.5 ppm, which were attributed to the acyl carbon of species (x) or (xi).

The signal for CO coordinated to palladium resonated at 168.9 ppm. The carbon signals appeared upfield compared to those which have been reported in literature. However, the spectra in this study were obtained in $CDCl_3$ instead of CD_2Cl_2, which was used by other researchers.[5] On the other hand, the appearance of an acyl carbon upfield, compared to the downfield signal around 220.9 – 222.3 ppm observed by Bastero *et al.*,[12] could be due to differences in the donor ligands. In addition, the interaction of triphenylphosphine with the Pd-centre, as was observed in the ^{31}P spectrum, could also have played a role. Upon introduction of three equivalents of styrene to a solution of catalyst (**57**) in an NMR tube and exposing the solution to the carbon monoxide atmosphere overnight, no noticeable changes in the ^{31}P NMR spectrum were observed (see **Figure 4.2.6** (iii)).

The signals due to styrene remained intact even after 36 h of reaction. These observations support the ^1H NMR spectral studies and imply that the styrene monomer does not insert into the Pd-acyl bond. After bubbling carbon monoxide into the solution of complex (**48**), the ^{31}P spectra displayed two new phosphorus signals at δ 26.6 and 27.0 ppm in the ratio of 1 : 10 in intensity, respectively. The signal which originally resonated at 39.9 ppm for coordinated phosphine disappeared after 18 h of the reaction. Interestingly, the new signals which appeared did not correspond to the phosphorus atom of the free uncoordinated triphenylphosphine (-5.2 ppm). The two peaks which appeared at 26.6 and 27.0 ppm were postulated to be due to phosphorus atoms in species (x) and (xi), respectively. Traces of triphenylphosphine oxide ($PPh_3P=O$) were observed at δ 29.2 ppm.

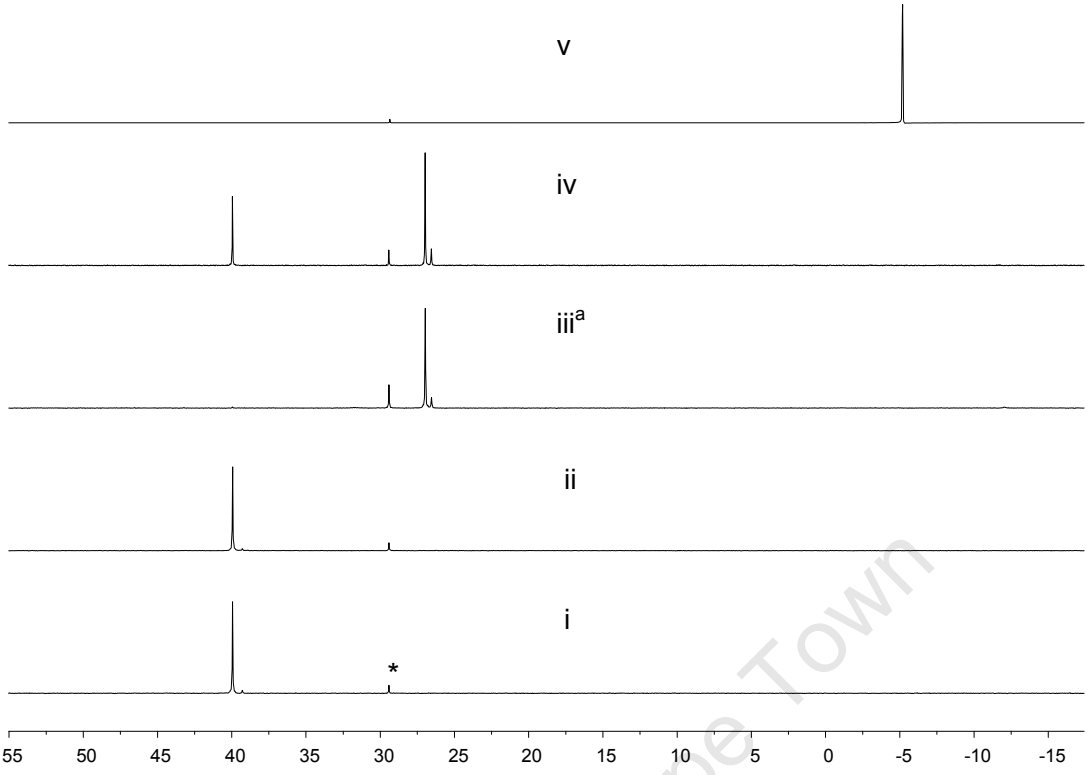

FIGURE 4.2.6: The ^{31}P NMR spectra in $CDCl_3$ of compound (**57**): (i) immediately after preparation; (ii) (**57**), after exposing the solution to CO atmosphere for ten minutes; (iii) after solution was exposed to carbon monoxide atmosphere for 18 h; (iv) (**57**) + three equivalents of styrene and exposing solution to CO atmosphere for 18 h; (v) commercial triphenylphosphine.
[a]Similar spectrum was observed after 36 h of reaction for compound (**57**) + three equivalents of styrene. *Impurity ($Ph_3P=O$).

This observation confirms the interaction of triphenylphosphine with the palladium centre. The studies support the ^{13}C and ^{1}H NMR data for CO insertion in the Pd-acyl bond. In addition, the triphenylphosphine in the solution displayed some interaction with the palladium centre. The interaction stabilizes the Pd-centre through back donation, and thus the resulting species $[Pd(PPh_3)(CO)(CO)\text{-}CH_3)$ $(N\text{^}N)]^+$ most likely hinders the insertion of styrene when using the NMR reaction conditions.

It was then concluded that triphenylphosphine was the main inhibitor of the catalytic cycle in these catalysts under the conditions investigated. As an aside, the interaction of triphenylphosphine with a Pd centre suggests that these catalysts could be stable enough for future use in the copolymerization of CO with monomers such as methyl acrylate and other olefins.[11] In order to achieve styrene

polymerization, harsher conditions could be investigated using catalysts (**57**), (**58**) and (**60**).

A possible mechanism is proposed comprising plausible steps which could be taking place to explain the inactivity of the catalysts, as illustrated in **Figure 4.2.5.** In this proposal, the first step is coordination of carbon monoxide to the Pd centre, forming a five-coordinate intermediate (i). At this stage two pathways are possible: associative path A or dissociative pathway B, both reaction paths ultimately forming the Pd-styryl intermediate following the insertion of the styrene monomer.

In path A, carbon monoxide displaces triphenylphosphine and CO molecular orbitals interact with one of the d-orbitals of Pd(II). Since triphenylphosphine has a high affinity for palladium, the new five-coordinate intermediate (ii) is formed with interaction of molecular orbitals of triphenylphosphine with the palladium centre through an axial out-of-plane orbital.[13] Migratory insertion then takes place to form the Pd-acyl intermediate (x). At high CO pressure, intermediate (xi) is formed, with CO occupying one of the square-planar coordination sites. However, at ambient pressure species (x) is more likely dominant. If species (xi) is formed then no polymers would be isolated as styrene insertion would be prevented.

The coordination of styrene to the metal centre in intermediate (x), followed by insertion in the Pd-acyl bond to form species (iv) in process C could be kinetically favoured. This is because triphenylphosphine is a better elctron donor compared to styrene. The resulting intermediate (iv) isomerizes to form a Pd-allyl intermediate (v) which has been found to be stable for phosphine-containing palladium complexes.[3] The intermediate (v) favours β-hydride elimination due to the Lewis acidity of the metal centre as provided by triphenylphosphine through the π back-donation process; subsequently, the oligoketone or ketone (vi) is produced.[12]

Process B on the other hand, is proposed to involve the dissociation of one nitrogen atom which is *trans* to triphenylphosphine through the *trans*-effect to form intermediate (iii). Migratory insertion of carbon monoxide takes place and then styrene inserts into the palladium-acyl bond to form intermediate (iv). The ketone (vi) is then produced. Once the ketone is produced, the palladium hydride species

(vii) is generated and then reacts with TFE through alcoholysis to form the palladium-trifluoroethoxide species (viii). Similar steps as in the formation of intermediates (iv) and (v) take place, but in this case the final product formed at the end of the catalytic cycle is a different ketone (ix). This product would be dominant compared to ketone (vi), as was observed in this study with the molecular weight M_n = 240, close to the molecular weight of the ketone (ix).

4.2.9 Effect of varying temperature, CO pressure and solvent on copolymerization when using catalysts bearing triphenylphosphine

Catalyst (**57**) was used at 50 ºC and ambient CO pressure for 24 h reaction time and gave a low molecular weight oligoketone with M_n = 220. No solid material for polymers was isolated when the polymerization was conducted under the same conditions with catalyst (**58**). The reaction solution was not analysed to confirm ologoketone formation. When the pressure of the system was increased to 30 bar and temperature raised to 80 ºC, no improvement in the catalytic performance was observed. Using these conditions no solid material was isolated from the use of catalysts (**57**) or (**58**) (**Table 4.2.4)**. The results in **Table 4.2.4** represent an average of three repeat experiments and the data were reproducible. Interestingly, no palladium black decomposition product was observed under these harsh conditions, implying that the complexes were very stable.

TABLE 4.2.4: Carbon monoxide/styrene copolymerization, using palladium complexes (**57**) and (**58**): effect of increasing temperature and pressure of the catalytic reaction[a]

Catalyst	CP Yield (mg),[b] [Activity, g CP (g Pd)$^{-1}$ h^{-1}]	50 ^{0}C, 1 bar	80 ^{0}C, 30 bar
		Mn[c] x 10^3 (PDI)	
(**57**)	2.30, [0.19]	0.22, (1.10)	0, (-)[d]
(**58**)	-	0, (-)	0, (-)

[a]Reaction conditions: see Table 4.2.1. [b]Mass of isolated polymer. [c]Determined by GPC. [d]Not determined.

When catalysis was performed in methanol at room temperature and at 10 bar, no polymers were isolated. Increasing the temperature to 80 ºC gave a small amount of polyketones. Moreover, the molecular weight of the polymers obtained (M_n = 11.93 x 10^3) was higher than those isolated at ambient conditions for other

catalysts investigated in this work. An increase in CO pressure to 20, 40 and 50 bar in methanol did not yield any polymers.

In summary, the catalysts prepared in this study displayed activity for styrene/CO copolymerization. The triphenylphosphine-containing complexes displayed poor activity. Ferrocenyl-containing complexes were less active than the tolyl analogues. Oxidation of ferrocenyl moeity resulted in a remarkable activity. An increase in pressure affected catalyst activity, while the variation of the amount of trifluoroethanol and benzoquinone influenced the yield and dispersity of the polyketones. Prolonged reaction times did not increase the molecular weights. An increase in catalyst loading did not improve the molecular weight or the yield of polymers.

4.3 Characterization of CO/styrene copolymers

4.3.1 Characterization using ^{1}H and ^{13}C NMR spectroscopy

As already discussed in the preceding Section, the molecular weights of the polymers obtained were analysed using Gel Permeation Chromatography. The ^{1}H and ^{13}C NMR spectra displayed all the signals comparable to those reported in literature.[14] The ^{1}H NMR spectra of the polymer samples in $CDCl_3$ displayed proton peaks as broad signals. The catalysts investigated in this study were stabilized with achiral ligands, and no stereochemical control was possible during polymerization. Hence, the broad signals in the ^{1}H NMR spectra are due to polymers with various stereochemical configurations [atactic, stereoregular, syndiotactic (SRSRSR-sequence) or isotactic (RRRRRR- or SSSSSS-sequence)]. On the other hand, polymers with various molecular weights were produced (PDI>1). By comparison to literature reports, the proposed polymers that were formed during polymerization are shown in **Figure 4.3.1**.[1b,2,5,14]

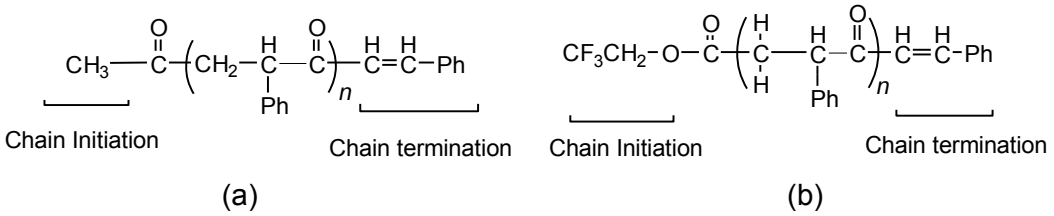

FIGURE 4.3.1: Proposed types of polymers formed as a result of initiation by insertion of CO on (a) the Pd-CH_3 bond, (b) the Pd-OCH_2CF_3 bond.[1b,2,5,14]

Polymer (a) was initiated with a -CH_3 group, and this was followed by insertion of CO in the Pd-Me bond. Polymer (b) was initiated with a –OCH_2CF_3 group, in the second cycle of the polymerization process where CO inserts in the Pd-OCH_2CF_3 bond. The second type of polymer was found to be dominant due to the abundance of TFE, which is able to initiate the polymerization reaction, as compared to Pd-CH_3, which is present only in the catalyst; this is further discussed in the next section on characterization using mass spectrometry.

The ^{1}H NMR spectrum (see **Figure 4.3.2**) displayed three sets of broad signals in the aliphatic region centred at δ 2.25, 3.10 and 4.00 ppm, while the protons in the aromatic region displayed a broad signal in the range δ 6.80 – 7.50 ppm. The broad signal at 6.60 ppm was postulated to be due to the alkenyl protons labelled 14 and 15, which form during the termination step.[5,10] The broad signals are a result of the formation of an atactic polymer by catalyst (**55**). No peaks were detectable in the region of δ 5.9 – 6.2, where *exo*-methylene protons would resonate if the CH_2=CPh-C(O)- termination group existed. [1b,2,5,14]

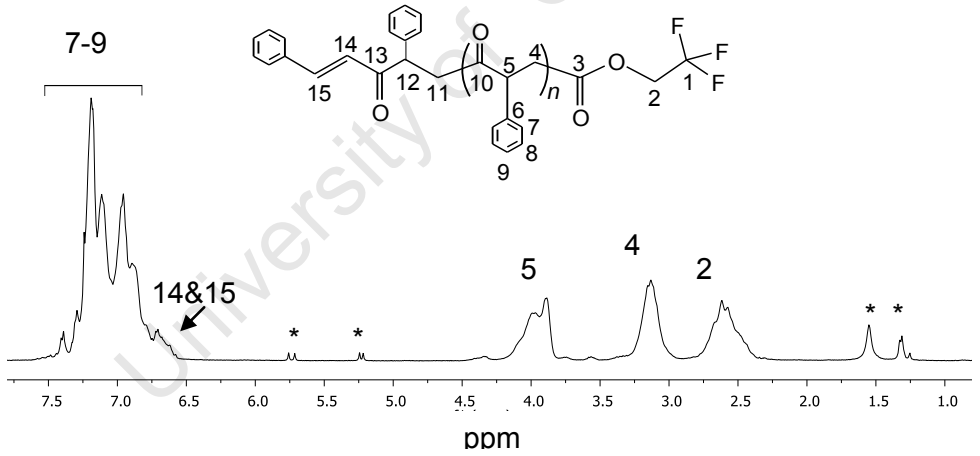

FIGURE 4.3.2: ^{1}H NMR (400 MHz, $CDCl_3$) spectrum of styrene/CO copolymer obtained with catalyst (**55**). The assigned chemical shifts are comparable to those obtained in literature; a broad signal at δ 6.60 is due to the alkenyl protons PhC*H*=C*H*−C(=O)−. *Impurities: 5.75 and 5.25 ppm, styrene; 1.51 ppm, water from solvent.

The ^{13}C NMR spectrum of a solution of the copolymer is shown in **Figure 4.3.3**, on the next page. The resonances at 45.4, 52.4 and 206.5 ppm were assigned to the backbone methylene (C4), methyne (C5) and carbonyl (C10) carbon atoms of the repeating molecular unit, –CH_2CHPhCO–, respectively. The aromatic carbon

resonances are located at δ 127.3, 128.2, 128.7 and 137.6 ppm, as depicted in **Figure 4.3.3**.

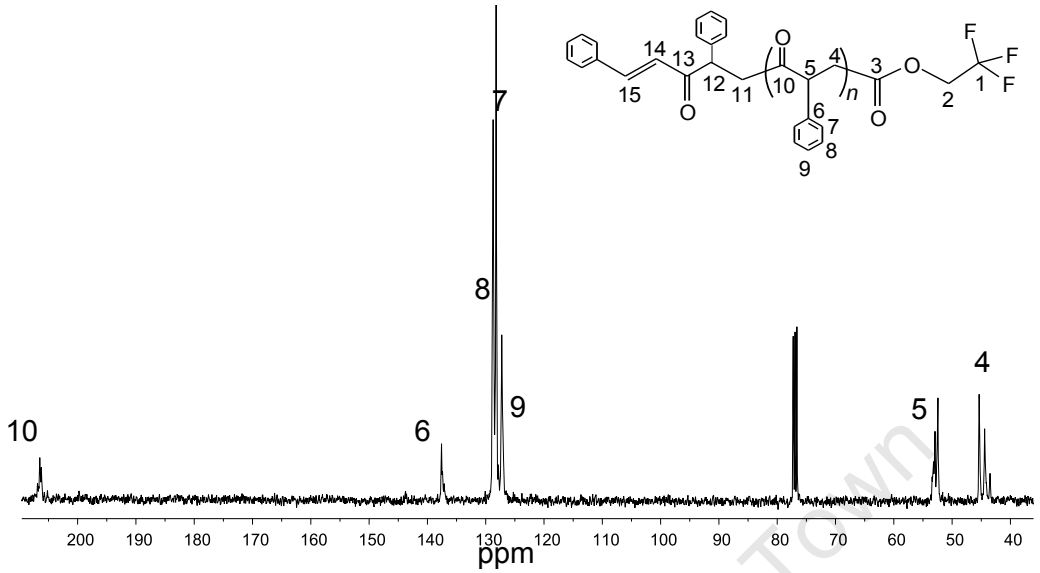

FIGURE 4.3.3: ^{13}C NMR (400 MHz, $CDCl_3$) spectrum of styrene/CO copolymer obtained with catalyst (**55**). The multiple peaks in the range δ 43 – 45 and 52 – 53 ppm are due to the atactic nature of the polymer.

The carbon signals for C13-C15 and C1 and C2 for the chain end-groups are usually not observed in the higher molecular weight polymers as they are suppressed by the abundant carbon signals from the polymer chain.[14] The additional peaks appearing in the methyl and methyne region in the ^{13}C NMR spectrum are believed to be due to the carbon atoms of various stereoisomers in the atactic polymer.[15]

4.3.2 Characterization using infrared spectroscopy

The polymer samples were also analysed using infrared spectroscopy. The infrared spectrum displayed all expected signals, notably, an intense peak at 1710 cm^{-1} assigned to the carbonyl group in the polyketones (see **Figure 4.3.4**).[6] In addition, two intense peaks at 699 and 757 cm^{-1} were attributed to either the C-F stretching frequency of the $–CF_3$ end-group, to the C-H deformation vibration of the -CH=CH- end-group in the *cis* form, or to an out-of-plane C-H deformation of a monosubstituted benzene ring.[6,16,17] It is not possible to assign the signals to a specific group unambiguously as they all absorb in a similar range.

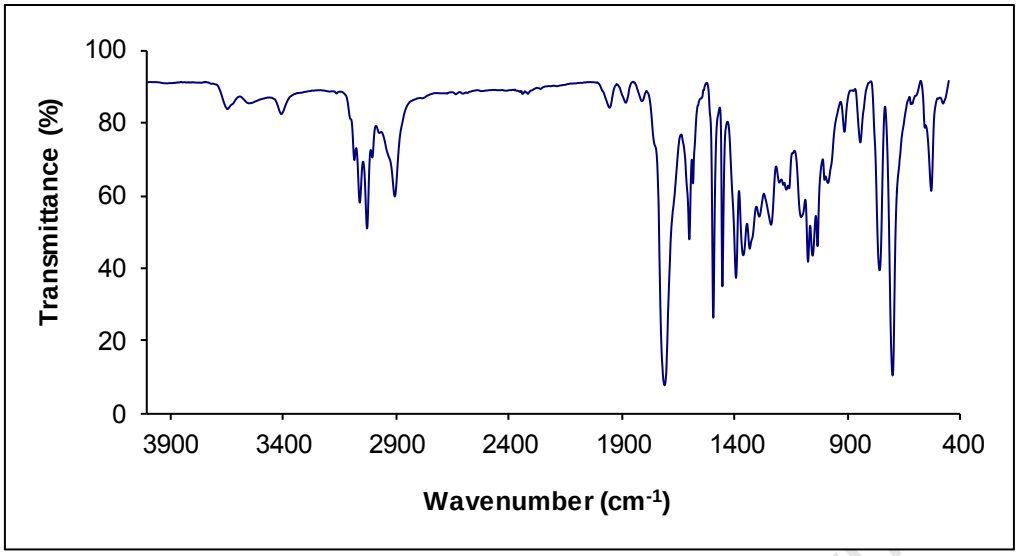

FIGURE 4.3.4: Infrared spectrum (KBr disc) of styrene/CO copolymer obtained with catalyst (**55**). The carbonyl vibration frequency appeared at 1710 cm^{-1}.

The C-H stretching frequencies for aromatic and aliphatic groups can be observed in the range 2890 − 3090 cm^{-1}, while deformation vibrations and in-plane C-H vibration for a substituted benzene ring appear between 1200 and 1493 cm^{-1}. The stretching vibration of the -C=C- bond in a monosubstituted phenyl group and for a -CH=CH- end-group appear at 1583 and 1598 cm^{-1}. The spectrum displays the characteristic signals for a compound containing phenyl and carbonyl groups, a further confirmation that polyketones were successfully produced.

4.3.3 Characterization using mass spectrometry

Some of the polyketones prepared with catalyst (**55**) were analysed with electrospray ionization mass spectrometry (ESI MS). Mass spectrometry using this soft ionization method can accurately produce intact molecular ions. The synthetic polymer sample solution is directly introduced into a stream of solvent-mixture containing volatile solvent (e.g. acetonitrile) and a weak organic acid (e.g. formic acid), leading to a sample-to-acid ratio of 1 : 1000. The liquid containing the analyte is dispersed by electrospray into a fine aerosol, introduced and heated in a vacuum where the solvent is evaporated. As the solvent evaporates the analyte loses a small percentage of its mass along with a relatively large percentage of its charge. The ions observed by mass spectrometry may be quasimolecular ions created by the

addition of a proton, i.e. a hydrogen ion, and are denoted $[M + H]^+$, or of another cation such as sodium ion, $[M + Na]^+$. ESI mass spectrometry has been found to be useful for the determination of both molecular weight distribution and end groups for polymeric samples. Various polymeric chains have been observed for CO/styrene copolymers (see **Figure 4.3.5**).[1b,2,5,14,17] All of the chains have in common one unsaturated end-group, while the other end group is different in each case.

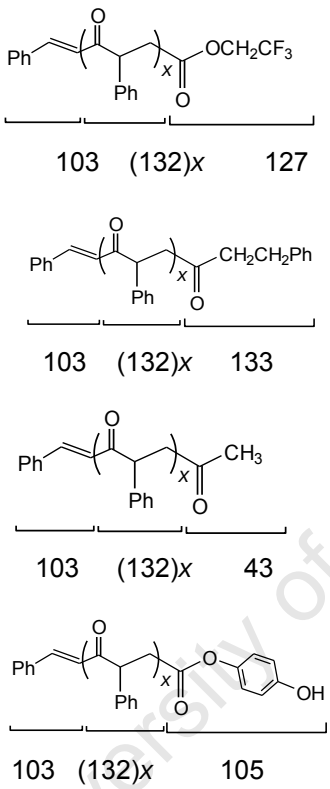

FIGURE 4.3.5: Polymeric chains present in CO/styrene polyketones prepared in trifluoroethanol in the presence of benzoquinone. [1b,2,5,14,17]

Two of the polymeric chains terminate with an ester end-group, which derives either from trifluoroethanol (chain a) or benzoquinone (chain d). The other two chains terminate with saturated groups, a phenylethyl group (chain b) and a methyl group (chain c). The mass spectrum (**Figure 4.3.6**) of the polyketones prepared here, in a solvent mixture of dichloromethane and trifluoroethanol (TFE) and in the presence of 1,4-benzoquinone (BQ), showed dominance of the polymeric chain terminated with an ester group that derives from TFE (chain a). The other peaks were attributed to the presence of other chains as already described.

The difference in chain growth was $\Delta(m/z)$ = 132, which corresponded to the CO/styrene repeating unit. The polymer chains observed here were in agreement with the literature reports for polymers obtained when polymerization is performed in the presence of TFE and BQ.[17] As was described in Chapter 1 (Section 1.2.4) on the mechanism of CO/styrene copolymerization, the first cycle of polymerization is initiated by methyl migration when CO inserts between Pd-Me bond followed by styrene insertion and then polymer growth. Termination step in the first cycle forms molecular palladium(0) which is oxidized to Pd(II) by BQ. In the second polymerization cycle, TFE coordinate to Pd(II) forming Pd-(OCH_2CF_3), followed by CO and styrene insertion and the polymerization growth step takes place. Polymers terminated with trifluoromethoxy group will be dominant since TFE is in abundance in the reaction mixture.

4.4 Concluding remarks

The cationic palladium complexes (**55**), (**56**) and (**59**) bearing acetonitrile donor ligands, produced copolymers with medium-size molecular weight using ambient conditions. The activity of the catalyst depended on the anion: catalysts containing a PF_6^- anion displayed higher activity than those with a BF_4^- anion.

The cationic complexes (**57**), (**58**) and (**60**) bearing the triphenylphosphine donor ligand displaced low activity. It is believed that the π-acceptor property of triphenylphosphine, which was shown to interact with the palladium centre even after insertion of CO in the Pd-Me bond most likely prevented insertion of the weak-donor styrene on Pd(II), and finally, no polymers were produced.

An electronic property of the ferrocenyl group was found to improve copolymerization activity: complex (**59**) bearing a ferrocenyl moiety, displayed improved activity when this group was oxidized *in situ*.

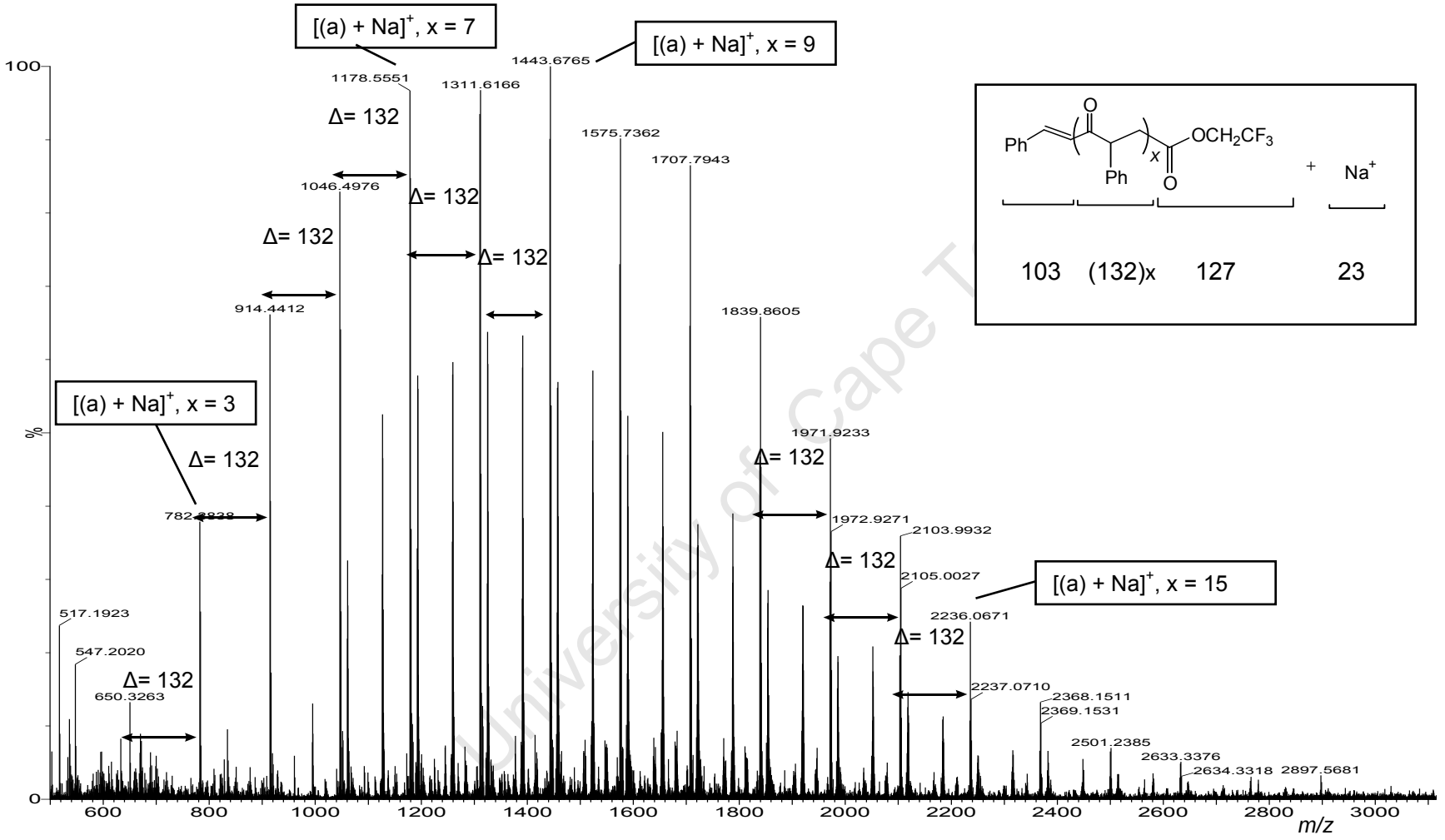

FIGURE 4.3.6: The electron spray ionization mass spectrum (ESI MS) for CO/styrene copolymer prepared using catalyst (**55**) in a mixture of dichloromethane and trifluoroethanol and in the presence of benzoquinone.

The polymers prepared here were then utilized in reactions for their functionalization with polylactide to produce a degradable block copolymer, the results of which will be discussed in the next chapter.

4.5 References

1. (a) B. Milani, A. Anzilutti, L. Vicentini, A. S. O Santi, E. Zangrado, S. Geremia and G. Mestroni, *Organometallics*, 1997, **16**, 5064; (b) A. Scarel, J. Durand, D. Franchi, E. Zangrado, G. Mestroni, C. Carfagna, L. Mosca, R. Seraglia, G. Consiglio and B. Milani, *Chem. Eur. J.*, 2005, **11**, 6014.
2. (a) C. Bianchini and A. Meli, *Coord. Chem. Rev.*, 2002, **225**, 35; (b) A. Nakamura, S. Ito and K. Nozaki, *Chem. Rev.*, 2009, **109**, 5234; (c) G. W. Coates, *Chem. Rev*., 2000, **100**, 1242; (d) E. Drent and P. H. M. Budzelaar, *Chem. Rev*., 1996, **96**, 663.
3. A. Macchioni, G. Bellanchioma, G. Cardaci, M. Travaglia and C. Zuccaccia, *Organometallics*, 1999, **18**, 3061.
4. A. Schätz, A. Scarel, E. Zangrando, L. Mosca, C. Carfagna, A. Gissibi, B. Milani and O. Reiser, *Organometallics*, 2006, **25**, 4065.
5. A. D'Amora, L. Fanfoni, D. Cozzula, N. Guidolin, E. Zangrando, F. Felluga, S. Gladiali, F. Benedetti and B. Milani, *Organometallics*, 2010, **29**, 4472.
6. J. Guo, B. Wang and C. Zhu, *eXpress Polym. Lett*., 2007, **1**, 69.
7. (a) M. Barsacchi, G. Consiglio, L. Medici, G. Petrucci and U. W. Suter, *Angew. Chem., Int. Ed. Engl*. 1991, **30**, 989, (b) G. Consilglio, S. C. A. Nefkens and A. Pisano, *Inorg. Chim. Acta*., 1994, **220**, 273.
8. J. Durand and B. Milani, *Coord. Chem. Rev*., 2006, **250**, 542.
9. R. van Asset, E. E. C. G. Gielens, R. E. Rulke and C. J. Elsevier, *J. Chem. Soc., Chem. Commun*., 1993, 1203.
10. K. Nozaki, H. Komaki, Y. Kawashima, T. Hiyama and T. Matsubara, *J. Am. Chem. Soc*. 2001, **123**, 534.
11. J. S. Brumbaugh, R. R. Whittle, M. Parvez and A. Sen, *Organometallics*, 1990, **9**, 1735.

12. A. Bastero, A. Ruiz and C. Claver, *Organometallics*, 2002, **21**, 5820.
13. M. J. Green, G. J. P. Britovsek, K. J. Cavell, F. Gerhards, B. F. Yates, K. Franckcombe, B.W. Skelton and A. H. White, *J. Chem. Soc. Dalton Trans*., 1998, 1137.
14. C. Carfagna, G. Gatti, D. Martini and C. Pettinari, *Organometallics*, 2001, **20**, 2175.
15. A. D. Cross and R. A. Jones, *An Introduction to Practical Infra-Red Spectroscopy*, 3rd Ed., Butterworth, London, 1969, pp. 65 – 97.
16. F. Yao, L. Deng, J. Men, Y. Feng and J. Sun, *J. Appl. Polym. Sci.*, 2001, **82**, 8.
17. B. Milani, G. Corso and G. Mestroni, *Organometallics*, 2000, **19**, 3435.

CHAPTER 5: POLY(LACTIDE-*co*-CO/STYRENE) BLOCK COPOLYMERIZATION

5.1. Introduction

The increasing amount of non-degradable plastic waste causes environmental contamination, such as pollution of the oceans[1] and destruction of arable land.[2,3] Furthermore, the global daily demand of plastics as packaging materials has contributed to the gradual depletion of the fossil fuels used to produce the petrochemical precursors for the manufacturing of the plastics. The most common plastics used for packaging and their petrochemical sources are outlined in **Figure 5.1.1.**

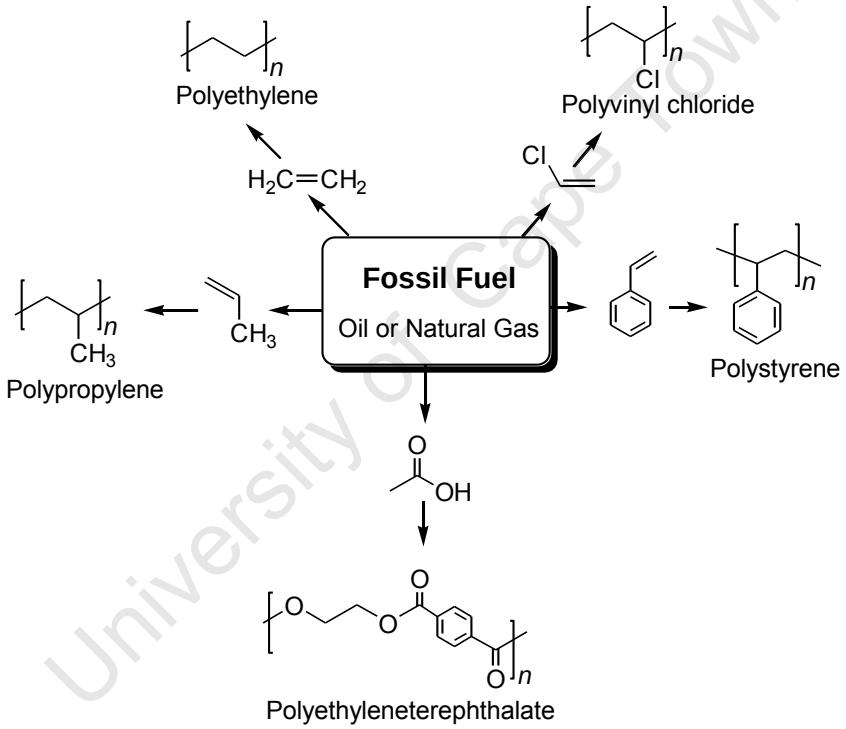

FIGURE 5.1.1: Common petrochemically-derived polymers which are used for packaging purposes.[2]

The polymer recycling process has been proposed as a form of intervention; however, this has displayed little impact on the annual production of plastic material. A consequence of this was the formulation of the twelve Principles of Green Chemistry concept during the early 1990s.[1-4] The following Principles are of interest here: Principle number one, which promotes the prevention of waste; Principle number seven, which encourages the use of renewable feedstocks; and Principle number ten, which promotes the design of degradable chemical products so that they do not persist

in the environment.[1] Since the inception of the Green Chemistry concept various alternative packaging materials have been considered, for example, the use of paper bags in place of the usual plastics. Moreover, some plastics have been designed in which the resulting material is composed of a degradable polymer fraction and partially degradable polymer, the resulting material then becoming partially degradable.

There have also been successes in the production of biodegradable polymers which are derived from agricultural feedstocks, e.g. polylactide, which is derived from lactic acid produced from beets and corn.[5] Most of the biodegradable materials have displayed poor mechanical stability, thus hampering their use for packaging purposes. These polymers have mostly been used for biological applications. Various methods, therefore, have been investigated in order to solve the stabilization problem, and some of the methods have been described in Chapter 1. The best-investigated methods involve incorporation of a degradable polymer with another relatively stable polymer through a chemical process, i.e. by reaction between different polymers,[2] or by physical methods, i.e. by the blending together of different polymers.[6] In some instances, stabilization additives have been added to strengthen the polymer material.[2]

5.2. Results and discussion

The current preliminary study was aimed at synthesizing a new degradable block-copolymer which is composed of a biodegradable polymer (polylactide) and a photodegradable polymer (styrene/carbon monoxide copolymer).[2,7] The CO/styrene copolymer used here was prepared using the new palladium catalysts as described in the previous chapter. The reaction scheme for the preparation of the new block-copolymer is outlined in **Figure 5.2.1**, and the full experimental method is described in Chapter 7, Section 7.6.3.

The first step in the preparation involved the C-C coupling reaction between 4-bromobenzyl alcohol and the alkenyl tail of the copolymer using palladacycle (**63**) as a catalyst. The palladacycle complexes have been reported to display a well-controlled production and stabilization of the Pd(0) active species which ultimately

enables the coupling reaction.[8] Similarly, phosphorus containing catalysts have also been reported to display good activity in the C-C coupling reactions.[8]

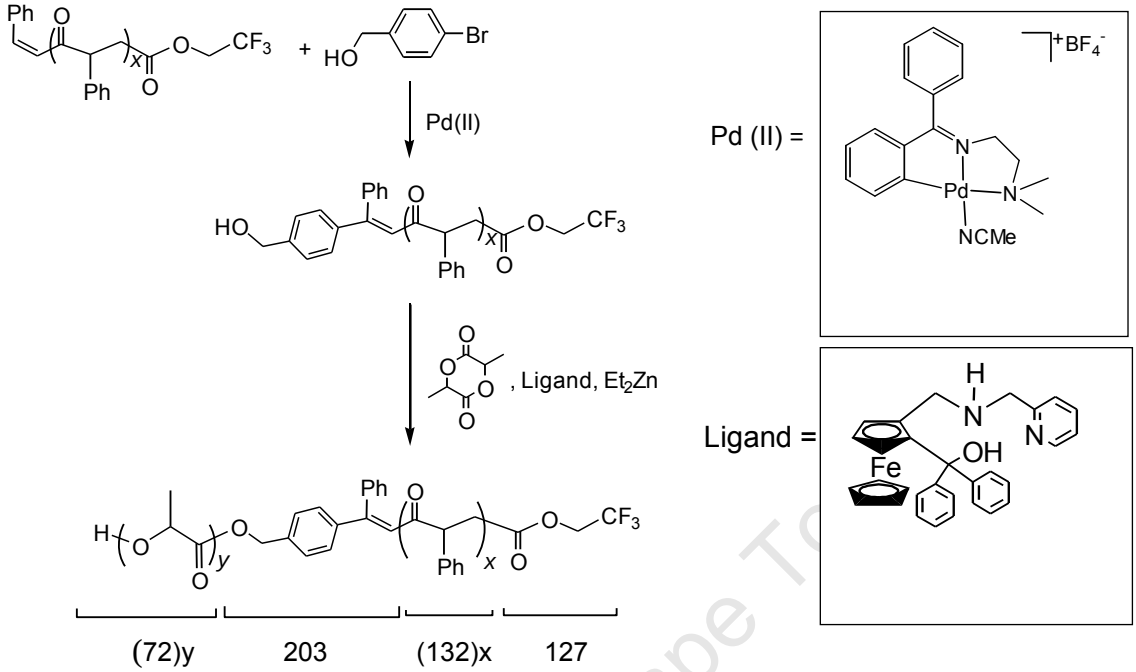

FIGURE 5.2.1: Synthesis of poly(lactide-*co*-CO/styrene) block copolymer. The molecular weight of the polymer was calculated using the formula: MW = 331 + (72)y + (132)x.

A reaction mechanism for the C-C coupling reaction which is similar to the one taking place in Suzuki or Heck reactions has been proposed.[8] In this coupling reaction, the catalytic cycle is initiated by oxidative addition of Pd(0) through coordination of the brominated substrate. The bromide which is coordinated to palladium is then extracted by $CsCO_3$, and this is followed by coordination of the alkenyl substrate. Finally, a reductive elimination step takes place; at the same time, C-C bond formation of the two species which are coordinated to palladium occurs to produce the desired product.

The new functionalized polymer which was terminated with a benzyl alcohol group was then used in the initialisation of lactide polymerization. The new ligand (**64**) was added to stabilize the ethylzinc complex *in situ*, presumably due to formation of Zn^{II}(O^N) seven-membered and Zn^{II}(N^N) five-membered rings.[9] The polymer terminated with a benzyl alcohol group was then introduced in the ethyl zinc solution, and the zinc-benzylalkoxide group (Zn-$OCH_2C_6H_4$-COP) was formed which was able to initiate lactide polymerization. Finally, the polymerization reaction was terminated

with an acidic aqueous solution. The new functionalized block copolymer was characterized using various analytical techniques. The peak due to the carbonyl stretching frequency of the residual lactide obscured the ν(C=O) signal of the copolymer, so characterization using IR spectroscopy was not pursued. The block copolymer was then characterized using gel permeation chromatography, ^{1}H NMR spectroscopy and mass spectrometry, and the data will be discussed in the next sections.

5.2.1 Characterization using gel permeation chromatography (GPC)

Three peaks were observed in the GPC chromatogram at different retention times: R_t = 17.0, 19.0 and 19.5 minutes. These peaks were, respectively, assigned to the styrene/CO copolymer, poly(lactide-*co*-CO/styrene) block copolymer and lactide monomer. The assignment of peaks was based on the molecular weight of the molecules since in gel permeation chromatogram column, higher molecular weight molecules are eluted easily than smaller molecules. The GPC data analysis of weight distribution in the sample confirmed formation of materials with a range of molecular weights. The presence of different molecules in the sample led to a broad polymer distribution, with PDI = 3.36. The presence of the lactide monomer at M_n = 144, which proved difficult to remove from the final polymeric material despite repeated recrystallization attempts, led to an overall low molecular weight (M_n = 1348), which was smaller than the M_n = 2925 for the CO/styrene copolymer. The larger retention time of the block copolymer as compared to the starting polyketone suggested that mostly smaller polymer chains of CO/styrene copolymer incorporated with alkoxy-derivative were functionalized with the polylactide chain forming a block copolymer.[1,10] The smaller polymer chains ultimately interacted strongly with the stationary phase and were retained longer on the GPC column.

5.2.2 Characterization using ^{1}H NMR Spectroscopy

The ^{1}H NMR spectrum displayed signals which confirmed the block copolymer formation (see **Figure 5.2.2).** The signals appeared as broad peaks due to the high polymer molecular weight distributions. The peaks at δ 5.20 and 1.51 ppm were

attributed to the methine and methyl protons of the polylactide group, respectively, i.e., peaks 6 and 7 in **Figure 5.2.2**.

The aliphatic peaks due to the CO/styrene copolymer were observed at 2.48, 3.12 and 4.30 ppm, while the aromatic peaks appeared in the range 6.75 – 7.25 ppm. The peaks due to the residual lactide monomer also appeared in the spectrum, further supporting the GPC observations for presence of lactide monomer in the final polymeric mixture.

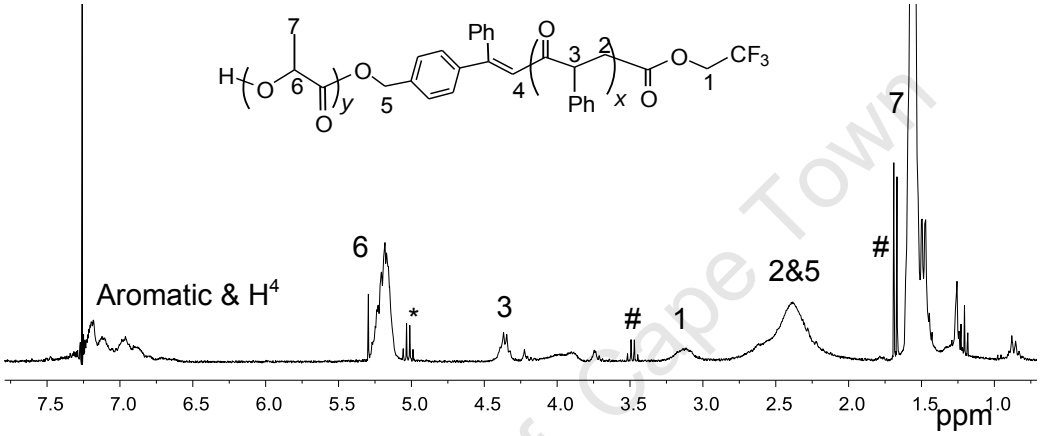

FIGURE 5.2.2: The ^{1}H NMR spectrum for poly(lactide-*co*-CO/styrene) block copolymer conducted in $CDCl_3$. *Residual lactide monomer. # Solvent impurity (diethylether).

5.2.3 Characterization using mass spectrometry

The ESI mass spectrum of the CO/styrene polyketone which was coupled with bromobenzyl alcohol is similar to the spectrum obtained for the polyketone itself, which was described in the previous chapter. This suggests that the functionalization process investigated here does not affect the polyketone chain as was expected. When the block-copolymer samples were analysed a number of peaks were observed in the spectrum (see **Figure 5.2.3**). The intense peaks in the spectrum exhibit values of Δ *m/z* 72 which suggests the presence of lactide repeating units. The *m/z* repeating units are not due to polylactide itself, i.e. the values in the spectrum do not correspond to those calculated using the formula: MW = (72)*n* + 2 for polylactide itself. This suggests that a certain initiating group is responsible for ring opening of the lactide and the proposed structure of the block copolymer is shown below.

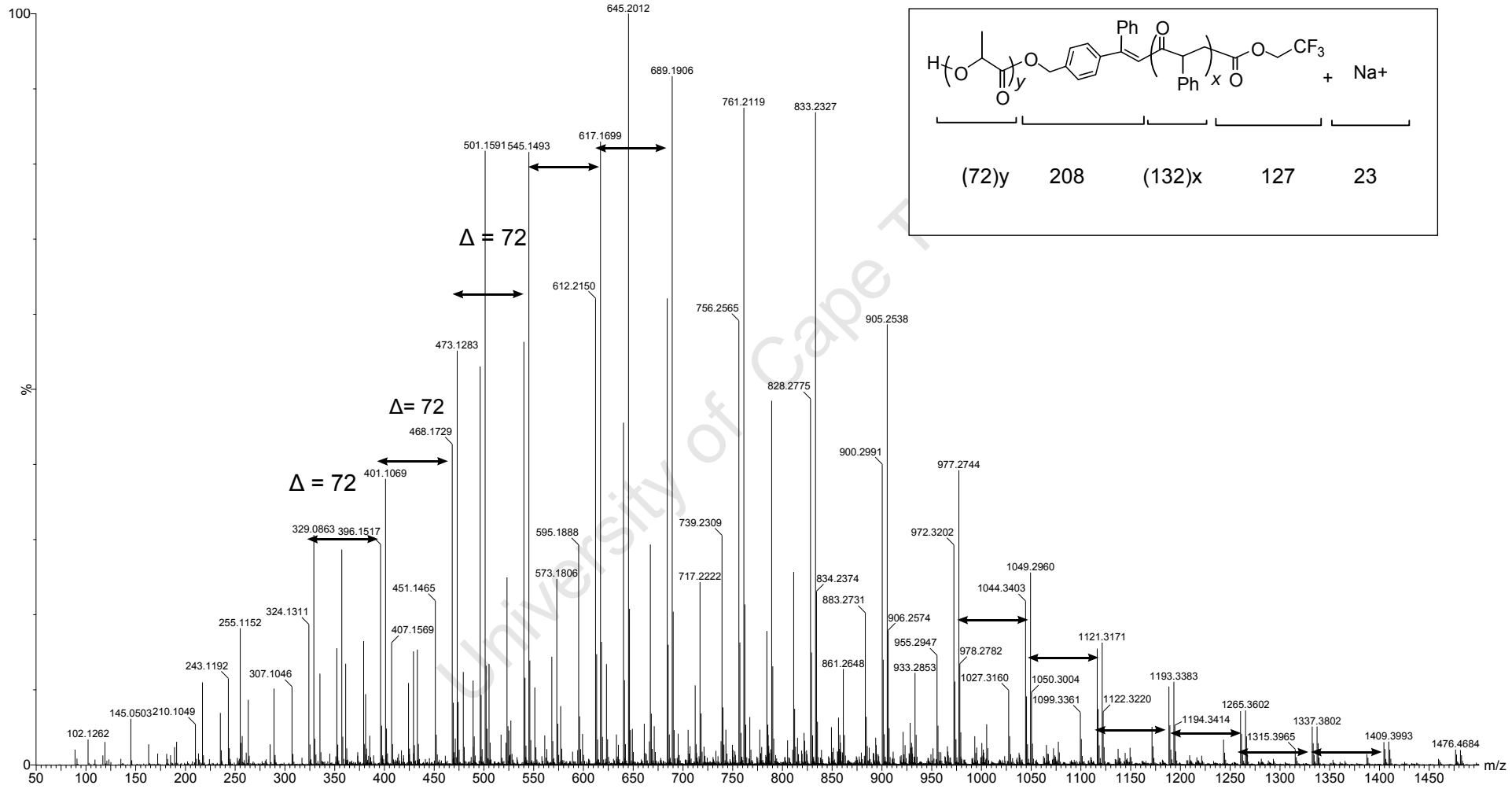

FIGURE 5.2.3: The electron spray ionization mass spectrum (ESI MS) for poly(lactide-*co*-CO/styrene) block copolymer.

The peaks in the spectrum were attributed to polymers with different chain lengths. The chain length in the polylactide fragment is determined by the value of y while the chain length in the polyketone side is determined by the value of x. This means that formation of a range of polymer chains with different molecular weights is possible.

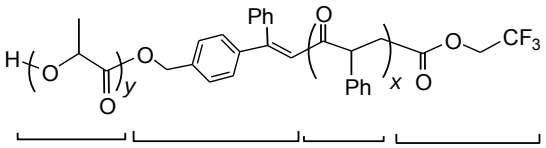

(72)y 208 (132)x 127

MW = 358 + (72)y + (132)x

The appearance of numerous peaks with small *m/z* values in the mass spectrum corroborates the smaller value of M_n = 1348, large retention time and broad polymer distribution (PDI = 3.36) which is observed in the gel permeation chromatogram. The mass spectrum, however, does not unambiguously confirm the formation of specific chain lengths of polylactide fraction (x) and polyketone side (y). Instead, it provides evidence of the presence of polylactide chain growth. In future work, it will be necessary to investigate the functionalization of lactide with commercial polyketones having a narrow polydispersity index. This could hopefully enable the isolation of a block copolymer with a narrow PDI and which might easily be characterized using mass spectrometry. Other characterization techniques, such as differential scanning calorimetry (DSC) and thermogravimetric (TGA) analysis, could also be used to determine the polymer stability.

5.3 Concluding remarks

In summary, it can be concluded that the synthesis of a poly(lactide-*co*-CO/styrene) block copolymer was successful. However, the formation of polymers with a broad distribution made it difficult to assign the *m/z* peaks to specific chain lengths. The ^{1}H NMR spectra displayed peaks which were assignable to a block copolymer composed of polylactide and polyketones chains. The method investigated here could be used for the production of block copolymers incorporating polylactide into other CO/olefin copolymers.

5.4 References

1. J. Clark and D. Macquarrie, *Handbook of Green Chemistry and Technology*, Blackwell Science Ltd, Great Britain, 2002, p. 52.
2. (a) A. Azapagic, A. Emsley and I. Hamerton, *Polymers, the Environment and Sustainable Development*, John Wiley and Sons Ltd, England, 2003, pp. 48 – 188; (b) M. Dirany, P. Lacroix-Desmazes, M. Vayer, R. Erre, B. Boutevin and C. Sinturel, *J. Appl. Polym. Sci*., 2011, **122**, 2944; (c) K. Huang, A. Jacobs and J. Rzayez, *Biomacromolecules*, 2011, **12**, 2327; (d) M.-L. Hsueh, B.-H. Huang, J. Wu and C.-C. Lin, *Macromolecules*, 2005, **38**, 9482; (e) A. S. Zalusky, R. Olayo-Valles, J. H. Wolf and M. A. Hillmyer, *J. Am. Chem. Soc*., 2002, **124**, 12761.
3. M. Lancaster, *Green Chemistry: an Introductory Text*, Royal Society of Chemistry, Great Britain, 2002, pp. 5 – 51.
4. P. T. Anastas and J. C. Warner, *Green Chemistry Theory and Practice*, Oxford University Press, Oxford, 1998.
5. R. E. Drumright, P. R. Gruber and D. E. Henton, *Adv. Mater*., 2000, **12**, 1841
6. W. Amass, A. Amass and B. Tighe, *Polym. Int.*, 1998, **47**, 89.
7. (a) D. R. Tyler, *Coord. Chem. Rev*., 2003, **246**, 291; (b) M. R. Rubin, *Chem. Rev*., 1975, **75**, 177.
8. (a) J. Dupont, C. S. Consorti and J. Spencer, *Chem. Rev*., 2005, **105**, 2527; (b) V. Polshettiwar, C. Len and A. Fihri, *Coord*. *Chem*. *Rev*., 2009, **253**, 2599; (c) J. G. de Vries, *Dalton Trans.*, 2006, 421.
9. (a) M. Watanabe, S. Araki and Y. Butsugan, *J. Org. Chem*., 1991, **56**, 2218; (b) C. Bolm, K. Muńiz-Fernández, A. Seger, G. Raabe and K. Günther, *J. Org. Chem*., 1998, **63**, 7860; (c) O. Riant, O. Samuel, T. Flessner, S. Taudien and H. B. Kagan, *J. Org. Chem*., 1997, **62**, 6733.
10. (a) K. Huang, D. P. Canterbury and J. Rzayez, *Macromolecules*, 2010, **43**, 6632; (b) X. Jiang, E. B. Vogel, M. R. Smith III and G. L. Baker, *Macromolecules*, 2008, **41**, 1937; (c) X. Jiang, E. B. Vogel, M. R. Smith III and G. L. Baker, *Macromolecules*, 2008, **41**, 318; (d) M. J. Stanford and A. P. Dove, *Macromolecules*, 2009, **42**, 141; (e) F. F. Wolf, N. Friedemann and H. Frey, *Macromolecules*, 2009, **42**, 5622.

CHAPTER 6: CONCLUSIONS AND FUTURE WORK

6.1 Project overview

In this project neutral zinc(II) and cationic palladium(II) complexes were successfully prepared and characterized using an array of analytical techniques. The chemical properties of some complexes were predicted using electron density calculations using the density functional theory method. The calculations were found to support the experimental observations. Spectral analysis confirmed the integrity of the complexes. Application of the zinc complexes was investigated for functionalization of polylactide, while the palladium complexes were investigated for CO/Styrene copolymerization. The CO/styrene copolymer which was produced here was utilized in the preparation of the new poly(lactide-*co*-CO/styrene) block copolymer using a new method. The polymers were characterized by several analytical techniques.

6.2 Polylactide functionalization

For the preparation of zinc complexes, ligands which comprised thiazole and thiosemicarbazone groups were designed and prepared. The choice of the ligands was determined by the existence of these groups in many drug lead molecules. The following approach was taken:

- Various ligands were prepared by reacting salicylaldehyde and salicylaldehyde derivatives bearing 3-*tert*-butyl- or 3,5-*tert*-butyl substituents with aminobenzothiazole. Of all the ligands which were prepared and, which contains a benzothiazole group, the reaction between the unsubstituted salicylaldehyde derivative and the zinc salt successfully produced the desired homoleptic complex.
- In order to investigate the effect of compounds with bulky groups on the lactide polymerization reaction, the ligand 2,4-di-*tert*-butyl-6-[(5-phenyl-2-thiazolyl)hydrazonomethyl]phenol was prepared. The reaction of this ligand with a zinc salt yielded the desired complex.
- Ligands based on the thiosemicarbazone group were prepared and ferrocenyl and aryl analogues were isolated. These analogues contained the 4-fluorophenyl or methyl substituents on the thiosemicarbazone moiety.

- Control experiments were conducted by testing the ligands for lactide polymerization, followed by testing of the zinc complexes in the same process.

The zinc complexes displayed different reactivity in the lactide polymerization reaction:

- The zinc complex bearing the benzothiazole ligand displayed the highest activity for lactide polymerization, while the complex stabilized with a ligand bearing bulky groups was found to be inactive. This inactivity was postulated to be due to the bulky groups restricting coordination of the lactide monomer, thus inhibiting polymerization.
- Complexes stabilized with the thiosemicarbazone ligands displayed low activity towards lactide polymerization. The low activity displayed by these complexes was attributed to the lower reactivity of the thiolate group initiator as compared to the phenolate initiator in the complex stabilized with a benzothiazole ligand.
- The ferrocenylthiosemicarbazone ligand bearing a fluorophenyl substituent, unexpectedly displayed activity towards lactide in the presence of methanol. This activity was attributed to the highly electrophilic nature of the ligand which was provided by the fluorophenyl substituent. The reaction mechanism is similar to that which has been proposed for the compound containing a thiourea derivative, with similarities to the thiosemicarbazone group.

Polymers which incorporated a benzothiazole group and with molecular weights up to M_n = 3000 g/mol and relatively narrow distribution were isolated. Various factors influenced the polymerization reaction. For example, variation of the solvent used for the lactide polymerization reaction led to a decrease in the rate of polymerization. The time needed for the lactide monomer to be converted to polymer increased from 24 h when conducting the reaction in tetrahydrofuran to three days when reaction was conducted in dichloromethane at 50 ºC. When the quantities of the monomer and catalyst were increased while keeping the Zn(II) : lactide ratio of 1 : 20 constant, polymers with broad molecular weight distribution were produced.

The functionalization of polylactide by a new method using homoleptic zinc complexes as catalysts was successful. The polymers might be utilized as delivery vehicles for biological or agricultural applications.

6.3 CO/styrene copolymerization

The ligand bearing two pyridyl groups was modified with a tolyl group through an amide linkage. This ligand was used as a model compound in which the tolyl group represented a carbon nanotube. In future work the ligand will be incorporated on the surface of carbon nanotubes through an amide formation reaction. Functionalized carbon nanotubes will then be reacted with the palladium precursor salt in order to produce a heterogeneous catalyst system. The ferrocenyl analogue was also prepared. The ligands were reacted with palladium(II) to form cationic complexes.

The complexes displayed different activity when investigated for CO/styrene copolymerization using ambient conditions:

- The cationic complexes stabilized with an acetonitrile donor ligand and the hexafluorophosphate anion displayed higher activity for CO/styrene copolymerization. The complexes stabilized with the triphenylphosphine donor ligand were inactive for the copolymerization reaction. The lack of activity displayed by these catalysts was attributed to the π-back-acceptor triphenylphosphine ligand which mitigated against the coordination of styrene under ambient conditions.
- The copolymers produced here were found to be influenced by variation of the reaction conditions. For example, when the concentration of trifluoroethanol in dichloromethane was varied while keeping the volume of the copolymerization solvent-mixture constant, polymers with a moderate increase in molecular weight distribution were produced. The amount of benzoquinone used in the polymerization reaction displayed an influence on catalyst activity. The highest activity was observed when a Pd(II) : BQ ratio of 1 : 20 was employed.

- The catalysts prepared and investigated here produced polymers with an average molecular weight between 2000 and 4000 g/mol.
- The cationic compounds containing a ferrocenyl group were found to be less active than the tolyl-containing counterparts. Interestingly, a change of the electronic environment in the ferrocenyl group by chemical oxidation led to an improvement in catalytic performance. This observation shows the fact that

variation of the electronic properties of the ligands does affect the catalyst performance for the production of CO/styrene copolymers.

- In the future, other oxidation methods, such as electrochemical oxidation by applying electricity to the polymerization solution or photo-oxidation using ultraviolet light, could be utilized for catalysts containing the ferrocenyl group and the copolymerization reaction investigated. Polymerization using these oxidation methods could provide a relatively cleaner copolymerization catalytic system.

Since the complexes investigated here displayed activity for CO/styrene copolymerization, the incorporation of the complexes on carbon nanotubes could lead to an improved heterogeneous catalyst system. In addition, these catalysts could be recyclable. The cationic Pd(II) complexes containing the triphenylphosphine donor could be active for the copolymerization reaction of carbon monoxide and olefins other than styrene, such as ethylene, propylene or methylacrylate.

6.4 Poly(lactide-*co*-CO/styrene) block copolymer

A new method was investigated for the synthesis of poly(lactide-*co*-CO/styrene) block copolymer. The method involved two steps: firstly, the CO/styrene copolymer was incorporated with benzyl alcohol using a new palladacycle-catalysed reaction. The second step involved functionalization of the CO/styrene polymer, which was terminated with an alcohol group, with lactide using a zinc catalyst which was generated in the solution. The molecular structure of the new ligand which stabilized the zinc complex *in situ* was determined using X-ray diffraction. In addition, the molecular structure of the palladacycle catalyst which was used for the functionalization of the CO/styrene copolymer was also determined.

- Although the method investigated here led to the formation of the block copolymer, characterization of the polymer chains using mass spectroscopy was not straight forward. A suggested improvement would be to employ a CO/styrene copolymer with a narrow molecular weight distribution.
- Further investigation to find an ideal lactide : catalyst ratio should assist in improving conversion of lactide monomer, which was found to remain in the resulting polymer material and made characterization difficult.

The new method could be used for the synthesis of block copolymers of lactide and other CO/olefin copolymers. These types of polymers should represent a new class of degradable polymers which do not harm the environment.

CHAPTER 7: EXPERIMENTAL DETAILS

7.1 Instrumentation

Melting points of the compounds were determined on a Kofler hotstage microscope (Reichart-Thermovar) coupled to a digital thermometer. Electron impact mass spectrometry (EI-MS) was carried out using a Jeol GC-MateII GC-MS system. Microanalyses for all compounds were performed using a Thermo Flash 1112 Series CHNS-O Analyser by Mr. Piero Benincasa (University of Cape Town), except for compounds (**44**), (**48**), (**59**), (**60**) and (**63**), for which a Carlo Erba NA 1500 Nitrogen Carbon Sulfur Analyser was used (analyses were conducted by Mr. Mike Philpott, at the Agricultural Research Council, Pretoria, South Africa).

The ^{1}H, ^{31}P and ^{13}C NMR spectra were recorded in $CDCl_3$ unless otherwise stated at ambient temperature using either Unity Varian 400 MHz a Varian or Bruker 300 MHz instruments. Infrared spectra were recorded on a Perkin Elmer Spectrum 100 FT-IR spectrometer. Crystallographic data for the compounds were collected at 113 K on a Nonius Kappa CCD diffractometer using graphite-monochromated Mo-Kα radiation (λ = 0.71073 Å, 54 kV, 22 mA). Data were reduced and scaled using DENZO-SMN software.[1] The structure was solved and refined using the program SHELX97.[2]

Molecular modelling calculations for electron density estimations were conducted by Ms. Feng Zheng, using the Sun Hybrid System hardware. Computational data were obtained using the DMol^3 density functional theory (DFT) code as implemented in Accelrys Materials Studio (Version 5.5).[3] The non-local generalized gradient approximation (GGA) exchange-correlation function was employed in all geometry optimizations, *viz*., the PW91 functional by Perdew and Wang.[4] DMol^3 utilizes a basis set of numeric atomic functions, which are exact solutions to the Kohn-Sham equations for the atoms.[5]

Electron spray ionisation mass spectrometry (ESI-MS) analysis using a Waters Synapt G2 machine was conducted for complexes and also for compounds having molecular weights greater than 500 g/mol at the University of Stellenbosch Analytical Service. The samples were dissolved in a mixture of 50% acetonitrile and 0.1% formic acid in

water and then directly injected (1 μl) using a Waters Ultra Performance Liquid Chromatography (UPLC) instrument at a flow rate of 0.2 ml/min. The ligands and compounds with molecular weight <500 g/mol were analysed at the University of Cape Town.

The molecular weights of the polymers were analysed by Gel Permeation Chromatography. MALDI MS spectrometry was performed using a 4800 MALDI TOF/TOF system (AB SCIEX) with instrument control through 4000 Series Explorer, at the University of Cape Town, Centre for Proteomic and Genomic Research, Medical School. Polymer samples were dissolved in 50% acetonitrile/water for mass analysis. A matrix solution (7.5 mg/ml) was prepared from α-cyano-4-hydroxycinnamic acid (CHCA) in 50% acetonitrile (ACN)/water and 0.15% triflouro acetic acid (TFA). The samples were mixed in a 1:2 ratio with the matrix solution to form a final matrix concentration of 5 mg/ml in 50% ACN/water, 0.1% TFA. The samples (0.5 μl) were manually spotted onto a MALDI target plate.

Cyclic voltammograms were recorded at room temperature on a BAS 100W Electrochemical Analyzer with a one-compartment three-electrode cell system consisting of a platinum disk working electrode, a platinum wire auxiliary electrode and a $Ag/AgNO_3$ reference electrode (0.01 M $AgNO_3$ and 0.1 M [n-Bu_4N][ClO_4] in anhydrous acetonitrile). An IR compensation circuit was used for all measurements. A scan rate of 100 mV s^{-1} was used throughout, beginning from the most negative potential and initially scanning in the anodic direction. The half-wave potential of the ferrocene/ferrocenium couple in this cell never varied by more than 30 mV from a mean value of $E_{1/2}$ = 261 mV *versus* the $Ag/AgNO_3$ reference electrode, with a peak separation falling between ΔE_p = 59 and ΔE_p = 66 mV. Solutions were purged with argon and voltammograms were recorded under a blanket of argon. The platinum disk working electrode was polished between runs. The voltammograms of samples were recorded using dichloromethane solutions (1-2 mM, with 0.1 M [n-Bu_4N][ClO_4] as a background electrolyte).

All chromatographic columns were packed with either Merck 0.063 – 0.200 mm silica gel or 0.063 – 0.200 mm alumina (neutral). Thin layer chromatography was performed on Merck silica gel 60 F_{254} aluminium-backed TLC plates. All reagents

were purchased from Sigma-Aldrich Co. and were not purified prior to use. The complex [PdMeCl(COD)] was prepared following a literature procedure.[6] All reaction solvents were AR grade, purchased from Kimix Chemicals or Merck. Standard drying procedures were followed in cases where dry solvents were required.

7.2 Zinc complexes and corresponding ligands

2-[2-(2-Benzothiazolyl)]phenyliminomethylphenol (**37**)

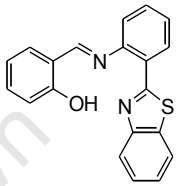

2-Aminobenzothiazole (1.50 g, 6.60 mmol) was added to a solution of salicylaldehyde (0.81 g, 6.6 mmol, 0.71 ml) in ethanol (75 ml). The reaction mixture was then heated under reflux for 5 h. After which the solvent was reduced under reduced pressure and the Schiff base product precipitated as a grey microcrystalline material (1.92 g, 88%). The product was placed in the refrigerator overnight and finally the mixture was filtered, washed with cold methanol and dried. The melting point of the product was found to be 130 - 131 ºC.

^{1}H NMR (C_6D_6) δ_H ppm: 12.49 (s, O*H*), 8.61 (s, -*H*^{7}C=N-), 8.40 (dd, *J* = 1.50 Hz, H^{18}), 8.13 (d, *J* = 8.15 Hz, H^{17}), 7.89 (d, *J* = 7.97 Hz, H^{5}), 7.30 – 7.60 (m, 6H$^{2,3,9\text{-}12}$), 7.10 (m, 2H$^{19\&20}$) and 6.98 (m, H^{4}). ^{13}C NMR (C_6D_6) δ_C ppm: 165.1 (C^{14}), 164.1 (C^{7}), 160.7 (C^{1}), 152.9 (C^{15}), 148.1 (C^{8}), 136.2 (C^{16}), 133.9 (C^{3}), 132.9 (C^{5}), 131.5 (C^{13}), 130.0 (C^{10}), 127.2 (C^{12}), 126.7 (C^{11}), 126.2 (C^{19}), 125.0 (C^{20}), 123.3 (C^{18}), 121.4 (C^{17}), 120.1 (C^{9}), 119.4 (C^{4}), 119.3 (C^{6}) and 117.5 (C^{2}). IR (KBr disc) ν(cm^{-1}): 3200 (O-H), 1611 (C=N), 1592, 1566 and 1482. Elemental analysis for $C_{20}H_{14}N_2OS$, [found (calculated)]: C 72.50 (72.70), H 4.30 (4.27), N 8.37 (8.48), S 9.77 (9.71). Electron impact mass spectrometry (EI MS) *m/z*: 330.40 (M^{+}, 100%), 212.02, 197.21 and 134.31.

Bis{2-[2-(2-Benzothiazolyl)]phenyliminomethylphenolato}zinc(II) (**39**)

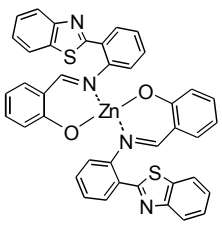

The Schiff base ligand (**37**), (0.10 g, 0.27 mmol) was dissolved in 10 ml of tetrahydrofuran under an atmosphere of argon and cooled to 0 °C in ice. To this solution, a solution of diethylzinc (0.14 mmol, 0.20 ml, 1.00 M) in hexane was

added. The reaction mixture was stirred at room temperature for 2 hours. After this time the solvent was reduced and hexane was added to precipitate the product. The isolated product was re-dissolved in tetrahydrofuran and the mixture was filtered, the filtrate was concentrated, dried and then recrystallized from tetrahydrofuran/hexane. The product was obtained as a yellow powder (0.08 g, 79%). The melting point of the product was found to be 220 ºC (decomposed).

^{1}H NMR (C_6D_6) δ_H ppm: 8.87 (-*H*^{7}C=N-), 8.12 (H^{5}), 7.85 (H^{17}), 7.64 (H^{18}), 7.48 (H^{2}), 7.25 (H^{3}), 6.65 (4H$^{9\text{-}12}$), 6.45 (H^{4}) and 6.25 (2H^{19,20}). ^{13}C NMR (C_6D_6) δ_C ppm: 174.5 (C^{14}), 170.0 (C^{7}), 164.0 (C^{1}), 161.7 (C^{15}), 153.9 (C^{8}), 152.9 (C^{16}), 148.7 (C^{3}), 136.7 (C^{13}), 135.7 (C^{5}), 134.3 (C^{10}), 133.0 (C^{12}), 130.1 (C^{11}), 126.4 (C^{20}), 125.7 (C^{19}), 125.1 (C^{9}), 124.7 (C^{4}), 123.8 (C^{17}), 121.6 (C^{18}), 120.8 (C^{6}) and 119.0 (C^{2}). ESI MS, *m/z*: 722.08 (M^{+}, 2 %), 650.02, 616.11, 486.32 and 381.20. IR (KBr disc) ν(cm^{-1}): 1609 (C=N), 1579, 1529 and 1482: Elemental analysis for $C_{40}H_{26}N_4O_2S_2Zn$ [found (calculated)]: C 66.52 (66.34), H 3.99 (3.62), N 7.39 (7.74) and S 8.77 (8.86).

2-[2-(2-Benzothiazolyl)]phenyliminomethyl-3-tert-butyl-2-hydroxybenzene (**49**)

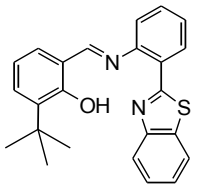

2-Aminobenzothiazole (1.50 g, 6.60 mmol) was added to a solution of 3-*tert*-butyl-2-hydroxybenzaldehyde (2.55 g, 6.60 mmol, 0.85 ml) in methanol (75 ml). The reaction mixture was then heated under reflux for 5 h. Thereafter which the solvent was reduced under reduced pressure and the product precipitated as a light yellow microcrystalline material (1.92 g, 88%). The product was placed in the refrigerator overnight and finally the mixture was filtered washed with cold methanol and dried. The melting point of the product was found to be 135 - 137 ºC.

^{1}H NMR (C_6D_6) δ_H ppm: 12.45 (s, O*H*), 8.63 (s, -*H*C=N-), 8.40 (dd, *J* = 1.50 Hz), 8.13 (d, *J* = 8.15 Hz), 7.89 (d, *J* = 7.97 Hz), 7.25 – 7.55 (m), 7.10 (m), and 1.52 [-(C*H*$_3$)$_3$]. ^{13}C NMR (C_6D_6) δ_C ppm: 164.9, 164.1, 160.5, 152.0, 148.1, 136.2, 133.2, 132.9, 131.5, 130.0, 127.2, 126.7, 126.2, 125.0, 123.3, 121.4, 120.1, 119, 119.3, 117.5, 34.2 [C(*C*H$_3$)$_3$] and 33.9 [*C*(CH$_3$)$_3$]. IR (KBr disc) ν(cm^{-1}): 3209 (OH), 1611 (C=N), 1595, 1566 and 1482. Elemental analysis for $C_{24}H_{22}N_2OS$, [found (calculated)]: C 75.50 (75.58), H 5.80 (5.74), N 7.32 (7.25) and S 8.35 (8.30).

Electron impact mass spectrometry (EI MS) *m/z*: 386.21 (M^+, 100%), 212.02, 197.20 and 134.34.

2-[2-(2-Benzothiazolyl)]phenyliminomethyl-3,5-di(tert-butyl)-2-hydroxybenzene (***50***)

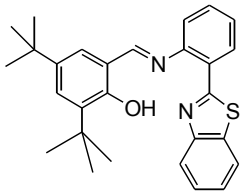

2-Aminobenzothiazole (0.75 g, 3.30 mmol) was added to a solution of 3,5-di(*tert*-butyl)-2-hydroxybenzaldehyde (1.46 g, 3.30 mmol) in methanol (75 ml). The reaction mixture was then heated under reflux for 5 h. Thereafter which the solvent was reduced under reduced pressure and the imine product precipitated as light yellow microcrystalline material (2.00 g, 88%). The product was placed in the refrigerator overnight and finally the mixture was filtered, washed with cold methanol and dried. The melting point of the product was found to be 120 - 125 ºC.

^{1}H NMR (C_6D_6) δ_H ppm: 12.50 (O*H*), 8.54 (-*H*C=N-), 8.40 (dd, *J* = 1.50 Hz), 8.13 (d, *J* = 8.15 Hz), 7.28 – 7.60 (m), 7.10 (m), 6.98 (m), 1.36 [5-C(C*H*$_3$)$_3$] and 1.29 [3-C(C*H*$_3$)$_3$]. ^{13}C NMR (C_6D_6) δ_C ppm: 165.1, 164.1, 160.7, 152.9, 148.1, 136.2, 133.9, 132.9, 131.5, 130.0, 127.2, 126.7, 126.2, 125.0, 123.3, 121.4, 120.1, 119.4, 119.3, 117.5, 33.6 [5-*C*(CH$_3$)$_3$], 34.1 [5-C(*C*H$_3$)$_3$], 32.0 [3-*C*(CH$_3$)$_3$] and 33.1 [3-C(*C*H$_3$)$_3$]. IR (KBr disc), ν(cm^{-1}): 3210 (O-H), 1615 (C=N), 1592, 1566 and 1482. Elemental analysis for $C_{28}H_{30}N_2OS$, [found (calculated)]: C 76.00 (75.98), H 6.52 (6.83), N 6.29 (6.33) and S 7.00 (7.24). Electron impact mass spectrometry (EI MS) *m/z*: 442.50 (M^+, 100%), 212.04, 197.25 and 134.31.

2,4-Di(tert-butyl)-6-[(5-phenyl-2-thiazolyl)hydrazonomethyl]phenol (**38**)

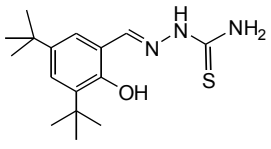

The intermediate 3,5-di(*tert*-butyl)-2-hydroxyphenylthiosemicarbazone derivative was firstly prepared following a literature procedure.[7] A solution of 3,5(di-*tert)*-butyl-2-hydroxybenzaldehyde (0.50 g, 2.10 mmol), aminothiocarbazide (0.19 g, 2.10 mmol) and acetic acid (0.1 ml) in ethanol (60 ml) was heated under reflux for 48 h. The solvent was then reduced under reduced pressure to yield the product as a white powder. The product (0.60 g, 92%) was collected through suction filtration and dried. The melting point of the product was found to be 220 – 221 ºC.

^{1}H NMR (DMSO-d^{6}) δ_H ppm: 11.24 (O*H*), 9.82 (N-N*H*-C), 8.24 (*H*C=N), 7.98 (2H, NH_2), 7.30, 7.08, 1.40 [9H, C(CH_3)$_3$], and 1.23 [9H, C(CH_3)$_3$]. ^{13}C NMR (DMSO-d^{6}) δ_C ppm: 177.2 (C=S), 152.2 (C=N), 149.8, 141.2, 136.2, 126.2, 118.6, 35.2, 34.3, 31.8 and 29.9. IR (KBr disc) ν (cm^{-1}): 3461 (OH), 3263 (NH), 3168, 2953, 2866, 1608 (C=N), 1574 (C=N, thiazole), 1464 and 706 (C=S).

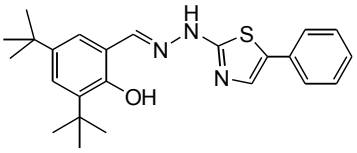

A solution of α-bromoacetophenone (0.23 g, 1.14 mmol) in ethanol 20 ml, was added to a solution of 3,5-di(*tert*-butyl)-2-hydroxyphenylthiosemicarbazone (0.35 g, 1.14 mmol) in the same solvent (20 ml). The reaction mixture was heated under reflux overnight.[7] After this time the solvent was reduced under reduced pressure. Water (40 ml) was then added to the resultant precipitate and the mixture was neutralized with a solution of sodium bicarbonate (10 %). The solid was collected by suction filtration, washed with water, cold ethanol and then dried under reduced pressure. The product (0.20 g, 77 %) was purified by repeated recrystallizations with ethanol and was isolated as a brown microcrystalline material. The melting point of the product (**38**) was found to be 219 - 223 ºC.

^{1}H NMR (DMSO-d^{6}) δ_H ppm: 10.80 (O*H*), 8.26 (*H*^{11}C=N), 7.83 (2H$^{13\&16'}$), 7.81 (N*H*), 7.38 (2H^{17}, t, *J* = 8.15 Hz), 7.25 – 7.29 (m, 4H^{5,9,18,16}), 1.24 [9H^{4}, C(CH_3)$_3$] and 1.38 [9H^{8}, C(CH_3)$_3$]. ^{13}C NMR (DMSO-d^{6}) δ_C ppm: 167.6 (C^{12}), 154.2 (C^{11}), 147.6 (C^{1}), 141.4 (C^{6}), 136.0 (C^{13}), 134.5 (C^{14}), 129.1 (C^{17}), 128.3 (C^{2}), 126.1 (C^{16}), 125.8 (C^{18}), 125.4 (C^{5}), 118.1 (C^{9}), 103.4 (C^{10}), 35.0 (C^{7}), 34.6 (C^{3}), 32.0 (C^{4}) and 29.8 (C^{8}). Elemental analysis for $C_{24}H_{29}N_3OS$ [found (calculated)]: C 70.70 (70.73), H 7.00 (7.17), N 10.29 (10.31) and S 7.80 (7.87). Mass spectrometry (FAB MS) *m/z*: 406.82 (M^{+}, 100%), 391.90, 218.00, 175.92 and 133.95. IR (KBr disc) ν(cm^{-1}): 3134 (O-H), 3052 (N-H), 2957, 2905, 2871, 1622 (C=N), 1587 (C=N, thiazole), 1439 and 706 (C-S).

Bis{2,4-Di-tert-butyl-6-[(5-phenyl-2-benzothiazolyl)hydrazonomethyl] phenolato}zinc(II) (**40**)

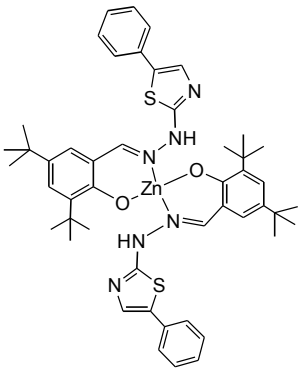

A solution of the ligand (**38**) (0.20 g, 0.49 mmol) and triethylamine (0.70 ml) in ethanol (50 ml) was added to a flask containing a solution of zinc acetate (0.054 g, 0.25 mmol) in the same solvent (5 ml).[7] The reaction mixture was then heated under reflux for 3 h, and then the mixture was left stirring at room temperature overnight. After this time the solvent was removed under reduced pressure, the solid which remained was dissolved in dichloromethane and washed with water and then dried. The solvent was reduced and hexane was added to the remaining mixture. The flask was placed in the refrigerator overnight to precipitate the product as brown microcrystalline solid (0.15 g, 68 %). The melting point of the product was found to be 228 – 233 ºC.

^{1}H NMR (DMSO-d^{6}) δ_H ppm: 10.80 (NH), 8.38 (H^{11}C=N), 7.80 (d, J = 3 Hz, 2H^{16}), 7.48 (t, J = 8.15 Hz, 2H^{17}), 7.25 – 7.35 (m, 2H$^{13\&9}$), 7.25 (d, J = 8.15 Hz, H^{18}), 7.20 (d, J = 8.15 Hz, H^{5}), 1.38 [9H^{8}, C(CH_3)$_3$], 1.24 [9H^{4}, C(CH_3)$_3$]. ^{13}C NMR (DMSO-d^{6}) δ_C ppm: 167.2 (C^{12}), 154.0 (C^{11}), 147.3 (C^{1}), 141.4 (C^{6}), 136.0 (C^{14}), 134.8 (C^{13}), 129.1 (C^{16}), 128.2 (C^{2}), 126.0 (C^{15}), 125.8 (C^{17}), 125.4 (C^{5}), 118.1 (C^{9}), 103.4 (C^{10}), 35.1 (C^{3}), 34.4 (C^{7}), 31.8 (C^{4}) and 29.9 (C^{8}). Elemental analysis for $C_{48}H_{56}N_6O_2S_2Zn$ [found (calculated)]: C 65.09 (65.62), H 6.92 (6.42), N 9.84 (9.57) and S 7.58 (7.30). Mass spectrometry (FAB-MS): 877.00 (M^{+}, 20%), 391.92, 218.03, 175.93 and 133.94. IR (KBr disc) ν(cm^{-1}): 3168 (N-H), 3056, 2953, 2909, 2871, 1607 (C=N), 1589 (C=N, thiazole), 1572 (C=C, thiazole ring), 1439, 1056 and 704 (C-S).

5-(4-fluorophenyl)ferrocenylthiosemicarbazone (**42**)

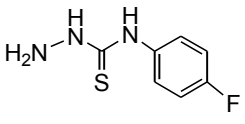

The intermediate 4-(4-fluorophenyl)thiosemicarbazide was firstly prepared as follows: hydrazine hydrate (13.2 M, 0.74 ml, 9.77 mmol) was added dropwise to a solution of 4-fluoro-isothiocyanate (1.50 g, 9.77 mmol) in ethanol (30 ml) at 0 ºC. The reaction mixture was stirred at room temperature for one hour; during this time white crystals

appeared. The crystals (1.61, 89%) were collected by suction filtration washed with ethanol and dried under reduced pressure. The melting point of the product was found to be 172 - 173 ˚C.

^{1}H NMR (DMSO-d^{6}) δ_H ppm: 9.12 [2H, N-N*H*-C and C-N*H*-R^{2}], 4.62 (NH_2), 7.71 (2H, m), 7.11 (2H, m). ^{13}C NMR (DMSO-d^{6}) δ_C ppm: 178.0, 161.1, 136.2, 126.3, 114.6. Elemental analysis for $C_7H_8N_3FS$, [found (calculated)]: C 44.99 (45.39), H 4.20 (4.35), N 22.10 (22.69) and S 17.40 (17.31). Mass spectrometry (EI): 185.20 (M^{+}, 98 %), 95.11 and 90.10. IR (KBr disc) ν(cm^{-1}): 3310 (NH_2), 3276 N(N-H)C, 3164 C(N-H)R^{2}, 3108, 2970, 1639 (C=N, thiol form), 1602, 1525, 1501, 1288, 1211, 906, 839 (C-S, thiol form) and 813 (C=S).

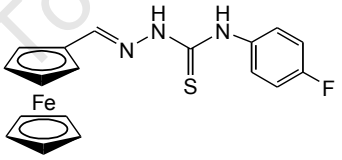

A solution of ferrocenecarboxyaldehyde (0.34 g, 1.60 mmol) in methanol (10 ml) was added dropwise to a flask containing an equimolar amount of 4-(4-fluorophenyl)thiosemicarbazide (0.30 g, 1.60 mmol) in the same solvent (20 ml). The reaction mixture was heated under reflux with stirring for three hours; during this time a maroon precipitate appeared. The solvent was then reduced under reduced pressure and the product was collected by suction filtration as a maroon microcrystalline material (0.52 g, 82%). The product was washed with petroleum ether (40 – 60 ˚C) and dried under reduced pressure. The product was further purified by recrystallization in an ethanol-hexane mixture. The melting point of the product (**42**) was found to be 120 – 123 ºC.

^{1}H NMR (DMSO-d^{6}) δ_H ppm: 11.51 [N(N*H*)C], 9.71 [C(N*H*)R^{2}], 7.97 (*H*^{5}C=N), 7.52 (2H^{8}, dd, *J* = 6.5 Hz), 7.14 (2H^{9}, t, *J* = 6.2 Hz), 4.74 (2H^{3}, t, *J* = 6.3 Hz), 4.49 (2H^{2}, t, *J* = 6.0 Hz) and 4.21 (5H^{1}). ^{13}C NMR (DMSO-d^{6}) δ_C ppm: 175.6 (C^{6}), 161.1 (C^{10}), 158.7 (C^{7}), 144.8 (C^{5}), 135.9 (C^{5}), 128.1 (C^{8}), 128.0 (C^{8}), 115.2 (C^{9}), 114.9 (C^{9}), 79.2 (C^{4}), 70.7 (C^{3}), 69.5 (C^{1}) and 68.4 (C^{2}). Elemental analysis for $C_{18}H_{16}N_3FSFe$, [found (calculated)]: C 56.80 (56.71), H 4.20 (4.23), N 10.92 (11.02) and S 8.30 (8.41). IR (KBr disc) ν(cm^{-1}): 3323 N(N-H)C, 3129 C(N-H)R^{2}, 2970, 1604 (C=N), 1540, 1508, 1276, 1207, 850 (C=S) and 822. Mass spectrometry (EI-MS) *m/z*: 381.12 (M^{+}, 73%), 287.00, 271.00, 228.06, 212.00, 198.00, 185.00, 155.01, 127.07 and 95.04.

Bis[5-(4-fluorophenyl)ferrocenylthiosemicarbazonato}zinc(II) (**46**)

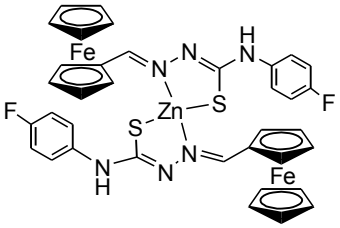

A solution of zinc acetate (0.03 g, 0.13 mmol) in methanol (10 ml) was added to a solution of two molar equivalents of 5-(4-fluorophenyl)-ferrocenylthiosemicarbazone (0.10 g, 0.26 mmol) in methanol (20 ml). The reaction mixture was stirred at room temperature overnight upon which the mixture turned cloudy. The solvent was reduced under reduced pressure and the product was collected by suction filtration as red fluffy solid material [0.80 g, 80%, based on Zn(II)]. The product was then washed with petroleum ether (40 – 60 ˚C) and dried under reduced pressure. The product was further purified by recrystallization in an ethanol-hexane mixture. The melting point of the product was found to be 195 - 198 ˚C.

^{1}H NMR (DMSO-d^{6}) δ_H ppm: 9.41 (CN*H*R^{2}), 7.68 (2H^{8}, dd, *J* = 6.3 Hz), 7.48 (H^{5}), 7.15 (2H^{9}), 5.05 (2H^{3}), 4.48 (2H^{2}) and 4.20 (5H^{1}). ^{13}C NMR (DMSO-d^{6}) δ_C ppm: 170.1 (C^{6}), 153.1 (C^{10}), 138.7 (C^{5}), 124.0 (C^{7}), 123.4 (C^{8}), 125.0 (C^{9}), 74.1 (C^{4}), 73.3 (C^{3}), 73.4 (C^{1}) and 70.0 (C^{2}). Elemental Analysis for $C_{36}H_{32}N_6F_2S_2Fe_2Zn$ [found (calculated)]: C 52.70 (52.35), H 3.74 (3.66), N 10.02 (10.18) and S 7.62 (7.77). IR (KBr disc) ν(cm^{-1}): 1600 [C(C=N)N], 1527 [N(C=N)C(S)N], 839 (C-S), 3306 [C(N-H)R^{2}], 3086, 1508 and 1484. Mass spectrometry (ESI-MS) *m/z*: 824.00 (M^{+}, 20%), 713.80, 425.97 and 380.04.

(5-methyl)ferrocenylthiosemicarbazone (**41**)

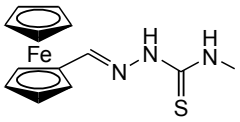

A solution of ferrocenecarboxyaldehyde (0.50 g, 4.80 mmol) in methanol (10 ml) was added dropwise to a solution containing an equimolar amount of 4-methylthiosemicarbazide (0.89 g, 4.80 mmol) in the same solvent (20 ml). The reaction mixture was heated under reflux with stirring for three hours; during this time a maroon precipitate appeared. The solvent was then reduced under reduced pressure and the product was collected by suction filtration as a maroon microcrystalline material (1.00 g, 69%). The product was washed with petroleum ether (40 – 60 ˚C)

and dried under reduced pressure. The melting point of the product was found to be 193-195 ˚C.

^{1}H NMR (DMSO-d^{6}) δ_H ppm: 11.10 [N(N*H*)C], 8.07 [C(N*H*)R^{2}], 7.84 (*H*^{5}C=N), 4.67 (2H^{3}, t, *J* = 6.1 Hz), 4.37 (2H^{2}, t, *J* = 3.8 Hz), 4.16 (5H^{1}) and 2.94 (H^{7}, d, *J* = 5.9 Hz). ^{13}C NMR (DMSO-d^{6}) δ_C ppm: 177.6 (C^{6}), 143.3 (C^{5}), 79.6 (C^{4}), 70.4 (C^{3}), 69.9 (C^{1}), 68.0 (C^{2}) and 31.2 (C^{7}). IR (KBr disc) ν(cm^{-1}): 1609 (C=N), 1551, 3336 [C(N-H)CH$_3$], 3297 [N(N-H)C(S)N], 3250, 3142, 2931 and 854 (C=S). Elemental analysis for $C_{13}H_{15}N_3SFe$, [found (calculated)]: C 51.90 (51.84), H 5.00 (5.02), N 13.50 (13.95) and S 10.50 (10.65). Mass spectrometry (EI-MS) *m/z*: 301.05 (M^{+}, 73%), 284.71, 271.00, 238.59, 226.68, 212.02 and 185.00.

Bis[(5-methyl)ferrocenylthiosemicarbazonato]zinc(II) (**45**)

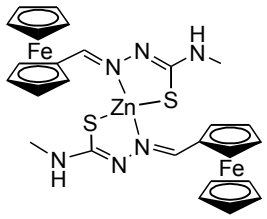

An ethanol solution of zinc acetate (0.08 g, 0.36 mmol) was added to a solution of two molar equivalents of (5-methyl)-ferrocenylthiosemicarbazone (0.20 g, 0.67 mmol) in methanol (20 ml). The reaction mixture was then heated under reflux with stirring overnight. The solvent was reduced under reduced pressure and the product was collected by suction filtration as a red solid material. The product [0.18 g, 82% with respect to Zn(II)] was then washed with petroleum ether (40 – 60 ˚C) and dried under reduced pressure. The product was further purified by recrystallization in ethanol-hexane mixture. The melting point of the product was found to be 195 - 198 ˚C.

^{1}H NMR (DMSO-d^{6}) δ_H ppm: 7.30 (2H, CN*H*R^{2} and *H*^{5}C=N), 5.16 (2H^{3}), 4.48 (2H^{2}), 4.12 (5H^{1}) and 2.95 (3H^{7}). ^{13}C NMR (DMSO-d^{6}) δ_C ppm: 151.2 (C^{6}), 143.8 (C^{5}), 74.9 (C^{4}), 72.9 (C^{3}), 71.8 (C^{1}), 69.7 (C^{2}) and 30.9 (C^{7}). Elemental Analysis for $C_{26}H_{28}N_6F_2S_2Fe_2Zn$ [found (calculated)]: C 47.40 (46.91), H 4.64 (4.24), N 12.20 (12.62) and S 9.50 (9.63). IR (KBr disc) ν(cm^{-1}): 1598 [C(C=N)N], 1495 [S(NH)(C=N)N], 3349 (N-H), 3353, 3095 and 2940 and 815 (C-S). Mass spectrometry (ESI-MS) *m/z*: 663.00 (M^{+}, 20%), 395.93, 302.02 and 271.00.

(5-methyl)(4-tert-butylphenyl)thiosemicarbazone (**43**)

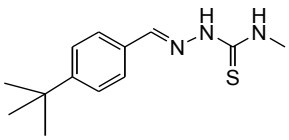

4-*tert*-Butylbenzaldehyde (0.46 g, 2.90 mmol, 0.50 ml) was added dropwise to a solution of an equimolar amount of thiosemicarbazide (0.30 g, 2.90 mmol) in methanol (40 ml). The reaction mixture was heated under reflux for 48 h. The solvent was then removed under reduced pressure and dichloromethane (1 ml) was added to the sticky oil which remained. To the remaining solution was added hexane (10 ml) and the product was isolated as a white microcrystalline solid (0.42 g, 58%). The material was collected by suction filtration, washed and dried under reduced pressure. The melting point of the product was found to be 193 – 195 ˚C.

^{1}H NMR (DMSO-d^{6}) δ_H ppm: 11.32 (N-*NH*-C), 8.34 (C-*NH*R^{2}), 8.04 (H^{7}), 7.70 (H^{5}), 7.42 (H^{4}), 3.02 (3H^{9}), 1.31 (9H^{1}). ^{13}C NMR (DMSO-d^{6}) δ_C ppm: 177.1 (C^{8}), 152.7 (C^{7}), 142.2 (C^{3}), 131.8 (C^{5}), 126.8 (C^{5}), 125.7 (C^{4}), 34.5 (C^{9}), 30.6 (C^{1}) and 21.7 (C^{2}). IR (KBr disc) ν(cm^{-1}): 3319 [N(N-H)C], 3177 [C(N-H)R^{2}], 3017, 2953, 1609 (C=N), 1548, 1521, 1269, 1033 and 835 (C=S). Elemental analysis for $C_{13}H_{19}N_3S$ [found (calculated)]: C 62.51 (62.61), H 7.62 (7.68), N 16.90 (16.85) and S 12.56 (12.86). Mass spectrometry (EI-MS): 248.81 (M^{+}, 100%), 246.91, 1756.00, 174.98, 161.02, 160.08, 146.97, 145.96, 134.09, 115.94, 104.00 and 89.95.

Bis[(5-methyl)(4-tert-butylphenyl)thiosemicarbazonato]zinc(II) (**47**)

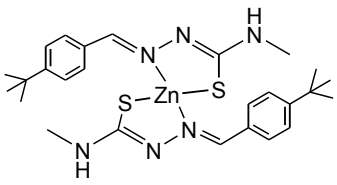

A solution of zinc acetate (0.07 g, 0.32 mmol) in methanol (20 ml) was added to a solution of two mole equivalents of (5-methyl)(4-*tert*-butylphenylthiosemicarbazone (0.16 g, 0.64 mmol) in methanol (20 ml). The reaction mixture was heated under reflux for 48 h. The solvent was then removed under reduced pressure and dichloromethane (1 ml) was added to the sticky oil which remained. To this solution was then added hexane (10 ml) to precipitate the product as a white microcrystalline solid (0.10 g, 55%). The material was collected by suction filtration, washed and dried under reduced pressure. The product was purified by recrystallization from a mixture of methanol-petroleum ether. The melting point of the product was found to be 108 – 110 ˚C.

^{1}H NMR (DMSO-d^{6}) δ_H ppm: 8.33 (C*NH*R^{2}), 8.04 (*H*^{7}C=N), 7.71 (H^{5}), 7.44 (H^{4}), 3.03 (3H^{9}), 1.33 [9H^{1}, C(C*H*$_3$)$_3$]. ^{13}C NMR (DMSO-d^{6}) δ_C ppm: 173.1 (C^{8}), 152.7 (C^{7}), 142.2 (C^{3}), 130.8 (C^{5}), 126.8 (C^{5}), 125.7 (C^{4}), 34.5 (C^{9}), 30.6 (C^{1}) and 21.7 (C^{2}). IR (KBr disc) ν(cm^{-1}): 3177 [C(N-H)R^{2}], 2966, 2909, 2862, 1613 [C(C=N)N)], 1579 [N(C=N)C(S)N, shoulder], 1510, 1084, 831 (C-S) and 669. Elemental analysis for $C_{26}H_{36}N_6S_2Zn$ [found (calculated)]: C 54.98 (55.55), H 6.42 (6.46), N 13.86 (14.95) and S 11.54 (11.41). Mass spectrometry (FAB-MS): 562.00 (M^{+}, 40%), 547.10, 531.14, 298.04 and 234.11.

5-(4-fluorophenyl)(4-tert-butylphenyl)thiosemicarbazone (**44**)

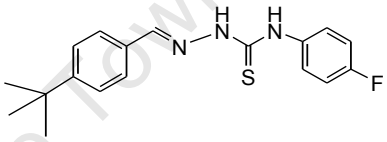

4-*tert*-Butylbenzaldehyde (0.18 g, 0.20 ml, 1.10 mmol), was added dropwise to a solution containing an equimolar amount of (4-(fluorophenyl)thiosemicarbazide (0.20 g, 1.10 mmol) in methanol (40 ml). The reaction mixture was heated under reflux for 48 h. The solvent was then removed under reduced pressure and dichloromethane (1 ml) was added to the sticky oil which remained. To the remaining solution was added hexane (10 ml) and the product was isolated as white microcrystalline solid (0.25 g, 69%). The material was collected by suction filtration, washed and dried under reduced pressure. The melting point of the product was found to be 200 – 205 ˚C.

^{1}H NMR (DMSO-d^{6}) δ_H ppm: 11.76 (N-N*H*-C), 10.11 (-CN*H*-R^{2}), 8.14 (H^{7}), 7.81 (H^{11}), 7.53 (H^{10}), 7.46 (H^{5}), 7.17 (H^{4}) and 1.30 (9H^{1}). ^{13}C NMR (DMSO-d^{6}) δ_C ppm: 176.9 (C^{8}), 161.4 (C^{12}), 158.5 (C^{7}), 153.4 (C^{3}), 143.7 (C^{9}), 136.2 (C^{5}), 132.0 (C^{4}), 128.5 (C^{6}), 127.8 (C^{10}), 126.1 (C^{12}), 35.3 (C^{2}) and 31.1 (C^{1}). IR (KBr disc) ν(cm^{-1}): 3198 [N(N-H)C], 3065 [C(N-H)R^{2}], 2967, 2897, 2866, 1607 [C(C=N)N)], 1529 [N(C=N)C, shoulder], 1512, 1265, 929 and 836 (C=S). Elemental analysis for $C_{18}H_{20}N_3FS$ [found (calculated)]: C 65.50 (65.63), H 6.18 (6.12), N 12.50 (12.76) and S 10.01 (9.73). Mass spectrometry (ESI-MS) *m/z*: 329.44 (M^{+}, 100%), 314.61, 234.03 and 90.11.

Bis[5-(4-fluorophenyl)(4-tert-butylphenyl)thiosemicarbazonato]zinc(II) (**48**)

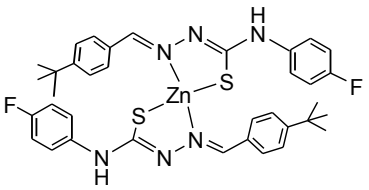

A solution of zinc acetate (0.033 g, 0.015 mmol) in methanol (20 ml) was added to a solution containing two mole equivalents (0.10 g, 0.03 mmol) of 5-[(4-fluorophenyl)(4-*tert*-butylphenyl)thiosemicarbazone in methanol (20 ml). The reaction mixture was heated under reflux for 48 h. The solvent was then removed under reduced pressure and dichloromethane (1 ml) was added to the sticky oil which remained. To this solution was added hexane (10 ml) to precipitate the product as white microcrystalline solid (0.10 g, 45%). The material was collected by suction filtration, washed and dried under reduced pressure. The product was purified by recrystallization from a mixture of methanol-petroleum ether. The melting point of the product was found to be 175 – 177 ˚C.

^{1}H NMR (DMSO-d^{6}) δ_H ppm: 9.48 (2H, N*H*), 8.12 (2H^{7}), 7.00 – 7.70 (16H) and 1.25 [18H^{1}, 2xC(C*H*$_3$)$_3$]. ^{13}C NMR (DMSO-d^{6}) δ_C ppm: 172.0 (C^{8}), 162.4 (C^{12}), 158.5 (C^{7}), 153.4 (C^{3}), 140.7 (C^{9}), 136.2 (C^{5}), 132.0 (C^{4}), 128.5 (C^{6}), 122.3 (C^{10}), 115.1 (C^{12}), 32.1 (C^{2}) and 31.1 (C^{1}). IR (KBr disc) ν(cm^{-1}): 3069 (N-H), 2966, 2909, 2866, 1609 [C(C=N)N)], 1592 [CN(S)(C=N)N], 1572, 1538, 1220 and 835 (C-S). Elemental analysis for $C_{38}H_{46}F_2N_6S_2Zn$ [found (calculated)]: C 60.02 (60.50), H 6.01 (6.15), N 10.76 (11.14) and S 8.02 (8.50). Mass spectrometry (FAB-MS) *m/z*: 754.33 (M^{+}) 643.42, 533.42, 520.10, 421.93 and 300.02.

7.3 Palladium complexes and corresponding ligands

4-Methyl-N,N-di(2-pyridyl)benzamide (**51**)

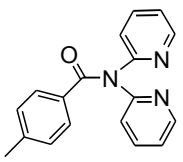

Solution of tolyl chloride (1.90 g, 12.30 mmol, 1.62 ml) in dry dichloromethane was added drop-wise to a flask containing *N,N*-di(2-pyridyl)amine (2.10 g, 12.30 mmol) and triethylamine (1.27 g, 13.00 mmol, 1.70 ml) in the same solvent at ºC. When addition was complete, the reaction mixture was stirred at this temperature for 1 h. The mixture was then allowed to slowly reach room temperature and left to react

while stirring for 24 h. The solvent was then removed under reduced pressure and the white solid which remained was subjected to purification on a short plug of alumina by column chromatography (2 x 10 cm), eluting with a mixture of dichloromethane : ethanol (99:1). After the solvent was removed, the crude gummy oil was recrystallized from dichloromethane and hexane to afford product (**51**) (3.00 g, 84 %) as white crystals. The melting point of the product was found to be 125 - 130 ºC.

^{1}H NMR ($CDCl_3$) δ_H ppm: 8.40 ($2H^{10}$, d, *J* = 3 Hz), 7.66 ($2H^{4}$, d, *J* = 12 Hz), 7.40 ($2H^{8}$, d, *J* = 9 Hz), 7.25 ($2H^{3}$, d, *J* = 6 Hz), 7.12 ($2H^{7}$, d, *J* = 3 Hz), 7.02 ($2H^{9}$, *J* = 6 Hz) and 2.29 ($3H^{1}$). ^{1}H NMR (Acetone-d^6) δ_H ppm: 8.16 ($2H^{10}$, d, *J* = 3 Hz), 7.65 ($2H^{4}$, dd, *J* = 12 Hz), 7.25 ($2H^{8}$, d, *J* = 6 Hz), 7.20 ($2H^{3}$, *J* = 3 Hz), 7.05 ($2H^{7}$, dd, *J* = 3 Hz), 6.96 ($2H^{9}$, d, *J* = 6 Hz), 2.15 ($3H^{1}$). ^{13}C NMR ($CDCl_3$) δ_C ppm: 172.0 (C^{6}), 156.2 (C=O), 149.0 (C^{10}), 142.1 (C^{2}), 137.8 (C^{8}), 134.1 (C^{5}), 129.2 (C^{3}), 128.7 (C^{4}), 122.5 (C^{9}), 121.4 (C^{7}), 21.4 (C^{1}). IR (KBr disc) ν(cm^{-1}): 3043, 3004, 2918, 1656 (C=O), 1609 (C=N), 1583, 1570 and 1465. Elemental analysis for $C_{18}H_{15}N_3O$ [found (calculated)]: C 74.51, (74.72), H 4.92 (5.23), N 14.32 (14.52). Mass spectrometry (ESI-MS) *m/z*: 289.33 (M^+, 100%), 120.10 and 171.21.

(Chlorido)(methyl)[4-methyl-N,N-di(2-pyridyl)benzamide]palladium(II) (**53**)

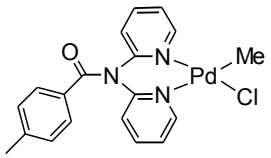

A mixture of 4-methyl-*N*,*N*-di(2-pyridyl)benzamide (0.30 g, 1.05 mmol) and [PdMeCl(COD)][6] (0.30 g, 1.05 mmol) in dry tetrahydrofuran was stirred at room temperature for 3 h. After this time the solvent was reduced under reduced pressure to afford a yellow oil. The oil was then dissolved in dichloromethane (5 ml) and to this solution diethyl ether was added and a cloudy mixture formed; upon placing the flask in liquid nitrogen the product precipitated as a white solid. The complex (**53**) (0.38 g, 81 %) was collected by suction filtration, washed with diethyl ether and dried. The melting point of the complex was found to be 180 ºC (decomposed).

^{1}H NMR ($CDCl_3$) δ_H ppm: 9.02 (H^{10}, d, *J* = 6 Hz), 8.63 ($H^{10'}$, d, *J* = 9 Hz), 7.87 (H^{4}, d, *J* = 3 Hz), 7.70 ($H^{4'}$, d, *J* = 3 Hz), 7.60 ($2H^{8,8'}$, d, *J* = 3 Hz), 7.52 ($H^{3/3'}$, d, *J* = 3 Hz), 7.29 - 7.40 ($3H^{3/3',7,7'}$, m), 7.12 ($2H^{9,9'}$, d, *J* = 9 Hz), 2.31 ($3H^{1}$), 1.11 (Pd-CH_3).

IR (KBr disc) ν(cm^{-1}): 3108, 3073, 3043, 2987, 2953, 2871, 1690 (C=O), 1600 (C=N), 1570, 1465, 1321 and 826. Elemental analysis for $C_{19}H_{18}ClN_3OPd$ [found (calculated)]: C 51.00 (51.14), H 3.98 (4.07) and N 9.50 (9.42).

(Methyl)(methylcyanide)[4-methyl-N,N-di(2-pyridyl)benzamide]palladium(II) tetrafluoroborate (**56**)

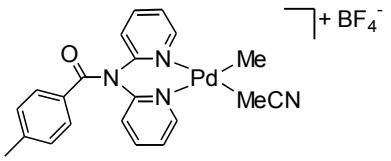

The neutral palladium complex (**53**) (0.28 g, 0.63 mmol) was dissolved in 20 ml of dichloromethane and the reaction flask was covered with aluminium foil. To this solution was added a solution of silver tetraflouroborate (0.13 g, 0.63 mmol) in acetonitrile (10 ml), and a white silver chloride precipitate formed immediately. The reaction mixture was further stirred at room temperature for 1 h. After this time the silver chloride was filtered off through celite under reduced pressure. The solvent was then reduced under vacuum. The oil which remained was dissolved in dichloromethane (5 ml) and diethyl ether (0.5 ml) was added. The mixture was cooled in liquid nitrogen to afford the product as a white powder. The product (**56**) (0.25 g, 74 %) was filtered, washed with diethyl ether and then dried under reduced pressure. The melting point of the product was found to be 190 ºC (decomposed). The product decomposed rapidly in deuterated solvents; therefore, the ^{1}H and ^{13}C NMR spectra were measured immediately after sample preparation.

^{1}H NMR ($CDCl_3$) δ_H ppm: 8.78 (H^{10}, d, *J* = 3 Hz), 8.40 ($H^{10'}$, d, *J* = 6 Hz), 7.90 (H^4, d, *J* = 3 Hz), 7.74 ($H^{4'}$, d, *J* = 6 Hz), 7.60 ($H^{8/8'}$, d, *J* = 6 Hz)), 7.57 ($H^{8/8'}$, *J* = 6 Hz), 7.42 ($4H^{3,3',7,7'}$, m), 7.10 ($2H^{9,9'}$, d, *J* = 6 Hz), 2.29 ($3H^1$), 2.53 (Pd-NCCH_3), and 1.01 (3H, Pd-CH_3). ^{1}H NMR (Acetone-d^6) δ_H ppm: 8.72 ($2H^{10}$), 8.57 ($2H^4$, d, *J* = 3 Hz), 7.98 ($2H^8$), 7.73 ($2H^3$), 7.46 ($2H^7$), 7.05 ($2H^9$), 2.15 ($3H^1$), 1.93 (3H, Pd-NCCH_3) and 0.96 (3H, Pd-CH_3). ^{13}C NMR ($CDCl_3$) δ_C ppm: 159.0 (C=O), 152.2 (C^7), 150.0 (C^7), 143.0 (C^{10}), 142.1 (C^2), 134.4 (C^9), 128.0 (C^5), 127.0 (C^3), 126.2, 125.2.1, 125.7, 125.0 (C^4), 126.0, 125.0, 21.0 (-C_6H_4-CH_3), 29.2 (CH_3CN-Pd) and 4.97 (Pd-CH_3). Mass spectrometry (ESI-MS) *m/z*: 451.00 [$(M\text{-}BF_4^-)^+$, 100%] and 87.00 (BF_4^-). IR (KBr disc) ν(cm^{-1}): 3078, 2966, 2879, 2328 (Me*C*≡*N*), 2297 (Me*C*≡*N*), 1686 (C=O), 1598 (C=N), 1570, 1464, 1329, 1286, 1060 (BF_4^-) and 828.

Elemental analysis for $C_{21}H_{21}N_4OBF_4Pd$ [found (calculated)]: C 46.55 (46.83), H 3.89 (3.93) and N 10.00 (10.40).

(Methyl)[4-methyl-N,N-di(2-pyridyl)benzamide](triphenylphosphine)palladium(II) tetrafluoroborate (**58**)

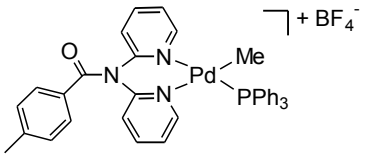

To solution of neutral complex (**53**) (0.10 g, 0.22 mmol) in 20 ml of dichloromethane was added a solution of triphenylphosphine (0.06 g, 0.22 mmol) and ammonium tetrafluoroborate (0.02 g, 0.22 mmol) in anhydrous methanol. The reaction mixture was stirred at room temperature for 24 h. After this time the solvent was removed under reduced pressure. Dichloromethane was then added to the flask to precipitate ammonium chloride, which was filtered off under reduced pressure through celite. The oil which remained was dissolved in dichloromethane (5 ml) and to this solution was added diethyl ether (0.10 ml). The mixture was cooled in liquid nitrogen to afford the product as a white microcrystalline powder. Product (**58**) (0.91 g, 54 %) was filtered, washed with diethyl ether and then dried under reduced pressure. The melting point of the product was found to be 219 – 221 ºC.

^{1}H NMR ($CDCl_3$) δ_H ppm: 8.60 (H^{10}, d, J = 3 Hz), 7.91 ($H^{10'}$, d, J = 12 Hz), 7.30 - 7.75 (21H, $(C_6H_5)_3P$ and $H^{3,3',4,4',7,8}$, m), 7.02 ($H^{7'}$, d, J = 6 Hz), 6.81 ($2H^{9,9'}$, d, J = 3 Hz), 2.33 ($3H^1$), 0.82 (3H, d, $J_{H\text{-}P}$ = 3 Hz, Pd-CH_3). ^{31}P ($CDCl_3$) δ_P ppm: 39.94 (Pd-PPh$_3$) and -144.36 (PF_6^-). ^{13}C NMR ($CDCl_3$) δ_C ppm: 169.2 (C=O), 150.5 (C^6), 141.7 (C^{10}), 140.5 (C^2), 134.4 (C^8), 134.3, (C^5), 131.6 (PPh$_3$-*ortho*), 129.2 (PPh$_3$-*meta*, and *para*), 129.1(C^3), 129.0 (C^4), 125.8(C^7), 125.6 (C^9), 124.5, 21.5 (C^1) and 5.2 (Pd-CH$_3$, d, $J_{C\text{-}P}$ = 21 Hz,). Mass spectrometry (ESI-MS) *m/z*: 672.06 [(M-BF_4^-)$^+$, 100%], 470.02, 383.12 and 87.00 (BF_4^-). IR (KBr disc) ν(cm^{-1}): 3078, 3056, 2978, 2884, 1669 (C=O), 1602 (C=N), 1570, 1316, 1295, 1061 (BF_4^-) and 831. Elemental analysis for $C_{38}H_{33}BF_4N_3OPd$ [found (calculated)]: C 58.06 (58.48), H 4.79 (4.38) and N 5.08 (5.53).

(Methyl)(methylcyanide)[4-methyl-N,N-di(2-pyridyl)benzamide]palladium(II) hexafluorophosphate (**55**)

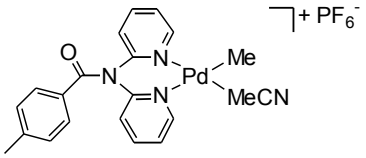

A solution of sodium tetrafluorophosphate (0.041 g, 0.22 mmol) in acetonitrile (5 ml) was added to a solution of the neutral complex (**53**) (0.10 g, 0.22 mmol) in dichloromethane (20 ml). After mixing the reagents sodium chloride appeared as a white solid. The reaction mixture was then stirred at room temperature for 24 h. When the reaction was over sodium chloride was filtered off under reduced pressure through celite and then the solvent was reduced under vacuum. The oil which remained was dissolved in dichloromethane (5 ml) and diethyl ether (0.50 ml) was added to the final solution. The mixture was cooled in liquid nitrogen to afford the product as a cream-white precipitate. Product (**55**) (0.11 g, 85 %) was filtered, washed with diethyl ether and then dried under reduced pressure. The melting point of the product was found to be 225 ºC (decomposed). The product was not soluble in $CDCl_3$ and decomposed quickly in other deuterated solvents; therefore, the ^{1}H and ^{13}C NMR spectra were measured immediately after sample preparation.

^{1}H NMR (Acetone-d^6) δ_H ppm: 8.76 (H^{10}), 8.75 (H^{10}, d, J = 6 Hz), 8.15 ($2H^{4,4'}$), 7.80 ($2H^{8,8'}$, d, J = 6 Hz), 7.62 ($2H^{3,3'}$), 7.55 ($2H^{7,7'}$, d, J = 3 Hz), 7.22 ($2H^{9,9'}$), 2.30 ($3H^{1}$), 2.05 (3H, CH_3CN-Pd) and 1.05 (Pd-CH_3). ^{31}P (Acetone-d^6) δ_P ppm: 145.0 (PF_6^-). ^{13}C NMR (Acetone-d^6) δ_C ppm: 159.0 (C=O), 152.2 (C^7), 150.0 (C^7), 143.0 (C^{10}), 142.1 (C^2), 134.4 (C^9), 128.0 (C^5), 127.0 (C^3), 126.2, 125.2.1, 125.7, 125.0 (C^4), 126.0, 125.0, 21.0 (C^1), 6.2 (CH$_3$CN-Pd), 4.97 (Pd-CH$_3$). Mass spectrometry (ESI-MS) *m/z*: 451 [(M-PF_6^-)$^+$, 100%], and 145. IR (KBr disc) ν(cm^{-1}): 3121, 3026, 2974, 2944, 2897, 2232, (Me$C\equiv N$), 2306 (Me$C\equiv N$), 1690 (C=O), 1602 (C=N), 1570, 1484 and 839 (PF_6^-). Elemental analysis for $C_{21}H_{21}N_4OF_6PPd$ [found (calculated)]: C 42.01 (42.26), H 3.74 (3.55) and N 9.37 (9.39).

(Methyl)[4-methyl-N,N-di(2-pyridyl)benzamide](triphenylphosphine)palladium(II) hexafluorophosphate (**57**)

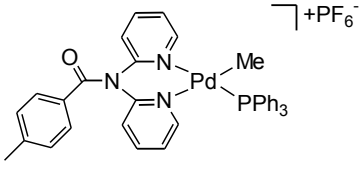

The neutral complex (**53**) (0.10 g, 0.22 mmol) was dissolved in 20 ml of dichloromethane in the reaction

flask. To this solution was added a solution of sodium hexafluorophosphate (0.04 g, 0.22 mmol) and triphenylphosphine (0.06 g, 0.22 mmol) in 10 ml of tetrahydrofuran. The reaction mixture was stirred at room temperature for 24 h. Sodium chloride salt formed and was filtered off and the filtrate was collected; the solvent volume was reduced under reduced pressure. The oil which remained was dissolved in dichloromethane (5 ml) and diethyl ether (0.5 ml) was added; this mixture was cooled in liquid nitrogen to afford the product as a white precipitate. Product (**57**) (0.15 g, 83 %) was filtered, washed with diethyl ether and then dried under reduced pressure. Single crystals suitable for X-ray crystallography were grown from a mixture of dichloromethane and diethyl ether in the refrigerator. The melting point of the product was found to be 190 ºC (decomposed).

^{1}H NMR ($CDCl_3$) δ_H ppm: 8.78 (H^{10}, d, J = 3 Hz), 8.60 ($H^{10'}$, d, J = 12 Hz), 7.30 - 7.75 (21H, $(C_6H_5)_3P$ and $H^{3,3',4,4',7,8}$, m), 7.02 ($H^{7'}$, d, J = 6 Hz), 6.81 ($2H^{9,9'}$, d, J = 3 Hz) 2.31 ($3H^{1}$), 0.78 (3H, Pd-CH_3), d, J_{H-P} = 3Hz). ^{31}P ($CDCl_3$) δ_P ppm: 39.94 [Pd-*P*$(C_6H_5)_3$] and -144.34 (PF_6^-). ^{13}C NMR ($CDCl_3$) δ_C ppm: 150.5 (C^6), 149.7 (C=O), 141.7 (C^{10}), 140.5 (C^2), 134.4 (C^8), 134.3, (C^5), 131.6 [($P(C_6H_5)_3$, *ortho*)], 129.2 [$P(C_6H_5)_3$-*meta* and *para*], 129.1(C^3), 129.0 (C^4), 125.8(C^7), 125.6 (C^9), 124.5, 21.5 (C^1) and 5.2 (d, J_{C-P} = 21 Hz, Pd-*C*H_3). Mass spectrometry (ESI-MS) *m/z*: 672 [$(M-PF_6^-)^+$, 100%], 528.03, 383.12 and 145.00 (PF_6^-). IR (KBr disc) ν(cm^{-1}): 3078, 3060, 2983, 2957, 2892, 1675 (C=O), 1604 (C=N), 1570, 1482, 1312, 1291 and 841 (PF_6^-). Elemental analysis for $C_{37}H_{33}N_3OF_6P_2Pd$ [found (calculated)]: C 53.83 (54.32), H 3.97 (4.07) and N 4.68 (5.14).

N,N-Di(2-pyridyl)ferrocenylamide (**52**)[8,9]

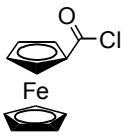

Chlorocarbonylferrocene was firstly prepared following a literature procedure.[8] Oxalyl chloride (1.36 g, 10.75 mmol, and 0.92 ml) was added drop-wise to a solution of ferrocenecarboxylic acid (1.00 g, 4.30 mmol) in carbon tetrachloride (20 ml) at 0 ºC under nitrogen atmosphere. When addition was complete, the solution was stirred at 0 ºC for 1 h, then the mixture was allowed to react further while stirring for an additional 3 h at room temperature. After this time excess oxalyl chloride was removed under reduced pressure at 30 ºC. The

acyl-chloride product was obtained as a red solid and dried under reduced pressure and then used in the subsequent reaction without further purification.

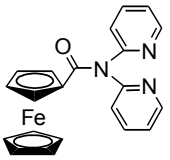

A solution of chlorocarbonylferrocene (1.05 g, 4.20 mmol) in dichloromethane (20 ml) was added drop-wise to a solution of *N*,*N*-di(2-dipyridyl)amine (0.72 g, 4.20 mmol) and triethylamine (0.42 g, 4.20 mmol, 0.60 ml) in the same solvent (20 ml) at 0 ºC. When addition was complete, the solution was stirred at this temperature for 1h, and then left to react while stirring at room temperature for 24 h. The solvent was then removed under reduced pressure; the red-orange solid which remained was subjected to purification on a preparative thin layer chromatography plate, eluting with a mixture of dichloromethane : methanol (99:1). The first orange band was collected and the product extracted with dichloromethane. The solvent was removed under reduced pressure and the product (**52**) (1.10 g, 69 %) was obtained as an orange solid. The melting point of the product was found to be 150 – 153 ºC (lit.[9] m.p. 150 – 152 ºC).

^{1}H NMR ($CDCl_3$) δ_H ppm: 8.44 ($2H^{9,9'}$, d, J = 9 Hz), 7.72 ($2H^{8,8'}$, d, J = 9 Hz), 7.36 ($2H^{7,7'}$, d, J = 6 Hz), 7.10 ($2H^{6,6'}$, t, J = 3 Hz), 4.28 ($5H^{1}$, C_5H_5, s) and 4.21 ($4H^{2,3}$, m). ^{13}C NMR ($CDCl_3$) δ_C ppm: 70.2 (C^1), 70.4 (C^2), 71.1 (C^3), 121.3 ($C^{9,9'}$), 122.4 ($C^{8,8'}$), 137.6 ($C^{7,7'}$), 148.9 ($C^{6,6'}$), 155.6 ($C^{5,5'}$) and 173.0 (C=O). IR (KBr disc) ν(cm^{-1}): 3058, 2983, 1674 (C=O), 1558, 1567 (C=N) and 1435. Mass spectrometry *(*EI-MS) *m/z*: 383.12 (M^+, 100%), 306.10, 199.20 and 186.00. Elemental analysis for $C_{21}H_{17}N_3OFe$ [found (calculated)]: C 65.82 (65.53), H 4.47 (4.40), N 10.96 (10.81).

(Chlorido)(methyl)[N,N-di(2-pyridyl)ferrocenylamide]palladium(II) (**54**)

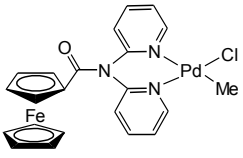

A mixture of *N*,*N*-di(2-pyridyl)ferrocenylamide (**52**) (0.21 g, 0.55 mmol) and [PdMeCl(COD)] (0.15 g, 0.55 mmol) in tetrahydrofuran (20 ml) was stirred at room temperature for 3 h. After this time the solvent was reduced under reduced pressure. Hexane was then added to the resulting solution to afford an orange precipitate. The desired complex (**54**), (0.26 g, 88 %) was collected by suction filtration, washed with hexane and dried under reduced pressure. The melting point of the product was found to be 178 ºC dec.

^{1}H NMR ($CDCl_3$) δ_H ppm: 9.03 (H^{9}, d, *J* = 6 Hz), 8.67 ($H^{9'}$, d, *J* = 6 Hz), 7.95 ($H^{8'}$, d, *J* = 3Hz), 7.78 ($2H^{8}$, d, *J* = 3Hz), 7.70 – 7.67 ($4H^{6,6',7,7'}$, m), 4.65 ($H^{2/2'}$), 4.45 ($6H^{1,\ 2/2'}$), 4.30 ($H^{3/3'}$), 3.82 ($H^{3/3'}$) and 1.13 (3H, Pd-C*H*$_3$). ^{13}C NMR ($CDCl_3$) δ_C ppm: 151.2 (C^{5}), 150.6 (C=O), 139.3 ($C^{5'}$), 139.1 (C^{9}), 126.3 (C^{7}), 124.8 (C^{6}), 124.2 (C^{8}), 123.8 (C), 119.2, 115.2, 112.1, 72.6 (C^{4}), 71.8 (C^{3}), 71.6 (C^{1}), 71.3 (C^{2}) and -2.1 (Pd-*C*H$_3$). IR (KBr disc), ν(cm^{-1}): 3444, 3284, 2953, 2871, 1656 (C=O), 1632 (C=N), 1594, 1465 and 1284. Elemental analysis for $C_{22}H_{20}N_3ClOFePd$ [found (calculated)]: C 48.82 (48.92), H 3.52 (3.73) and N 7.44 (7.78).

(Methyl)(methylcyanide)[N,N-di(2-pyridyl)ferrocenylamide]palladium(II) hexafluorophosphate (**59**)

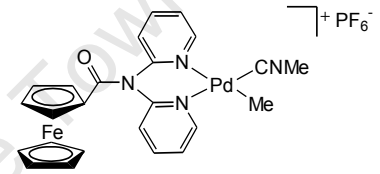

The neutral complex (**54**) (0.10 g, 0.19 mmol) was dissolved in 20 ml of dichloromethane in a reaction flask. To this solution was added a solution of sodium hexafluorophosphate (0.032 g, 0.019 mmol) in acetonitrile (10 ml). The reaction mixture was stirred at room temperature for 24 h. The sodium chloride which formed was then filtered off by gravity, the filtrate was collected and the solvent was reduced under reduced pressure. The oil which remained was dissolved in dichloromethane and a few drops of diethyl ether were added; this mixture was cooled in liquid nitrogen to afford the product as a yellow powder. Product (**52**) (0.09 g, 69 %) was filtered, washed with diethyl ether and then dried under reduced pressure. Single crystals suitable for X-ray crystallography were grown from a mixture of dichloromethane and diethyl ether in the refrigerator. The melting point of the product was found to be 190 ºC (decomposed). The product decomposed rapidly in deuterated solvents; therefore, the ^{1}H and ^{13}C NMR spectra were measured immediately after sample preparation.

^{1}H NMR ($CDCl_3$) δ_H ppm: 8.84 (H^{9}, d, *J* = 6 Hz), 8.50 ($H^{9'}$, d, *J* = 6 Hz), 8.02 (H^{8}, d, *J* = 6 Hz), 7.94 ($H^{8'}$, d, *J* = 6 Hz), 7.73 ($2H^{7,7'}$, m), 7.56 ($2H^{6,6'}$, m), 4.43 [7H, $5H^{1}$ (C_5H_5), $2H^{2,2'}$(C_5H_4)], 3.99 ($2H^{3,3'}$, C_5H_4), 2.52 (3H, Pd-CNC*H*$_3$) and 1.12 (3H, Pd-C*H*$_3$). ^{13}C NMR ($CDCl_3$) δ_C ppm: 170.2 (C^{5}), 151.9 (C=O), 141.2 (C^{9}), 126.6 (C^{7}), 125.8 (C^{6}), 124.7 (C^{8}), 73.0 (C^{4}), 72.7 (C^{2}), 72.4 (C^{3}), 70.9 (C^{1}), 3.76 (Pd-CN*C*H$_3$) and 1.27. (3H, Pd-C*H*$_3$). ^{31}P NMR ($CDCl_3$) δ_P ppm: 144.3 (*P*F_6^-). IR (KBr disc) ν(cm^{-1}): 3366, 3108, 2970, 2328 (Me*C*≡*N*), 2297 (Me*C*≡*N*), 1667

(C=O), 1632 (C=N), 1598 (C=N), 1467, 1282 and 843 (PF_6^-). Elemental analysis for $C_{24}H_{23}N_4F_6OPFePd$ [found (calculated)]: C 42.25 (41.73), H 3.18 (3.36), N 7.61 (8.11). Mass spectrometry (ESI-MS) *m/z*: 545.00 $[(M\text{-}PF_6^-)^+$, 100%] 488.03 and 145.00 (PF_6^-).

(Methyl)[N,N-di(2-pyridyl)ferrocenylamide](triphenylphosphine)palladium(II) hexafluorophosphate **(60)**

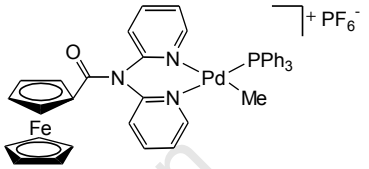

The neutral complex (**54**) (0.10 g, 0.19 mmol) was dissolved in 20 ml of dichloromethane in a reaction flask. To this solution was added a solution of sodium hexafluorophosphate (0.032 g, 0.19 mmol) and triphenylphosphine (0.05 g, 0.19 mmol) in 10 ml of tetrahydrofuran. The reaction mixture was stirred at room temperature for 24 h. The sodium chloride salt which formed was filtered off by gravity, the filtrate was collected and the solvent was then reduced under reduced pressure. The oil which remained was dissolved in dichloromethane and diethyl ether (0.10 ml) was added; this mixture was cooled in liquid nitrogen to afford the product as a yellow powder. Product (**60**) (0.12 g, 71 %) was filtered, washed with diethyl ether and then dried under reduced pressure. Single crystals suitable for X-ray crystallography were grown from a mixture of dichloromethane and diethyl ether in the refrigerator. The melting point of the product was found to be 191 ºC (decomposed).

^{1}H NMR ($CDCl_3$) δ_H ppm: 8.60 (H^9), 7.90 ($H^{9'}$), 6.80 – 7.80 {21H, 15H [$P(\text{-}C_6H_5)_3$], $6H^{5,5'\text{-}7,7'}$, m}, 4.30 ($2H^{2,2'}$, C_5H_4, m), 4.22 ($5H^1$, C_5H_5), 3.99 ($2H^{3,3'}$, C_5H_4, m), 0.72 (3H, Pd-C*H*$_3$, d, $J_{H\text{-}P}$ = 3Hz). ^{13}C NMR ($CDCl_3$) δ_C ppm: 170.8 (C^5), 151.3 (C=O), 141.0 (C^9), 134.6 (C^7), 134.5 [$P(C_6H_5)_3$-*ipso*], 131.6 [$P(C_6H_5)_3$-*ortho*], 130.4, 129.1 [$P(C_6H_5)_3$-*meta,* and *para*], 125.0 (C^6), 115.2 (C^8), 71.3 (C^1 – C^4, m), 5.5 (Pd-*C*H_3, d, $J_{C\text{-}H}$ = 22 Hz). ^{31}P NMR ($CDCl_3$) δ_P ppm: 39.54 [*P*$(C_6H_5)_3$], 144.25 (*P*F_6^-). IR (KBr disc) ν(cm^{-1}): 3082, 3047, 2974, 1710 (C=O), 1658 (C=N), 1602 (Ph*C*=*C*), 1437, 1286 and 839 (PF_6^-). Elemental analysis for $C_{40}H_{35}N_3F_6OP_2FePd$ [found (calculated)]: C 52.22 (52.68), H 3.50 (3.87) and N 4.32 (4.61). Mass spectrometry (ESI-MS) *m/z*: 767.00 $[(M\text{-}PF_6^-)^+$, 100%] 384.08, 277.12 and 145.00 (PF_6^-).

7.4 Palladium complex for coupling reactions

N'-Benzhydrylidene-N,N-dimethylethane-1,2-diamine **(61)**

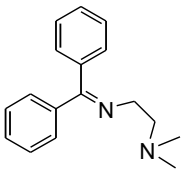

A solution of *N,N*-dimethylethane-1,2-diamine (1.61 g, 18.30 mmol, 2 ml) and benzophenone (3.34 g, 18.30 mmol) in ethanol was heated under reflux for 24 h.[10] After this time the solvent was removed under reduced pressure to afford a yellow oil. The oil was further dried under reduced pressure at 40 ºC, and then exposed to short column chromatography (silica), eluting with a mixture of dichloromethane : methanol (99:1). The product was obtained as the second band by fractional collection. The solvent was then removed under reduced pressure to afford product (**61**) as an oil (2.10 g), which was further dried under reduced pressure at 40 ºC for 12 h.

^{1}H NMR ($CDCl_3$) δ_H ppm: 7.76 (2H, d, *J* = 6 Hz), 7.50 – 7.59 (2H, m), 7.40 (2H, m), 7.30 (2H, m), 7.12 (2H, d, *J* = 3 Hz), 3.49 (2H, t, *J* = 3 Hz), 2.60 (2H, t, *J* = 6 Hz) and 2.19 [6H, $N(CH_3)_2$]. ^{13}C NMR ($CDCl_3$) δ_C ppm: 46.2, 49.1, 60.3, 124.3, 127.9, 130.3, 130.7, 131.0, 132.0, 134.3, 150.3. IR (DCM), ν(cm^{-1}): 3034, 2948, 2815, 2772, 1658 (C=N), 1624, 1598 and 1579. Mass spectrometry (ESI-MS) *m/z*: 252.00 (M^+), 176.10 and 87.11. Elemental analysis for $C_{17}H_{20}N_2$ [found (calculated)]: C 80.52 (80.91), H 7.80 (7.99) and N 10.90 (11.10).

(N'-Benzhydrylidene-κC^2-N,N-dimethylethane-1,2-diamine-κ^{2}N,N')(chlorido) palladium(II) (**62**)

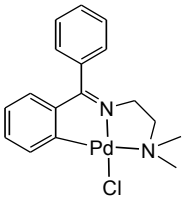

To a solution of *N,N*-dimethylethane-1,2-diamine (**61**) (0.21 g, 0.85 mmol) and sodium acetate (0.15 g, 1.10 mmol) in dry methanol (10 ml) was added solid Na_2PdCl_4 (0.25 g, 0.85 mmol) in one portion. Upon addition of the salt a yellow precipitate appeared and the mixture was further stirred at room temperature until the precipitate turned grey (over 8 h). After this time the product (**62**), (0.22 g, 65%) was collected by suction filtration, washed several times with methanol, and then dried under reduced pressure. The melting point of the product was found to be 229 – 231 ºC.

^{1}H NMR ($CDCl_3$) δ_H ppm: 7.80 (d, *J* = 6 Hz), 7.58 (3H, m), 7.30 (2H, m), 7.13 (d, *J* = 3 Hz), 6.92 (d, *J* = 3 Hz), 6.68 (d, *J* = 3 Hz), 3.70 (2H, t, *J* = 6 Hz), 2.85 (2H, t, *J* = 6 Hz) and 2.72 [N(CH_3)$_2$]. ^{13}C NMR ppm ($CDCl_3$) δ_C ppm: 47.9, 50.3, 62.1, 125.3, 127.5, 129.1, 130.7, 131.0, 132.0, 134.3, 156.9 (Pd-*C*) and 185.2 (*C*=N). IR (DCM) ν(cm^{-1}): 3034, 2948, 2815, 2772, 1607, 1590, 1572 and 1550. Mass spectrometry (ESI-MS) *m/z*: 393.02 (M^+, 100%), 357.06, 251.16 and 238.15 Elemental analysis for $C_{17}H_{19}N_2ClPd$ [found (calculated)]: C 51.60 (51.93), H 4.50 (4.87), N 6.80 (7.12).

(N'-Benzhydrylidene-κC^2-N,N-dimethylethane-1,2-diamine-κ^{2}N,N')(methylcyanide) palladium(II) tetrafluoroborate (**63**)

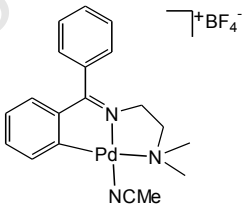

To a solution of (**62**) (0.15 g, 0.38 mmol) was added silver tetrafluoroborate (0.08 g, 0.38 mmol) dissolved in acetonitrile (5 ml). A precipitate of silver chloride immediately appeared. The flask was covered with aluminium foil and the reaction mixture was further stirred at room temperature for one hour. The silver chloride was filtered by suction filtration, the filtrate was collected and solvent was removed under reduced pressure. The oil which remained was dissolved in dichloromethane and dried with anhydrous magnesium sulfate. The drying agent was filtered by gravity and the solvent volume reduced. Product (**63**) (0.15 g, 83%) was then precipitated as white powder by addition of diethyl ether. Crystals suitable for X-ray diffraction were grown by slow diffusion of hexane into a solution of compound (**63**) in dichloromethane. The melting point of the product was found to be 219 – 221 ºC.

^{1}H NMR ($CDCl_3$) δ_H ppm: 7.55 (3 H, d, *J* = 6 Hz), 7.36 (2H, d, *J* = 6 Hz), 7.13 (2H, m), 6.98 (m), 6.72 (d, *J* = 6 Hz), 3.70 (2H, m), 2.85 (2H, t, *J* = 6Hz), 2.78 [N(CH_3)$_2$] and 2.62 (CH_3CN). ^{13}C NMR ($CDCl_3$) δ_C ppm: 3.0 (CH_3CN-Pd), 48.1, 51.3, 63.1, 125.3, 127.5, 129.1, 130.7, 131.0, 132.0, 134.3, 157.1 (Pd-*C*) and 185.2 (*C*=N). IR (DCM) ν(cm^{-1}): 3034, 2948, 2815, 2772, 2328 (Me*C*≡*N*), 2297 (Me*C*≡*N*), 1604 (C=N), 1589, 1574 and 1555. Mass spectrometry (ESI-MS) *m/z*: 398.00 [(M-BF_4^-)$^+$, 100%)], 357.80 and 87.00 (BF_4^-). Elemental analysis for $C_{19}H_{22}N_3BF_4Pd$ [found (calculated)]: C 47.28 (46.99), H 4.39 (4.57) and N 8.11 (8.65).

7.5 Ferrocenyl ligand for in situ stabilization of zinc complex

*Diphenyl(2-{[(2-pyridylmethyl)amino]methyl}ferrocenyl)methanol (***65**)

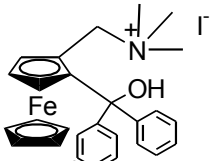

(**64**)

The intermediate methiodide salt (**64**) was firstly prepared following a literature method.[11] A stirred solution of *N*,*N*-dimethylaminomethylferrocene (2.44 g, 10.00 mmol) in 20 ml of freshly dried diethylether was treated dropwise with *n*-butyllithium (25.00 mmol, 16.00 ml, 1.50 M) in hexane over a period of 10 min. Metallation was completed by stirring for an additional hour at room temperature. After this time, an ethereal solution (20 ml) of benzophenone (7.30 g, 40.00 mmol) was added dropwise over 10 min (moderate refluxing) and the reaction continued for 4 h at 25 ºC. The reaction mixture was then hydrolysed by careful addition of water. Separation of the organic layer was followed by extraction of the remaining aqueous layer with several portions of diethylether. The organic layers were combined and extracted with 1:10 phosphoric acid, and the resulting acid solution was neutralized by slow addition to a large excess of 10 % sodium carbonate solution with stirring. The yellow precipitate which appeared was collected by suction filtration and dried under reduced pressure. The dried crude material was subjected to column chromatography (alumina), eluting with dichloromethane : methanol (49 : 1). The solvent was removed under reduced pressure and the solid which remained was recrystallized from methanol-diethylether to afford 2-(α,α diphenylhydroxymethyl)dimethylaminomethylferrocene (3.00 g, 70%) as orange crystals. The melting point of the compound was found to be 122 − 125 ºC (lit.[11] 121 − 125 ºC). Finally, the methiodide product was prepared from a reaction of this resulting compound (2.46 g, 5.80 mmol) and excess methyl iodide (1.23 g, 8.70 mmol, 0.54 ml) in acetonitrile (50 ml) at 35 ºC for 1 h. A precipitate of the desired product (**64**) (2.50 g, 76%) appeared and was collected and dried under reduced pressure. The melting point of the product which was recrystallized from ethanol, was found to be 166 − 169 ºC (lit. m.p 166 – 168 ºC).[11]

^{1}H NMR data of compound (**64**) ($CDCl_3$) δ_H ppm: 7.50 (d, J = 8 Hz), 7.39 (t, J = 8 Hz), 7.20 – 7.35 (m, 8H), 5.21 (2H, CH_2), 4.91 (C_5H_3), 4.63 (C_5H_3), 4.45 (C_5H_3), 4.32 (C_5H_5) and 2.91 [N(CH_3)$_3$]. Elemental analysis for $C_{27}H_{30}NOIFe$ [found (calculated)]: C 58.90 (58.72), H 4.80 (4.62) and N 8.36 (8.56).

To a mixture of the methiodide compound (**64**) (0.80 g, 1.8 mmol) and potassium carbonate (0.25 g, 3.60 mmol) in acetonitrile (10 ml) was added slowly a solution of picolylamine (0.20 g, 1.80 mmol, 0.20 ml) in the same solvent (20 ml). The reaction mixture was heated under reflux for 24 h. After this time, the mixture was cooled and then filtered to remove inorganic material. The solvent was removed under reduced pressure followed by addition of chloroform to the resulting residue, and the mixture was then filtered to further remove inorganic salts. The solution was washed with water and the organic fraction was dried with magnesium sulfate. The solvent was removed under reduced pressure and the product (**65**) (0.60 g, 60%) was obtained as a yellow powder. Recrystallization of the crude material from chloroform-hexane afforded orange crystals. The melting point of the product was found to be 150 – 154 °C.

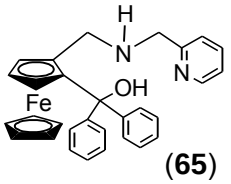

(**65**)

^{1}H NMR ($CDCl_3$) δ_H ppm: 8.58 (H^{18}, d, J = 8 Hz,), 7.63 (H^{17}, d, J = 16 Hz), 7.49 ($2H^{15,16}$, d, J = 8 Hz), 7.20 – 7.40 [$10H^{1-3}$, $2x(C_6H_5)$, m], 4.33 ($5H^{6}$, C_5H_5), 4.13 (H^{9}, C_5H_3), 4.02 (H^{8}, C_5H_3), 3.80 ($H^{13'}$, d, J = 12 Hz), 3.67 (H^{13}, d, J = 16 Hz), 3.48 (H^{10}, C_5H_3), 3.20 ($H^{12'}$, d, J = 16 Hz) and 2.64 (H^{12}, d, J = 12 Hz). ^{13}C NMR ($CDCl_3$) δ_C ppm: 158.1 (C^{14}), 149.4 (C^{18}), 146.8 (C^{2}), 136.6 (C^{16}), 127.6 (C^{4}), 127.4 (C^{3}), 127.0 (C^{5}), 122.4 (C^{15}), 122.2 (C^{17}), 98.1 (C^{1}), 84.8 (C^{10}), 72.6 (C^{9}), 70.8 (C^{8}), 69.8 (C^{6}), 64.5 (C^{7}), 54.2 (C^{13}) and 46.3 (C^{12}). Mass spectrometry (EI-MS) *m/z*: 488.03 (M^+, 80%). IR (KBr disc) ν(cm^{-1}): 3297 (O-H), 3060 (N-H), 2797, 1592 (C=N), 1567 and 1443. Elemental analysis for $C_{30}H_{28}N_2OFe$ [found (calculated)]: C 73.78 (72.83), H 5.78 (5.77) and N 5.74 (5.62).

7.6 Polymerization conditions

7.6.1 Lactide polymerization

A Schlenk flask containing lactide and catalyst was purged with nitrogen and evacuated (5 cycles). Toluene (5 ml) was added and similar cycles of purging and evacuating were again performed. The reaction mixture was heated at 70 ºC in an oil bath under a nitrogen atmosphere for a specified time. The reaction was quenched with aqueous acetic acid (5 mM, 0.1 ml) and stirred for 1 h. and then transferred to a

flask containing hexane cooled to -70 ºC. A precipitate of a polymer appeared, and was collected by suction filtration, washed with hexane and dried under reduced pressure. The NMR scale reactions were conducted in a J. Young's NMR tube and all reagents were weighed in a glove box. The tube was further purged with nitrogen and evacuated on the Schlenk line. The reaction setup for reactions performed in the Schlenk tube is shown in **Figure 7.6.1.**

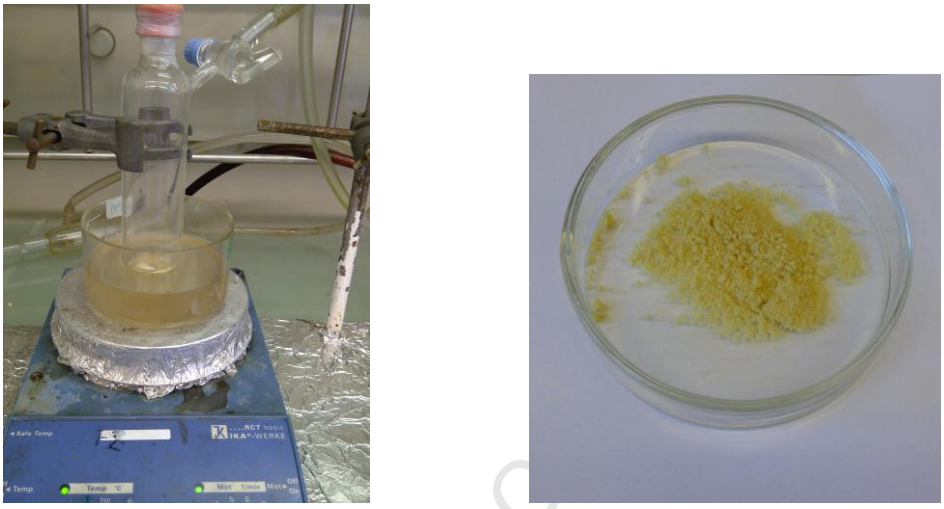

(a) (b)

FIGURE 7.6.1: Pictures representing (a) the experimental setup for the lactide polymerization reaction and (b) the product which was isolated.

7.6.2 CO/styrene copolymerization

A carbon monoxide purged balloon was introduced to a flask containing styrene monomer, catalyst, 1,4-benzoquinone, trifluoroethanol and dichloromethane. The total volume of the mixture was kept constant at 10 ml in all experiments conducted. The solution was stirred at room temperature for 18 h. After this time, the solvent volume was reduced under reduced pressure by rotary evaporation and the flask was placed in a liquid nitrogen-acetone mixture at -70 ºC, followed by the addition of hexane and diethyl ether to precipitate the polymer as a white powder. The polymer was collected by suction filtration, dried under reduced pressure for 2 days, then analysed by GPC and MALDI-TOF spectrometry. The reactions conducted at higher pressure (10 - 30 bar) and temperature (25 - 90 ºC) were conducted in a 100 ml stainless steel autoclave reactor. The reaction setup for polymerization reaction at ambient conditions is shown in **Figure 7.6.2.**

(a) (b) (c)

FIGURE 7.6.2: Pictures representing the experimental setup for CO/styrene copolymerization reaction: (a) polymerization at ambient conditions (1 bar, 25 ºC); (b) polymerization at various conditions (1 - 30 bar, 25 - 90 ºC) in the autoclave reactor; (c) the NMR-scale reactions at ambient conditions in Young's NMR tube.

The polymerization utilizing the oxidized form of compound (**59**) was performed as follows: silver tetrafluoroborate was dissolved in trifluoroethanol (1 ml) and placed in a two-necked round-bottom flask and the solution was stirred. An equimolar amount of compound (**59**) in dichloromethane (4 ml) was transferred with a syringe through a rubber septum. The orange solution of compound (**59**) immediately turned green upon contact with the solution of silver salt. The reaction mixture was stirred for 10 min then styrene (5 ml) was introduced with a syringe through a septum. Carbon monoxide was then introduced and the reaction was continued for 18 h at room temperature with stirring. The reaction setup is shown in **Figure 7.6.3.**

The styrene/CO copolymer was initially functionalized with 4-bromobenzyl alcohol by a C-C coupling method. The Schlenk flask containing $CsCO_3$ and palladium catalyst (**63**) or (**57**) was purged with nitrogen and evacuated (three cycles). To this flask was added copolymer dissolved in toluene through a rubber septum. The flask was then heated to 100 ºC for 48 h. The inorganic salts were filtered off and the functionalized polymer was precipitated by addition of hexane. The material was collected using suction filtration, washed with hexane and dried under reduced pressure.

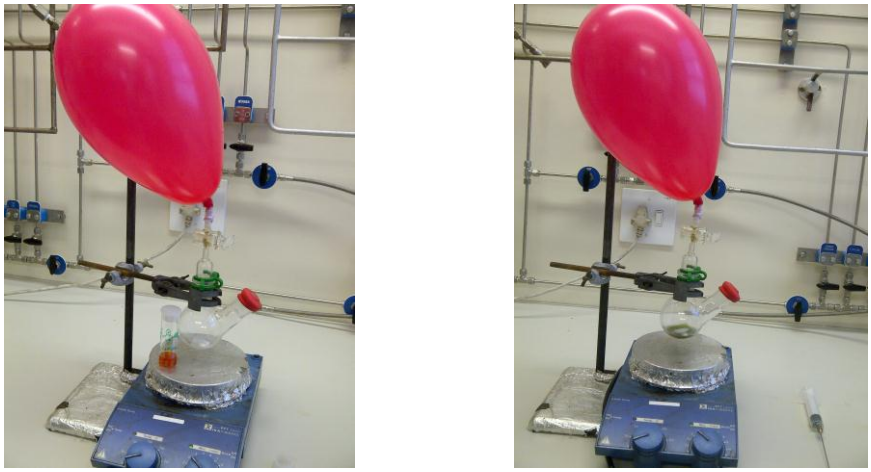

(a) (b)

Figure 7.6.3: Pictures representing the experimental setup for the CO/styrene copolymerization reaction when the oxidized form of compound (**59**) was utilized: (a) round-bottom flask containing a solution of silver tetrafluoroborate in TFE, the sample vial next to the flask contains a solution of the complex (**59**) in DCM; (b) solution after the reagents were mixed.

7.6.3 Poly(lactide-co-CO/styrene) block copolymerization

The ferrocenyl ligand (**65**) was dissolved in freshly dried toluene and the flask was purged with nitrogen and evacuated (three cycles). To this solution was added diethylzinc in hexane at –78 ºC. The reaction mixture was allowed to slowly reach room temperature and was further stirred for 3 h. After this time, the functionalized CO/styrene copolymer which was prepared as outlined above was dissolved in toluene and transferred to the flask, and the mixture was further stirred at room temperature for 3 h. After this time, the lactide monomer was added to the reaction mixture and the flask was heated at 80 ºC under a nitrogen atmosphere with stirring for 48 h. The polymerization process was quenched with an acidic aqueous solution and the polymer was precipitated with hexane at –78 ºC. The polymer was collected using suction filtration, washed with hexane and dried under reduced pressure.

7.7 Polylactide degradation conditions

Six sample vials containing functionalized polymer (20 mg) and phosphate buffer solution, pH =7.4 (20 ml), were heated at 37 ºC on the oil bath with stirring. At a given time, a sample vial was removed from the oil bath and the contents were transferred to the separating funnel. The mixture was extracted with dichloromethane

and the organic layer was collected, dried with magnesium sulfate and then concentrated under reduced pressure. The sample was then analysed using ^{1}H NMR spectroscopy. For the sample analysed at time t = 0, the sample vial containing the polymeric material was shaken vigorously for ten minutes and then treated the same way as other samples. A control experiment was conducted by transferring the benzothiazole ligand (**37**) and this sample was also treated in the same way as other samples.

7.8 References

1 G. M. Sheldrick, SHELXS97, *Programme for Solving Crystal Structures*, University of Göttingen, Germany, 1997.

2 G. M. Sheldrick, SHELXL97, *Programme for the Refinement of Crystal Structures*, University of Göttingen, Germany, 1997.

3 (a) B. Delley, *J. Chem. Phys*., 1992, **92**, 508; (b) B. Delley, *J. Phys. Chem*., 1996, **100**, 6107; (c) B. Delley, *J. Chem. Phys*., 2000, **113**, 7756.

4 J. P. Perdew and Y. Wang, *Phys. Rev. B*., 1992, **45**, 13244.

5 B. Delley, in *Modern Density Functional Theory: A Tool for Chemistry*; J. M. Seminario, P. Politzer, Eds; *Theoretical and Computational Chemistry*, Vol. **2**; Elsevier, Amsterdam, The Netherlands, 1995.

6 (a) D. Drew and J. R. Doyle, *Inorg. Synth.*, 1972, **13**, 52; (b) B. Milani, A. Marson, E. Zangrando, G. Mestroni, J. M. Ernsting and C. J. Elsevier, *Inorg. Chim. Acta*, 2002, **327**, 188.

7 (a) S. K. Bharti, G. Nath, R. Tilak and S. K. Singh, *Eur. J. Med. Chem.*, 2010, **45**, 651; (b) V. Vrdoljak, I. Đilovic, M. Rubčić, S. Pavelić, M. Kralj, D. Matković-Calogović, P. Novak, A. Rožman, I. Piantanida and M. Cindrić, *Eur. J. Med. Chem.*, 2010, **45**, 38; (c) T. D. Thangadurai and S.-K. Ihm, *Trans. Met. Chem*., 2004, **29**, 189; (d) I. Yilmaz and A. Çukurovali, *Synth. React. Inorg. Metal-Org. Chem.*, 2003, **33**, 657.

8 (a) C. T. Cioffi, A. Palkar, F. Melin, A. Kumbhar, L. Echeqoyen, M. Melle-Framco, F. Zerbertto, G. M. Aminu-Rahman, C. Ehli, V. Sgobba, D. M. Guldi and M. Prato, *Chem. Eur. J.*, 2009, **15**, 4419; (b) A. S. Batsanov, D. Herault, J. A. K. Howard, L. G. F. Patrick, M. R. Probert and A. Whiting, *Organometallics*, 2007, **26**, 2414.

9 (a) J. E. Aguado, O. Crespo, M. C. Gimeno, P. G. Jones, A. L. Laguma and Y. Nieto, *Eur. J. Inorg. Chem.*, 2008, 3031; (b) S. Quintal, M. Gimeno, A. Laguma, M. J. Calhorda, *J. Organomet. Chem*., 2010, **695**, 558; (c) S. Quintal, S. Fedi, J. Barbetti, P. Pinto, V. Félix, M. G. B. Drew, P. Zanello, M. J. Calhorda, *J. Organomet. Chem*., 2011, **696**, 2142.

10 M. Cohen and D. H. Smith, *J. Med. Chem*., 1981, **24**, 336.

11 D. W. Slocum, B. W. Rocket and C. R. Hauser, *J. Am. Chem. Soc*., 1965, **87**, 1241.

APPENDICES

Full crystallographic structural analysis of single crystal X ray diffraction data of the following compounds (on the CD rom):

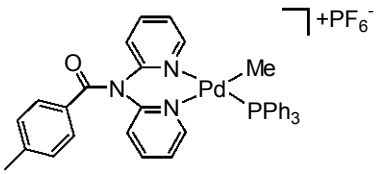

Compound (**57**)

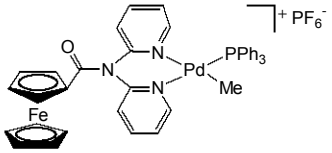

Compound (**60**)

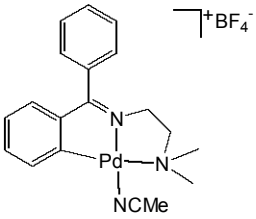

Compound (**63**)

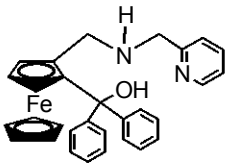

Compound (**65**)